767c

FLOW-INDUCED VIBRATIONS
INSIDE A TUBE-BANK

# CROSS-FLOW-INDUCED VIBRATIONS DEEP INSIDE A CLOSELY-PACKED TUBE-BANK

by

L. K. GROVER, M.A.Sc. (Sask.)

A Thesis

Submitted to the School of Graduate Studies

in Partial Fulfillment of the Requirements

for the Degree of

Doctor of Philosophy

McMaster University

May 1977

| | |
|---|---|
| DOCTOR OF PHILOSOPHY (1977)<br>(Mechanical Engineering) | McMASTER UNIVERSITY<br>Hamilton, Ontario |

| | |
|---|---|
| TITLE: | Cross-Flow-Induced Vibrations Deep Inside a Closely-Packed Tube-Bank |
| AUTHOR: | L. K. Grover, M.A.Sc., (Eng.) Univ. of Saskatchewan |
| SUPERVISOR: | Dr. D. S. Weaver |
| NUMBER OF PAGES: | xi, 248 |

## ABSTRACT

Heat-exchangers designed and fabricated in accordance with the existing design standards may be susceptible to damage as a result of excessive tube vibrations caused by the shell-side fluid flow. The present investigation was undertaken to further our understanding of the vibration behaviour of tube arrays.

An experimental facility and techniques have been developed by means of which the major mechanisms that cause flow-induced vibrations in tube arrays due to cross-flow can be produced and properly identified.

The experiments were conducted in a low-speed wind-tunnel having 305 x 305 mm.working section. The tube-bundle was a parallel-triangular tube-array with pitch/diameter = 1.375. The array was 27 rows deep with 5 tubes in each row. The tubes were designed such that they could be conveniently removed from outside the wind-tunnel, in order to facilitate studying the effect of tube-bundle size on vibration and flow characteristics. Nineteen identical tubes in the middle of the tube-array were movable and specially designed so that natural frequency and damping could be controlled precisely over a range of values.

The experiments have verified that deep inside a closely-packed tube-bank the existence of discrete vortex-

shedding is not a working hypothesis and the response of a tube in a tube-bundle is expected to be a function of Reynolds number and the number of upstream rows of tubes. From the flow-field velocity power-spectra obtained for the array tested and from the available data existing in the literature, it is seen that there is a strong possibility of predicting the dominating frequency in the flow from a universal Strouhal number. For the first time a fluidelastic stability boundary for the array has been derived and it is noticed that the slope of this boundary is significantly different from that derived by other authors from theoretical considerations.

ACKNOWLEDGEMENTS

The author is grateful to Dr. R. T. Hartlen for suggesting the problem and to other members of the Supervisory Committee for their continued interest in the work.

In addition, sincere gratitudes are expressed to my supervisor, Dr. D. S. Weaver, for his infinite patience with me (while I was making all kinds of mistakes) and from whom I have learnt much more than what is contained in this thesis.

The kind help of Departmental technicians, Mr. Robert Brown, Mr. Frank Drieman and Mr. Dave Schick is highly appreciated. The painstaking efforts of Ms. BettyAnne Bedell for her excellent typing of this manuscript is also greatly appreciated.

The financial support provided through the National Research Council Operating Grant A8284 is gratefully acknowledged.

CONTENTS

## LIST OF SYMBOLS

| | |
|---|---|
| $a$ | Speed of sound in fluid |
| $A$ | Area of cross-section |
| $c$, $c_n$ | Absolute damping of the tube |
| $c_c$ | Critical damping of the tube |
| $c$ | A constant |
| $c'$ | A constant |
| $C_D$ | Coefficient of drag |
| $C_f$ | Coefficient of friction |
| $C_L$ | Coefficient of lift |
| $d$ | Outside diameter of tube or cylinder |
| $D$ | Characteristic length |
| $E$ | Young's modulus of elasticity |
| $f$ | Vibration frequency |
| $f_b$ | Frequency of boundary displacement |
| $f_s$ | Frequency of vortex-shedding |
| $f_n$ | Natural frequency of tube or cylinder |
| $F$ | Force acting on the cylinder |
| $F_e$ | Externally applied force |
| $F_L$ | Alternating lift-force |
| $G$ | Minimum-gap between two tubes in an array |
| $\Delta H$ | Pressure drop |
| $k$ | Spring rate of the tube |
| $K$ | Fluidelastic constant |

| | |
|---|---|
| $\ell$ | Longitudinal spacing of tubes |
| $L$ | Length of the cylinder |
| $L_c$ | Correlation length |
| $m$ | Mass of the tube |
| $M_o$ | Virtual mass of the tube |
| $p$ | Pitch of the tubes in the array |
| $R$ | Reynolds number |
| $R_G$ | Reynolds numbers based on minimum-gap velocity |
| $R_T$ | Reynolds number based on velocity between two adjacent tubes in the transverse direction |
| $R_U$ | Reynolds number based on freestream flow velocity |
| $S$ | Strouhal number |
| $S_G$ | Strouhal number based on minimum-gap velocity |
| $S_T$ | Strouhal number based on velocity between two adjacent tubes in the transverse direction |
| $S_U$ | Strouhal number based on freestream flow-velocity |
| $t$ | Time constant |
| $T$ | Transverse spacing of tubes |
| $V$ | Flow velocity |
| $V_G$ | Flow velocity in the minimum-gap between the tubes |
| $V_R$ | Reduced velocity = $V/fd$ |
| $V_U$ | Upstream flow velocity |
| $x,y$ | Vibration amplitude |
| $X_L$ | Geometric parameter = $\ell/d$ |
| $X_{2L}$ | Geometric parameter = $2\ell/d$ |
| $X_T$ | Geometric parameter = $T/d$ |

$Y_b$ Boundary displacement

Greek Symbols

$\sigma$ Tensile stress

$\xi$ A dimensionless number = $R.V_R/X_T$

$\xi'$ Damping factor

$\delta$ Logarithmic decrement of tube

$\rho$ Density of the fluid

$\mu$ Viscosity of the fluid

# CHAPTER 1

# INTRODUCTION

As the art of heat-exchanger design moves into new areas regarding size, temperature and unusual fluids, there has been a significant increase in the number of equipment failures due to vibrations. Hartlen [84]* and Shin and Wambsgnass [81] have described recent field experiences, where tube failures due to excessive vibrations have been recorded. With the construction of larger nuclear plants and chemical plants, and the increasing sophistication in their design, more exacting requirements are being placed on heat-transfer equipment. Large size units are being built, and for service at higher temperatures. Higher equipment performance often is required as manifested by lower pressure drop and higher heat-transfer rates. The economics sometimes dictate smaller components or minimum structural constraints, as illustrated by the small diameter tubes used in CANDU** nuclear steam generators to minimise heavy water inventory. High flow rates and decreased structural rigidity could lead to problems due to excessive flow-induced vibrations. Mechanical wear, fatigue failure,

---

* Numbers in brackets designate references at the end of the thesis.

** CANDU - CANADA DEUTERIUM URANIUM

fretting failure, acoustic noise and mixing of shell-side and tube-side fluids are the problems caused by flow-induced vibrations. Failures in the larger heat-transfer units are costly both in repairs and in plant down-time or production loss. In some cases specialized repair techniques, such as remote operations are required when heat-exchangers operate in exotic fluid environments such as sodium, mercury or molten salts or in a nuclear radiation environment.

Recent surveys - [5], [6], [81]-[83] of vibration problems in heat-transfer equipment have indicated a wide range of uncertainties involved in currently available predictive methods for the designer. Our understanding of the mechanism of excitation of oscillating tubes deep inside a tube-bundle seems to be far from complete and anomalies in the literature exist. The lack of information for the designer in this important field has been mainly due to the complexity of fluid-structure interaction problems which so far have defied reasonable analytical solution and present considerable difficulties if an experimental study is to be initiated.

Cross-flow-induced vibrations in a tube-bundle can be correlated in terms of a dimensionless velocity parameter $(V_G/fd)$ and a damping parameter $(m\delta/\rho d^2)$. Figure 1.1 shows a generalized stability diagram, expressed in terms of these two parameters.

There appear to be at least three excitation mechanisms; a vortex-shedding mode, turbulent buffeting and a

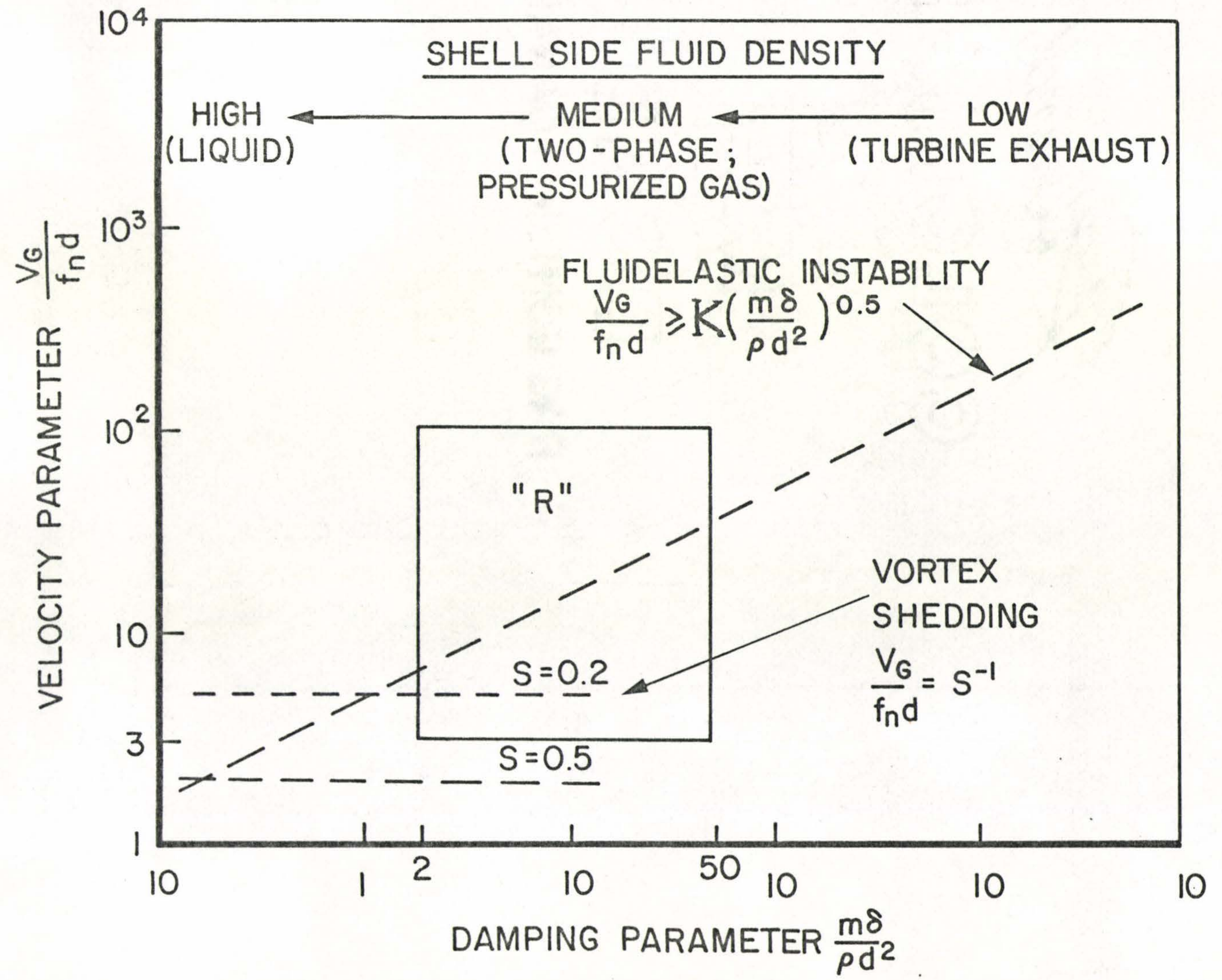
SHELL SIDE FLUID DENSITY
HIGH (LIQUID)
MEDIUM (TWO-PHASE; PRESSURIZED GAS)
LOW (TURBINE EXHAUST)
FLUIDELASTIC INSTABILITY
$\frac{V_G}{f_n d} \geq K\left(\frac{m\delta}{\rho d^2}\right)^{0.5}$
"R"
VORTEX SHEDDING
$\frac{V_G}{f_n d} = S^{-1}$
S = 0.2
S = 0.5
VELOCITY PARAMETER $\frac{V_G}{f_n d}$
DAMPING PARAMETER $\frac{m\delta}{\rho d^2}$
$10^4$
$10^3$
$10^2$
10
3
1
10
1
2
10
50
10
10
10

FIGURE 1.1

fluidelastic mode as discussed in the literature by Chen [89], Owen [100], Connars [78], Savkar [82] and Gorman [113], etc.

The vortex-shedding mode is excited when the frequency of vortex-shedding in the tube-bank coincides with the natural frequency of the tube. The coupling occurs at a constant value of Strouhal number. The vortex-shedding frequency is a function of tube-pattern and pitch and is shown by the constant velocity parameter lines in figure 1.1. However, it is still uncertain if such a phenomenon occurs deep inside a tube-bank as most of the investigations conducted so far have been done by modelling only a few rows of the tube-array.

Turbulent buffeting is due to random pressure fluctuations which give rise to a behaviour associated with a randomly forced, damped vibration. Owen [100] has stated that the tube structure acts as a mechanical filter and selects for its response predominantly that part of the force spectrum neighbouring on a natural frequency and a peak displacement occurs at such a flow speed that the dominant frequency in the force spectrum coincides with a natural structural frequency. However, this hypothesis has not been verified by experimental evidence yet.

Connars [78] has established a fluidelastic stability threshold as shown in figure 1.1. He conducted a quasi-steady analysis wherein he equated the energy added by a fluidelastic tube displacement mechanism to that dissipated by damping. As his analysis was done on a single row of tubes only, its validity in predicting the onset of vibrations in a tube-bundle is very questionable. The fluidelastic stability threshold is also expected to be a function of tube-pattern and pitch. No systematic investigation has been published so far which provides fluidelastic stability boundaries for the various types of tube arrays.

It is also seen in figure 1.1 that for low values of the damping parameter, the fluidelastic boundary tends to merge with that for vortex-shedding. The parameter range over which the vortex-shedding and fluidelastic thresholds are expected to crossover and one criterion replace the other as the design criterion, is not known yet.

A source of considerable confusion has been the widely varied tube arrays used in experimentation. Not only have numerous staggered and in-line arrays been studied using different values of reduced damping but the number of tubes used to represent a tube-bundle has varied greatly. In addition, some of the experiments have been conducted with flexible tubes while others have used rigid tubes. It seems reasonable that excitation mechanisms, turbulence levels and stability thresholds are all dependent on array configuration and the number of tubes in a given array. Thus many of the results reported in the literature are not really comparable. It would be particularly useful to know just how many tubes are required to properly model the phenomena occurring deep inside a tube-bank.

Our lack of knowledge as described above is primarily due to the difficulties encountered in modelling the tube vibrations in an array (including time and expense) and in devising effective means to control the various parameters involved.

The purpose of the present investigation is to develop a single experimental facility and the accompanying techniques whereby the various mechanisms that cause cross-flow-induced vibrations in tube-bundles could be produced and properly identified. Of particular interest is to determine:

(a) Whether both vortex-shedding and fluidelastic instability will occur in the same tube array and to ascertain their relative importance.

(b) Whether vortex-shedding occurs deep inside a tube-bundle.

(c) The effect of the number of tubes on the vibration characteristics and stability of the tube array and thus the number of tubes required to model a tube array.

(d) the nature of the fluidelastic instability deep inside a tube array and the validity of the simple fluidelastic stability criteria proposed by Connars and commonly used in current design practice.

It is hoped that this experimental program will demonstrate useful investigative techniques, help in the design of more meaningful future experiments and result in an improvement of our understanding of the mechanism of tube vibrations in tube arrays of practical interest.

# CHAPTER 2

# LITERATURE SURVEY OF FLOW-INDUCED VIBRATION PROBLEMS

## 2.1 Basic Concepts of Fluid-Structure Interaction

Flow-induced vibration problems involve mutual interactions among inertial, fluid-dynamic and elastic forces. Various uncertainties and non-linearities associated with determining the exact nature and magnitudes of these forces for different classes of problems render their analyses a formidable task. This field finds its greatest applications in the vastly growing areas of naval and space science [1] and more recently in problems related to vibration and fretting in nuclear fuel assemblies [2], vibrations of hydraulic components and structures [3], [4] and tube vibrations in nuclear heat-exchangers and steam generators [5], [6]. Wind effects on buildings and structures [7] is another very important area encompassed by this field.

Flow-induced vibration phenomena are relatively complex and diverse. This has resulted in a large volume of research and analysis, scattered throughout a wide variety of journals. A number of general papers [8], [9],[10] and [11] have been written, which shed some light on the nature of the complexities involved. Naudascher [12] has attempted to classify various hydroelastic phenomenon by their common flow-instability mechanisms. Most of the flow-induced vibrations can be characterized in three categories (a) dynamic response (b) self-controlled vibrations and (c) self-excited vibrations [4].

Dynamic response problems are the forced vibrations induced by turbulence or pressure fluctuations in the flow or by fluid impact. Response of aircraft panels to jet noise, or response of space-craft structures to boundary-layer excitation are problems which are of great practical interest and rely for their solution on the use of statistical techniques. High-performance marine craft experience many different types of dynamic excitation and response. The marine vehicle operates at an interface between air and water and thus is subjected to wave actions and therefore loading conditions are complex and difficult to describe accurately. Secondly, a vehicle operating at this interface may entrain air in cavities formed behind those portions of the structure that penetrate the liquid surface - in fact, the entire concept of "cavitated" flows is vital to high-speed marine craft. Hydrodynamic impact is also associated with ship slamming. The phenomenon resulting from interaction of a missile system or of a supersonic vehicle with the shock front of a blast wave is another example which falls into this category. Additional examples are response of aircraft to gusts and response of tall buildings to ground boundary layer turbulence. A necessary condition for this class of response problems is that the deformation of the structure does not significantly alter the fluid forces acting on it.

In self-controlled vibrations, some periodicity exists in the flow. If this periodicity happens to coincide with one of the natural frequencies of the structure, the amplitude of vibration builds up to the point where the magnitude and frequency of the fluid forces are controlled by the motion of the structure and a dynamic feedback mechanism develops. The velocity range in which the flow periodicity is controlled by the structural vibration frequency is called the "lock-in" region. The width of this region is affected by the amount of damping in the structure. The most common source of this periodicity in the flow is the vortex-shedding phenomenon. Vortex-shedding in the wake of a bluff body results from a free shear layer that separates from each side of it. The shear layers roll up and form discrete vortices. Vortex-shedding can also cause acoustical resonance resulting in a severe structural loading and noise generation. Vibrations of smokestacks, pipes and submarine periscopes are perhaps the most obvious examples of this class of vibrations. Recently, however, investigations have revealed that vortex-streets occur for geometries other than the circular cylinders previously considered. In particular, the phenomenon has been studied in connection with the "singing" of vanes and propellers. The practical consequences of the "singing" of vanes and propellers are the generation of both structure-borne and water-borne sound, fatigue failure of the blade, loss of propulsive efficiency, etc. In all these problems, mutual interaction exists between inertial and elastic forces of the structure, with an already existing periodicity in the flow.

Self-excited vibrations are produced when the oscillations of the structure result in periodic fluid forces which in turn amplify the structure's motion. These vibrations are distinguished from those of the self-controlled type in that the periodic forces disappear in the absence of structural motion. Problems of dynamic aeroelasticity such as the "flutter" of plates and shells fall into this category [16]. "Flutter" is a dynamic fluid-elastic instability in which a structure, when perturbed, will oscillate with exponentially increasing amplitude, unless limited by some non-linear constraint. Other examples are self-excited vibrations of vertical-lift gates, oscillations of gate seals and hydroelastic vibration of swing check valves, etc. [3].

In bluff body vibrations, when the body shape is such that a small transverse or torsional motion of the body causes the shear layers to lie sufficiently asymmetrically with respect to the downstream body surfaces, a pressure loading is created on the body which forces it in the direction of its initial small motion, and galloping instability results. With a multi-component bluff structure, such as a transmission line conductor bundle, the wake of an upstream element may impinge on a downstream element to create pressure loadings on it, and wake galloping results [13], [14]. A stranded conductor may also gallop in a flow approaching at a small angle to the normal from the conductor span. In this case the instability results from asymmetric flow separation caused by the different surfaces presented to the flow by the helically wound strands [15].

Certain special forms of flow-induced vibration of bluff bodies occur also. If the cross-section of the body in the plane of the incident flow and of the transverse vibration is long, the initially separated flow will reattach to the downstream body surfaces, and the pressure loading may have enough similarity to that for an airfoil section that a combined plunging and twisting flutter oscillation can develop. This can occur for suspension bridge decks [3].

The analysis and development of mathematical models for fluid-structure interaction problems draws on four disciplines: (1) theory of elasticity; (2) mechanical vibrations; (3) fluid mechanics; and (4) mathematical stability theory. The formulation of the equations of fluidelasticity may be viewed as consisting of the determination of the so called structural operators, inertial operators, and fluid-dynamic operators [9]. The adequacy of formulating these equations depends on the degree to which the mechanism of excitation is understood. In fluidelasticity, stability problems often receive primary attention. The solution of the response problem consists of determining particular integrals of the equation of motion. Ordinary algebraic methods suffice when structural deformation and motions can be assumed to be harmonic. Laplace transformations and solution by indicial admittances are needed for transient motions. The results thus obtained are approximate because the linearity of operators has been assumed. The degree of approximation always remains subject to question. In addition, the response depends critically on structural damping. Yet the laws of damping are not known accurately. Finally, for stochastic responses, it remains to select fatigue criteria for design. In short, proper solution of response problems requires at least some attention to the non-linearity of the basic equations of solid and fluid mechanics.

The major difficulty of fluidelasticity centers around the fluid-dynamic operators. This is a result of the often nonlinear and/or stochastic nature of these operators. The degree of difficulty is dependent on structural characteristics among which geometric shape is viewed as the most important. When there is no flow separation along the structural surface, the flow field may usually be computed by means of potential flow theory and linearization of the nonlinear equations of fluid-mechanics is feasible. Flow separation will be absent only if the structural shape is properly streamlined and, furthermore, if the angle of attack is within a certain limited range. One of the simplifying assumptions is the so called "strip" assumption (i.e., the local fluid dynamic forces are considered dependent on the local shape only) by which marked three-dimensionality of the flow is held absent.

Many non-linear problems in fluidelasticity are related to free shear layer characteristics. Unsteady separated flows can not be analysed using the potential flow theory only. The latter's usefulness is therefore limited and the determination of the fluid-dynamic operators becomes more reliant on experimental information. Obtaining and interpreting such information places greater demands on the theories of boundary layers, cavitation, turbulence and wake mechanics.

The experimental tools for analysing fluid-structure interactions are in an advanced stage of development and under constant demands from an ever increasing number of new and unique problems for their further refinement. Indeed, fluidelastic phenomenon encountered at the forefront of modern design often do not yield to analytical methods, and if solutions are to be obtained within a reasonable length of time the employment of experimental methods is essential.

The needed experimental information is usually in the form of stability thresholds, fluid-dynamic coefficients, correction coefficients, pressure distributions, velocity profiles, noise spectrums, flow-visualization, vortex-shedding frequencies, amplitude-frequency-phase of oscillations and intensity-scale-spectrum of turbulence, etc.

The preliminary analysis of phenomena and the choice of a system of definite non-dimensional parameters is made possible by dimensional analysis and similitude theory. Dimensional analysis can be used to analyze very complex phenomenon and is of considerable help in setting up experiments.

Applying similarity principles, a model is constructed which is related to the physical system (prototype) such that observations on the model may be used to predict accurately the performance of a physical system in the desired respect. In a rigid body motion model, dynamic similarity requirements can be met independently of geometric similarity and kinematic similarity requirements. "Replica" dynamic models are used to aid in the design for prototypes which are complex and which have high potential for catastrophic damage in the event of a failure [18].

The model laws that arise in fluid-structure interactions impose stringent scaling requirements. To obtain a feasible model, it is usually necessary to allow several of the dimensionless parameters to be distorted. This can only be done with confidence when the physics of the problem is well understood. The modeler must know, for example, what kind of prototype responses are really important and what kinds can be neglected, for otherwise modelling may be impossible. Baker et al. [18] showed by giving a few examples, the nature of the complexities and difficulties involved in modelling the dynamic interaction between a flexible structure and a liquid. They state that the modelling problems of the flow-induced vibrations of heat-exchangers and nuclear reactors are particularly complicated and have to this day defied complete analysis and accurate modelling. This results in full-scale prototypes being vibration tested, and costly changes, if needed, must then be made on the already manufactured item.

Although it may be possible in concept to design, build and test dynamic models simulating every prototype structure or problem, there are a number of practical considerations which can limit one's ability to build and test such models. Some such factors are: cost, limitations imposed by physical properties, limitations imposed by an "unwanted" physical phenomenon, limitations with decreasing model size and limitations imposed by construction techniques, etc.

Wind-tunnels, water-tunnels, water-loops and two-phase flow loops are commonly employed to study the response and stability of these dynamic models.

## 2.2 Basic Flow-Induced Vibration Mechanisms for Cross-Flow over Circular Cylinders

### 2.2.1 Flow over a Single Circular Cylinder (both Fixed and Oscillating)

The principal mechanisms exciting flow-induced vibrations of a single cylinder appear to be vortex-shedding and turbulence.

When a fluid flows past a cylindrical obstacle, the wake behind it in certain ranges of Reynolds numbers is seen to contain numerous vortices arranged in a regular pattern, which was described and drawn accurately as early as the fifteenth century by Leonardo da Vinci [21]. The vortices appear alternately on each side of the cylinder and are washed away in the wake when they have reached a certain size. At the moment that a vortex has reached its maximum size, just before detaching itself from the cylinder, the velocity of the flow past that side of the cylinder is maximum and hence, by

Bernoulli's law, the pressure on that side is a minimum. The cylinder thus experiences an alternating force in a direction perpendicular to that of the flow. In 1878 Strouhal published a formula for the frequency of this vortex-shedding, based on observations only. This formula is now usually represented in a dimensionless form and is known as the "strouhal number", defined as:

$$S = \frac{f_s d}{V}$$

$f_s$ = frequency of vortex-shedding

$d$ = diameter of circular cylinder

$V$ = flow velocity in undisturbed stream

In 1911 von Karman made a stability analysis of the vortices and from it derived the geometrical pattern. This was the first theoretical investigation of the subject, and it is so important that the vortex wake now is generally referred to as the Karman Wake [20].

The major regimes of fluid flow across a rigid circular cylinder are shown in Fig. 2.1. At extremely low Reynolds number (<3) the flow about the cylinder follows Stokes law. The flow streamlines close behind the cylinder and the flow does not separate as shown in Fig. 2.1(a). As the Reynolds number is increased, the streamlines widen, and at a Reynolds number of 5-10, a pair of fixed "Foppl" vortices first appear immediately behind the cylinder, as shown in Fig. 2.1(b). This vortex pair behind the wake of cylinders becomes unstable at a Reynolds number of about 40, and the

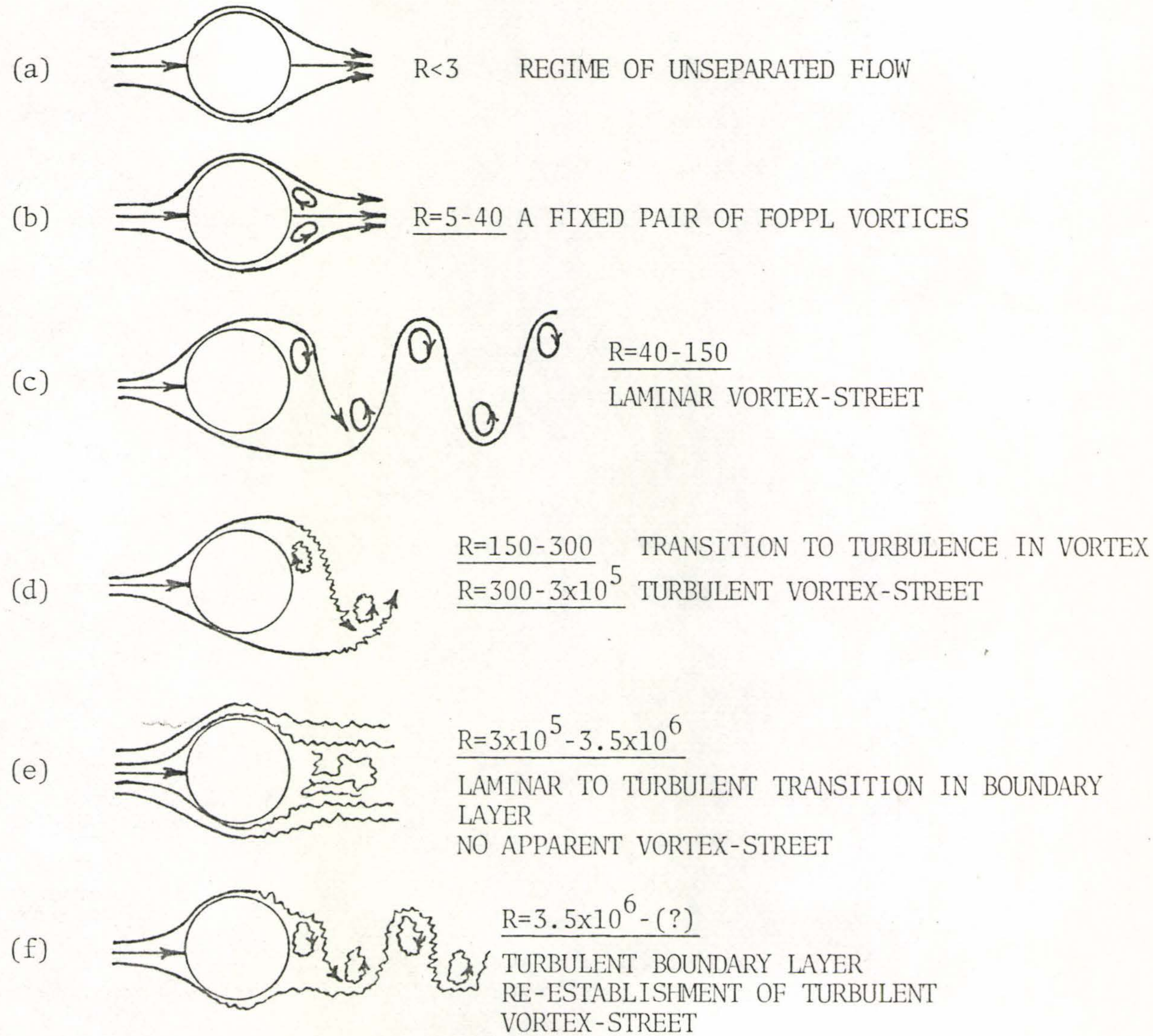


REGIMES OF FLUID FLOW ACROSS A CIRCULAR CYLINDER (FROM REF. 81)

FIGURE 2.1

fixed vortex pair separates from the main body of the fluid. At a Reynolds number of about 90, one of the fixed vortices breaks away from the cylinder. This causes a wake-pressure asymmetry and the other leaves, the process repeats itself, and the State of alternating vortex-shedding is attained, as shown in Fig. 2.1(c). The flow in this case is laminar, and the vortex street is preserved for many diameters downstream. As the Reynolds number is increased beyond the vortex-shedding point to 150-300, a laminar-to-turbulent transition begins in the free shear layers before breaking away into the street, as shown in Fig. 2.1(d). At a Reynolds number of about 300, and continuing up to approximately $3 \times 10^5$, the vortex street is fully turbulent. In the Reynolds number range $3 \times 10^5$ to $3.5 \times 10^6$, the laminar boundary layer on the cylinder has undergone turbulent transition, the wake is narrower and disorganized, and no vortex street is apparent, as shown in Fig. 2.1(e). As the Reynolds number is increased beyond $3.5 \times 10^6$, the turbulent vortex street forms [21] and the wake is thinner, as shown in Figure 2.1(f). A number of excellent papers on vortex street development have been written [22]-[29].

The turbulent vortex street region corresponding to Reynolds numbers range of $300\text{-}3 \times 10^5$ is the most important region from a practical standpoint. The Strouhal number is constant at about 0.2 for this range of Reynolds numbers. Fig. 2.2(a) shows the variation of Strouhal number (S) with Reynolds number (R). This figure provides a functional

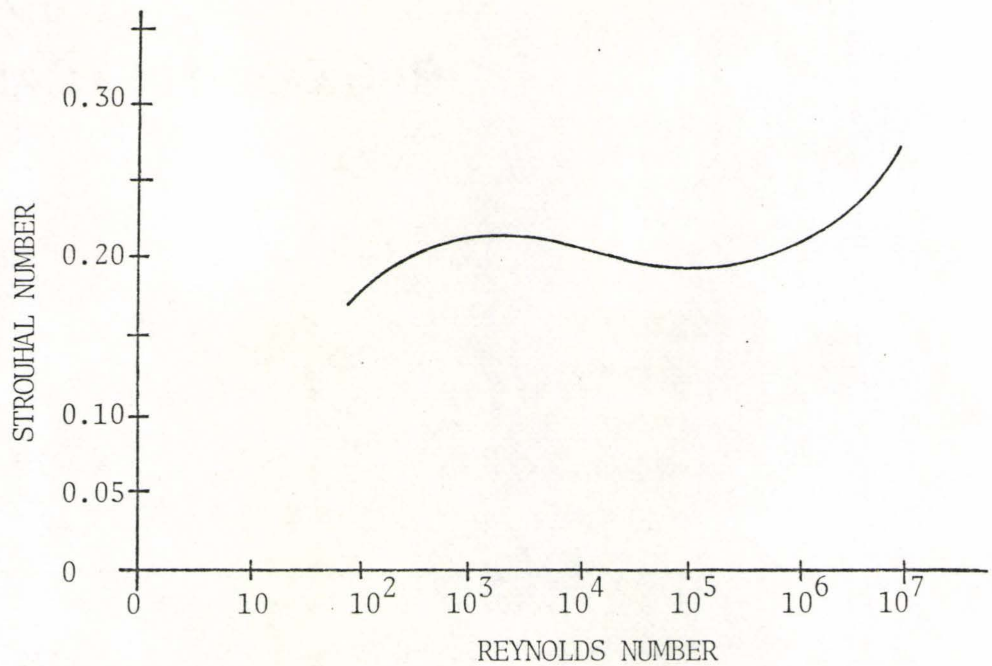


(a)

A LEAST SQUARE FIT OF PUBLISHED DATA (REF. 30)

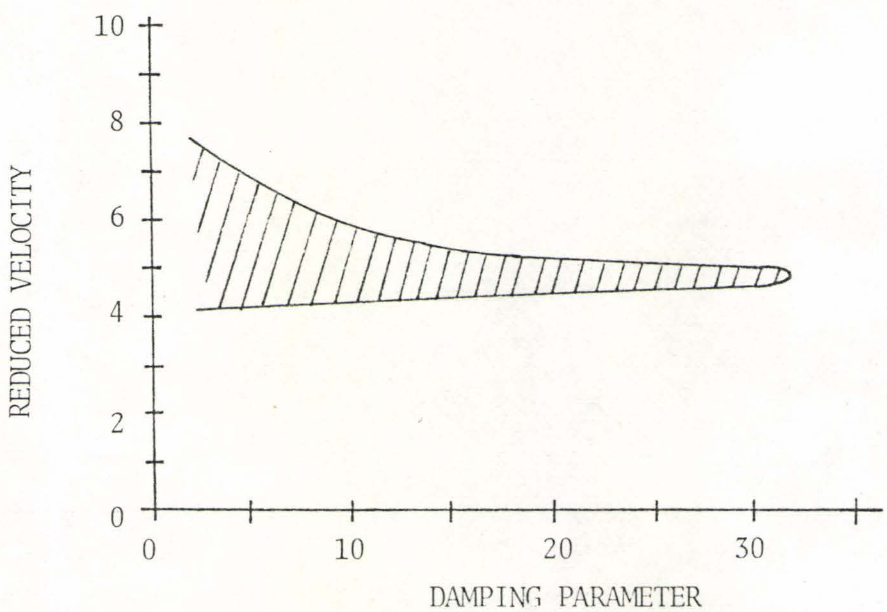


(b)

(SYNCHRONIZATION OCCURS WITH THE SHADED AREA) (FROM REF. 31)

FIGURE 2.2 (a) & (b)

relationship between R and S that reflects the research of many workers in the field. The relationship shown was developed from a "least squares" polynomial fit of 57 data points [30].

Vortex-shedding generally causes large vibration amplitudes only when the shedding frequency is close to the fundamental natural frequency of the cylinder. Once vibration begins, the shedding frequency and the cylinder natural frequency can become synchronized [31] - [33]. In effect, the motion becomes self-controlled as the tube vibration causes the shedding to continue to occur at the tube natural frequency as the flow velocity increases. For a spring-mounted cylinder in an air stream, Scruton [31] has shown that the velocity range over which synchronization persists depends upon the damping parameter $m\delta/\rho d^2$ (m is the mass of the cylinder per unit length, $\delta$ is the logarithmic decrement of damping, $\rho$ is the fluid density, and d is the cylinder diameter). In Fig. 2.2(b) the shaded area is the region of synchronization. The ordinate $v/f_n d$ is a reduced velocity ($f_n$ is the natural frequency of the flexibly mounted cylinder). Outside the shaded area, the cylinder experiences an alternating lift force at the vortex-shedding frequency for a stationary cylinder. With increasing $m\delta/\rho d^2$ the velocity range over which synchronization persists decreases, and, for $m\delta/\rho d^2 > 34$, no synchronization occurs.

The alternating lift-force (force transverse to flow) associated with vortex-shedding from a stationary circular cylinder, is usually expressed as:

$$F_L = C_L \frac{1}{2} \rho v^2 d L \sin (2\pi f_s t)$$

where $F_L$ = alternating lift force

$C_L$ = alternating lift force coefficient

$\frac{1}{2} \rho v^2$ = dynamic fluid pressure

$L$ = cylinder length

$t$ = time

The variation of the alternating lift coefficient with Reynolds number has been the subject of a number of investigations [34]-[36]. Although the vortex-shedding occurs at a discrete frequency for a given flow situation, the alternating force is randomly modulated. The lift coefficient is therefore usually given as an RMS value obtained with a suitable meter. In addition, it has been demonstrated by Keefe [37] that the flow over a cylinder is three-dimensional rather than two-dimensional, even at relatively low Reynolds number (R>300). The significance of the three-dimensional flow is that at a given instant the local forces at two different span-wise locations on the cylinder may or may not be acting in phase.

The distance over which the forces may be considered as acting in phase is called the correlation length. The lift coefficients measured in tests on a relatively short cylinder having a physical length less than or equal to the correlation length, $L_c$, are called local lift coefficients.

Knowing the local value, $C_\ell$, the effective lift coefficient, $C_L$, to use for calculating the force on a cylinder of length L where $L >> L_c$ is given by Keefe [37] as:

$$C_L = C_\ell \sqrt{\frac{2L_c}{L}}$$

In obtaining, reporting, and using experimental lift coefficients, proper allowance must be made for the span-wise correlation of the forces.

The drag force (force in the direction of flow) has two components: pressure drag and frictional drag. At very low Reynolds numbers, the drag will consist almost entirely of frictional drag. As the oscillating force appears, frictional drag gradually becomes negligible in comparison with pressure drag [38].

Many diversified experiments reporting values of coefficients of drag ($C_D$) and lift ($C_L$) are available in the literature. However, specific values of $C_D$ and $C_L$ can not be assigned with certainty because of the wide variation in measured values. Bishop and Hassan [35] reviewed the experimentally determined data on drag forces, and plotted the values of the drag coefficients over a wide range of Reynolds numbers. Chen [39] has compiled available data on mean oscillatory lift coefficients. Most of the measurements are in the Reynolds number range $10^4 < R < 10^6$. The scatter of the data is large, and the data are far less consistent than the drag coefficient data; values vary from 0.1-1.5. Since the excitation in the lift direction is 5 to 10 times higher than the excitation in the drag direction (because of the greater force coefficient), the lift direction is of primary importance. However, in water flows, the excitation in the drag direction may be significant.

The effective lift coefficient for a vibrating cylinder is greater than that for a stationary one. Weaver [32] suggests that the value of $C_L$ for a vibrating cylinder can be up to 1.5 times that for the stationary case. The reason for the increase has been variously attributed to increased circulation due to shifting separation points [20], increased eddy strength arising from the increased wake width [32] and increased span wise correlation of the shedding forces. Wake flow phenomenon and coefficients of lift and drag of an oscillating cylinder have also been studied by other authors [40]-[46].

Analytically the problem is very complicated due to the periodic separated flow around an oscillating boundary. A "wake-oscillator" model was initially suggested by Bishop and Hassan [43] and later developed by Hartlen and Currie [47] and refined by Landl [48] and Currie et al. [49]. A model based on the Karman vortex street for determining the drag force exerted by the vortex on the cylinder has been suggested by Chen [50]. Iwan and Blevins [51] have recently developed a quasi-steady model for vortex induced oscillation of structures. A number of mathematical models to describe the galloping of long bluff cylinders have also been developed [52].

When a cylinder body is immersed in a stream of fluid in a channel of finite breadth, the presence of walls influence the flow around the body. This means that its vortex shedding frequency and drag differs from that which is experienced in an infinite stream. A "Blockage correction" is usually applied to account for this effect. This correction factor is based on theories and empirical equations which have been developed over a number of years [53], [54].

The characteristics of the separated wake downstream from a bluff cylinder can be greatly affected when a splitter plate is placed downstream of a circular cylinder in cross-flow. At Reynolds numbers at which a regular vortex street is shed from the plain cylinder, the vortex shedding may be altered or even suppressed and the drag force experienced by the cylinder may be affected. A suitably selected length of a splitter plate can reduce the drag markedly [55].

An increase in upstream turbulence can result in the amplification of the vortex shedding motion and also produces improvements in heat transfer. The effect of free stream turbulence on vortex shedding has been studied by Petrie [56] and Surry [57].

A practical problem is to determine the effect of non-uniform upstream flow on vortex shedding from a circular body. One case of importance where there is such a velocity variation is that of a structure, such as a chimney, present in the earth's boundary layer. Maull and Young [58] have studied the effect on vortex shedding from bluff bodies in a shear flow. They have shown that vortex shedding can occur in span wise cells, the frequency being constant in each cell.

There has been a recent interest in studying the unsteady wake characteristics of non-circular cylinders, e.g., Square [59], Triangular [60], Elliptical [61], and Conical [62], etc., the data for these and other non-circular sections of potential engineering interest are not quite so extensive as those for circular cylinders.

Vibrations have also been observed in parallel fluid flow situations. The usual forcing function here is the fluctuating pressure in the turbulent boundary layer and the oscillations are of a self-excited type. This problem has been analysed by Paidoussis [63], Reavis [64], Burgreen et al. [65] and Basile et al. [66]. Nuclear fuel elements are most vulnerable to this type of vibration.

A circular cylinder can also be set into vibrations by the turbulent pressure fluctuations occurring in its wake or carried to it from an upstream disturbance [67]. The energies associated with velocity or pressure fluctuations in turbulent flow, rather than being concentrated at a discrete frequency (as is the case for vortex shedding), are normally continuously distributed over a wide band of frequencies. Turbulent pressure fluctuations, generated in the boundary layer and in the wake, act on the cylinder and generate fluctuating forces having lift and drag components. Similar forces arise from turbulence that already exists in the approaching flow. In some instances, the energy spectrum associated with the approaching flow, rather than being smoothly continuous, may contain peaks at discrete frequencies due to pump pulsations, to the vibration of upstream structures, to vortices from upstream structures, or to impinging jet flows. If the frequency of the spectral peak coincides with a tube natural frequency, a large amplitude response can occur.

### 2.2.2 Flow Over a Pair of Circular Cylinders

The situation encountered when two circular cylinders are located in the flow field has been investigated by a number of authors [68]-[72].

Spivak [68] showed that when two cylinders normal to an air-stream are separated by a gap just smaller than the diameter, instability occurs. As the gap is decreased, the main sequence of frequencies changes from a value corresponding to a single cylinder, of diameter, d, to a value associated with a solid body of breadth equal 2d (at zero gap). The picture is complicated by vortices generated within the gap. At spacings less than one half diameter, a low gap-frequency is found. Between one half and one diameter a high gap-frequency is present, decreasing to the independent cylinder value at the critical spacing. In addition, doubled frequencies of the main sequence are also found, generally on the centre line of the wake, attributed to overlapping vortices from the external sides of the cylinders. At larger gaps the cylinders behave like independent bodies.

Thomas and Kraus [69] observed by flow visualization studies that the interference effects were more pronounced when the cylinders were in the plane of the flow than when they were perpendicular to the flow.

Zdravkovich [70] recently studied vibrations of two cylinders in tandem. His experiments showed that a hysteresis in the lift and restoring forces may cause or maintain low frequency large amplitude aeroelastic vibrations. A method of suppressing these vibrations is also described.

Wilson and Caldwell [73] while acquiring data for the design of multiple ocean piping systems nearer to the ground plane observed that for spacings of about one diameter, and for mass ratios (mass ratio = mass per unit length of pipe, including the fluid inside/mass per unit length of the environmental fluid which the pipe displaces) near one, the apparent vortex shedding frequencies for two parallel, flexible cylinders near a ground plane could exceed five times the vortex shedding frequency for one isolated cylinder.

The analysis of the vibration modes and responses of a group of cylinders in a fluid is difficult because of the difficulty in accounting for the coupling effect of the surrounding fluid. Chen [71] has analytically studied two parallel cylinders vibrating in a liquid. He derived equations of motion using the added mass concept and included the fluid coupling terms. He has recently extended the analysis to the problem for many cylinders [137]. However, the inertia coupling term is probably not important in gas flows. Also, it remains to be determined how the fluid-elastic mode shape is related to the natural mode shapes considered by Chen in a quiescent fluid.

### 2.2.3 Flow Over a Single Row of Circular Cylinders

Circular cylinders or tubes in a single row perpendicular to the direction of flow can be excited to vibrate by vortex shedding, a jet-switch mechanism or by a fluid-elastic mechanism. Each of these mechanisms of vibration is known to exist for a certain range of velocity parameters $V_G/f_n d$ and tube spacings.

Vibrations of the vortex excited type where the motion of the tubes is principally transverse to the flow direction were shown by Livesey and Dye [74] to occur for a velocity parameter range of 3.5 to 8.75 (G/D = Gap/Diameter = 0.785). The Reynolds number range for their experiments was $3.7\text{-}9.5 \times 10^3$. They also observed two main and two subsidiary modes of vibration, all principally transverse to the flow direction. In a subsequent paper Dye [75] has given the critical flow speed ranges for seven different tube spacings. Both in-phase and out-of-phase vibrations were shown to have occurred for G/D < 1.4 and two distinct vortex shedding frequencies were reported to have been recorded in the wake.

Streamwise vibrations with no transvere component were apparently first observed by Dumpleton [76] and later analysed by Roberts [77]. Roberts argued that as the tubes are displaced alternately, one upstream and one downstream, the jet, as it issues from between the tubes, can be switched back and forth producing different "pairing". He proved theoretically that this switch produces a significant change in drag force which feeds large amplitude vibrations in the streamwise direction. Due to a finite time required for the jet entrainment process to effect an inversion, this type of vibration was presumed to occur for $(V/f_n d) > 0(3)$ only.

The concept of fluid-elastic oscillations due to the effect of aerodynamic hysteresis was experimentally verified by Connars [78] for a row of tubes normal to the direction of flow. He showed that as the flow field is altered by the displacement of a tube, the energy is extracted from the flow by the tube and when during a cycle of vibration this energy exceeds the energy dissipated by the damping, a fluid-elastic vibration is established resulting in an oval motion. Connars found two possible modes for three adjacent flexible tubes. The centre tube moves downstream through a smaller than normal gap and upstream through a larger than normal gap. The side tubes move transversely to the flow direction. The actual motions are ellipses in the streamwise and transverse directions, respectively. The first mode, a symmetric one, is established if the side tubes produce the oval motions in clockwise and anti-clockwise directions, being in symmetric positions, respectively, relative to the central tube. The second, asymmetric mode is established when there is a phase shift of $180^{\circ}$ between the two side tubes. The stability threshold for these type of vibrations was in a velocity parameter range in between those corresponding to vortex shedding and jet switch type of instabilities. Connars developed a semi-empirical model to predict the onset of whirling of a tube row.

Neglecting added mass effects, Blevins [79] has analytically modelled fluid-elastic forces acting on a tube in a tube row transverse to the flow. The tubes were modelled with different stiffnesses and damping normal and parallel to the free stream to simulate effects which arise in actual heat exchangers. It was shown that critical velocity parameter required for the onset of instability increased sharply with the separation of natural frequency between the tubes. There appears to be some doubt about the validity of this analysis for tube bundles.

Added mass coefficients for vibrations of a row of circular cylinders in a quiescent liquid have been computed by Chen [80] using the potential flow theory. His results also give natural frequencies of tube rows for various modes of vibrating tubes. These results are valid only for small oscillations as the added mass may be affected by other factors such as vibration frequency, vibration amplitude and fluid viscosity. Chen [137] later extended the analysis to an array of tubes. It should be noted that the analysis of Chen does not contain cylinder velocity dependent terms which may be very important to the phenomena being studied.

### 2.2.4 Flow Over Two Rows of Circular Cylinders

The flow set up by two rows of cylinders was investigated for tandem and staggered arrangements of the cylinders by Borges [85]. The Reynolds numbers of his tests corresponded to the high subcritical range for a cylinder in isolation. The results showed that the interference between the two rows is restricted roughly to a spacing ratio $\ell/d < 4$. Borges observed some Reynolds numbers effects in his experiments and also showed that if the rear row of cylinders is so placed as to form a staggered arrangement the flow is much more sensitive to variations in $\ell/d$ than a tandem arrangement with the same value of $T/d$. Generally speaking the effect of reducing the distance between the rows is to increase the dominant vortex shedding frequencies. Zdrovkovich [110] found that in a two-row in-line arrangement, the front row tubes were more stable and developed large vibrations only when the tubes began banging in the second row. The second-row tubes were more unstable and large amplitude vibrations became sufficient to cause tube contact in the transverse direction. This type of response probably results from the second row tubes being directly in the unsteady wake of the first row tubes.

### 2.2.5 Flow Over a Tube-Bank

The dynamic response behaviour of a group of circular cylinders in cross flow is influenced by their mutual interactions with the surrounding fluid. Interaction with the fluid causes coupling motions of a group of cylinders. The problem is very difficult to model analytically or experimentally as compared to the case of flow over a single circular cylinder or over a single row of circular cylinders.

Surveys of flow induced vibrations of tube arrays in cross flow have been carried out by Nelms and Segaser [5], Shin and Wambsgnass [81] and recently by Savkar [82]. A technical report on tube vibrations in industrial shell and tube heat exchangers has also been issued recently by Heat Transfer Research, Inc. in California [83]. All of these surveys have reported that operating heat exchangers experience damage due to excessive flow induced vibration and the existing design techniques do not satisfactorily evaluate the potential for flow induced vibrations.

Banks of heat exchanger elements can be considered in two general classes, in-line and staggered and tube vibrations have been reported in both types. The four most common types of tube patterns are shown in Figure 2.3. Baird [86] reported a severe case of pulsations in the super-

COMMONLY USED TUBE ARRAYS

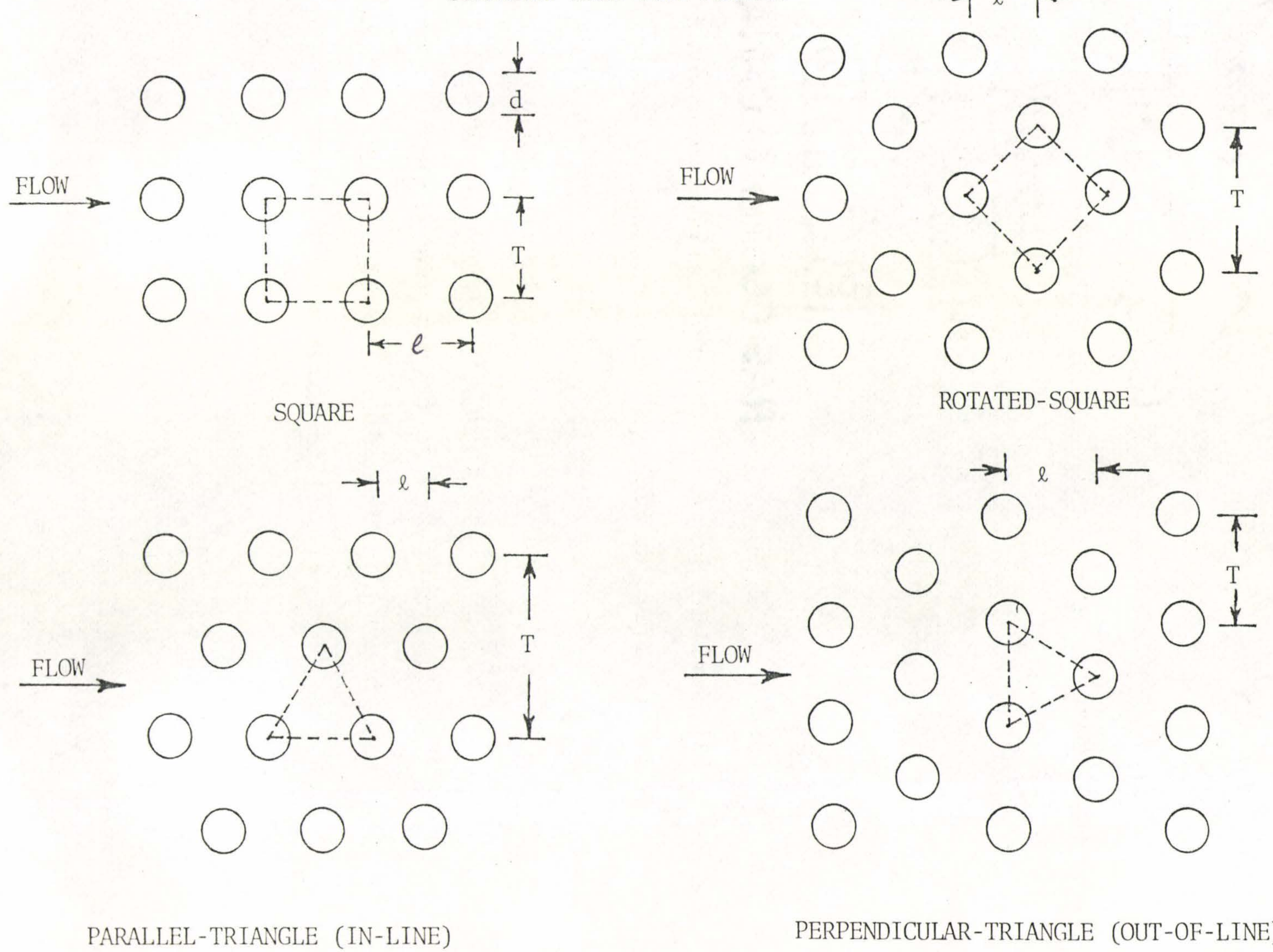


FIGURE 2.3

heater-economiser duct of the Etiwanda Steam Station. This pulsation was so severe that the duct walls were permanently distorted outwardly. Halliday [87] reported a case of vibration in the boiler uptake immediately above the economiser; this problem developed in the dockside trials of a rather large ship. The acoustic mode of vibration was the first transverse mode in the duct, in which the tubes were in an in-line pattern. Stallbrass [88] reported an intense noise during early calibration runs of the high speed icing wind tunnel in the low temperature laboratory of N.R.C. The problem was analysed and use of baffles on the centre line of the tubes was proposed which later effected a cure.

Chen [89] has also studied the noise problem and suggested the insertion of detuning baffles into the tube bank. These baffles are placed near the antinodes of the stationary velocity waves of the transverse gas column vibrations otherwise expected in the unmodified heat exchanger. These baffles make the natural frequencies in the transverse direction of the heat exchanger along its length as different as possible so that no coupling with the vortex shedding occurs.

For closely pitched staggered arrangements the fitting of detuning baffles is often impossible, and so an alternate solution is needed. One such solution suggested by Walker and Reising [90] was the complete removal of several judiciously placed tubes in order to prevent the build up of "in-phase" oscillations. The effect of this would be to reduce the sound intensity level and reduce the possibility of coupling. In their investigation they found that the best position for tube removal was longitudinally in the centre of the test bank and in the transverse direction, at the positions which would be the pressure nodes of the standing waves. It was suggested that the omission of every third tube from the positions where pressure nodes would exist will be sufficient to completely eliminate the excessive vibrations. Zdravkovich [108] has suggested the use of irregular longitudinal pitch to suppress the coupling with the acoustic standing waves.

Where none of the above methods are possible, then other steps to protect structural parts from excessive vibrations must be taken, by adjusting the natural frequency of the system, by increasing the mass or by incorporating damping devices in the supports.

The first systematic measurements of the vortex shedding frequencies in a simulated tube bank heat exchanger were apparently made by Grotz and Arnold [91]. They found that the Strouhal number in which velocity is taken as the mean velocity through the minimum area when the oscillation starts, varied from 0.093 to 0.45, depending on $T/d$ and $\ell/d$ However, not much confidence can be placed in the results, considering their claimed inaccuracy of as much as 30% in the experimental data. They presented an important condition for the generation of coupled acoustic-aerodynamic oscillations: the ratio of wavelength of noise generated to the width of the free passage for the wave has to be less than 120. Kays and Loeschner [92] observed a high frequency oscillation in a pin-fin heat exchanger, which started at a Reynolds number of about 1000 and continued to about 3000, but with the frequency increasing in steps and the amplitude generally decreasing. Using the Grotz and Arnold criteria, they found that only the second and higher modes could be driven.

There are few data on the effects of fins on tubes in a tube bundle. Cherrett [93] supplied one data point for $T/d = 1.812$, $\ell/d = 1.75$, fin-to-tube diameter ratio of 1.563, with 10.66 fins per unit of diameter, but the frequency was not measured and has to be computed from the assumed acoustic mode. The resulting value of Strouhal number was 0.473. It appears possible that, while the effect of the transverse spacing does not change with the presence of fins, the effect of longitudinal spacing does. The aerodynamic stability of a cross-flow type heat exchanger with a dense array of staggered rows of high finned tubes was examined by Dye and Abrahams [94]. They showed, by flow visualization techniques, that the finned tubes would shed vortices; and, by wind tunnel tests on a full scale model of a section of the heat exchanger, that two velocity dependent flow fluctuations were produced by the heat exchanger.

Hill and Armstrong [95] made some contribution to our understanding of the fluid dynamics of the vortex shedding mode associated with staggered tube arrays. In a study of a three-row tube array at various longitudinal spacings, $\ell/d$, but of a fixed transverse spacing, T/d, of 2.36, they noted that the mechanism did not seem to be the same as for in-line arrays. They rejected the idea of acoustic resonance due to vortex shedding through the array and rather attributed the possible cause to successive compressions and rarefaction of the air as it flows through the tube bank. A highest Strouhal number of 0.61 was recorded.

A theory of the mechanism of the formation of Karman vortices in in-line tube banks has been developed by Chen [96]. His simplified model assumes the tube columns and tube rows to be infinite in both directions and he makes a questionable assumption that the existence of the tubes does not prevent the influence of the vortices on each other. There are certain inconsistencies in his logic and the resultant arguments do not seem to give enough information.

Chen [89] has also developed empirical correlations for in-line and staggered tube banks. These are plots of the Strouhal number versus the tube spacing transverse to the flow direction with the longitudinal tube spacing as a parameter. The Strouhal number is based on the average velocity between adjacent tubes on a centre line normal to the direction of the flow and not upon the maximum velocity value that may exist in the bundle. As it is difficult to measure the velocity of flow accurately the accuracy of these correlations, in predicting the value of the Strouhal number is reported to be as good as 10 percent. These correlations show that the

Strouhal number or vortex shedding frequency is strongly dependent upon the tube pattern. Moreover, the shedding frequencies in the tube banks may be much greater than that for a single tube, for Strouhal number values as high as 0.7 are indicated in the figures. The correlations also show that the Strouhal number is independent of the Reynolds numbers range tested and that higher frequencies are encountered in banks with finned tubes than with bare tubes. However, very few data are available for closely packed tube arrays which are of special interest to the heat exchanger designers.

The data obtained by Chen [89] to develop Strouhal number correlations was taken for Reynolds number values up to $6.0 \times 10^4$ on tubes having an outside diameter of approximately 38 mm. The data of Grotz and Arnold [91] was taken with tube diameters of 1.6 mm., 7.9 mm. and 9.5 mm. and at a comparable value of the Reynolds numbers as the supper limit of the investigation. Drawing an analogy with the vortex shedding from a single tube, it is not surprising that the Strouhal number on simulated tube bank exchangers is independent of the Reynolds number in this range, for the Reynolds number values are subcritical. If the analogy between the vortex shedding from a single tube and a tube bank holds at higher Reynolds number values, then transition and transcritical regions could be found to exist for tube banks. However, these regions are not likely to be encountered in practical situations.

Chen's correlation does not provide sufficient information regarding the possibillty of flow induced vibrations throughout the tube bank. Along the length, the transverse baffling is such that the mean flow direction changes from being; in the baffle windows, esssentially parallel with the tube axis to making, between the baffles, an acute angle with the tube axis. Enough data is apparently not available on the vortex shedding in tube bundles when the mean flow meets the tube axis at an acute angle. Since vortex shedding is initiated by boundary layer separation, it is clear that as the angle between the tube axis and the mean flow direction approaches zero, so that boundary layer separation can not occur, vortex shedding must cease and with it the possibility for this kind of resonant vibration. The limiting value of the angle where this occurs has not been established.

An assessment of lift forces in tube bundles has been provided in another paper by Chen [97]. Here he attempts to derive the trend of the fluctuating $C_L$ and the Strouhal number in tube banks at higher Reynolds numbers from the course of the steady pressure drag coefficient at the corresponding Reynolds number range. Furthermore, some measurements of the vortex lift forces in tube bundles are also given. On this basis it is shown that at normal spacings ($X_T/X_L = 2.4/2.8$) ($X_T = T/d$, $X_L = \ell/d$), strong and practically sinusoidal vortices are shed. Small spacings ($X_T/X_L = 1.2/1.4$) are associated with weak vortices and a broad frequency band turbulence, whereas mixed spacings ($X_T/X_L = 1.2/2.8$) shed stronger vortices coupled by a broad frequency band turbulence. These vortices at mixed spacings possessed second harmonic and the tubes, therefore, were predicted to be excited to vibrate in resonance either at the critical flow velocity or at its half value.

In still another paper Chen [142] reports the effects of staggered tube bundles and inside baffles on measured values of $C_D$, $C_L$ and S. Five cases designated by the irregular ratio r = 0% (= in-line), 20, 30, 40% and 50% (= regularly staggered) are considered. It was observed that for regularly staggered tube bundles (r = 50%) without inside baffles, the resonance peaks increase the pressure drop a great deal, especially for vibration in second mode. He showed that the increase in $C_D$ in the case of staggered tubes after insertion of baffles is not only due to the narrowing effect on the flow passage by the boundary layer formed on the baffles' surfaces, but is also due to the modification of the flow path. A fall of the Strouhal number due to a rise in the pressure drop coefficient due to the inside baffles was also observed. From his results it is obvious that the lift coefficient for the regularly staggered tube bundle is much higher than that for the in-line bundle. Chen has further shown that at lower Reynolds numbers (low subritical range), for both in-line and staggered tube bundles, $C_D$ falls and S rises with an increasing R. These results are in line with the observations from the single circular cylinder experiments.

Chen's [89] vortex shedding frequency measurements were conducted in a five row deep stationary tube bundle. The effect of an increase in tube rows in an array on shedding of vortices has still not been studied and also the effect of tube vibrations on flow field characteristics is unknown.

Fitz-Hugh [98] has compiled all the available data on vortex shedding through tube arrays. He has arranged the data so as to show constant Strouhal number maps for staggered and in-line tube arrays. A Strouhal number as high as 1.18 has been shown to exist in narrowly spaced staggered tube arrays. His design relationships are based on frequency criterion only. Wallis [99] conducted some excellent flow visualization studies of water flow through a wide range of tube-bundle geometries for Reynolds numbers up to $2.7 \times 10^3$. He has shown the existence of vortices behind tubes in widely-spaced tube arrays. For narrowly-spaced tube bundles the flow field was seen to consist of streamwise "flow-lanes" through the gap between tubes and a "dead-water" region behind each tube.

In discussing the physical phenomenon associated with the vibrations in a tube bank, Owen [100] has pointed out that there are two possible causes for the vibration. Either they are fluidelastic in nature, resulting from the interaction between the motion of the tubes and the flow of fluid through the gaps between the tubes, or the tubes are rigid enough for their movement to be aerodynamically innocuous, and the vibrations arise from the buffeting forces imposed on the tubes by the unsteadiness of the flow. This latter type of excitation can be either random or periodic in nature, depending on whether the buffeting force arises from turbulence or periodic vortex shedding. Owen has made a fairly complete theoretical approach to the problem and his arguments hold for both in-line and staggered tube arrays. He disregards any theory of a superposed regular pattern, but rather states that "deep within a tube bank the cumulative growth of random irregularities in the labyrinthlike, high Reynolds number flow must lead to a state of almost complete incoherence". From this one would expect the tubes to vibrate randomly. Owen further concludes that "a tube is aerodynamically selective and responds by means of a force principally to that group of eddies whose dimensions are comparable with the tube diameter. As a consequence, the force frequency spectrum at any section of the tube is a good deal narrower than that of the turbulent energy, especially when the latter is presented in its one-dimensional form". He considers turbulent energy being produced at rows of tubes and being dissipated between rows, and from the assumption of energy equilibrium, derives a relationship between various geometric and flow parameters. However, his criterion has still not been verified experimentally.

Tube vibrations at flow velocities considerably higher than those predicted by vortex shedding relationships have been reported to have occurred in a number of industrial heat exchangers [101]-[107]. These vibrations are usually at very large amplitudes and unlike vortex shedding response the tube amplitude keeps on building up with an increase in flow rate till it is limited by some form of system non-linearity. Large amplitude vibrations are of a self-excited type and are usually designated "fluidelastic" oscillations. The mechanism causing such vibrations is far from being completely understood and the technological development in the field is at a rudimentary stage.

Zdravkovich [109] has attributed the cause of large amplitude self-excited vibrations to a flow pattern switch in front of the rearward tube in a staggered arrangement. Southworth and Zdravkovich [110] have also studied the response of one-, two- and three-row in-line arrangements for a range of $X_T$ and $X_L$. Two distinct vibrational responses seem to have been recorded. The first one, at low values of reduced velocity corresponded to the coincidence of the fundamental natural frequency of the tube with the vortex shedding frequency. It was characterized by a narrow resonance peak with vibrations in the transverse direction. The second vibrational response occurred at higher reduced velocities, depending on the tube arrangement and the position of the tube in the bank. It was characterized by a continuous build up of amplitudes in the transverse and streamwise directions up to a limit imposed by the gap between adjacent tubes. This fluidelastic response always occurred at the fundamental natural frequency of the tube. No effect of damping on the fluidelastic stability threshold was evaluated.

Effect of upstream turbulence on the vibrational response of tube arrays has been studied by Batham [111] and Southworth and Zdravkovich [112]. Southworth and Zdravkovich observed a large reduction in the maximum amplitudes due to the introduction of grid turbulence.

More recently Gorman [113] has reported his experimental vibration tests on a series of tube bundles in a water tunnel. He found that the main excitation mechanisms are turbulence, some vortex shedding and hydroelastic instability. However, all his tests were conducted for a single value of damping, corresponding to a damping parameter of approximately 0.22.

In summary, it can be said that the possible mechanisms causing tube vibrations in an array appear to be vortex shedding, turbulence and fluidelasticity. However, it is still not certain as to which one of these is the most dominant mechanism for a tube vibrating deep inside a tube bundle. Although the available data of various authors has been compiled and plotted by Shin and Wambsgnass [81], there is considerable scatter and there is not sufficient data for any given array to show any definite trend. No systematic investigation has been carried out so far to derive a fluidelastic stability boundary of an array. Current design against fluidelastic instability is based on a Connars [78] or Blevins [79] type equation:

$$\frac{V_G}{f_n d} = K\left(\frac{m\delta}{\rho d^2}\right)^{1/2}$$

where K has been determined experimentally and depends on array geometry. Typically, K is determined by a single experiment on the specific array. However, there appears little evidence to validate for tube banks the analysis on which the equation is based and, in particular, to verify that the exponent in such an equation should be 1/2.

# CHAPTER 3

# DIMENSIONAL ANALYSIS

In the present investigation model tests are being used to investigate the causes of flow-induced vibrations deep inside a tube bundle. Understanding of the appropriate similitude relationships is necessary for planning the model tests and for interpreting the results in terms of the prototype behaviour.

Four dependent variables and fourteen independent variables are involved in the general tube vibration in an array:

Dependent Variables:

| | | | |
|---|---|---|---|
| 1. | Vibration amplitude: | $y$ | |
| 2. | Vibration frequency: | $f$ | |
| 3. | Fluid force acting on the tube: | $F$ | |
| 4. | Frequency of periodic fluid phenomenon: | $f_s$ | |

Independent Variables:

| | | | |
|---|---|---|---|
| 1. | Characteristic length: | $D$ | |
| 2. | Transverse Spacing: | $T$ | Geometry |
| 3. | Longitudinal Spacing: | $\ell$ | |

| | | | |
|---|---|---|---|
| 4. | Mass of tube: | $m$ | Mechanical System |
| 5. | Spring rate of tube: | $k$ | |
| 6. | Mechanical damping of tube: | $c_n$ | |
| 7. | Velocity of fluid-flow: | $v$ | Fluid System |
| 8. | Density of fluid: | $\rho$ | |
| 9. | Viscosity of fluid: | $\mu$ | |
| 10. | Speed of sound in fluid: | $a$ | |
| 11. | Externally applied force: | $F_e$ | External System |
| 12. | Frequency of externally applied force: | $fe$ | |
| 13. | Boundary displacement: | $y_b$ | |
| 14. | Frequency of boundary displacement: | $f_b$ | |

In the above tabulation, to simplify the dimensional analysis, the tubes are assumed to have a linear spring rate and viscous damping (damping proportional to vibration velocity). One degree of freedom is treated and it is assumed that the spring and damping characteristics of the tubes are the same in all planes of motion.

If the tubes in the array are assumed to vibrate at their fundamental natural frequency only, then the response problem is reduced to one of determining the dynamic deflections of the tubes.

The dependent variable of most interest is the displacement y. Neglecting external forces and forced boundary displacements, the independent variables are D, T, $\ell$, $f_n$, $c_n$, v, $\rho$, $\mu$ ($f_n$ = natural frequency in quiescent fluid and $c_n$ = damping constant for the structure in quiescent fluid). Neither the spring rate nor the mass of the cylinder is now an independent variable since the tube is assumed to vibrate at the natural frequency only, and $c_n$ is the mechanical impedence at that frequency. An incompressible fluid flow is assumed so that the effects of Mach number do not appear.

Following the methods of Langhaar [114], the number of independent dimensionless groups appropriate to the above set of variables would be given by subtracting the rank of the dimensional matrix (three in this case; Force, length and Time) from the number of independent variables in the set (eight). Accordingly, a dimensional analysis of the above quantities produces the following set of five dimensionless groups:

$$\frac{y}{D} = \phi \left[\frac{\rho v D}{\mu}, \frac{v}{f_n D}, \frac{c_n}{\rho v D^2}, \frac{T}{D}, \frac{\ell}{D}\right]$$

A more convenient form can be obtained, by noting that:

$$\frac{c_n}{\rho v D^2} = c_c \left[\frac{c_n}{c_c}\right] . \frac{1}{\rho v D^2}$$

where $c_c$ = $2 M_o W_n$ (critical damping)

$M_o$ = virtual mass of the tube

= Mass of the tube + mass of the fluid

inside the tube + the added apparent fluid mass.

$$w_n = 2\pi f_n.$$

Substituting:

$$\frac{c_n}{\rho v D^2} = \frac{c_n}{c_c}\,(2M_o w_n)\,\frac{1}{\rho v D^2}$$

Also $\frac{c_n}{c_c} = \frac{\delta}{2\pi}$ where $\delta$ = logarithmic decrement in still fluid.

hence
$$\frac{c_n}{\rho v D^2} = \frac{M_o\delta}{\rho D^3}\,[\frac{w_n D}{v}].\,\frac{1}{\pi}$$

$$= \frac{M_o\delta}{\rho D^3}\,[2.\ \frac{f_n D}{v}].$$

Since $\frac{f_n D}{v}$ is already one of the similitude parameters, we can replace $\frac{c_n}{\rho v D^2}$ by $\frac{M_o\delta}{\rho D^3}$, and we have

$$\frac{y}{D} = \phi\ [\frac{\rho v D}{\mu},\ \frac{v}{f_n D},\ \frac{M_o\delta}{\rho D^3},\ X_T,\ X_L]$$

where $X_T$ = T/D and $X_L$ = $\ell$/D;

or in terms of virtual mass per unit length,

$$\frac{y}{D} = \phi\ [\frac{\rho v D}{\mu},\ \frac{v}{f_n D},\ \frac{M_o\delta}{\rho D^2},\ X_T,\ X_L]$$

This expression gives the scaling law and the similarity requirements for tube arrays. If geometrical similarity is assumed between the prototype and model, for a given tube array the above expression reduces to:

$$\frac{y}{D} = \phi \left[\frac{\rho v D}{\mu}, \frac{v}{f_n D}, \frac{M_o \delta}{\rho D^2}\right]$$

The various dimensionless groups are easily recognized as:

| | |
|---|---|
| Reynolds number: | $= \frac{\rho v D}{\mu}$ |
| Reduced velocity (or velocity parameter) | $= \frac{v}{f_n D}$ |
| Reduced damping (or damping parameter) | $= \frac{M_o \delta}{\rho D^2}$ |

Replacing the dependent variable y by F, and solving the resulting equations gives the alternate dimensionless group $\frac{F}{\rho v^2 D^2}$ which is also a function of the same three dimensionless numbers viz.: Reynolds number, velocity parameter and damping parameter.

Beavers and Plunkett [115] have enumerated the difficulties encountered in modelling an actual heat exchanger from the standpoint of flow induced vibrations. It is usually difficult to match both reduced velocity and Reynolds number simultaneously. To get around to some of these difficulties in the present investigation, a special tube was designed using discrete devices for its damping and stiffness controls, so that these two parameters could be varied over a wide range of values without actually changing the length, mass or material of the tube. Although the damping parameter range in which the present model study was conducted corresponded to two-phase shell-side flow in prototypes, economics dictated the use of a wind tunnel only. The remaining parameters were adjusted accordingly to obtain the desired range of reduced damping.

# CHAPTER 4

# EXPERIMENTAL EQUIPMENT

As it is desired to develop an experimental facility where both vortex-shedding and fluidelastic tube vibrations can be initiated in the same tube array, the rig must be designed so as to realise very low values of the velocity and damping parameters. Also, as the vortex shedding and fluid-elastic boundaries are not known yet, the parameter ranges must be carefully chosen so that the objective can be met. After careful consideration it was concluded that the desired result could be obtained with a rig in which the following parameter ranges could be achieved:

Damping parameter: 2 to 50 ($m\delta/\rho d^2$)

Velocity parameter: 3 to 100 ($V_G/f_n d$)

These parameters cover a region marked "R" in the stability diagram shown in Figure 1.1.

From an economics and convenience standpoint it was decided to build a wind-tunnel, though the above damping parameter range usually corresponds to two-phase shell-side flow in prototype heat exchangers. It was also decided to develop a special movable tube-model where the effective damping and natural frequency of vibration could be varied over a wide range of values by using some form of discrete devices

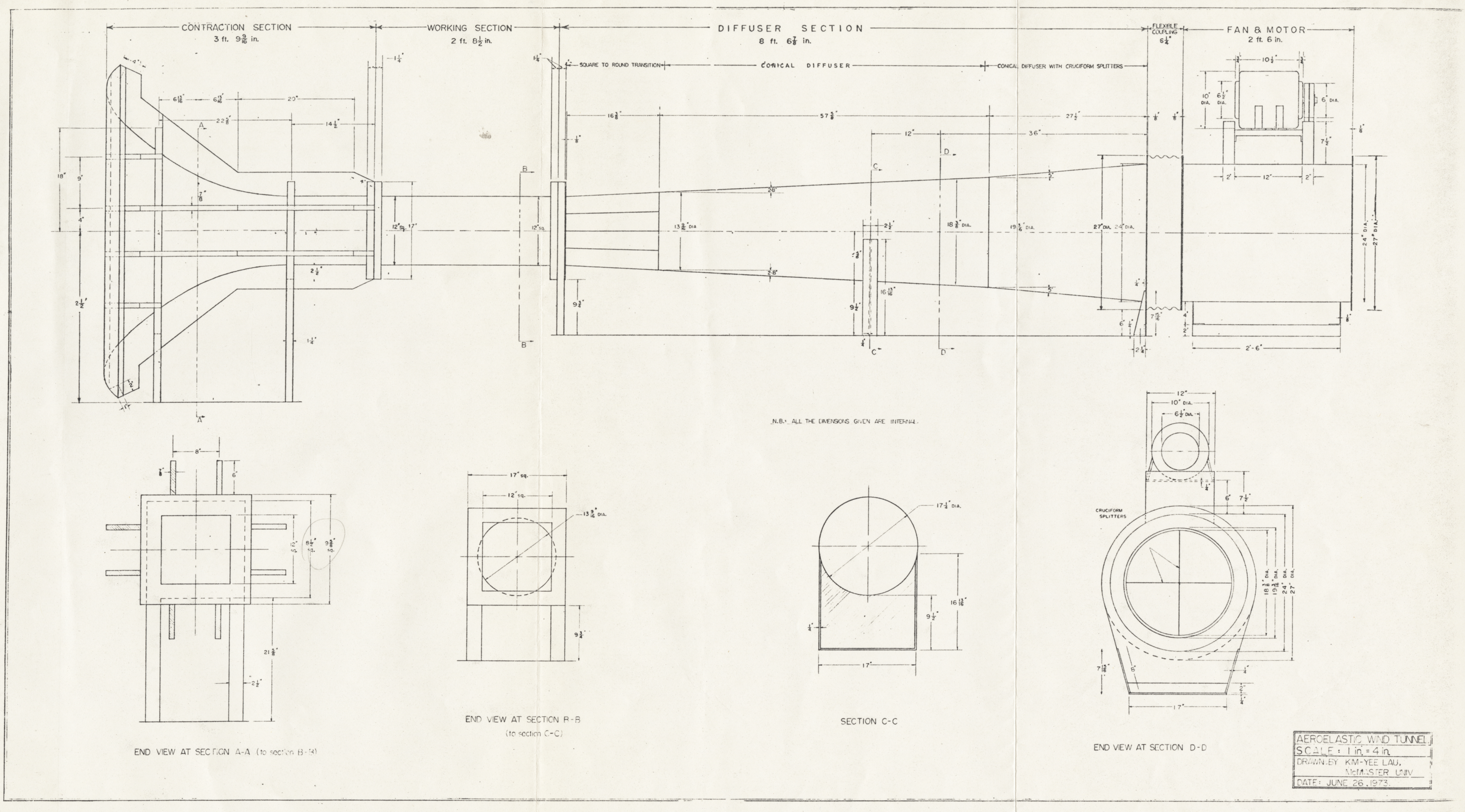
CONTRACTION SECTION
3 ft. 9 9/16 in.
WORKING SECTION
2 ft. 8 1/2 in.
DIFFUSER SECTION
8 ft. 6 7/8 in.
FLEXIBLE COUPLING
6 1/4"
FAN & MOTOR
2 ft. 6 in.
SQUARE TO ROUND TRANSITION
CONICAL DIFFUSER
CONICAL DIFFUSER WITH CRUCIFORM SPLITTERS
N.B.: ALL THE DIMENSIONS GIVEN ARE INTERNAL.
END VIEW AT SECTION A-A (to section B-B)
END VIEW AT SECTION B-B
(to section C-C)
SECTION C-C
CRUCIFORM SPLITTERS
END VIEW AT SECTION D-D
AEROELASTIC WIND TUNNEL
SCALE: 1 in. = 4 in.
DRAWN BY KIM-YEE LAU,
McMASTER UNIV.
DATE: JUNE 26, 1973.

FIGURE 4.1

without changing the diameter, length or mass of the tube. The development of such a tube-model is described later in this chapter.

## 4.1 Design of the Wind-Tunnel

A low-speed wind-tunnel shown in Figure 4.1 was specifically designed and constructed for this study. The general design procedures for wind-tunnels have been described in references [116]-[118].

The contraction section of the wind-tunnel is made of 3.2 mm. (1/8 in.) birch plywood mounted on oak bulkheads. The length of the section is approximately 1.14 m. (3 ft. 9 in.) and contraction takes place from 1.45 m. (4 ft. 9 in.) square at inlet to 0.31 m (12 in.) square at the exit (a contraction ratio of about 22:1). The use of a contraction section upstream of the working section considerably reduces spatial irregularities in the velocity distribution and also results in low turbulence levels at the working section. A number of papers are available for the design of wind-tunnel contractions [119]-[124]. The wall contours are designed so as to be free from adverse pressure gradients, since this might cause boundary layer separation. In the present design, one of the contracting cones developed by Smith and Wang [119] based on electric analogy has been used. Theoretically the velocity distribution at the exit is predicted to be uniform within 1% for the selected wall shape.

The skeleton of the working section is a box type structure made up of four perspex plates (13 mm. and 19 mm. thickness) bolted together. The front and back plates are easily removable. The nominal internal dimensions of the working section are 0.31 m (12 in.) square x 0.76 m. (2 ft. 6 in.) long. The complete design of the working section is described later in this chapter.

The diffuser section which is 2.59 m. (8 ft. 6 in.) long is constructed by welding 12 gauge mild steel sheet. A square-to-round transition is constructed at the front of the diffuser. The included angle for the main body of the diffuser is $6^{o}$. Cruciform splitters are installed at the end of the diffuser which afforded an increase in the included angle to $10^{o}$. The principal action of a diffuser is to decelerate the flow. Diffuser efficiency depends on wall angle, inlet and outlet velocity profiles. A knowledge of flow processes in general including flow separation, vortex formation, production and decay of turbulence, energy levels, etc., are all extremely important in predicting diffuser performance. The main design criterion of a diffuser is an efficient conversion of kinetic energy to pressure energy. The present diffuser design was based on the information supplied in a report by Wade and Fowler [125].

The fan and motor assembly was installed at the end of the wind-tunnel as shown in Figure 4.1. A 0.61 m (24 in.) vaneaxial fan having a maximum rating of 3.8 $m^3$/sec. (8230 C.F.M.) at 0.038 m. (1.5 in.) static pressure was used. A D.C. motor was employed to run the fan. The power requirements for the wind-tunnel and the detailed specifications of fan and motor are given in Appendix A. Speed control was obtained by employing a D.C. motor speed control arrangement also described in Appendix A. Over the operating range of 0-2500 R.P.M. the motor speed could be kept constant within $\pm$ 2 R.P.M. at lower speeds and within $\pm$ 5 R.P.M. at high speeds. Two different sizes of pulleys were used at the motor shaft to obtain the desired range of fan speeds.

A flexible sleeve is fitted between the diffuser and fan unit to prevent any fan vibration from reaching the main structure.

## 4.2 Performance of the Wind-Tunnel

The contraction section, working section, diffuser, fan and motor assembly were installed on frames as shown in Figure 4.17(a) such that the middle of the working section was at the eye level height. The turbulence intensity and velocity distribution upstream of the tube bundle were recorded. The average upstream turbulence intensity over the range of operating speeds was only about 0.2%. The normalized velocity distribution at an upstream location (with the tube bundle inside the working section) in the working section is shown in Figure 4.2. It is seen that the velocity distribution is uniform within 1% over the middle 80% of the area. At the middle of the walls the boundary layer thickness is about 1.27 cm. (1/2 in.) at an upstream velocity of 2.83 m/sec. (9.28 ft./sec.).

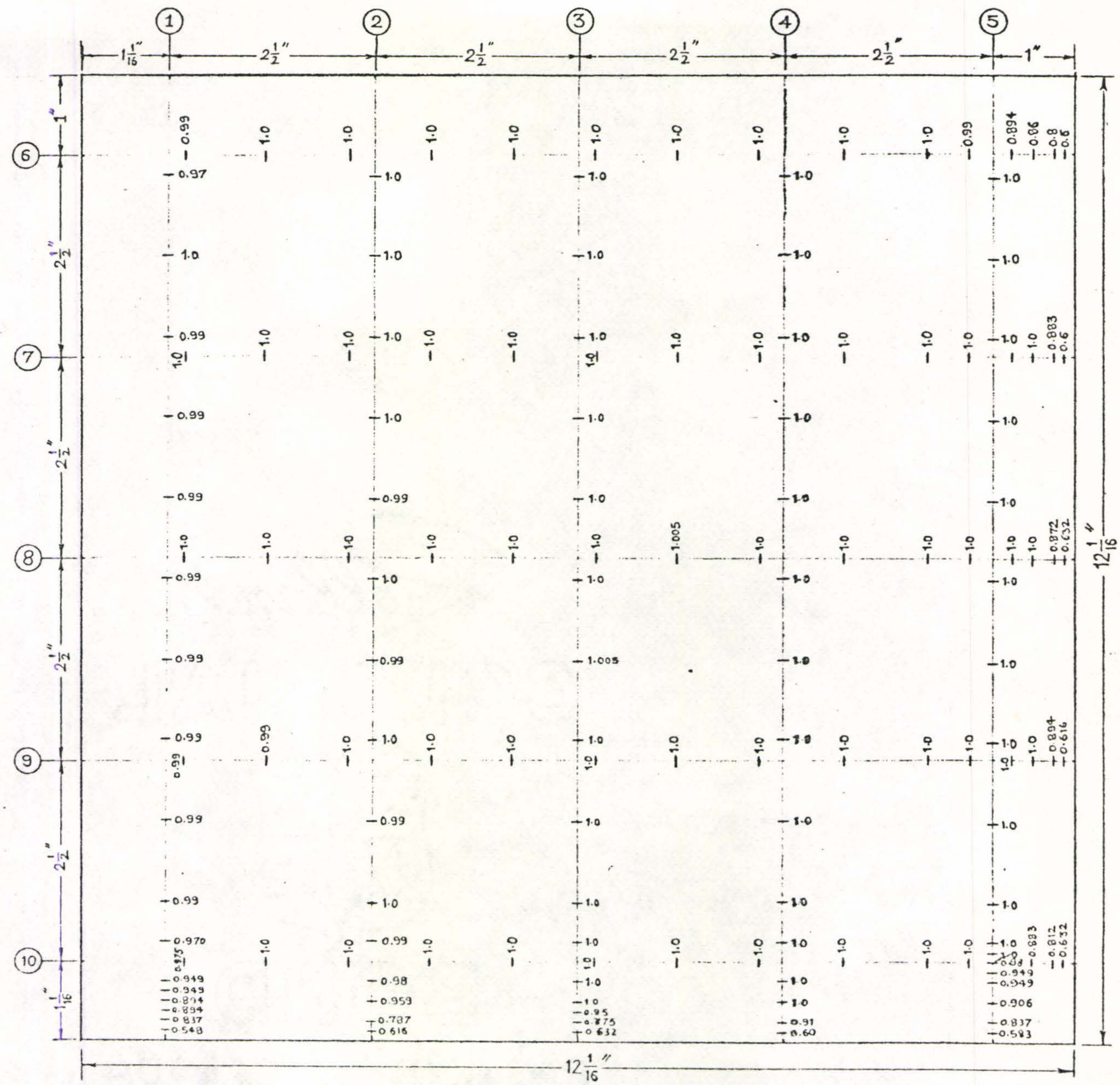

NORMALIZED UPSTREAM VELOCITY DISTRIBUTION

VELOCITY AT CENTER = 2.83 M./SEC.

FIGURE 4.2

As expected, non-uniform velocity distribution occurs at the corners. With the tube bundle in position the tunnel was run to a maximum upstream velocity of 4.6 m./sec. (15 ft./sec.). The noise and vibration levels of the tunnel were negligible.

## 4.3 The Development of a Movable Tube

As mentioned earlier it is desired to obtain damping parameter ($m\delta/\rho d^2$) values as low as 2 and velocity parameter ($V_G/f_n d$) values as low as 3. A preliminary analysis conducted at Ontario Hydro [135] showed that by using rubber, Teflon or P.V.C. tubing the lowest damping parameter that could be obtained was only 8. In addition, in order to obtain the desired range of $f_n$ and $\delta$ values we would have to change diameter, length and material of the tube every time. Also there were problems of decreasing $f_n$ and increasing $\delta$ with time, associated with materials having low elastic modulus. Accordingly it was decided to construct a tube-model in which:

a) the tube itself is effectively rigid, but elastically mounted.

b) the elastic constraint is linear (i.e., restoring action proportional to tube displacement) and can be varied over a range of values.

c) the damping is viscous (i.e., dissipative action proportional to cylinder velocity), and can be readily controlled and varied.

Two tube-models were developed and are described below:

### 4.3.1 Tube-Model Using Compression Coil Springs

A tube-model was conceived in which an aluminum tube 30.48 cm. (12 in.) long, 2.54 cm. (1 in.) O.D. and 1.6 mm. (1/16 in.) wall thickness was used. The tube had capped ends and extension pins were screwed on at its top and bottom as shown in Figure 4.3. The tube shown in this figure is, however, not an aluminum tube but an acrylic tube with a brass plug in the middle of it. This design of tube was developed earlier in order to separate the rocking mode and translational mode natural frequencies as far as possible but was later rejected due to the unacceptable weight of the tube.

The tube was suspended by a string attached to the top wall of the assembly (not shown in Figure 4.3). The damping control was exercised by using a small cup and paddle assembly on the working section walls at the top and bottom of the tube. Various kinds of fluids such as water and different grades of motor oils could be poured in to the cups. The amount of these fluids in the cups could also be varied and a wide range of damping values were realised. Also the cups could be left empty and a low value of damping could be obtained.

Four compression coil springs, mounted as shown in Figure 4.3 along four mutually perpendicular directions, provided the necessary restoring force. The maximum directional variation in effective stiffness of the tube was expected to be not more than 5%. Using only three coil springs instead would have produced a directional variation as large as 24%.

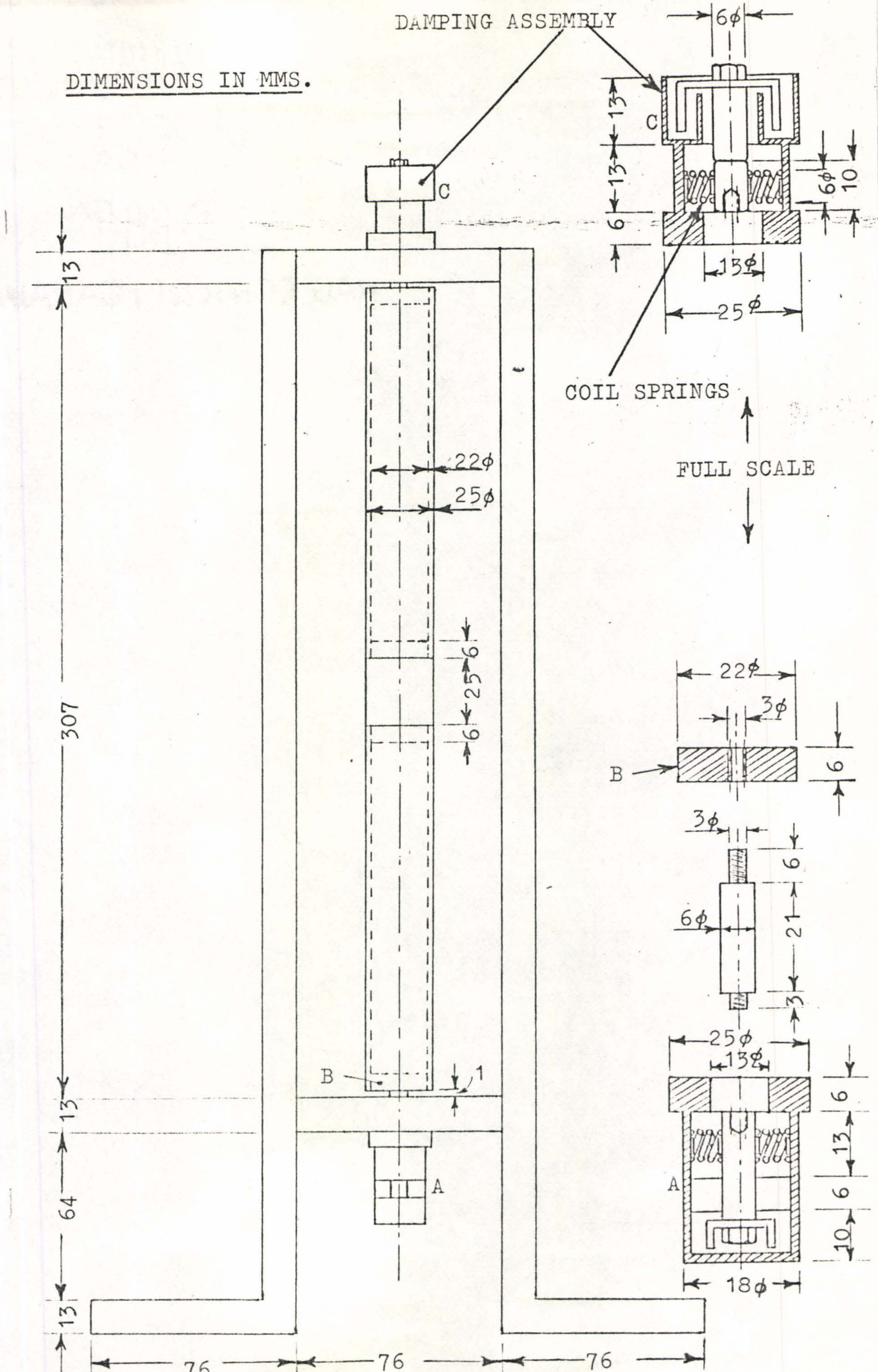


HALF SCALE

FIGURE 4.3

Springs of different gauge sizes could be used to obtain a wide range of effective tube spring rates. A linear restoring force was obtained for up to 1.3 mm. (0.050 in.) of tube deflection along two mutually perpendicular directions where the coil springs had been installed.

A DISA proximity transducer (Model 51D11) was used to record free oscillations of the tube. The detailed specifications of the probe are provided in Appendix D. The probe was installed at the centre of the tube as shown in Figure 4.10. No rocking mode was observed. However, the output of the probe occasionally showed a beating form of tube oscillations. the beats were first thought to be due to the coupling of natural frequency of the tube with that of the frame but a computer analysis of the problem (given in Appendix B) showed that the beat response is due to the slightly different spring rates of the tube along two mutually perpendicular directions.

Using five different sets of coil springs, natural frequencies of the tube within the range 22-59 Hz could be obtained. The accuracy was within $\pm$ 5.6% (the scatter is probably because of chafing at the spring seats). Not very low or consistent values of damping could be obtained with this model. The spread in values was very large (approximately $\pm$ 20% at low values of damping) and the minimum damping parameter that could be realised was only 12. Also it was very expensive to produce this model. For these reasons the performance of the tube-model was considered very unsatisfactory and a new tube-model was developed as described below.

## 4.3.2. Piano-Wire Tube-Model

The feasibility of using a light aluminum tube sprung on a piano-wire was examined analytically (details in Appendix C) and it was found that there was a good possibillity of obtaining a damping parameter down to approximately three. Also by eliminating compression coil-springs the large scatter in damping values and directional variation in the tube stiffness of the previous model should be eliminated. The tension in the piano-wire could be used to regulate the natural frequency of the tube. Wire material damping and windage will give the necessary low damping values required whereas high damping values could be obtained from various fluids using an arrangement similar to the previous tube-model.

A schematic of the new model developed is shown in Figure 4.4. An aluminum tube 30.48 cm. (12 in.) long, 2.54 cm. (1 in.) O.D. and 0.38 mm. (0.015 in.) wall thickness was mounted on a 1.04 mm. (0.041 in.) diameter piano-wire. The free length of the wire was 60.96 cm. (24 in.) and it passed through two 15.9 mm. (5/8 in.) steel plates at each end. The bottom of the wire passed through a concentric hole in a 6.4 mm. (1/4 in.) brass screw and was bent at the end. The movement of brass screw was regulated by a wing nut. At the top end the wire passed through a similar brass screw and a 15.9 mm. (5/8 in.) diameter compression coil spring was installed as shown in Figure 4.4. The tension in the piano-wire could

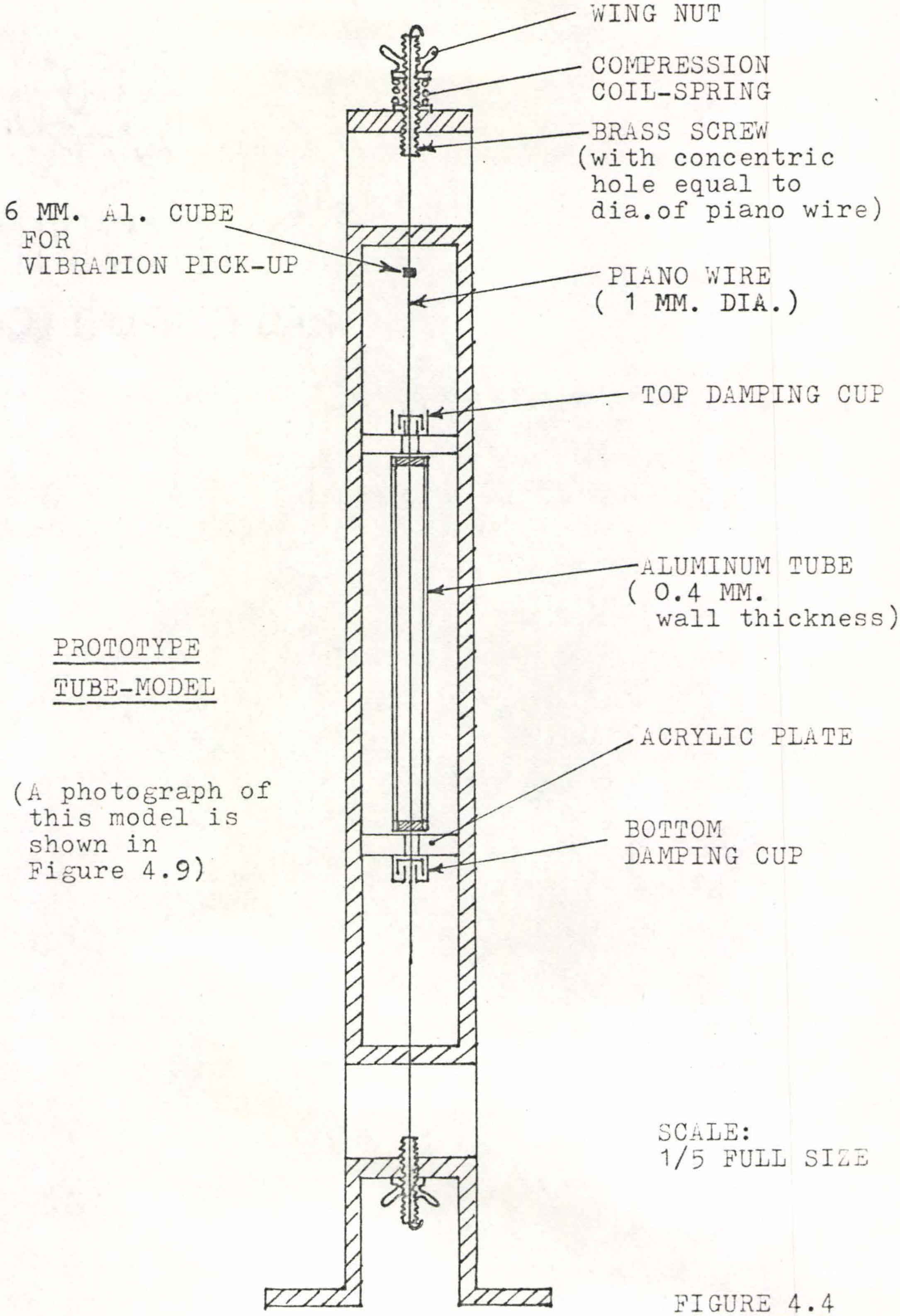
WING NUT
COMPRESSION COIL-SPRING
BRASS SCREW (with concentric hole equal to dia.of piano wire)
6 MM. Al. CUBE FOR VIBRATION PICK-UP
PIANO WIRE ( 1 MM. DIA.)
TOP DAMPING CUP
ALUMINUM TUBE ( 0.4 MM. wall thickness)
PROTOTYPE TUBE-MODEL
ACRYLIC PLATE
(A photograph of this model is shown in Figure 4.9)
BOTTOM DAMPING CUP
SCALE: 1/5 FULL SIZE

FIGURE 4.4

be controlled by regulating the compression coil-spring by a wing nut installed at the top. Two damping cup-and-paddle assemblies similar to the previous model were also mounted at the top and bottom walls of the working section.

This tube-model gave excellent performance characteristics. The tension in the piano-wire could be varied in order to obtain effective translational natural frequencies of the tube in the range from 22 to 40 Hz. The directional variation in the natural frequency was not more than $\pm$ 0.2%. In the following discussion, the damping of the tube without any oil in the damping cups will be designated 'AIR' damping and will be called 'OIL' damping when oil is used in the cups. Both of these damping values will in fact include material damping of the piano-wire and end damping. The 'AIR' damping of the tube was found to vary with the tuned natural frequency of the tube as shown in Figure 4.5. The increase in natural frequency of the tube from 22 to 40 Hz. resulted in a decrease in logarithmic decrement of damping by a factor of about two. The value of $\delta$ decreased from 0.003 at 22.5 Hz. to 0.0017 at 39.5 Hz. The uncertainty in computing logarithmic decrement of damping due to directional variations and due to readout errors varied from $\pm$ 10% at low frequencies to $\pm$ 6% at the higher end of the tuned natural frequencies. A capacitive displacement transducer was used to record free vibrations of the tube from which the tuned natural frequency and logarithmic decrement of damping were subsequently computed. The OIL damp-

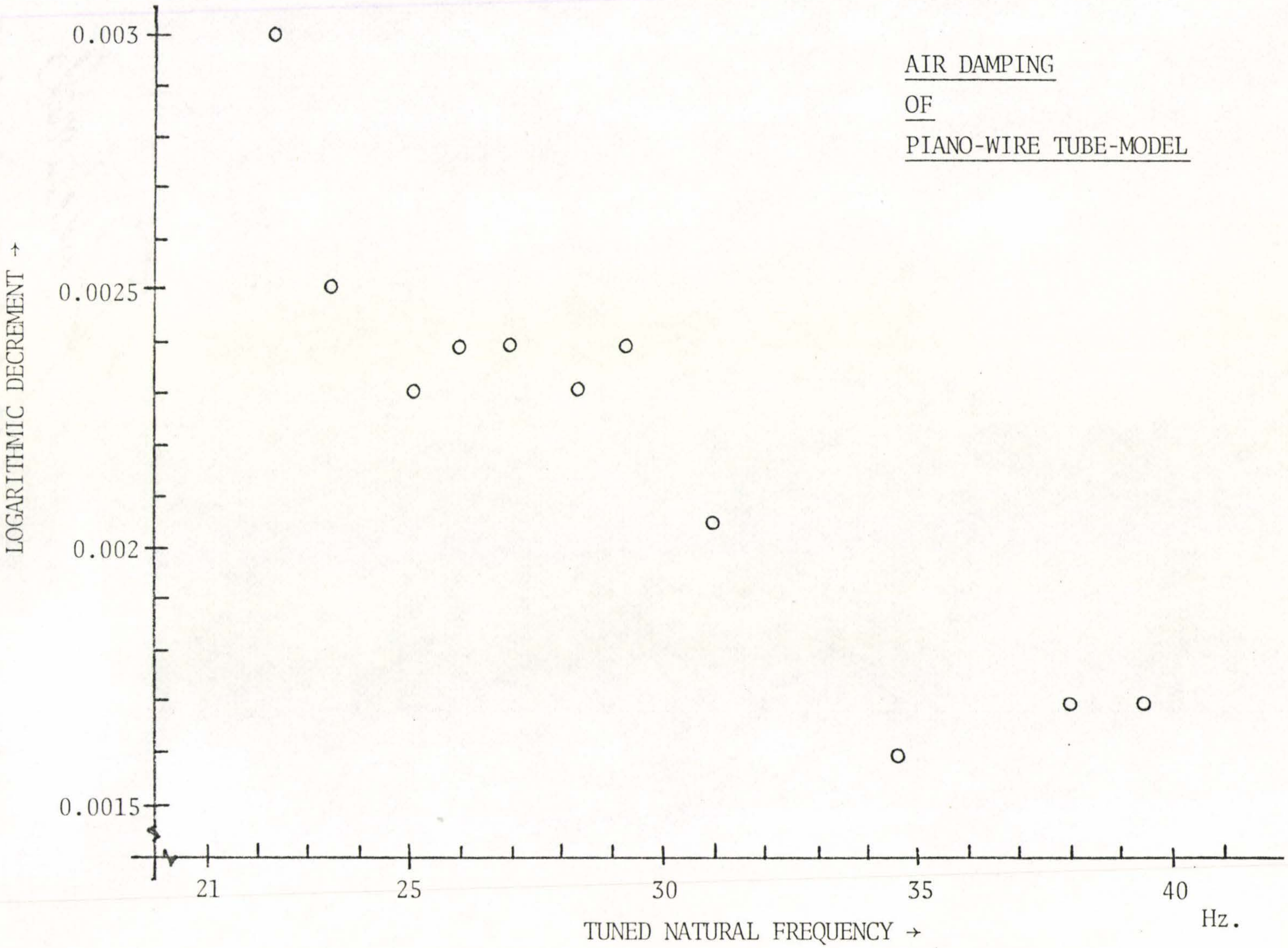
AIR DAMPING
OF
PIANO-WIRE TUBE-MODEL
LOGARITHMIC DECREMENT →
0.003
0.0025
0.002
0.0015
21
25
30
35
40
Hz.
TUNED NATURAL FREQUENCY →

FIGURE 4.5

ing was obtained by using two levels of SAE-10, 20 and 30 types of motor oils. The results have been shown in Figure 4.6 along with the AIR damping values obtained earlier. Also included in Figure 4.6 are two performance curves for two levels of water in damping cups. However, it was considered inappropriate to use water damping in actual tests due to the problems encountered with evaporation. The OIL damping was also found to decrease with an increase in tuned natural frequency. The highest value of logarithmic decrement of damping was seen to have decreased from 0.28 at 23 Hz. to 0.18 at 39.5 Hz. No directional variation in the data recorded for OIL damping was observed and damping was found to be linear. Typical amplitude decay traces recorded one each for AIR damping and OIL damping are shown in Figure 4.7. With this design of the tube-model the damping parameter of the tube could be varied from 0.35 to 56.

The tube-model was calibrated by hanging known weights at the middle of the tube and recording the tube deflection. The calibration curves so obtained have been shown in Figure 4.8. The tube was calibrated along four mutually perpendicular directions in the horizontal plane and similar results were obtained. The calibration indicates that the tube has a linear load-deflection characteristics for a maximum tube deflection of $\pm$ 1 mm. This feature of the tube-model was later used to obtain the coefficient of lift of a vibrating tube deep inside the tube-bundle. The tube could be deflected to a maximum peak amplitude of 6 mm. (7/32 in.) before the damping paddles would

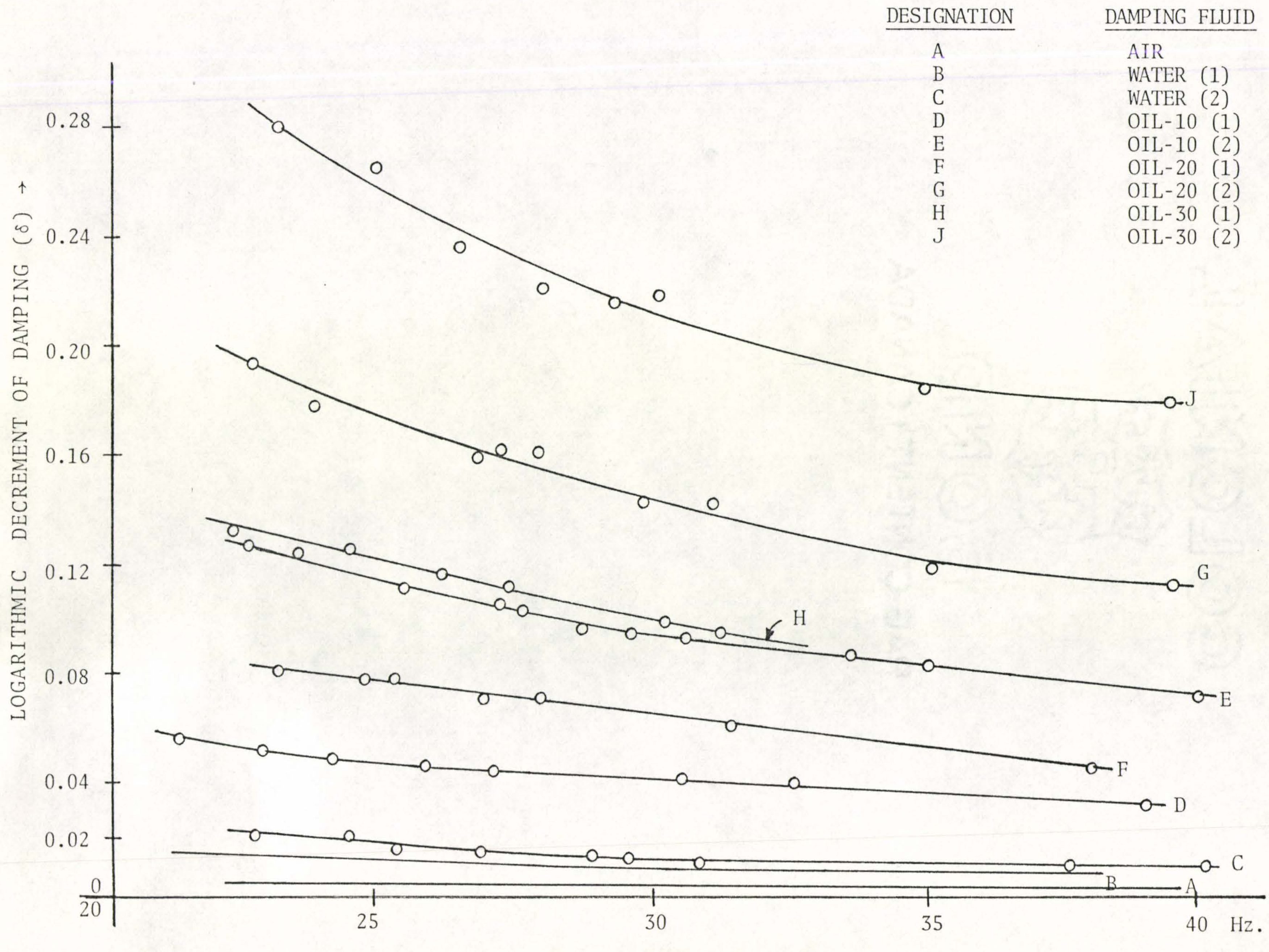
DESIGNATION
DAMPING FLUID
A AIR
B WATER (1)
C WATER (2)
D OIL-10 (1)
E OIL-10 (2)
F OIL-20 (1)
G OIL-20 (2)
H OIL-30 (1)
J OIL-30 (2)
LOGARITHMIC DECREMENT OF DAMPING (δ) →
0.28
0.24
0.20
0.16
0.12
0.08
0.04
0.02
0
20
25
30
35
40
Hz.
TUNED NATURAL FREQUENCY →
J
G
H
E
F
D
C
B
A

FIGURE 4.6

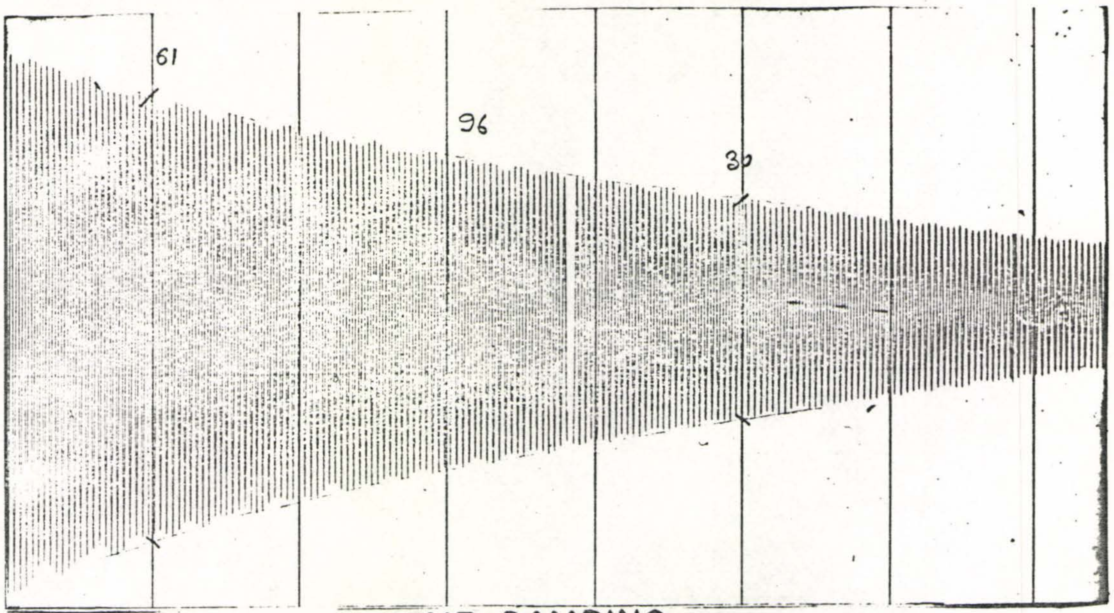


AIR DAMPING

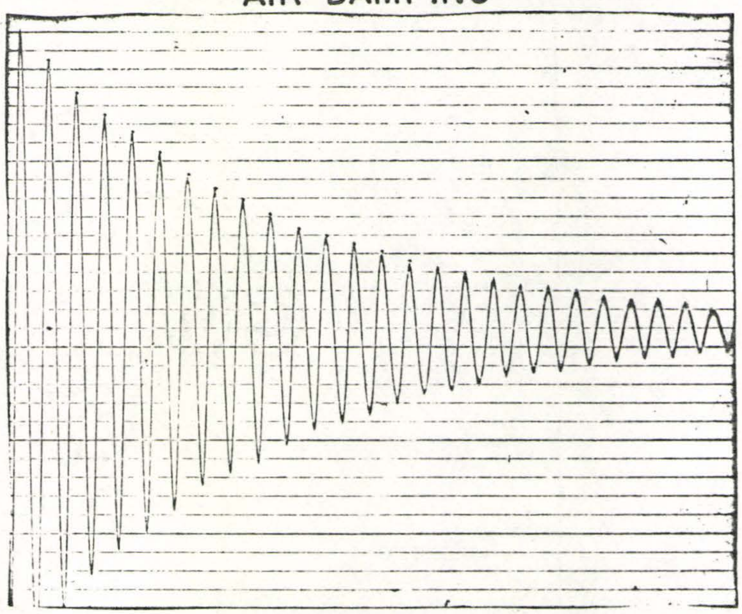

OIL DAMPING

TYPICAL AMPLITUDE-DECAY TRACES OF A MOVABLE-TUBE

FIGURE 4.7

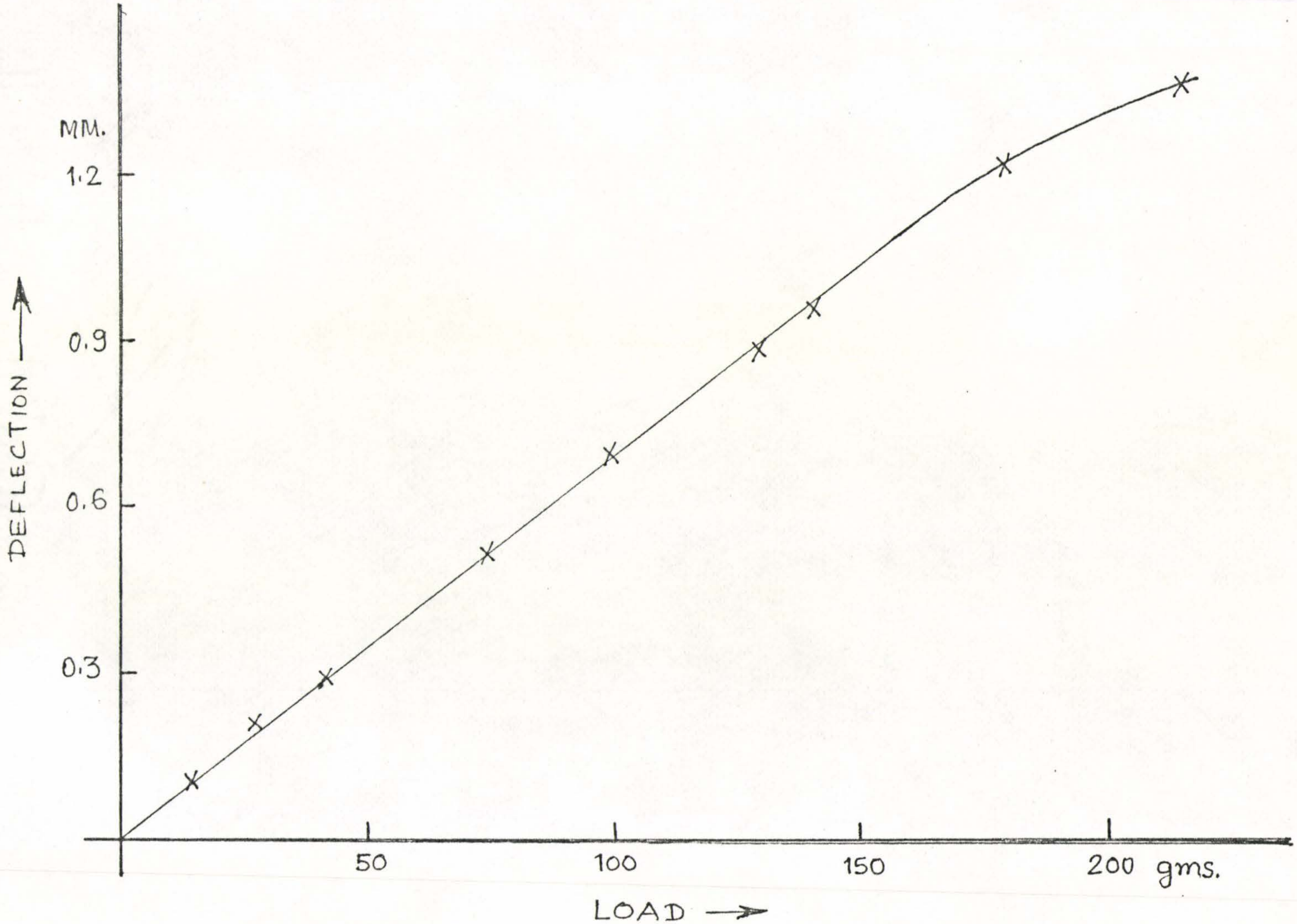


LOAD-DEFLECTION CHARACTERISTICS OF A MOVABLE TUBE

FIGURE 4.8

start striking the walls of the damping cups.

The rocking mode frequency of the tube-model was computed analytically and was expected to be about 1.5 times that of the rectilinear or fundamental natural frequency of the tube. This frequency separation seems to have been adequate as no rocking mode frequency was observed in tests.

The tube-model based on the concept of a hollow tube suspended on a piano-wire, therefore, enabled the natural frequencies of the tube to be varied easily and a far better control over both damping and natural frequency of the tube was obtained. No significant directional variation in effective tube stiffness could be discerned and the large scatter in damping values of the previous model was reduced to minimum by eliminating the coil springs. Also much lower values of damping could be realised in this tube-model which enabled exploring the tube-bundle characteristics at the required low values of the damping parameter.

The photographs of two tube-models developed are shown in Figure 4.9. Due to its far superior performance characteristics, the piano-wire tube-model was adopted for conducting further studies described in this thesis.

## 4.4 The Test Array

It was decided to conduct tests on a parallel-triangular array (also called in-line array) having a pitch/diameter ratio equal to 1.375. This particular array was selected because of its frequent use in actual heat exchangers.

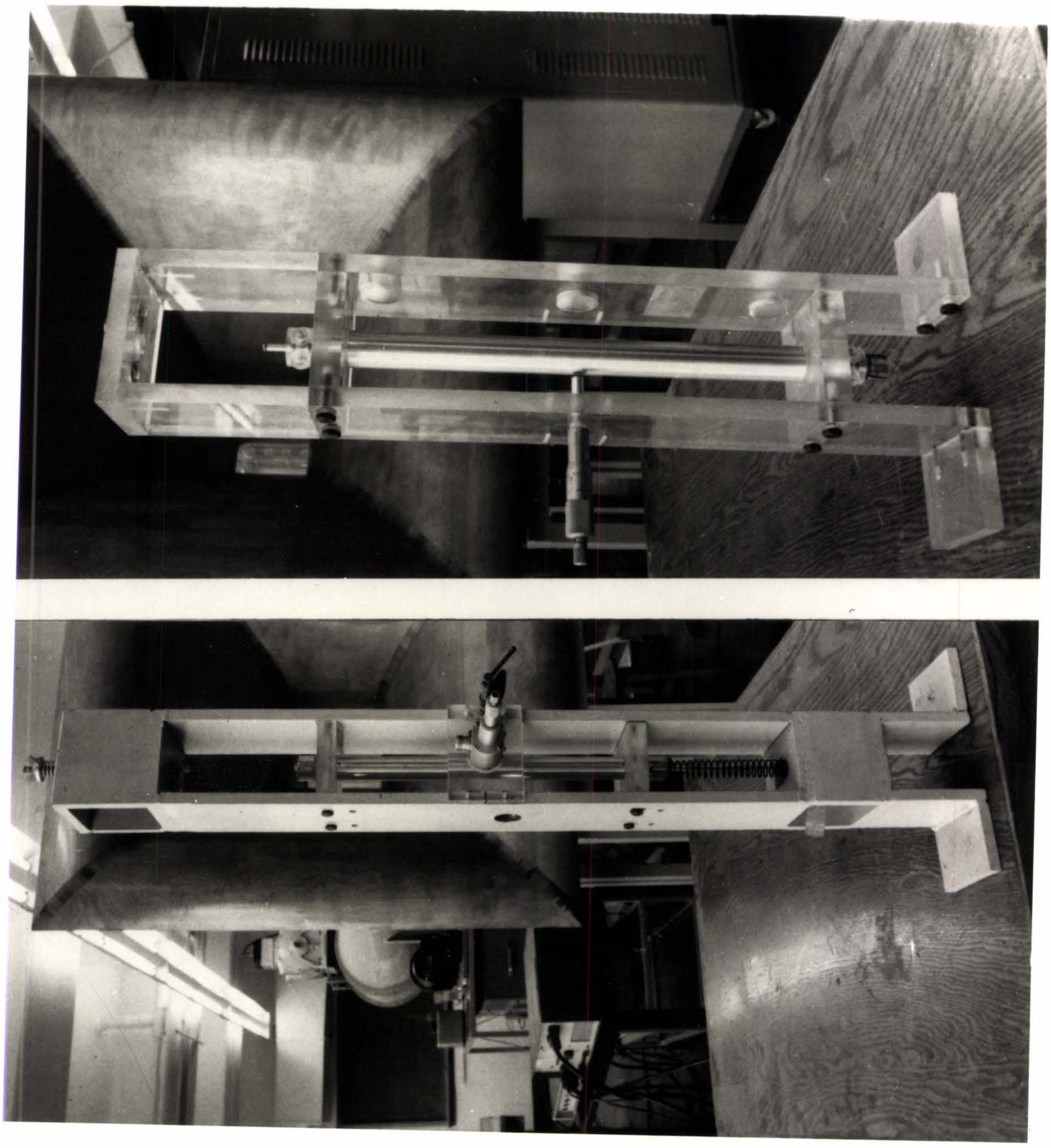

FIGURE 4.9

The conceived array had 27 rows of tubes with five tubes in each row as shown in Figure 4.10. Half tubes were installed at the ends to reduce wind-tunnel wall effects. Only 19 tubes in the middle of the tube-bundle were mounted flexibly. The design of each of these movable tubes was similar to the piano-wire tube-model described in the previous section. Not all the tubes in the array were made movable primarily from an economic standpoint. However, the rigid tubes were made easily removable to allow determination of the effect of number of tubes in the array on stability behaviour and flow-field characteristics.

A steel frame for mounting the 19 movable tubes was designed. The frame consisted of 16 mm. (5/8 in.) steel plates and 64 x 64 x 5 mm. (2 1/2 x 2 1/2 x 3/16 in.) square steel tubing and was bolted together. The steel frame was installed around the middle of the working section as shown by the photograph in Figure 4.11. Two reinforcement steel plates were installed in each of the two hollow box-type components of the steel frame. The designed value of deflection at the middle of the box due to maximum tension expected in all the piano-wires taken together was not more than 0.015 mm. (0.0006 in.). The structure was thus very rigid and no change in the tuned natural frequencies of the tubes would result from the tuning of subsequent tubes. A view of the top of the test section with 19 movable tubes in place is shown in Figure 4.12. The space between steel frame and working section (both at top and bottom) was enclosed

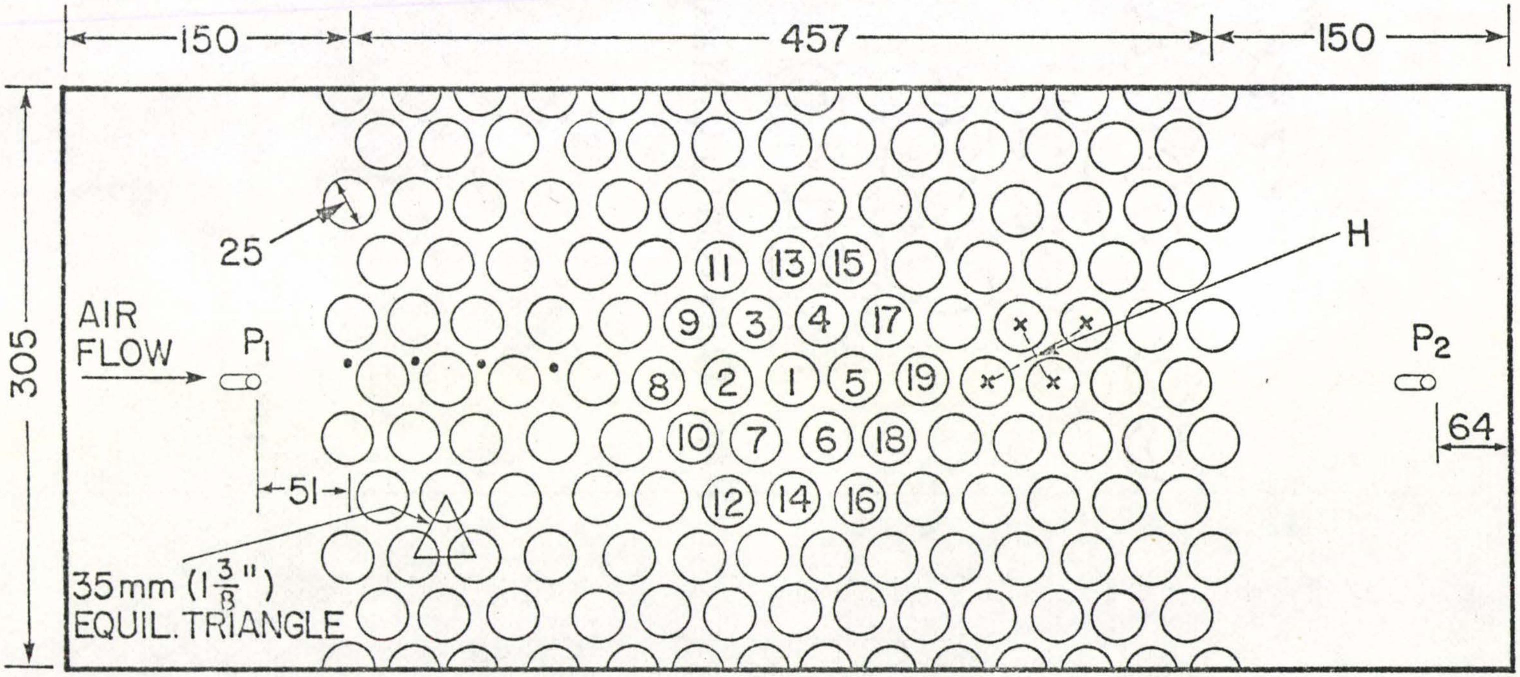


DIMENSIONS IN MM.

TUBES MARKED 1-19 ARE MOVABLE TUBES (REST ARE FIXED)

$P_1$, $P_2$ — LOCATIONS OF PITOT-PROBES

H — LOCATION OF HOT-WIRE PROBE

• — ADDITIONAL LOCATIONS FOR HOT-WIRE PROBE

FIGURE 4.10

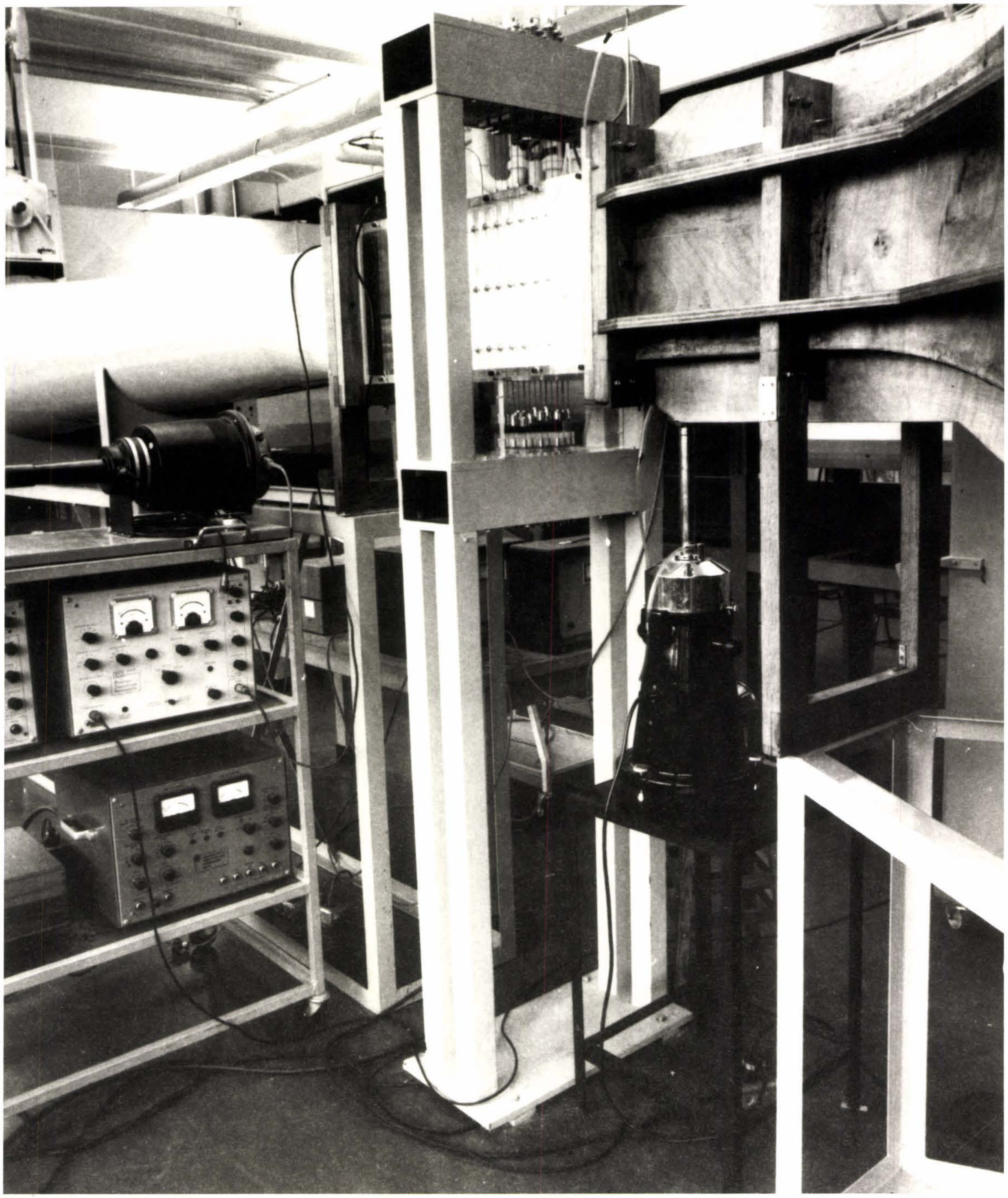

FIGURE 4.11

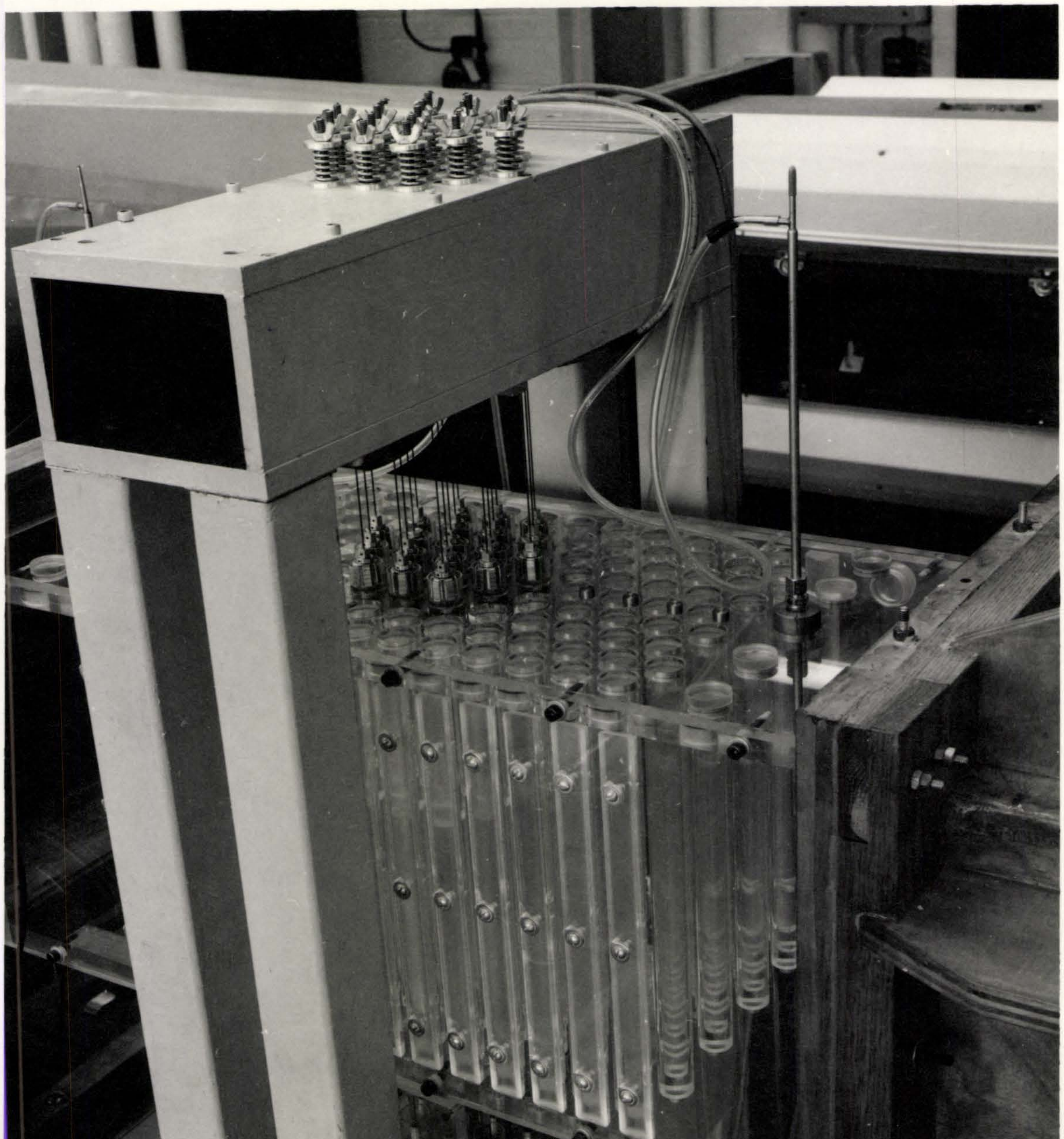

FIGURE 4.12

by four 13 mm. (1/2 in.) acrylic plates so as to form an enclosure for the 19 piano-wires. This arrangement prevented the leakage of air from the working section.

The flow velocities at location 'H' in the array as shown in Figure 4.10 were recorded by a hot-wire probe and designated 'Gap-stream velocities' ($V_G$). The corresponding upstream velocities were also recorded with a pitot-static probe and designated 'upstream velocities' ($V_U$). The ratio of $V_G/V_U$ was found to be a constant equal to 3.73.

The translational natural frequency of a movable tube was obtained by releasing the tube after displacement from its static equilibrium position and viewing the frequency count on an electronic digital counter. A capacitance probe was used for displacement pick-up. The tension in the piano-wire was adjusted in order to obtain a desired value of tuned frequency for the tube. The procedure was repeated for each of the 19 movable tubes til they were all tuned to a natural frequency of 24 Hz. within about $\pm$ 0.2% as shown in Table 4.1. The tuned frequencies were again checked after a period of about six months and the data recorded is also given in Table 4.1. There was an average drop in natural frequencies of about 0.2 Hz. (or about 1%) over this time period. This drop in frequencies was probably due to temporal relaxation or creep in the piano-wires. The new spread in natural

TABLE 4.1

NATURAL FREQUENCIES OF MOVABLE TUBES

| Tube No. | Initially tuned natural frequency | | Natural frequencies after about six months of initial tuning | |
|---|---|---|---|---|
| 1 | 24.00 | | 23.73 | |
| 2 | 23.99 | | 23.79 | |
| 3 | 23.96 | | 23.70 | |
| 4 | 24.00 | | 23.66 | |
| 5 | 24.03 | | 23.88 | |
| 6 | 23.97 | | 23.76 | |
| 7 | 23.98 | | 23.75 | |
| 8 | 24.02 | | 24.00 | |
| 9 | 23.99 | | 23.64 | |
| 10 | 24.04 | | 23.84 | |
| 11 | 23.97 | | 23.78 | |
| 12 | 24.03 | | 23.80 | |
| 13 | 24.02 | | 23.89 | |
| 14 | 24.04 | | 23.64 | |
| 15 | 24.00 | | 23.81 | |
| 16 | 23.99 | | 23.65 | |
| 17 | 24.02 | | 23.87 | |
| 18 | 24.04 | | 23.75 | |
| 19 | 24.01 | | 23.78 | |
| MEAN: | 24.01 | + 0.03<br>- 0.05 | 23.78 | +0.29<br>-0.14 |
| Standard Deviation: | 0.025 | | 0.10 | |

(Average of 1% reduction in frequencies)

frequencies was 23.86 $\pm$ 0.22 and was considered to be acceptable.

The logarithmic decrement of free vibration was measured by releasing the movable tube after displacement from its static equilibrium position and recording the subsequent amplitude decay on a U.V. recorder. The number of free vibration cycles required for the amplitude to decrease from a particular amplitude to a selected lower amplitude were counted. The computed values for each of the 19 movable tubes are given in Table 4.2. A certain amount of impact damping was observed in many tubes due to inevitable manufacturing tolerances among clearance holes drilled in the steel plates for the piano-wires. The problem was corrected by pouring aluminum filler in the grooves in the steel plates around the wires as shown in Figure 4.13. The logarithmic decrement of damping was determined again for each tube and is also given in Table 4.2. The average value of damping was consequently reduced by a factor of two. However, a large variation in the damping values of all the tubes is apparent (0.009 $\pm$ 0.003). It is to be noticed that the damping here is extremely small and the variation is undoubtedly due to variable end conditions which could not be precisely controlled. It should be noted that these are AIR damping values only and in later tests when the damping was controlled by oil in the damping cups, the damping values of all the movable tubes could be set to within about $\pm$ 2%. The AIR damping of movable tubes was measured again after the rig had been operating for 7-8

TABLE 4.2

AIR DAMPING OF MOVABLE TUBES

| Tube No. | Damping before applying Aluminum filler | Damping after applying Aluminum filler | Damping after about eight months |
|---|---|---|---|
| 1 | 0.013 | 0.009 | 0.015 |
| 2 | 0.016 | 0.010 | 0.015 |
| 3 | 0.021 | 0.010 | 0.014 |
| 4 | 0.018 | 0.011 | 0.016 |
| 5 | 0.014 | 0.007 | 0.010 |
| 6 | 0.016 | 0.012 | 0.020 |
| 7 | 0.021 | 0.012 | 0.018 |
| 8 | 0.017 | 0.009 | 0.019 |
| 9 | 0.020 | 0.011 | 0.017 |
| 10 | 0.018 | 0.006 | 0.008 |
| 11 | 0.018 | 0.006 | 0.020 |
| 12 | 0.021 | 0.006 | 0.009 |
| 13 | 0.021 | 0.011 | 0.016 |
| 14 | 0.018 | 0.007 | 0.011 |
| 15 | 0.015 | 0.012 | 0.020 |
| 16 | 0.020 | 0.007 | 0.009 |
| 17 | 0.011 | 0.006 | 0.008 |
| 18 | 0.021 | 0.007 | 0.011 |
| 19 | 0.014 | 0.012 | 0.018 |
| MEAN: | $0.018^{+0.003}_{-0.007}$ | $0.009 \pm 0.003$ | $0.014 \pm 0.006$ |
| Standard Deviation: | 0.003 | 0.002 | 0.004 |

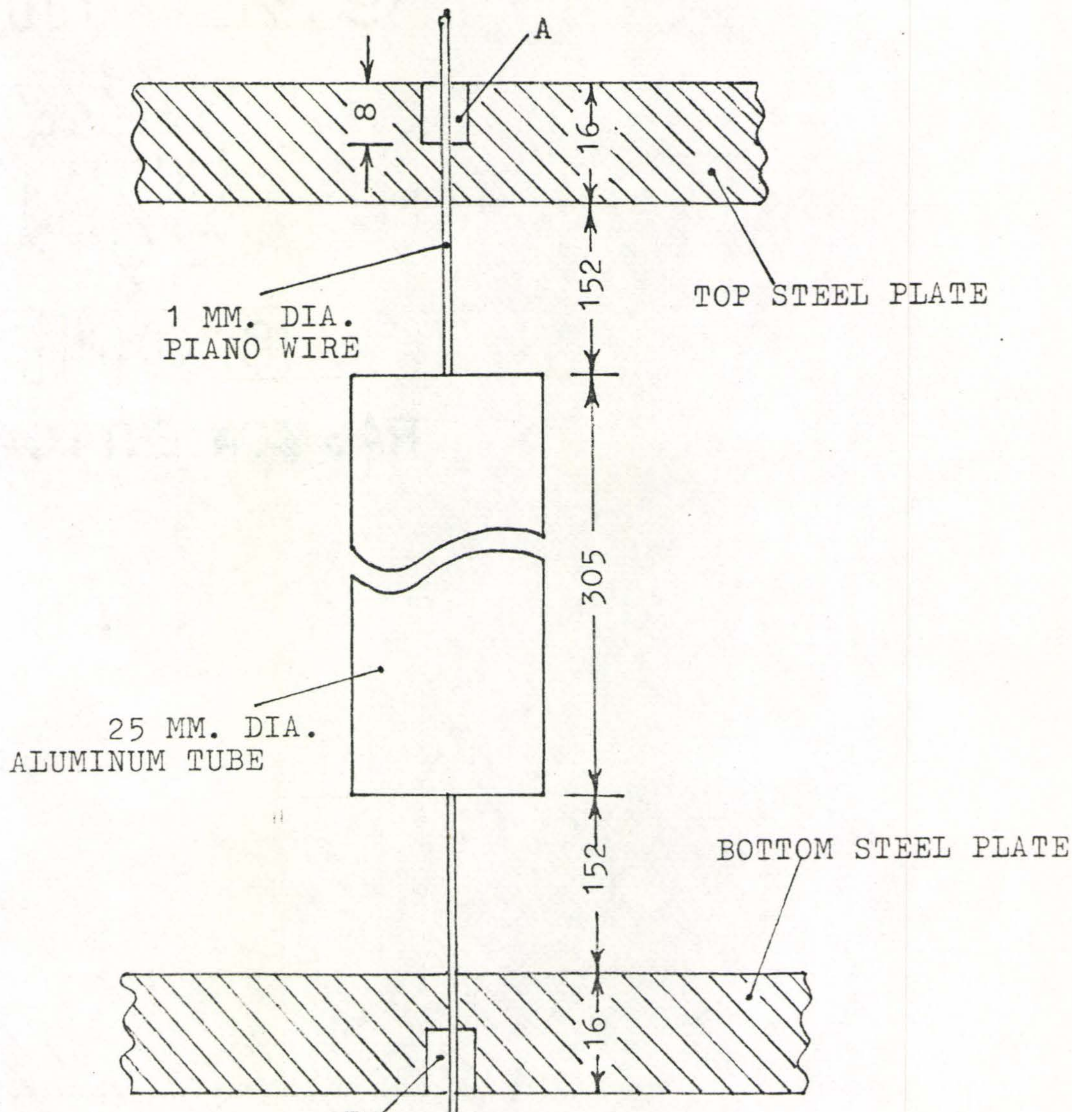


ALUMINUM FILLER WAS POURED IN GROOVES A & B

FIGURE 4.13

months and the data so obtained is given in Table 4.2. The average value of damping is seen to have increased by about 50%, probably due to wear in the aluminum filled wire clearance holes. However, the spread in damping values among the tubes stays rather large.

The average weight of a movable tube was 48.25 gms. and the weights of all the tubes were within $\pm$ 0.50 gm. ($\pm$ 1%) of this value.

## 4.5 Instrumentation

The free vibrations of a single tube assembly were recorded by using a DISA proximity transducer (DISA TYPE 51D11). A schematic of the complete instrumentation is shown in Figure 4.14.

In the main experiments on the tube-bundle, upstream flow velocity was measured by using a pitot-static probe and a Betz manometer. The gap-stream velocity was recorded by a $90^{\circ}$ miniature hot wire probe using a DISA constant-temperature anemometer and the output was displayed on a digital voltmeter. The signal for computing flow-field velocity power-spectra was also obtained from the same combination of hot-wire probe and constant-temperature anemometer and then processed in a Hewlett Packard Fourier analyser (Model 5475A). Two Wayne-Kerr capacitive probes (Type MC1 used in conjunction with vibration meter B731B) were employed to observe tube displacements on an oscilloscope and the signals were also recorded on a U.V. recorder. The

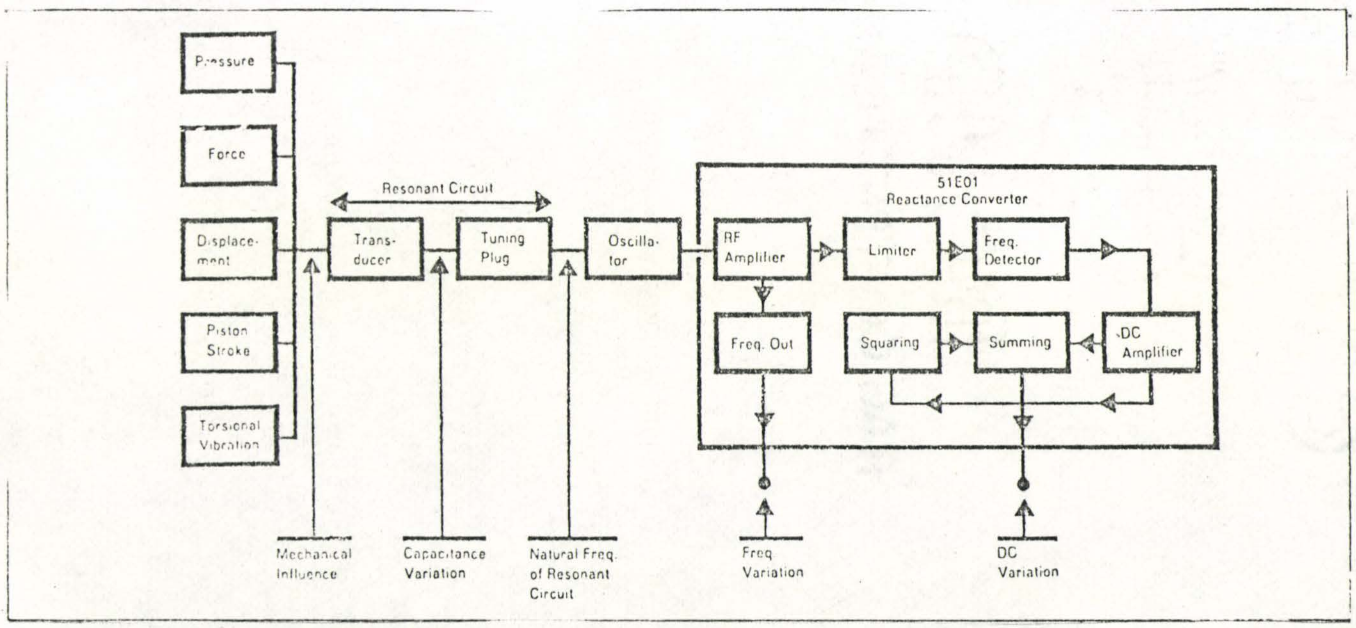


TRANSDUCER: DISA TYPE 51D11

PROXIMITY-VIBRATION TRANSDUCER
(Can be connected directly to the oscillator)

OSCILLATOR: DISA TYPE 51E62

REACTANCE CONVERTER: DISA TYPE 51E01

FIGURE 4.14

probes were installed at $90^{o}$ to each other and $45^{o}$ to the direction of flow as shown in Figure 4.15. The output of a capacitive probe when recorded on Kodak linegraph paper was used to compute the natural frequency and logarithmic decrement of damping of movable tubes. An ordinary tachometer was used to record the R.P.M. of the fan motor. The instrumentation system has been shown schematically in Figure 4.16.

Detailed description and specifications of all the instruments and probes is given in Appendix D and the calibration curves for the transducers and hot-wire probes have been included in Appendix E.

Two photographs showing various instruments in the general work area of wind-tunnel have been included in Figure 4.17. In Figure 4.18 is shown a photograph of a pitot-static probe, a Wayne-Kerr capacitive probe and a DISA $90^{o}$ miniature hot wire probe.

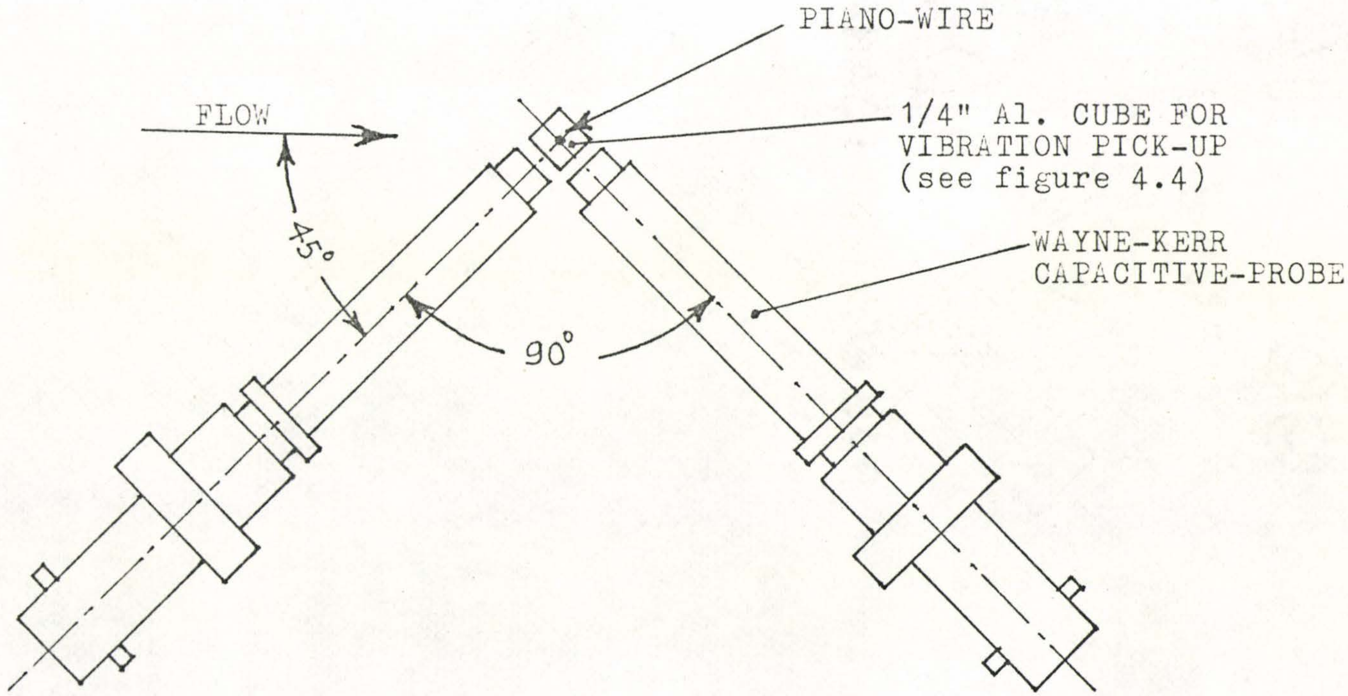


LOCATION OF PROBES

SCALE:
1.5 X FULL SIZE

FIGURE 4.15

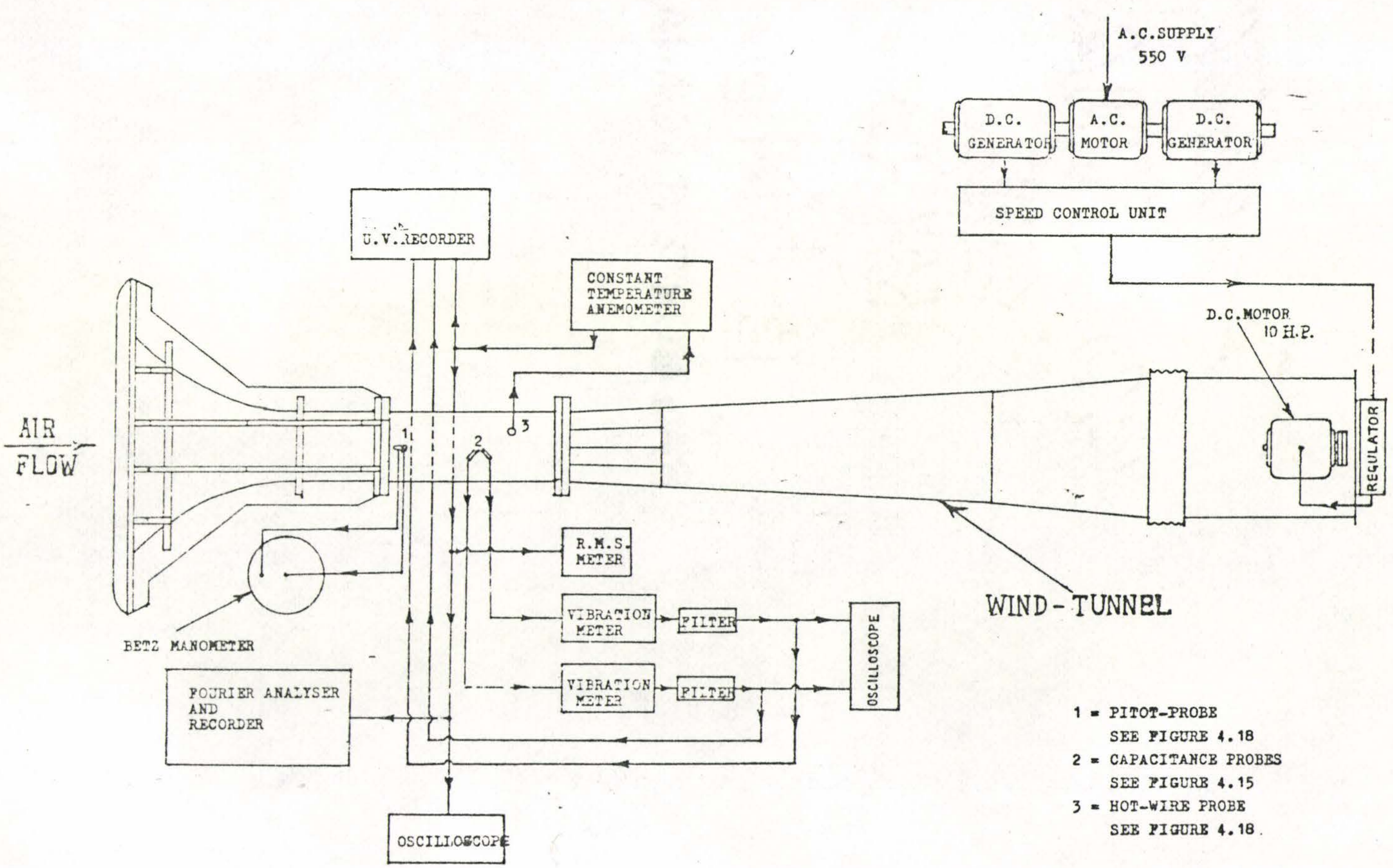


OVERALL LAYOUT OF THE WORK AREA

FIGURE 4.16

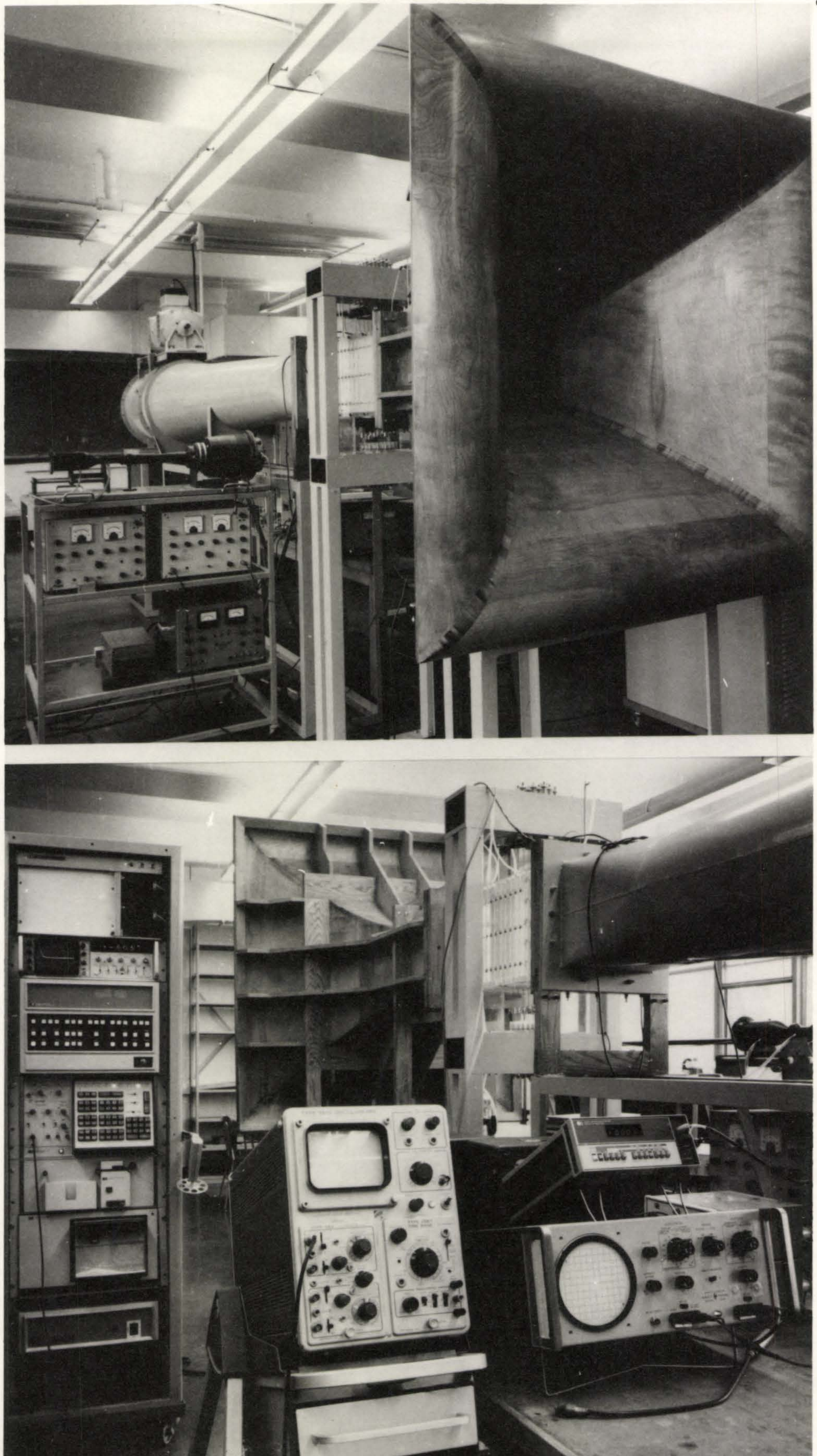

(a)

(b)

FIGURE 4.17

PITOT STATIC PROBE

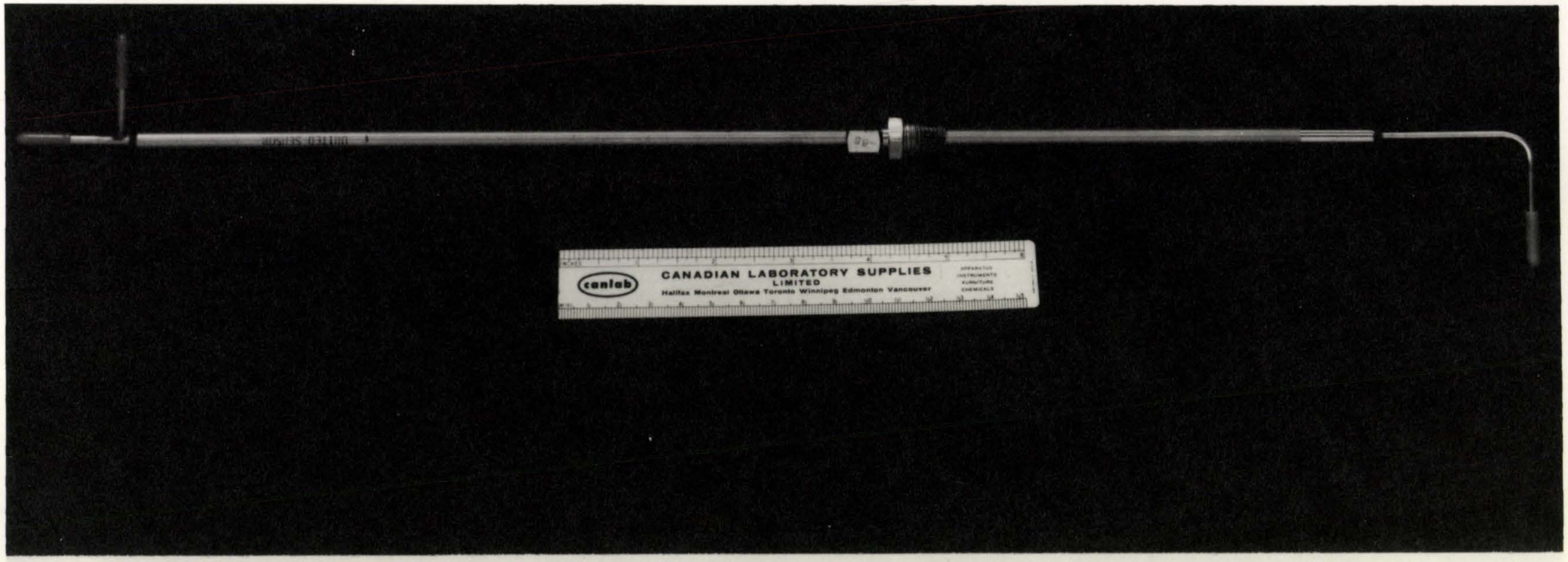


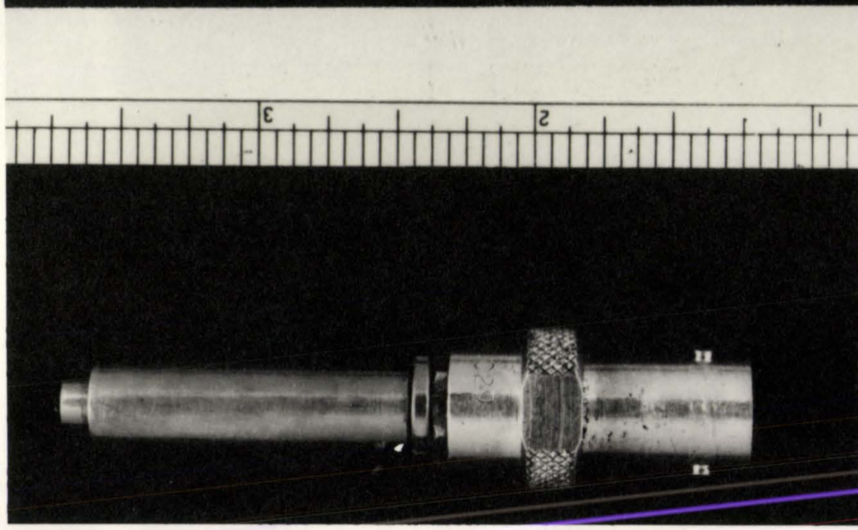

CAPACITIVE PROBE

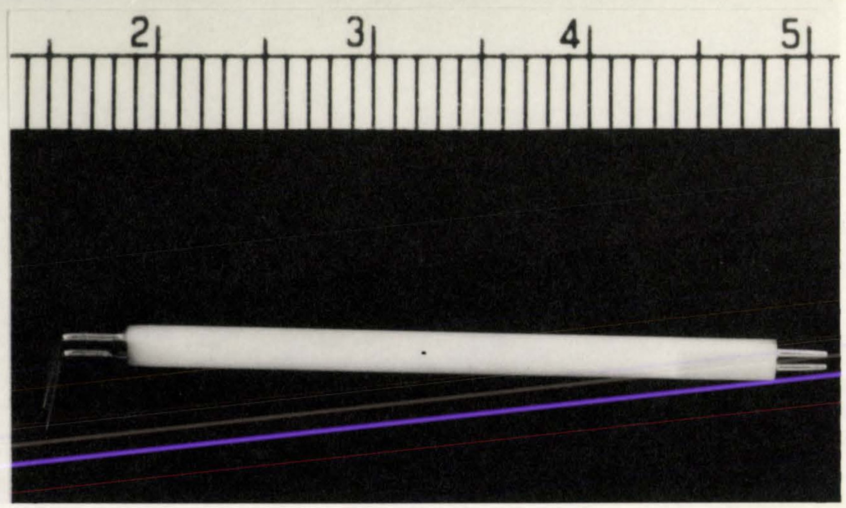


HOT-WIRE PROBE

FIGURE 4.18

# CHAPTER 5

# EXPERIMENTAL RESULTS

As described in the previous chapter, the experiments were conducted on a parallel-triangular (in-line) tube array having p/d = 1.375. The array was 27 rows deep with 5 tubes in each row. As shown in figure 5.1, half tubes were installed along the sides of the test section to minimise wall effects. Nineteen tubes in the array (as shown in figure 5.1) were movable and their stiffness and damping could be controlled independently. The movable tubes were specially designed to give a linear response for up to $\pm$ 1 mm. ($\pm$ 0.04 in.) of tube deflection. Nine rows of stationary tubes in the front of the tube-array were designed to be removable in order to study the effect of tube-bundle size on flow characteristics.

The test plans were modified slightly during the course of the investigation due to a minor equipment failure. The original intent was to instrument tube no. 1 (figure 5.1) to record typical tube response data. However, after a few days of running the equipment, it was noticed that the mounting blocks for the vibration pick-up probes for tube no. 1 had become loose. An attempt was made to fix them but unfortunately, due to very limited access room available on top of the movable tubes, the situation could not be corrected. It was decided

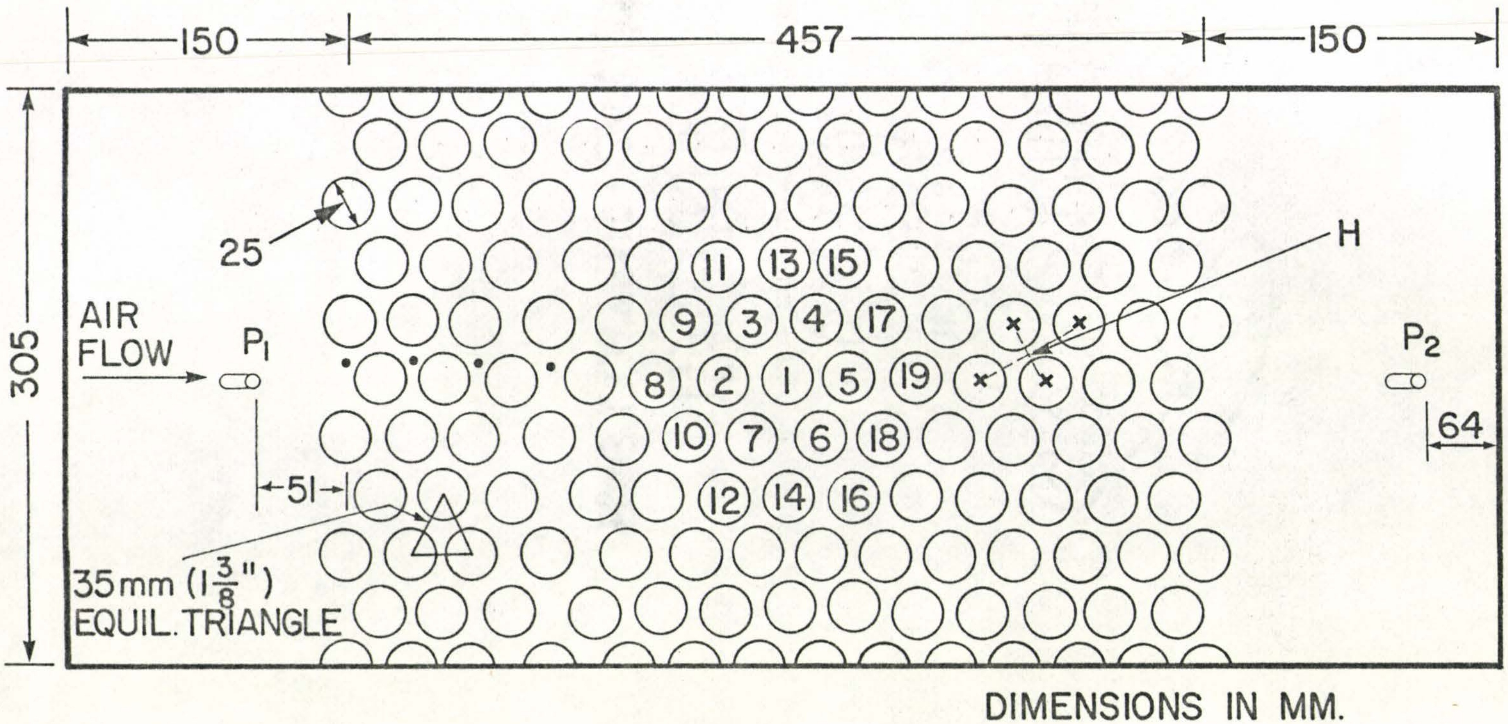


TUBES MARKED 1-19 ARE MOVABLE TUBES (REST ARE FIXED)

$P_1$, $P_2$ — LOCATIONS OF PITOT-PROBES

H — LOCATION OF HOT-WIRE PROBE

• — ADDITIONAL LOCATIONS FOR HOT-WIRE PROBE

FIGURE 5.1

to instrument tube no. 5 instead, to obtain representative response data.

As the flow rate in the wind-tunnel was increased the tubes responded to vortex-shedding, turbulent buffetting and fluidelastic effects respectively. Discussion of the tube response has therefore been considered under these headings below.

## 5.1 Vortex-Shedding Response

The tests were conducted with all the movable tubes tuned to a natural frequency of 24 $\pm$ 0.04 Hz. and an overall logarithmic decrement of 0.009 $\pm$ 0.003 (air and material damping only). Nine rows upstream of the movable tube-bundle were removed leaving an array of 18 rows only. The movable tube no. 8 was thus directly facing the upstream flow. The wind-tunnel fan was started and run at a very low speed.

The gap-stream velocity at the location marked 'H' in figure 5.1 was measured with a $90^{o}$ hot-wire probe and was recorded to be $V_G$ = 0.53 m./sec. The corresponding Reynolds number based on outside diameter of tube is R = 900. The output signal from the hot-wire probe was fed into a Hewlett Packard Fourier analyser and a velocity power-spectrum was computed. The power spectrum is shown as the top trace in figure 5.2. As is evident, the velocity fluctuations in the flow-field are concentrated at two discrete frequencies, 18 and 35 Hz. The existence of two discrete frequencies in the flow appears to be due to regular vortex-shedding through

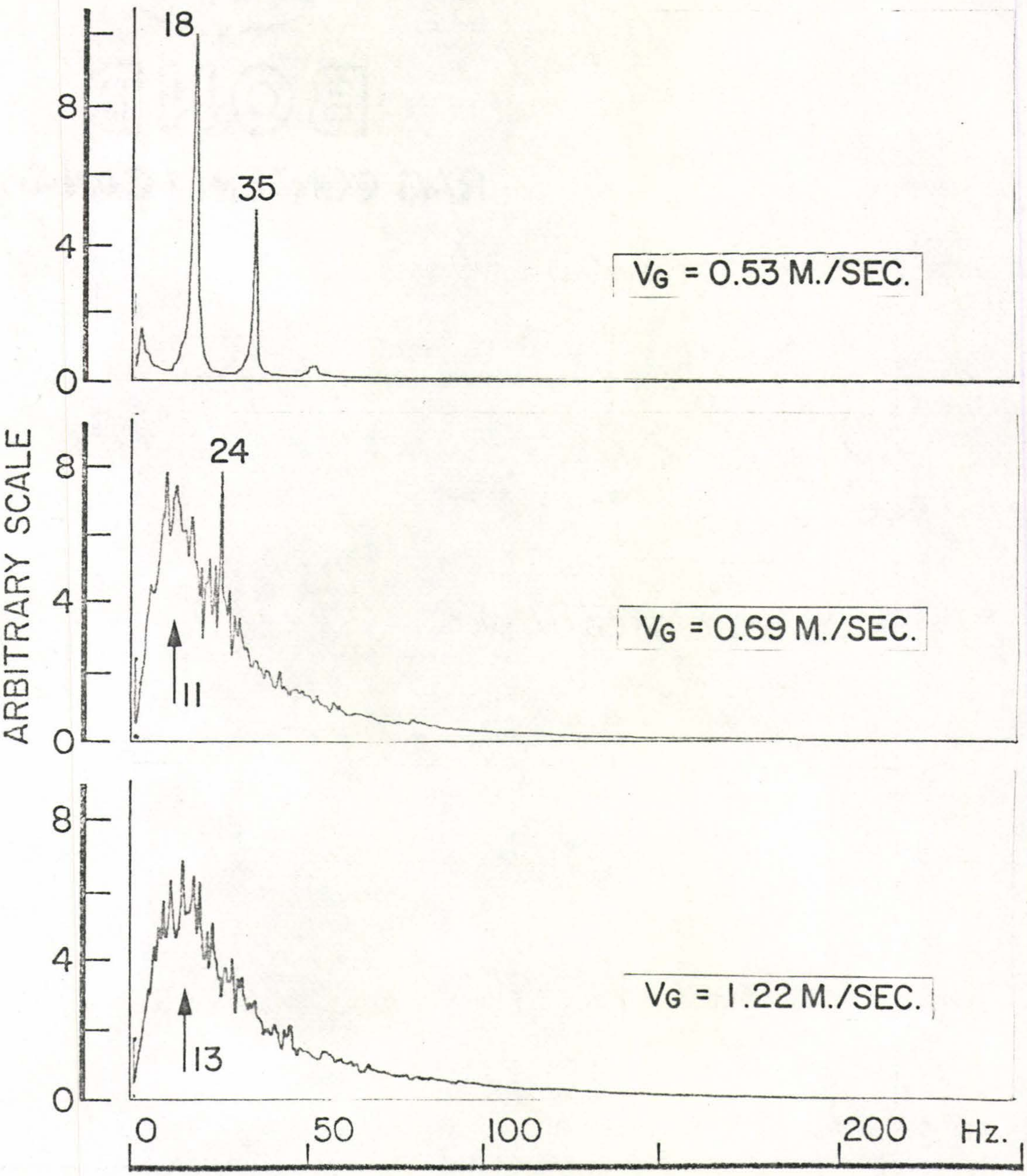


VELOCITY POWER-SPECTRA FOR 13 UPSTREAM ROWS

FIGURE 5.2

the tube-bank. The resolution of frequency record obtained from the Fourier analyser is 0.5 Hz., therefore, it is most likely that the higher frequency is equal to 2 x the lower frequency. Walker and Reising [90] and Dye and Abrahams [94] have also found two vortex-shedding frequencies in their investigations of flow over tube bundles.

The larger peak which occurs at 18 Hz corresponds to a Strouhal number ($S_G$) of 0.86 based on minimum-gap velocity and outside diameter of the tube. If the Strouhal number is based on the velocity between two adjacent tubes in the same row or on the upstream flow velocity the figures will be $S_T = 1.83$ and $S_U = 3.16$ respectively.

A high value of Strouhal number is usually anticipated for a closely packed array. However, no data exists in the literature on Strouhal number values for the array tests in the present experiments (p/d = 1.375, $X_T = 2.38$, $X_L = 0.688$, L = longitudinal distance between rows). Thus a direct comparison has to be ruled out. Using Fitz-Hugh's [98] maps the expected Strouhal number $S_T$ for the present array would be of the order of 1.0 (the maps are reproduced in figure 5.3a). This value is about 45% lower than the actual Strouhal number found in the present experiments. Chen's [89] data on Strouhal numbers has been reproduced in figure 5.3b. Although no data point exists in this plot for the present array, an extrapolation of the curves indicate a Strouhal number of $S_T = 0.82$. This value is again much lower than that actually observed (about 55% lower). Gorman [113] has recently

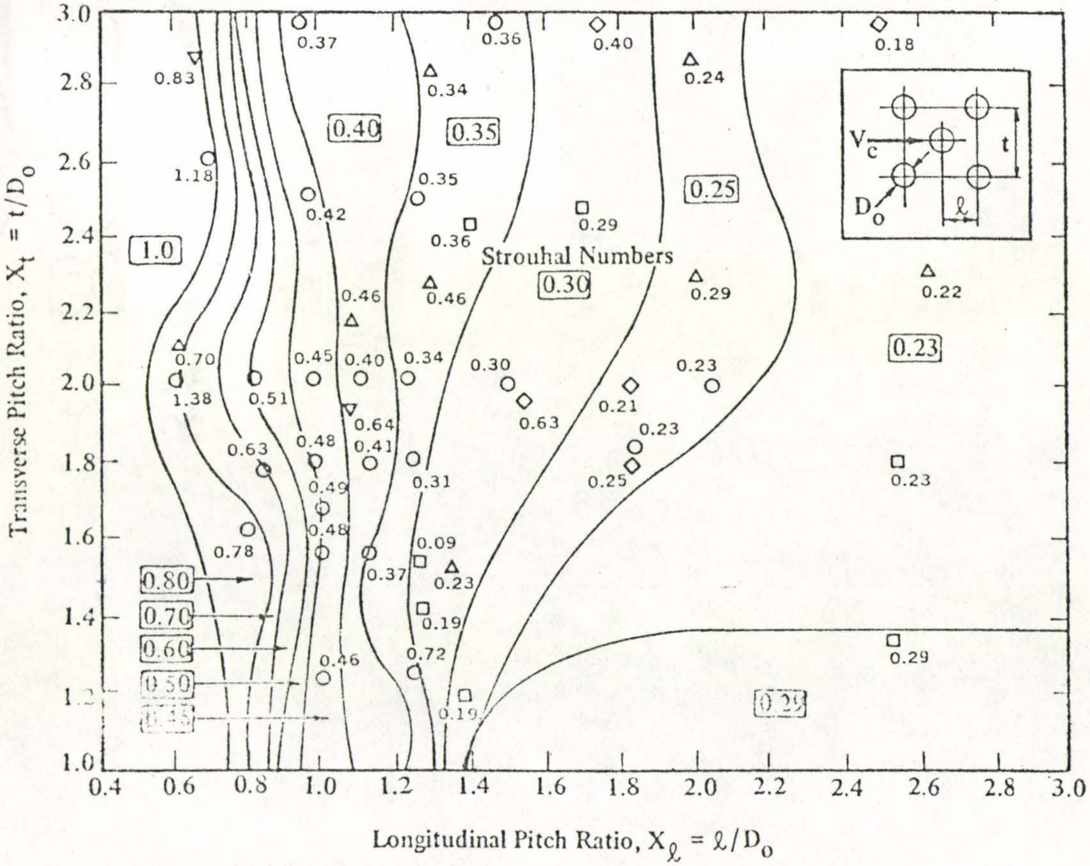


Map of Strouhal Numbers for Staggered Arrays by Fitz-Hugh (REF. 98)

FIGURE 5.3(a)

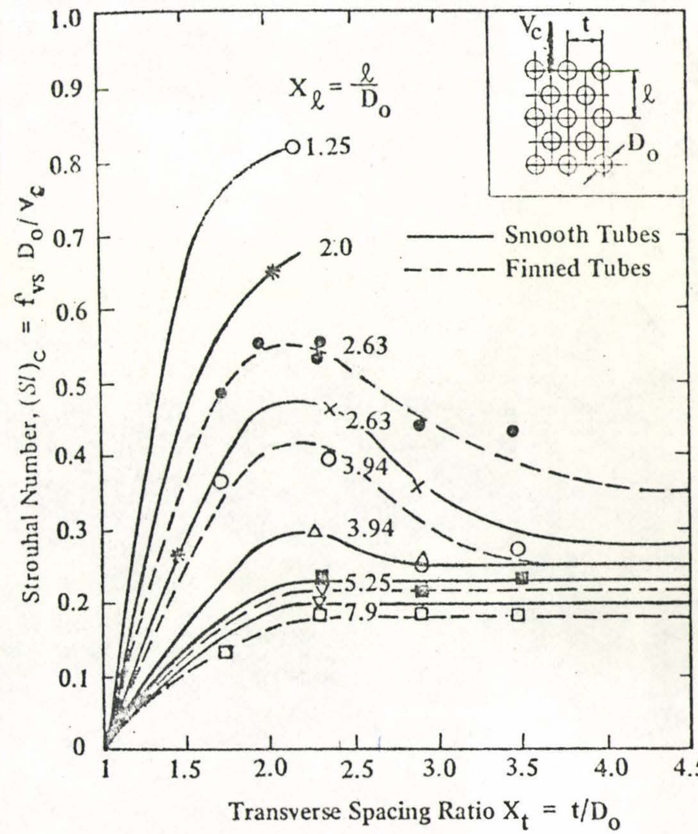


Strouhal Numbers for Staggered Tube Banks by Chen (REF. 89)

FIGURE 5.3(b)

conducted tests in a water-tunnel and did not observe any vortex-shedding response for in-line arrays at p/d = 1.33. However, he did observe a vortex-shedding response of an inlet tube only in an in-line tube-bundle for p/d = 1.57. The corresponding Strouhal number was $S_U$ = 1.19. This value is about 62% lower than that obtained in the present experiments.

The large difference between Gorman's and the present results can be attributed to (a) the larger pitch ratio of Gorman's tube-bundle and (b) a possible Reynolds number effect. Gorman conducted his tests at $R_U = 1.3 \times 10^4$ whereas the Strouhal number in the present experiments was recorded at $R_U$ = 245 only. The variation of Strouhal numbers for tube-bundles over this Reynolds number range is not known yet. However, Funakawa [6] recorded a decrease in Strouhal number with an increase in Reynolds number in the subcritical range ($R_U = 1.0 - 4.0 \times 10^4$). More data on Strouhal numbers in closely-packed arrays established at comparable Reynolds numbers is needed to improve our understanding of vortex-shedding relationships in the tube banks.

As the movable tubes were all tuned to a natural frequency of 24 Hz, no coupling existed between the tubes and the flow fluctuations at 18 and 35 Hz. Consequently no tube response was seen on the oscilloscope screen as shown in picture no. 1 of figures 5.4 and 5.5.

With an increase in flow velocity to $V_G$ = 0.69 m./sec. ($R_G$ = 1171) the shape of the velocity power-spectrum changed to that shown in the middle trace of figure 5.2. A concentration

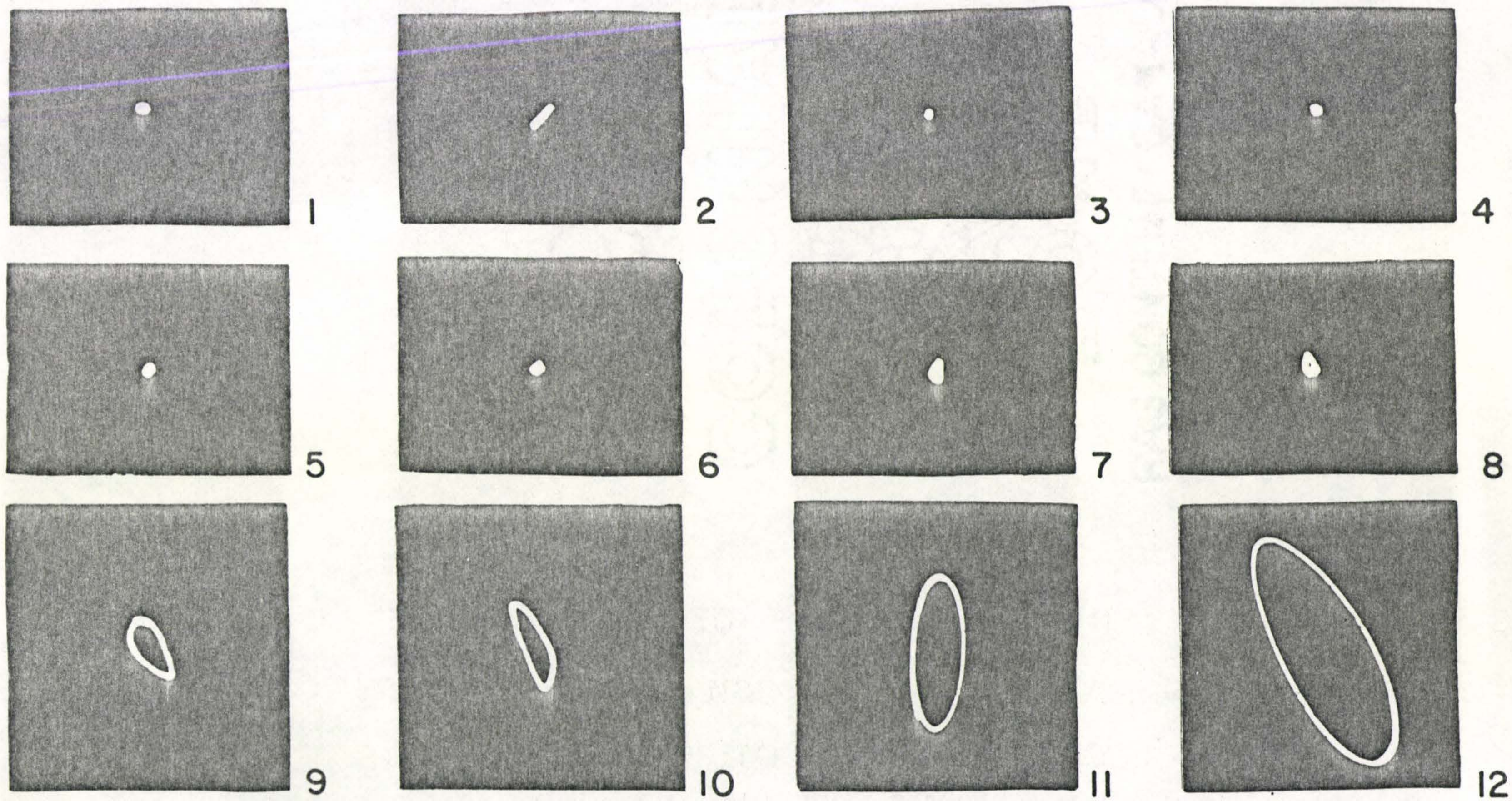


SERIAL NOS. INDICATE INCREASING FLOW-VELOCITY

TUBE RESPONSE UP TO 10 UPSTREAM-ROWS
(AS SEEN ON AN OSCILLOSCOPE)

FIGURE 5.4

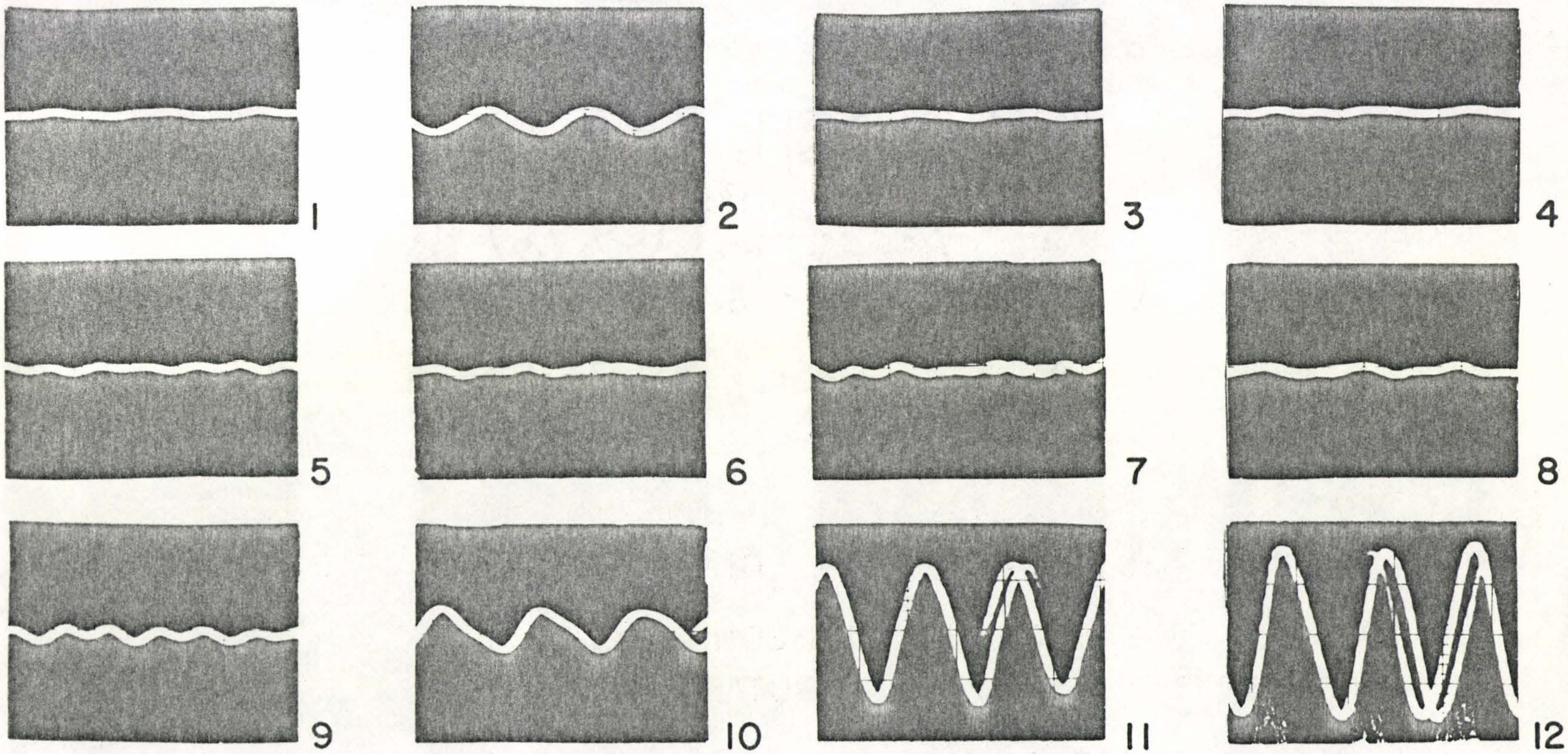


SERIAL NOS. INDICATE INCREASING FLOW VELOCITY
TUNED NATURAL FREQUENCY OF TUBE = 24 Hz.

TUBE RESPONSE UP TO 10 UPSTREAM - ROWS
(AS SEEN ON AN OSCILLOSCOPE)

FIGURE 5.5

of flow energy at 24 Hz on top of a narrow-band turbulence sprectrum is evident. The Strouhal number at 24 Hz and based on minimum-gap velocity is $S_G = 0.89$. The peak in the narrow-band spectrum (11 Hz) corresponds to $S_G = 0.41$.

The movable tubes being tuned to 24 Hz, now responded to flow-fluctuations at 24 Hz. The response as seen on the oscilloscope is shown in picture no. 2 of figures 5.4 and 5.5. The monitored tube which oscillated at its natural frequency of 24 Hz was seen to vibrate primarily in the transverse direction, occasionally drifting within $\pm 45^o$ to this direction. The amplitude of vibration stayed constant at about $\pm$ 0.08 mm. ($\pm$ 0.003 in.).

As the movable tubes had been specially designed to give a linear response up to $\pm$ 1 mm., this feature can be used to determine the coefficient of lift for the tube. The computation procedure has been described in Appendix F. The coefficient of lift based on the velocity between two adjacent tubes in a transverse row is $C_L = 0.41$.

No data is available in the literature for the lift-coefficient at vortex-shedding resonance for the present array. The closest comparison that can be made is with a data point given by Chen [142] for a staggered tube-bundle of $X_T = 1.46$, $X_{2L} = 2.84$ and at $R_T = 790$. He obtained $C_L = 0.63$. This compares well with the present value ($C_L = 0.41$) keeping in mind that in arrays with smaller longitudinal spacing the boundary layer on the cylinder separates further downstream than in arrays with larger longitudinal pitches, thus resulting in a greater drag and lower $C_L$. The effect of the difference in $X_T$ is probably compensated for by using the velocity between two adjacent tubes in the transverse row while computing $C_L$ in each case. In still another paper Chen [97] has obtained $C_L = 0.436$ at $R_T = 1.55 \times 10^4$ in a staggered tube-array. However, he has not given the geometry of the array for which the data was computed. Both these data points of Chen were obtained at resonant conditions. Batham [111] has obtained $C_L$ on a closely pitched in-line array (p/d = 1.25) by integrating the pressure distribution around a stationary tube. He derived $C_L = 0.19$. Presumably this value is lower first because $C_L$ in in-line arrays is expected to be smaller than in staggered arrays and second, because resonant conditions result in an improved spanwise correlation of forces and $C_L$ is expected to be higher. Ferguson and Parkinson [33] have shown for a single cylinder that there is a three-fold increase in the coefficient of lift when the cylinder is in resonance and interacts with its flow-field.

The wind-tunnel speed was further increased to $V_G = 1.22$ m./sec. ($R_G = 2.1 \times 10^3$). A velocity power-spectrum at the same location (location 'H' in the tube bundle, figure 5.1) in the tube-bundle was recorded and is shown as the bottom trace in figure 5.2. It is evident from this spectrum that the excess energy of the regular vortex-shedding over the energy associated with the random turbulence in the tube-bundle has completely disappeared. The flow-field velocity fluctuations are concentrated within a narrow band of frequencies. Only a very small amplitude random response of the tube was observed at this Reynolds number as shown in picture no. 3 of figures 5.4 and 5.5.

The above results indicate that discrete periodicity due to vortex-shedding in the tube-bundle exists up to Reynolds numbers of the order of $10^3$ (based on the minimum-gap velocity) only. As the Reynolds number is increased the discrete periodicity in the flow-field breaks down and gives way to a narrow-band turbulence spectrum. It was next decided to determine the effect of tube-bundle size on the vortex-shedding phenomenon and the following experiments were conducted.

Two rows of fixed tubes were installed upstream of the tube-bundle (making it 15 rows upstream of the hot-wire probe location). The wind-tunnel fan was run again and the air flow was set at approximately $V_G$ = 0.53 m./sec. A velocity power-spectrum was computed at location 'H' in the tube-bundle and is shown in figure 5.6. It is seen from this spectrum that most of the flow energy is concentrated at 17 Hz which corresponds to a Strouhal number of 0.81 (based on minimum-gap velocity). The second harmonic at 33 Hz is not very strong. Also, no appreciable tube response was seen on the oscilloscope at this flow velocity. With a further increase in flow velocity to $V_G$ = 0.69 m./sec., a large peak at 24 Hz was seen in the spectrum as shown in figure 5.6. This peak occurred at a Strouhal number of $S_G$ = 0.89. The movable tubes being tuned at 24 Hz responded in resonance to this vortex-shedding

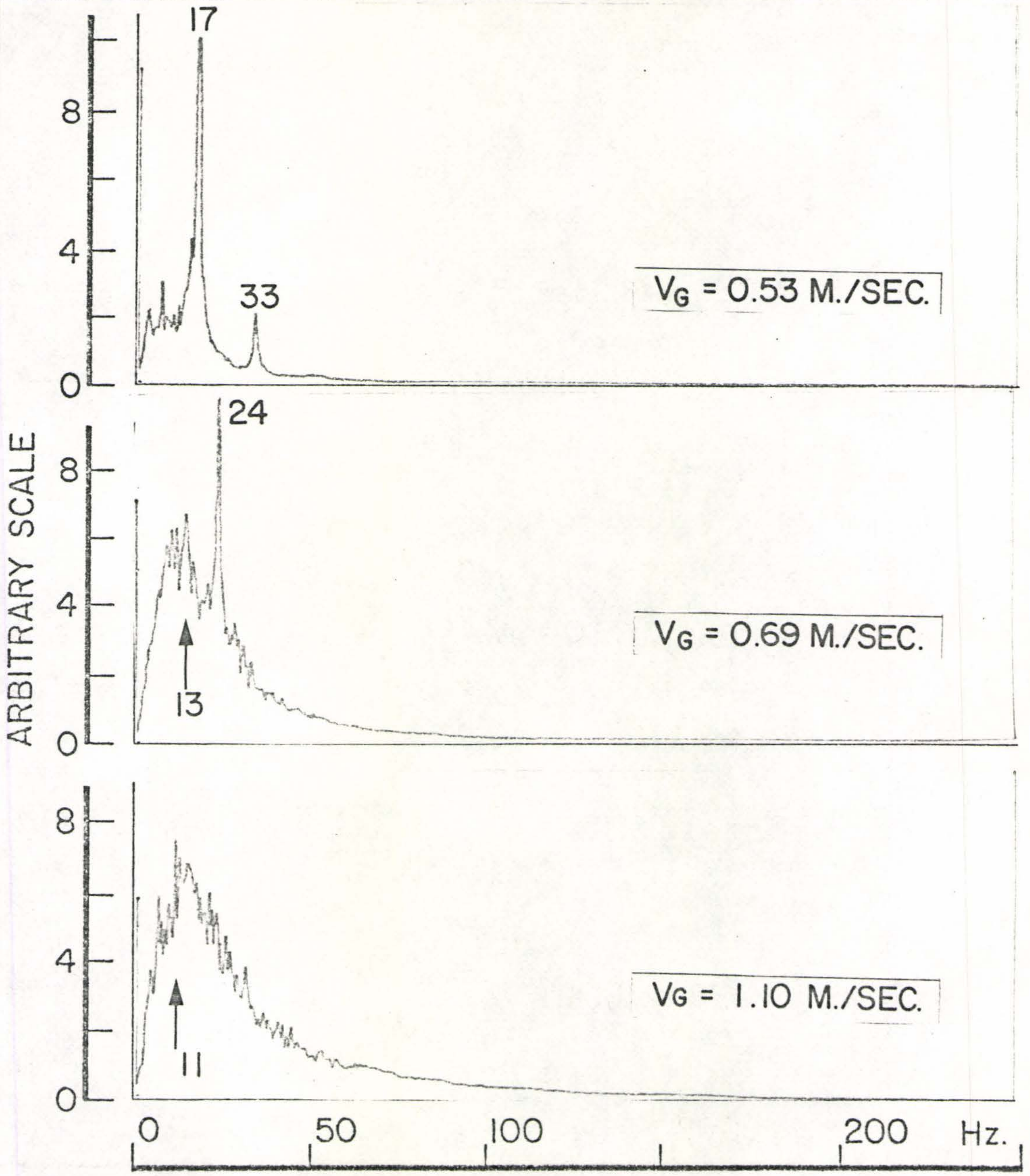


VELOCITY POWER-SPECTRA FOR 15 UPSTREAM ROWS

FIGURE 5.6

frequency. The amplitude of vibration was very small ($\pm$ 0.08 mm.) and the instrumented tube responded primarily in the transverse direction to the flow. A further increase in flow velocity to $V_G$ = 1.10 m./sec. resulted in the disappearance of any predominant frequency in the velocity power-spectrum and no regular tube response was recorded.

In order to determine whether the peak at 24 Hz was due to the tubes' motion at their natural frequency or due to periodicity in the flow, a simple test was carried out. The motion of all the movable tubes was physically blocked from outside the wind-tunnel by using acrylic strips and a velocity power-spectrum as shown in figure 5.7 was obtained at $V_G$ = 0.63 m./sec. A peak at 24 Hz is evident. However, this peak is not as large as when the movable tubes were free to vibrate, thus indicating that very small tube oscillations amplify an existing concentration of energy in the flow-field when frequencies coincide. Hence, the strength of periodicity in the flow is extremely sensitive to tube motions as was found by Batham [111].

An increase in the number of upstream rows to 16 (counted from the point where the hot-wire probe was installed, see figure 5.1) resulted in a set of frequency spectra as shown in figure 5.8. Two large peaks at 16 and 19 Hz instead of a single peak recorded at comparable flow velocities in previous records are apparent. This double peak is probably due to the unsteady nature of the vortex-shedding frequency occurring in the tube-bundle. Because of the time required

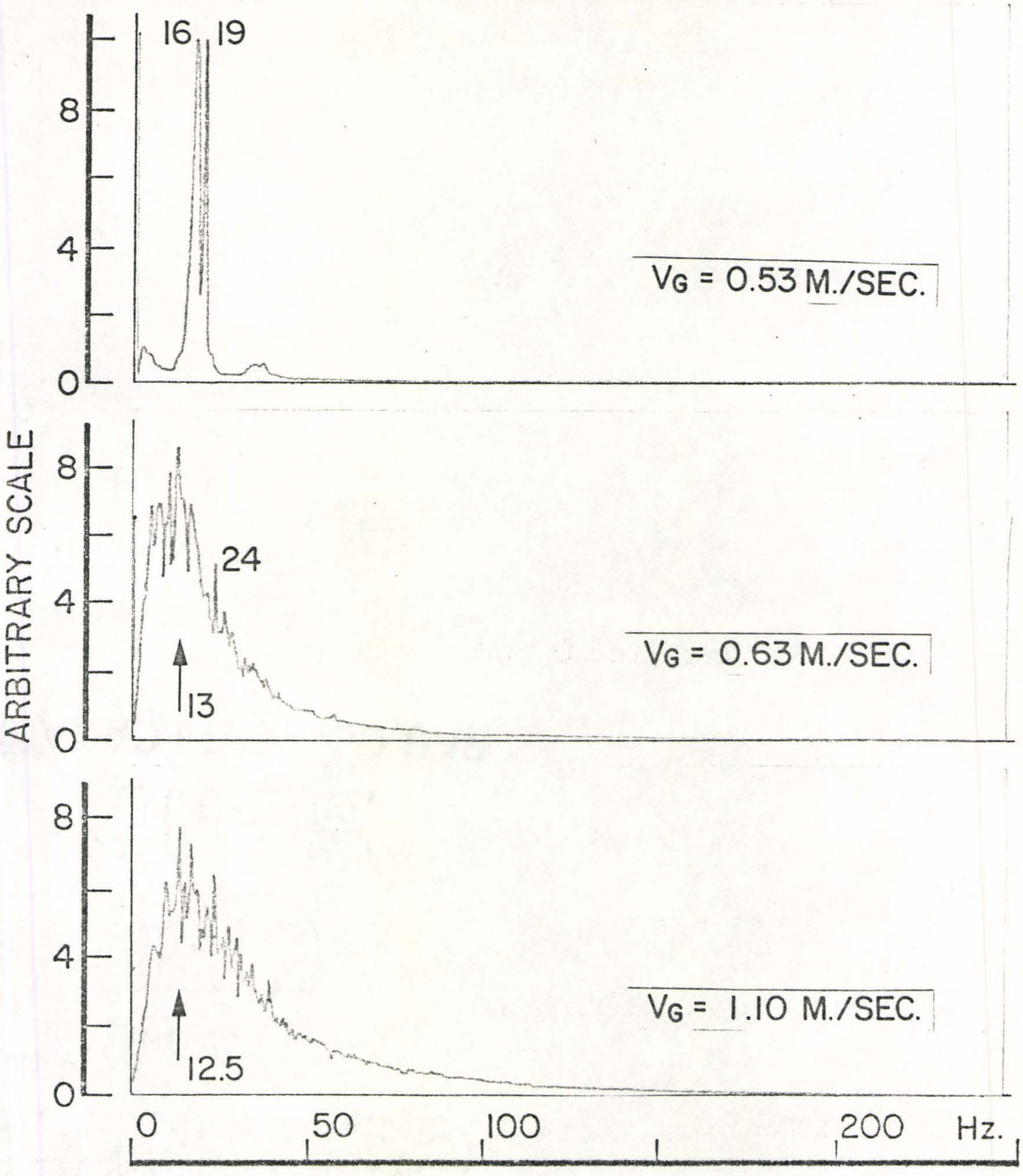


VELOCITY POWER-SPECTRA FOR 15 UPSTREAM ROWS
(MOVABLE TUBES BLOCKED)
FIGURE 5.7

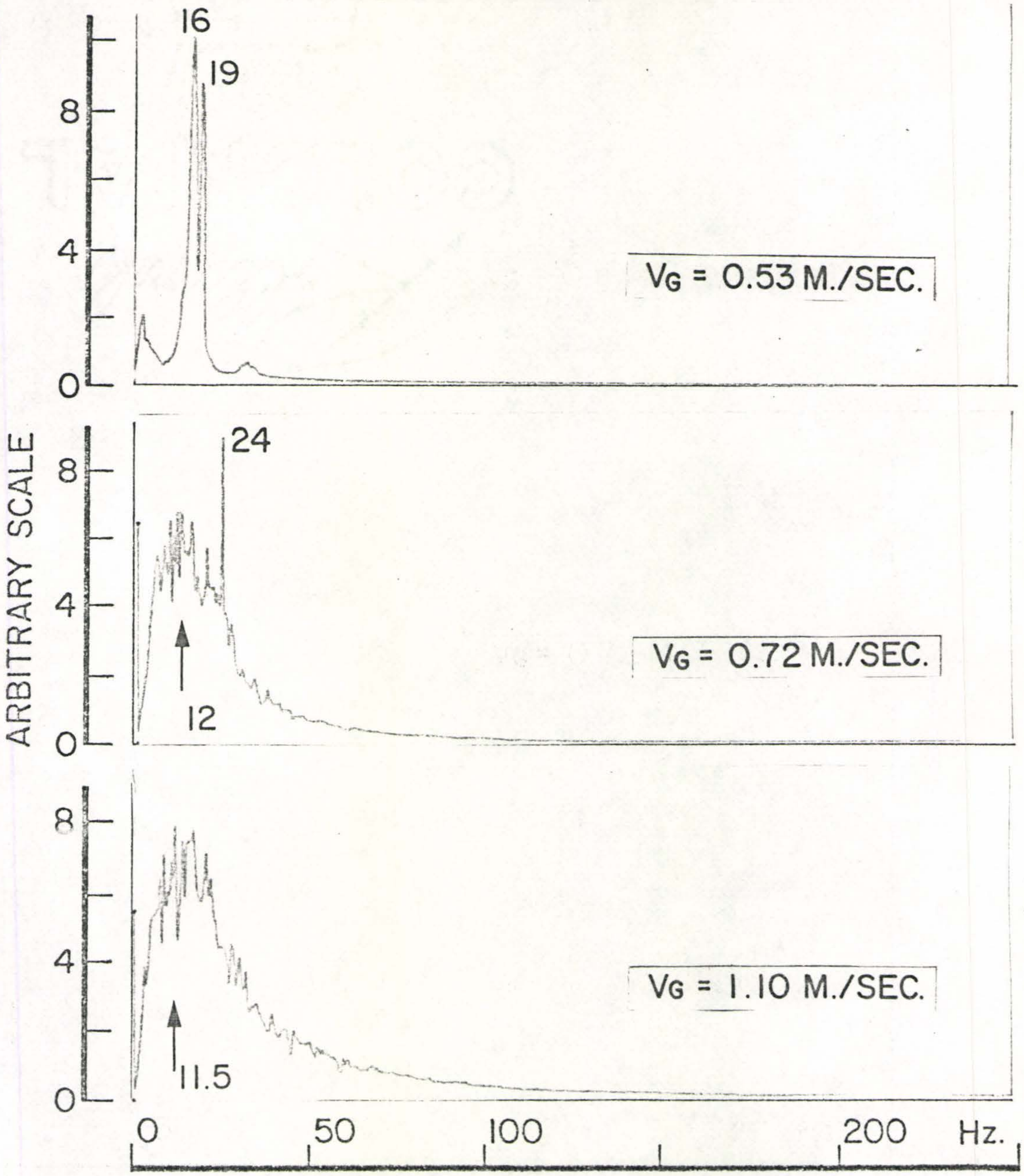


VELOCITY POWER-SPECTRA FOR 16 UPSTREAM ROWS

FIGURE 5.8

for sampling, the numerical Fourier transform of the signal leads to discrete peaks when the frequency is shifting slowly about some mean value. The energy content at the second harmonic around 35 Hz seen in previous records appears to have been reduced to a negligible amount. A dominant peak at 24 Hz for a flow velocity of $V_G$ = 0.72 m./sec. is again apparent and a corresponding regular tube response was also observed on the oscilloscope screen.

An interesting result was obtained when the number of upstream rows was further increased by one. At 17 rows upstream of the position where the hot-wire probe was located, a series of frequency spectra as shown in figure 5.9 were recorded. at $V_G$ = 0.68 m./sec. the large peak at 24 Hz seen so far has completely disappeared. No regular response of the movable tube on the oscilloscope screen was seen either. At this time there were 11 rows of tubes in the array upstream of the instrumented tube. A further increase in the number of upstream rows by two and four as shown in figures 5.10 and 5.11 respectively did not result in further changes in the velocity power spectra and no regular vibration of the instrumented tube was observed.

This result indicates that the discrete vortex-shedding which occurred at 24 Hz breaks down as the number of rows of tubes upstream of the instrumented tube is increased beyond ten. However, the large peak at the lower flow velocity ($V_G$ = 0.53 m./sec.) still exists even for the full array tested (figure 5.11). Thus, it appears that discrete vortex-shedding occurs

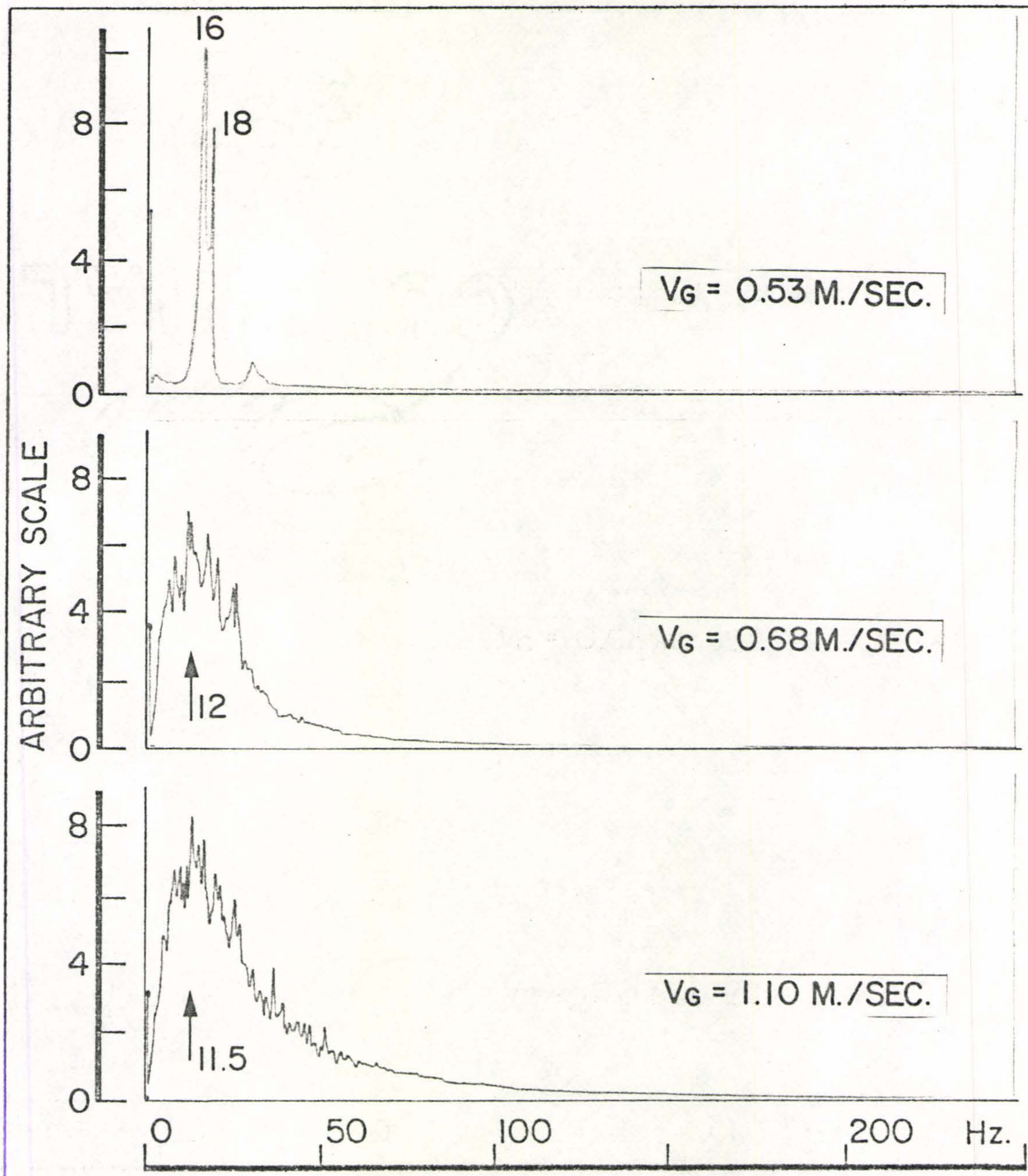


VELOCITY POWER-SPECTRA FOR 17 UPSTREAM ROWS

FIGURE 5.9

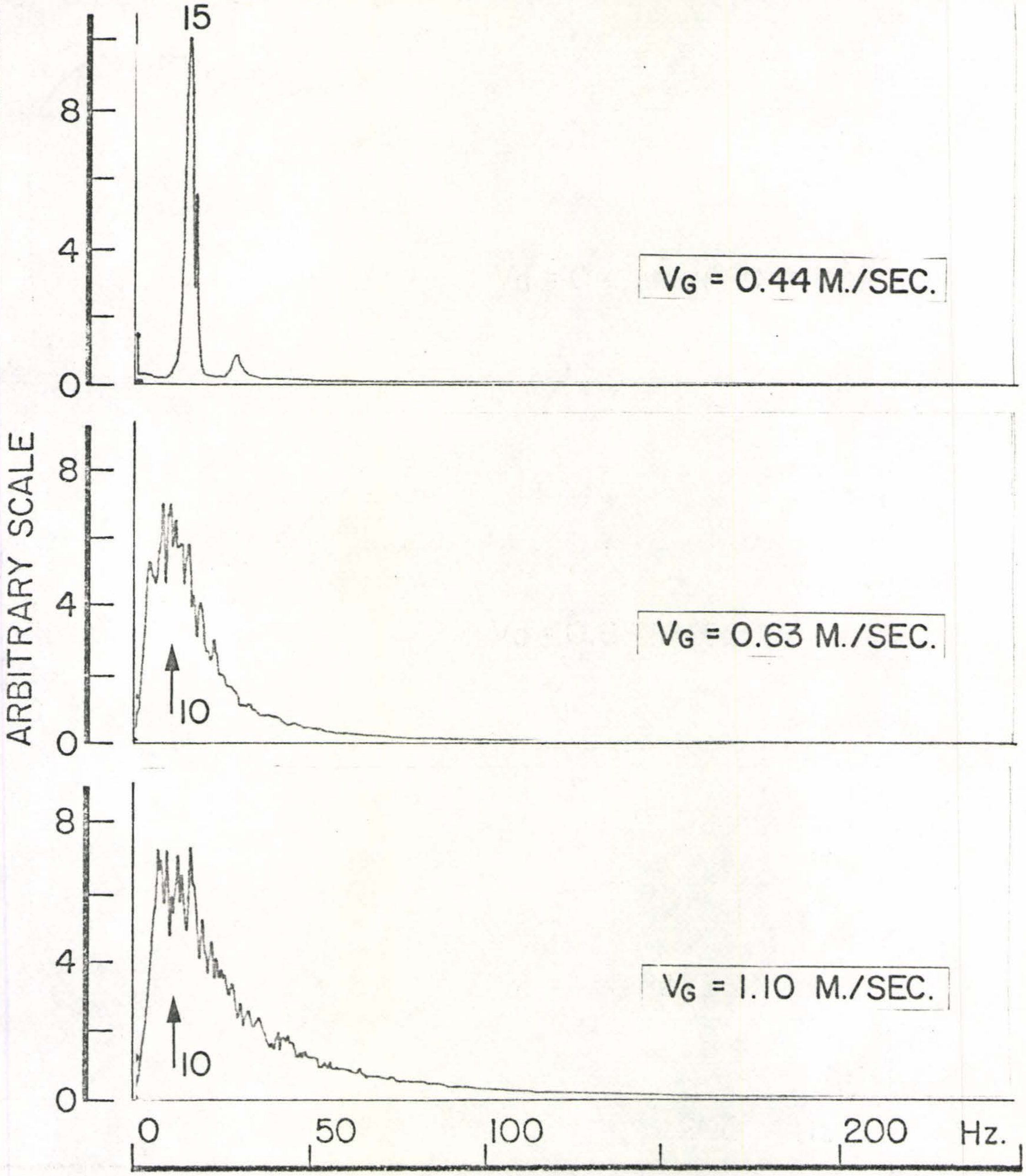


VELOCITY POWER-SPECTRA FOR 19 UPSTREAM ROWS

FIGURE 5.10

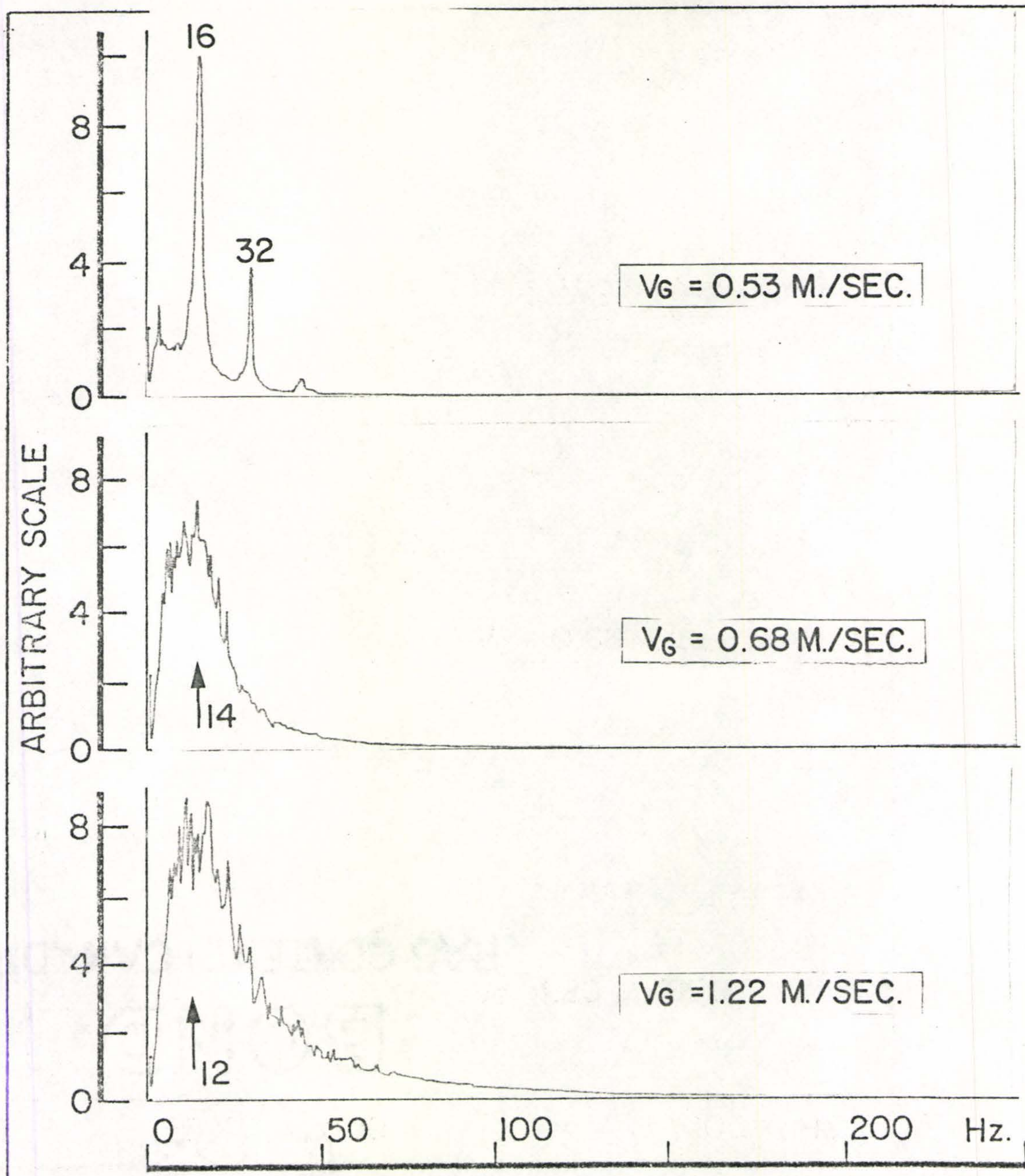


VELOCITY POWER-SPECTRA FOR 21 UPSTREAM ROWS
(FULL ARRAY)
FIGURE 5.11

at very low Reynolds numbers ($R < 10^3$) throughout the tube-bank of the type being tested but the tube response is a function of the number of tubes in the bank. In particular, the increase in turbulence deeper inside the tube-bank could have the effect of reducing the correlation length and hence preventing the tube from responding predominantly at its natural frequency. One might speculate that resonance could have been obtained had the tubes been tuned at about 16-18 Hz where the peak occurred in the velocity power-spectrum. By the time the velocity had been increased such that the peak at $S_G \simeq 0.83$ coincided with 24 Hz, the discrete vorticity had largely given way to narrow band turbulence. Any discrete vorticity remaining is probably washed out by the increase of turbulence intensity occurring with increased number of tube rows. It should be noted that even when the number of tube rows was small, the resonant tube amplitudes were extremely small.

Velocity power-spectra for the number of rows upstream of the hot-wire probe from 13 to 21 were recorded and corresponding Strouhal numbers were computed. The compiled data is given in table 5.1. The average value of Strouhal number as recorded in this table is $S_G \simeq 0.83$. Due to difficulty in precisely measuring the very low velocities involved, the Strouhal numbers could be estimated to an accuracy of $\pm$ 0.1 ($\pm$ 12%) only. The coefficient of lift described earlier in this section could also be estimated within an accuracy of $\pm$ 32% ($C_L = 0.41 \pm 0.13$) only. This

TABLE 5.1

| Number of Rows Up-stream of Hot-Wire Probe | Average Velocity in the Minimum-Gap $V_G$ = (m./sec.) | Peak Frequency in the Frequency Spectrum f = (Hz.) | Computed Strouhal Number $S_G = fd/V_G$ |
|---|---|---|---|
| 13 | 0.53 | 18 | 0.86 |
| | 0.69 | 11,24 | 0.41, 0.89 |
| | 1.22 | 13 | 0.26 |
| 14 | 0.53 | 17 | 0.81 |
| | 0.69 | 11,24 | 0.41, 0.89 |
| | 1.22 | 11.5 | 0.24 |
| 15 | 0.53 | 17 | 0.81 |
| | 0.69 | 13.5, 24 | 0.5, 0.89 |
| | 1.10 | 11 | 0.25 |
| 15 With all the movable tubes blocked | 0.53 | 16, 19 | 0.76, 0.90 |
| | 0.63 | 13, 24 | 0.53, 0.97 |
| | 1.10 | 11.5 | 0.26 |
| 16 | 0.53 | 16, 19 | 0.76, 0.90 |
| | 0.72 | 12, 24 | 0.43, 0.85 |
| | 1.10 | 11.5 | 0.26 |
| 17 | 0.53 | 16, 18 | 0.76, 086 |
| | 0.68 | 12 | 0.45 |
| | 1.10 | 11.5 | 0.26 |
| 18 | 0.53 | 16 | 0.76 |
| | 0.64 | 12 | 0.48 |
| | 1.10 | 12.5 | 0.28 |
| 19 | 0.44 | 14.5 | 0.83 |
| | 0.63 | 10 | 0.41 |
| | 1.10 | 10 | 0.23 |
| 20 | 0.53 | 15.5 | 0.74 |
| | 0.63 | 12 | 0.49 |
| | 1.10 | 11 | 0.25 |
| 21 | 0.53 | 16 | 0.76 |
| | 0.68 | 14 | 0.52 |
| | 1.22 | 12 | 0.25 |

seemingly large variation in data is primarily due to (a) uncertainty in the measurement of very small tube amplitudes involved (amplitudes of the order of 0.16 mm. could be measured within a precision of $\pm$ 15% only) and (b) uncertainty in the measurement of very small flow velocities (velocities of the order of 0.7 m./sec. could be measured within a precision of $\pm$ 10% only).

The effect of tube rows in an array on its velocity power-spectra has never been studied before. The study of Chen [89] on Strouhal numbers in tube-bundles was conducted for a five row deep tube-bundle only and vortex-shedding measurements were recorded after the third row to tubes. Chen covered a Reynolds number range of 1.5 - 6 x $10^4$ (based on velocity between two adjacent tubes in a transverse row). Dye and Abrahams' [94] experiments on vortex-shedding frequencies were conducted in a four row deep staggered tube model. Funakawa [6] recorded vortex-shedding response for a five row deep tube array only. He tested arrays having large longitudinal spacings and observed vortex-shedding response for Reynolds numbers up to approximately 9 x $10^3$ (based on upstream flow velocity). As is apparent, the studies of all these authors were restricted to a maximum of five rows of tubes in the tube-bundle. This may explain why vortex-shedding has been noted for such high Reynolds numbers.

Batham [111] and Heinecke [132] have noted that periodic vortex-shedding is unlikely to occur for arrays with $p/d < 2$.

However, the present experiments have clearly shown that vortex-shedding can be induced even in an array for p/d = 1.375 but at low Reynolds numbers only.

Thus from the results of the present experiments and the information available to date from the literature it can be conjectured that vortex-shedding exists even in a narrowly spaced tube-bundle and the existence of regular periodicity due to vortex shedding is a function of both Reynolds number and the number of rows of tubes in the array. Vortex-shedding seems to have become more coherent at low values of the Reynolds number. As the Reynolds number or the number of tube rows in the array is increased, turbulence increases and the periodicity in the flow-field breaks down. Therefore, deep inside the tube-bundle studied the assumption of regular vortex-shedding is not a working hypothesis at $R > 10^3$ and Chen's [89] correlations are not valid. Chen [89] has also observed that the excess energy of vortex-shedding over the broad turbulence spectrum will diminish to a negligible amount when $R = 6 \times 10^4$ (based on velocity betwwen two adjacent tubes in a transverse row). However, this observation was for a five row deep tube-bundle only and is not valid in general. The exact number of tube rows and the upper limit on Reynolds number beyond which no concentration of energy at Strouhal frequency is available in a particular tube-bundle is expected to depend on the longitudinal and transverse tube spacings in the array.

As seen in the present experiments the Strouhal frequency occurs at such low velocities that the von Karman vortex effect is expected to be of a negligible factor in promoting large amplitude tube vibrations. The dynamic pressure at these flows is too small to result in any noticeable vibratory build up, particularly if sufficient tube damping exists.

In summary, it can be stated that in the present tube-bundle of $X_T = 2.38$, $X_L = 0.688$ and $p/d = 1.375$, discrete periodicity in the flow has been observed up to a Reynolds number of $1.2 \times 10^3$ and for a maximum of 10 rows in the array. Strouhal number based on minimum-gap velocity is $0.83 \pm 0.1$. The coefficient of lift at $R_G = 1.2 \times 10^3$ as the tube responded to vortex-shedding frequency is $C_L = 0.41 \pm 0.13$ (based on the velocity between two adjacent tubes in a transverse row). However, as the Reynolds number is increased, the well-defined periodicity in the flow breaks down and the flow-field exhibits a narrow band velocity power-spectrum. A further increase in Reynolds number broadens the frequency band. The effect of increasing the number of rows of tubes in the array also results in discrete periodicty due to vortex-shedding giving way to a narrow-band turbulence spectrum. While the first few rows of tubes in a tube-bundle may be excited by vortex-shedding, the amplitudes are likely to be insignificant at least for tubes in a gas flow.

## 5.2 Flow-Field Characteristics at Higher Reynolds Numbers

As the rate of air flow in the wind-tunnel was increased beyond the point at which vortex-shedding response was observed, the flow-field velocity fluctuations became narrow band random fluctuations.

A typical hot-wire probe output signal recorded at location 'H' in the array (figure 5.1) is shown in figure 5.12. The top trace was recorded at $V_G$ = 4.57 m./sec. ($R = 7.8 \times 10^3$) and indicates a random signal. The bottom trace was recorded at a higher flow velocity, $V_G$ = 7.32 m./sec. ($R = 1.25 \times 10^4$). The output signal is again a random signal, however, the maximum level of the fluctuations appears to have reduced and the frequency band broadened at the higher Reynolds number.

### 5.2.1 Effect of Number of Samples and Probe-Orientation on Frequency Spectrum

The above signal was analysed using a Fourier Analyser and a velocity power-spectrum as shown in figure 5.13 was computed. It is apparent from this record that most of the velocity fluctuations in the flow-field are concentrated within a small band of frequencies. The spectrum exhibits a well defined peak at about 32.5 Hz. This spectrum was computed by taking an average of 50 records of the signal. In order to determine the effect of number of records on the shape of the frequency spectrum two more spectra were computed, one an average of 500 records and the second an average of 1000 records. The results are shown in figure 5.14. It is seen that the effect of an increase in the number of samples is to smooth out the frequency-spectrum slightly. However, the peak in

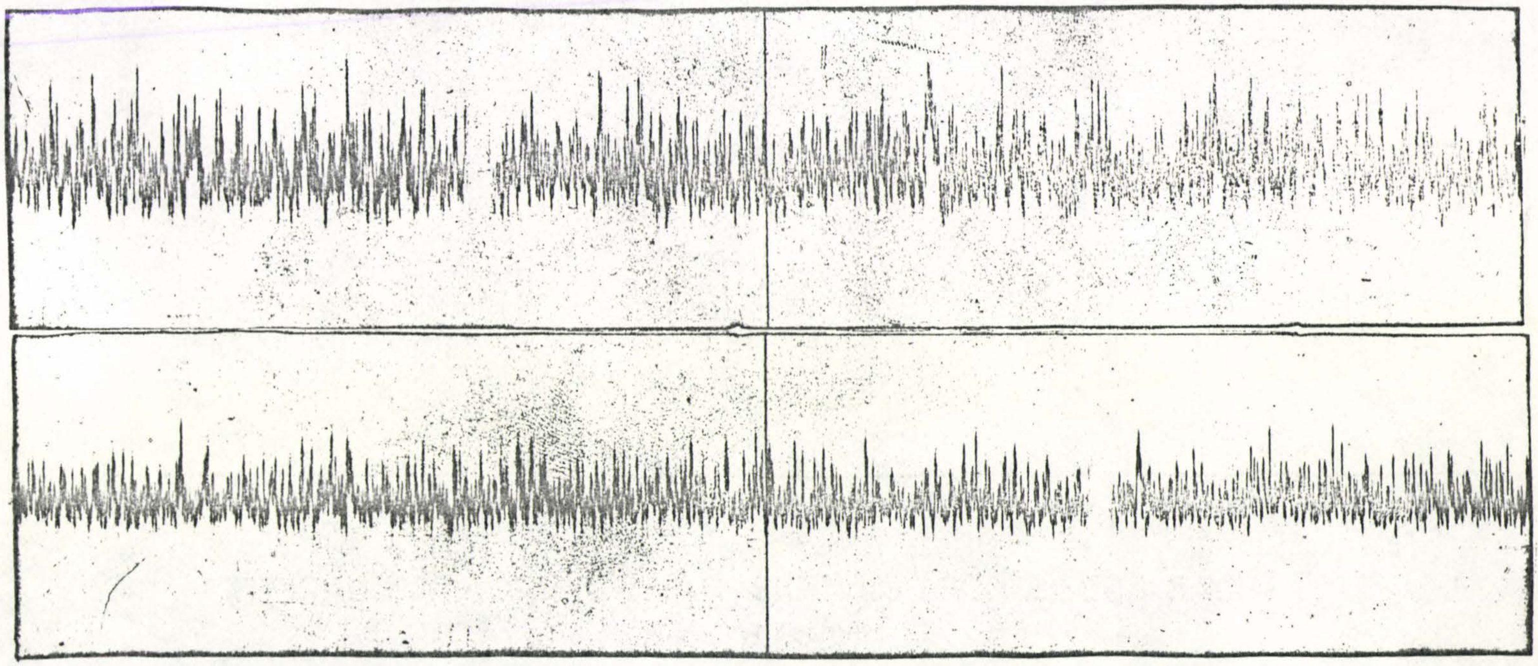

TYPICAL HOT-WIRE OUTPUT SIGNALS (FOR 2 SECS. EACH)
(AIR DAMPING)

TOP TRACE : TUBES NOT VIBRATING ; $V_G$ = 4.57 M/SEC.
BOTTOM TRACE : TUBES VIBRATING ; $V_G$ = 7.32 M/SEC.

FIGURE 5.12

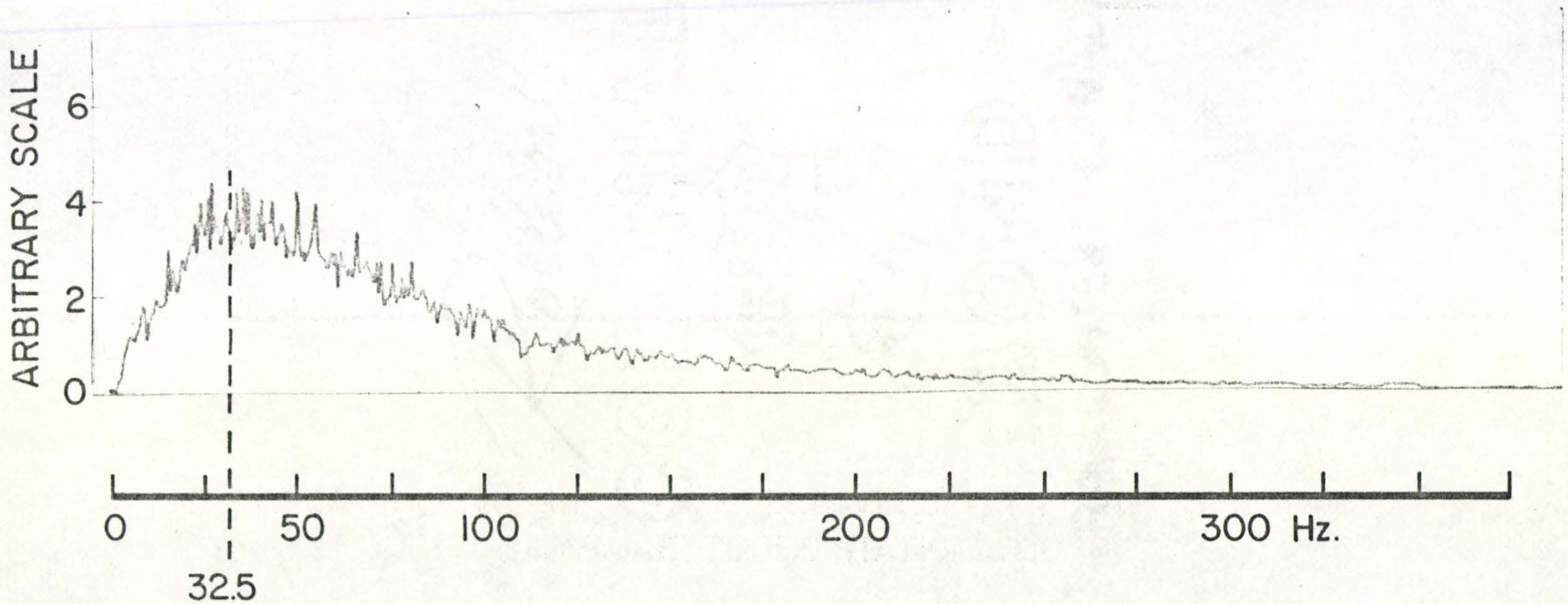


A TYPICAL RECORD OF FLOW-FIELD VELOCITY POWER-SPECTRUM
(MOVABLE TUBES STATIONARY)

FIGURE 5.13

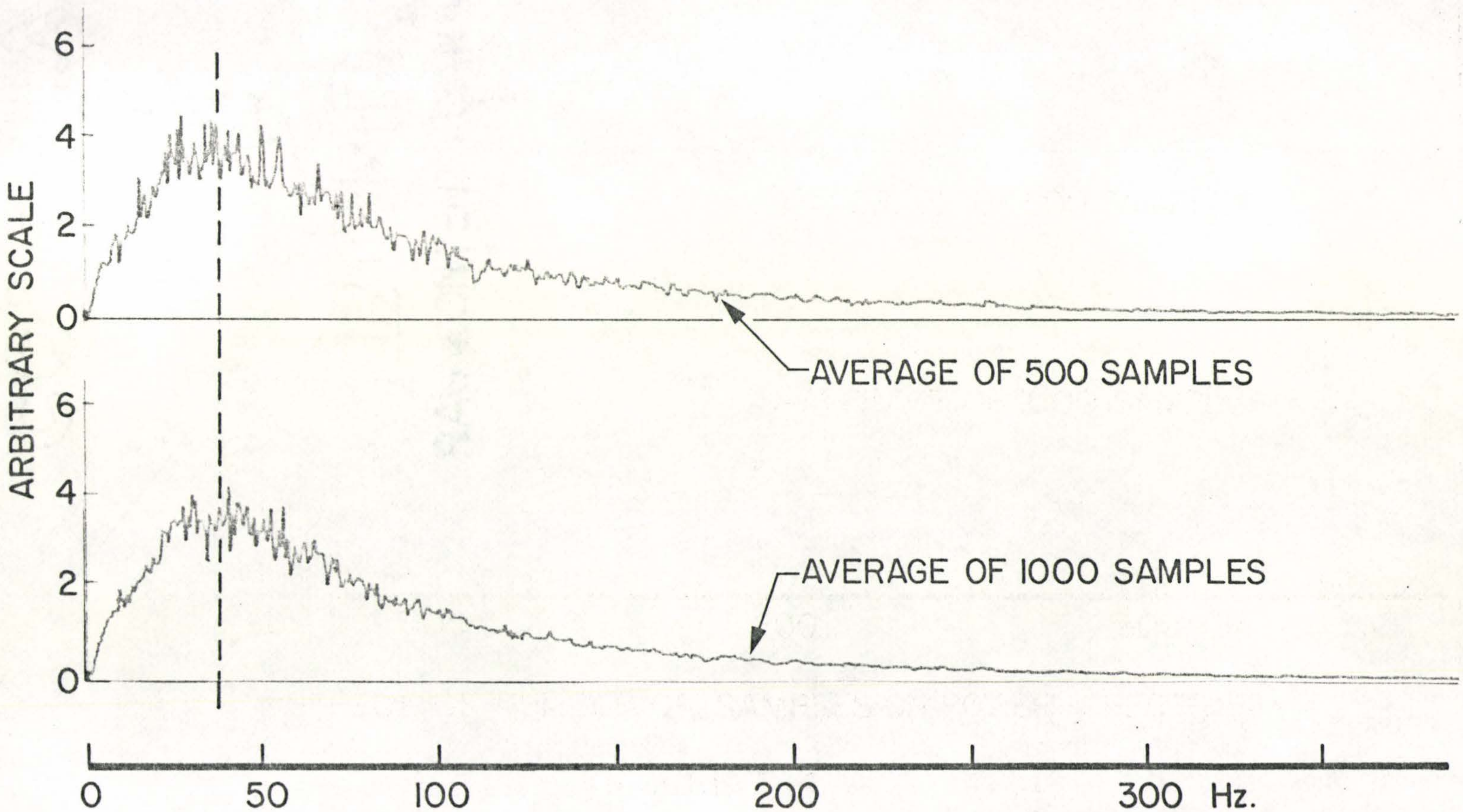


EFFECT OF NUMBER OF SAMPLES ON POWER-SPECTRUM

FIGURE 5.14

the spectrum still occurs at the same frequency. As the frequency corresponding to the highest peak in the spectrum is of most interest in the present analysis it was decided to use an average of only 50 records of signals for computing the frequency spectra. This resulted in (a) a savings in the computation time required and (b) a considerable reduction in the length of time the wind-tunnel had to be run to acquire the desired data.

The hot-wire probe was installed in the middle of the gap between two tubes and on the line joining the centres of these tubes as shown in figure 5.1 by the location marked 'H'. The effect of rotation of the probe about this mean position on the velocity power spectra was determined by rotating the probe $\pm$ $15^{\circ}$ to the mean position. The three frequency spectra so obtained are shown in figure 5.15. The peak in the three spectra is seen to occur at the same frequency thus indicating a relative insensitivity of location of the peak in the spectrum to small variations in probe orientation.

### 5.2.2 Turbulence Intensities in the Tube-Bundle

The turbulence intensities were measured in the full tube-bundle by installing a hot-wire probe after 2, 4, 6 and 20 upstream rows respectively. The data recorded at a Reynolds number of 1.41 x $10^4$ (based on minimum-gap velocity) is given below:

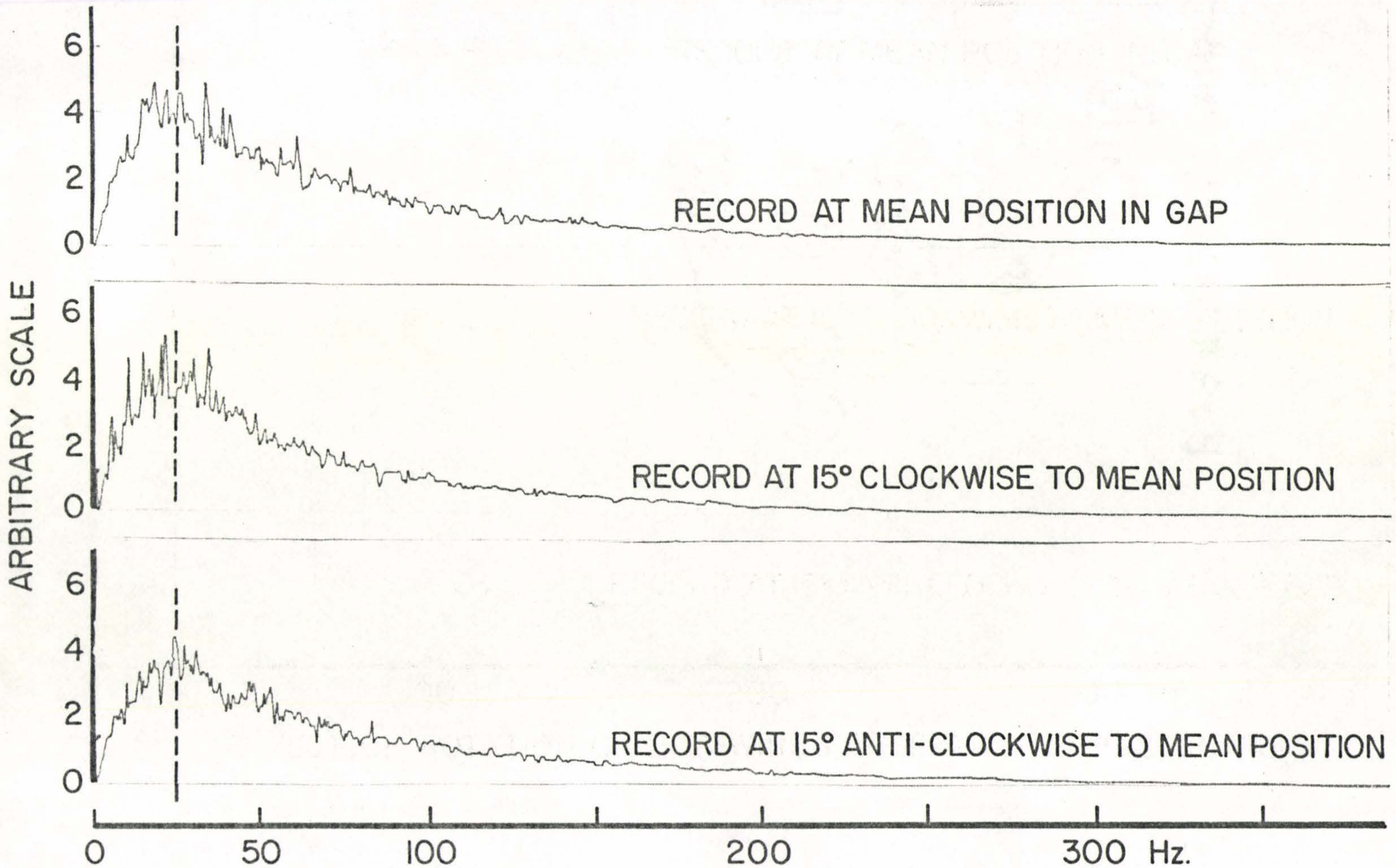


EFFECT OF ROTATION OF HOT-WIRE PROBE ON POWER-SPECTRUM

FIGURE 5.15

| Location of probe | Turbulence instensity (average) |
|---|---|
| Upstream of tube-bundle | 0.14% |
| After 2 upstream rows | 0.76% |
| After 4 upstream rows | 2.4% |
| After 6 upstream rows | 2.5% |
| After 20 upstream ros | 2.5% |

The turbulence intensity after 20 upstream rows decreased to about 2.27% at $R = 1.72 \times 10^4$ and was recorded to have increased to about 3.26% at $R = 0.68 \times 10^4$. The turbulence intensity appears to increase with a decrease in Reynolds number. The turbulence intensities could be measured to within a precision of $\pm$ 10% only.

The turbulence intensity in the present array seems to have attained a constant value after about four upstream rows. Batham [111] has measured mean pressure drops across successive tube rows and also observed that the pressure drop had attained an approximate constant value after the 4th row in case of uniform incident stream in a closely packed in-line array. It appears then, that at least four upstream rows of tubes are required for modelling phenomena deep inside a tube-bank.

A perforated sheet metal plate (3 mm. diameter holes, 5 mm. equilateral triangular pattern) was next installed upstream of the tube-bundle so as to increase the upstream turbulence intensity from 0.14% to 0.66%. Velocity power-spectra before and after installing the screen were computed and are shown in Figure 5.16. No significant difference in the two spectra is apparent. The peaks occur at very nearly the same frequencies. The turbulence intensity after 20 upstream rows was also not affected by the introduction of the upstream screen. Batham [111] also observed no effect of the incident turbulence on the excitation of the closely pitched array. However, he noticed that the high intensity turbulence would lead to the suppression of vortex-shedding in widely pitched tube banks, especially from the first few rows. This supports the observations made above regarding the effect of number of tube rows on vortex-shedding response. Zdrakovich [112] observed that the difference between the response of the tube with and without the upstream grid decreased as $X_L$ was decreased (for the present array, $X_L$ = 0.688 which is very small).

### 5.2.3 The Nature of the Flow Field

Wallis [99] has conducted flow-visualisation studies through a series of tube bundles. The highest water flow velocity reached was 5 cm./sec. (upstream) which corresponds to a Reynolds number of $2.7 \times 10^3$. Some of the photographs taken by him are shown in figure 5.17. It is noticed that in a staggered tube arrangement where $X_T > 2$ and in in-line arrangements of tubes, the main stream flows with continuous high speed in flow lanes and retains a definite regularity as distinct from the eddying motion in the spaces behind the tubes. The number of eddies present in the "dead-water" regions is to some extent determined by the longitudinal pitch. With

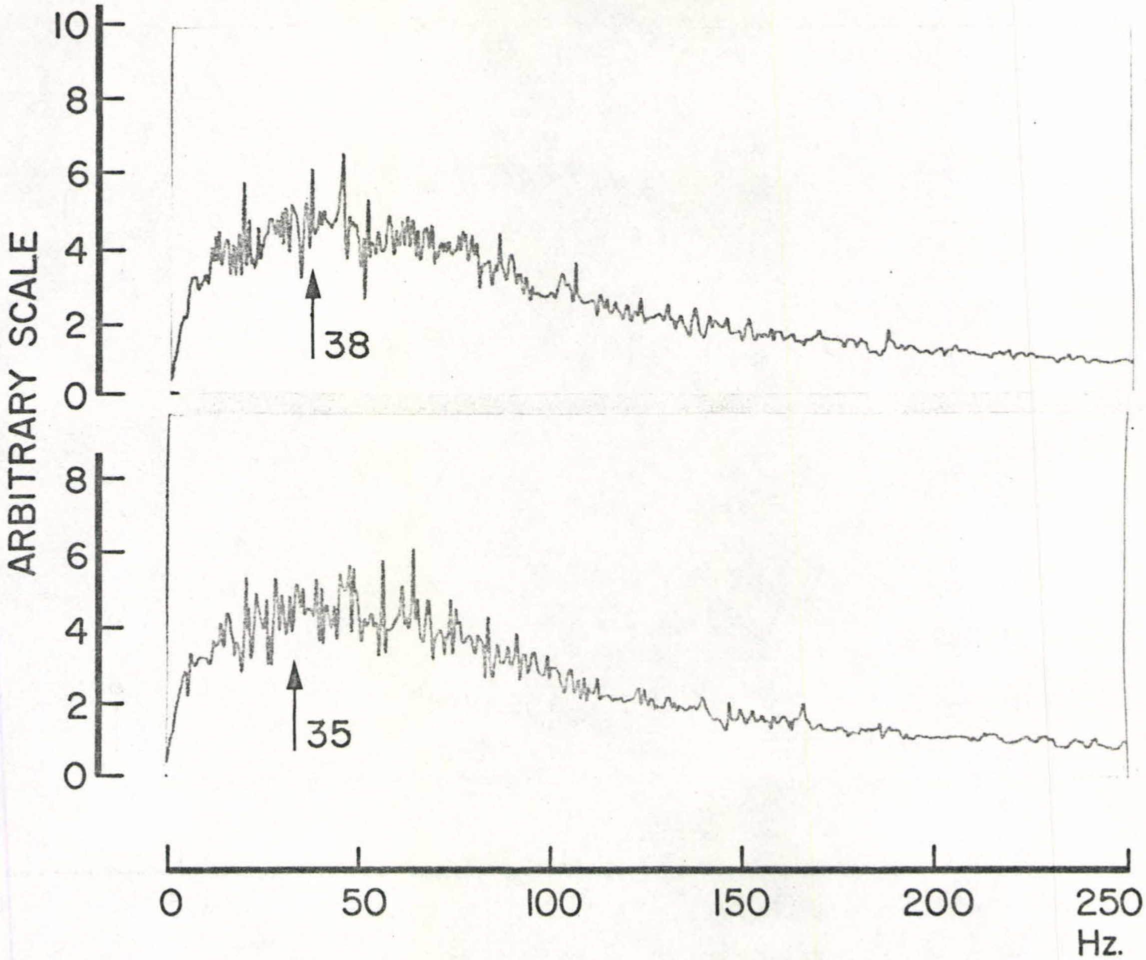


TOP : UPSTREAM - GRID INSTALLED
TURBULENCE INTENSITY = 0.66 %

BOTTOM : NO UPSTREAM GRID
TURBULENCE INTENSITY = 0.14 %

EFFECT OF UPSTREAM-GRID ON VELOCITY POWER SPECTRUM
( $V_G$ = 4.16 M/SEC )

FIGURE 5.16

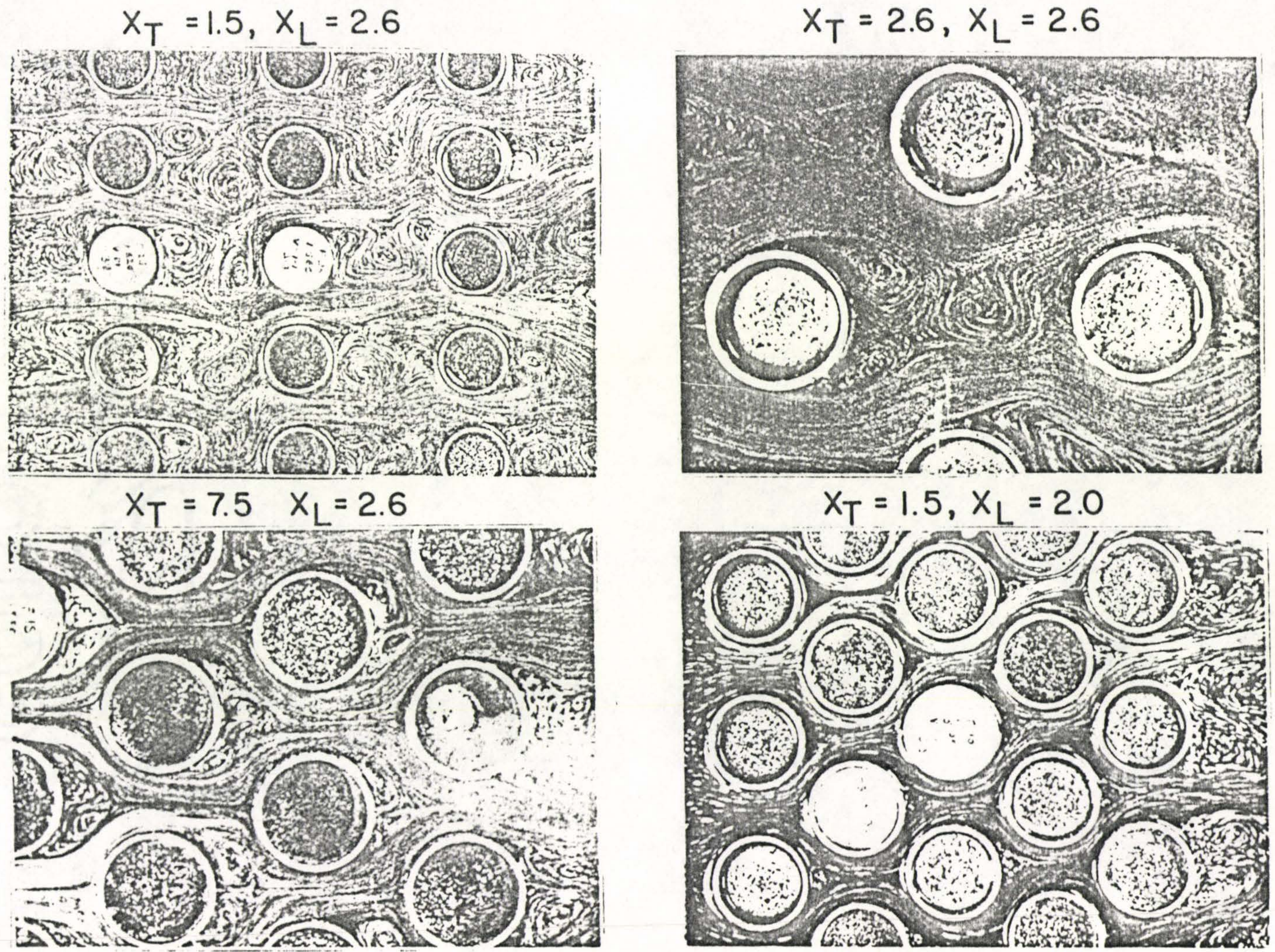


FLOW PATTERNS BY WALLIS (REF. 99)

FIGURE 5.17

longer longitudinal pitch the eddies are less rigidly held at the back of the tubes and are carried more freely downstream. For staggered arrays where $X_T < 2$, the "dead-water" regions are constricted and no longer extend from one tube to the tube directly behind it. In the extreme case with close pitching the "dead-water" region appears only as a very small triangular prism attached to the downstream side of each tube.

In the staggered array presently being tested, $X_T = 2.38$, and therefore, it is expected that the flow-field will consist of flow lanes and so called "dead-water" regions behind each tube in the sense described by Wallis. Few eddies are expected in the "dead-water" region as the longitudinal pitch is very small ($X_L$ = 0.688). Velocity power-spectra at locations marked 1, 2 and 3 in the flow-field as shown in figure 5.18 were recorded. It is noticed that the flow fluctuations at location-3 are far more intense than at locations-1 or 2. In fact, the spectrum at location-3 had to be replotted using a reduced scale as shown in the bottom trace. The peak in the three spectra occurred at essentially the same frequency. The flow fluctuations at location-2 are not as large as at location-3 thus indicating that the "dead-water" region is probably restricted to a very small area attached to the back of each tube and does not extend to the tube directly behind it. This qualitative test has indicated the possible existence of so called "flow lanes" and "dead-water" regions in the flow field. This test was run at $V_G \doteq 4.27$ m./sec. which corresponds to a Reynolds number of $7.3 \times 10^3$. With an increase in

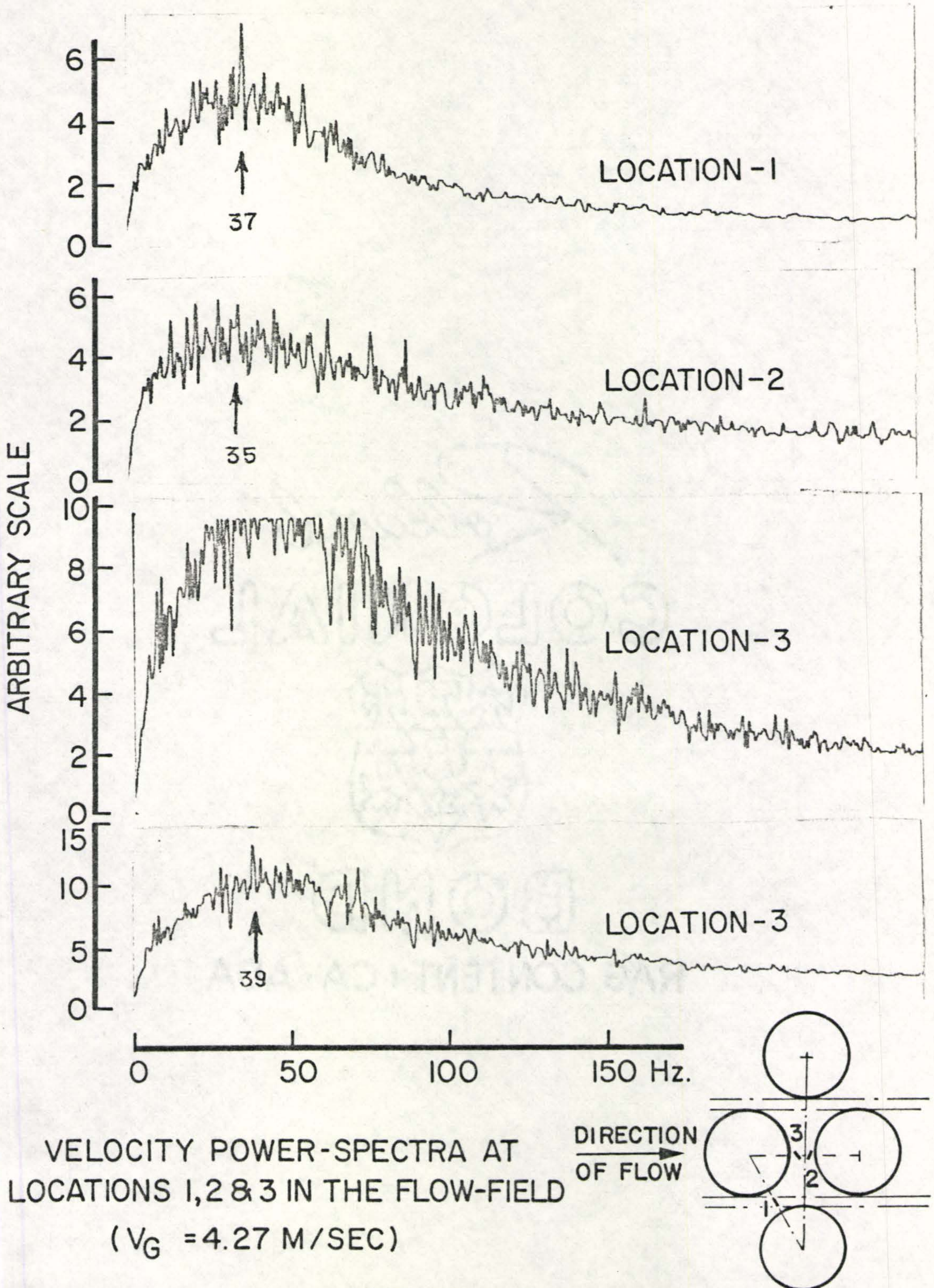


VELOCITY POWER-SPECTRA AT LOCATIONS 1,2 & 3 IN THE FLOW-FIELD ($V_G$ = 4.27 M/SEC)

FIGURE 5.18

Reynolds number to 1.2 x $10^4$ the flow-field remained unchanged. The nature of the flow-field was still unchanged even when the upstream turbulence intensity was increased from 0.14% to 0.66% by installing an upstream screen.

### 5.2.4 The Peak in the Frequency-Spectra

It is observed from the velocity power spectra recorded so far that although the flow-field is highly turbulent, a relatively large amount of energy is concentrated on a narrow frequency band. Therefore, it is possible to nondimensionalize the frequency spectrum using the diameter of the tube and the peak frequency, i.e., to use Strouhal number as a base rather than frequency. The result (shown in figure 5.19) is to collapse the various power-spectra so that their peaks coincide at a value around 0.21. This is nearly the same value as the Strouhal number for an isolated cylinder over most of the sub-critical range. To further establish this fact a series of frequency spectra were computed for a range of flow velocities and sizes of tube-bundles as shown in figures 5.20-5.25. The significance of a peak at 24 Hz observed in the bottom trace of figures 5.20-5.24 has been explained later in this chapter. The Strouhal numbers based on the frequency corresponding to the peak in the spectra were computed and the results are compiled in table 5.2. The average Strouhal number is 0.21 and the rest of the data lies within $^{+0.04}_{-0.03}$. No significant variation in the shapes of the power-spectra is apparent as the size of the tube-bundle is varied. A possible

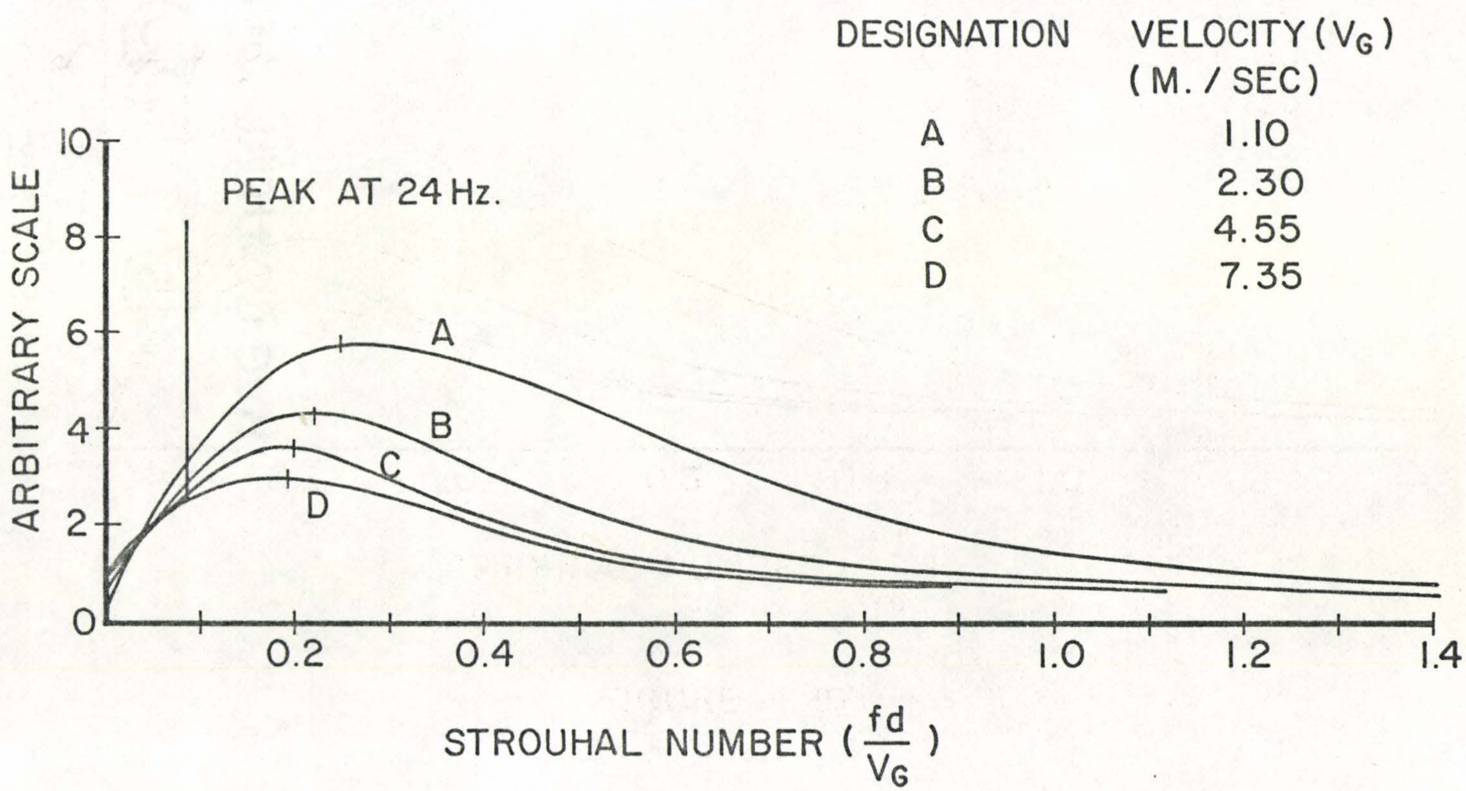
DESIGNATION
VELOCITY ($V_G$) (M. / SEC)
A 1.10
B 2.30
C 4.55
D 7.35
PEAK AT 24 Hz.
ARBITRARY SCALE
0
2
4
6
8
10
A
B
C
D
0.2
0.4
0.6
0.8
1.0
1.2
1.4
STROUHAL NUMBER ( $\frac{fd}{V_G}$ )

FIGURE 5.19

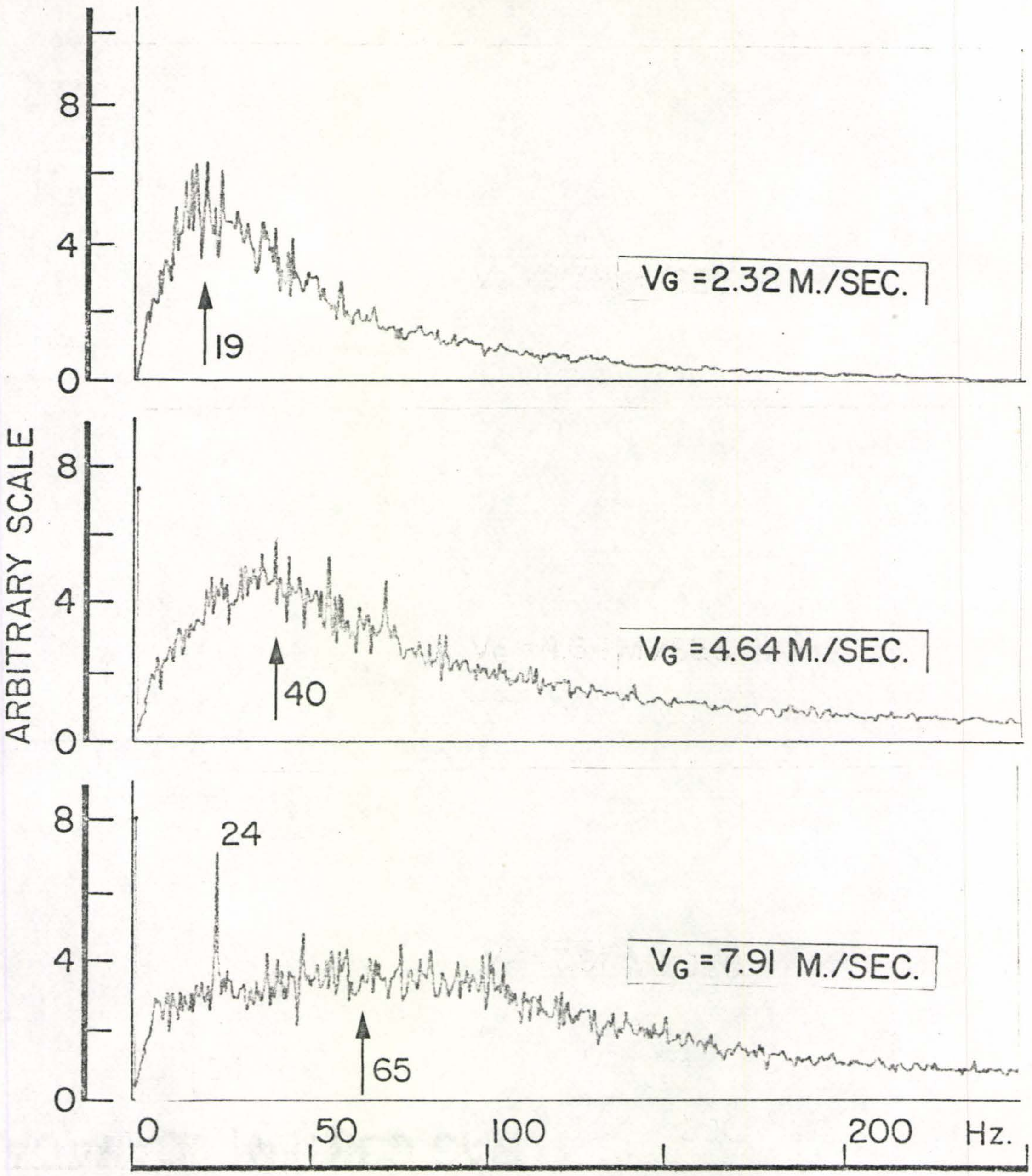


VELOCITY POWER-SPECTRA FOR 13 UPSTREAM ROWS

FIGURE 5.20

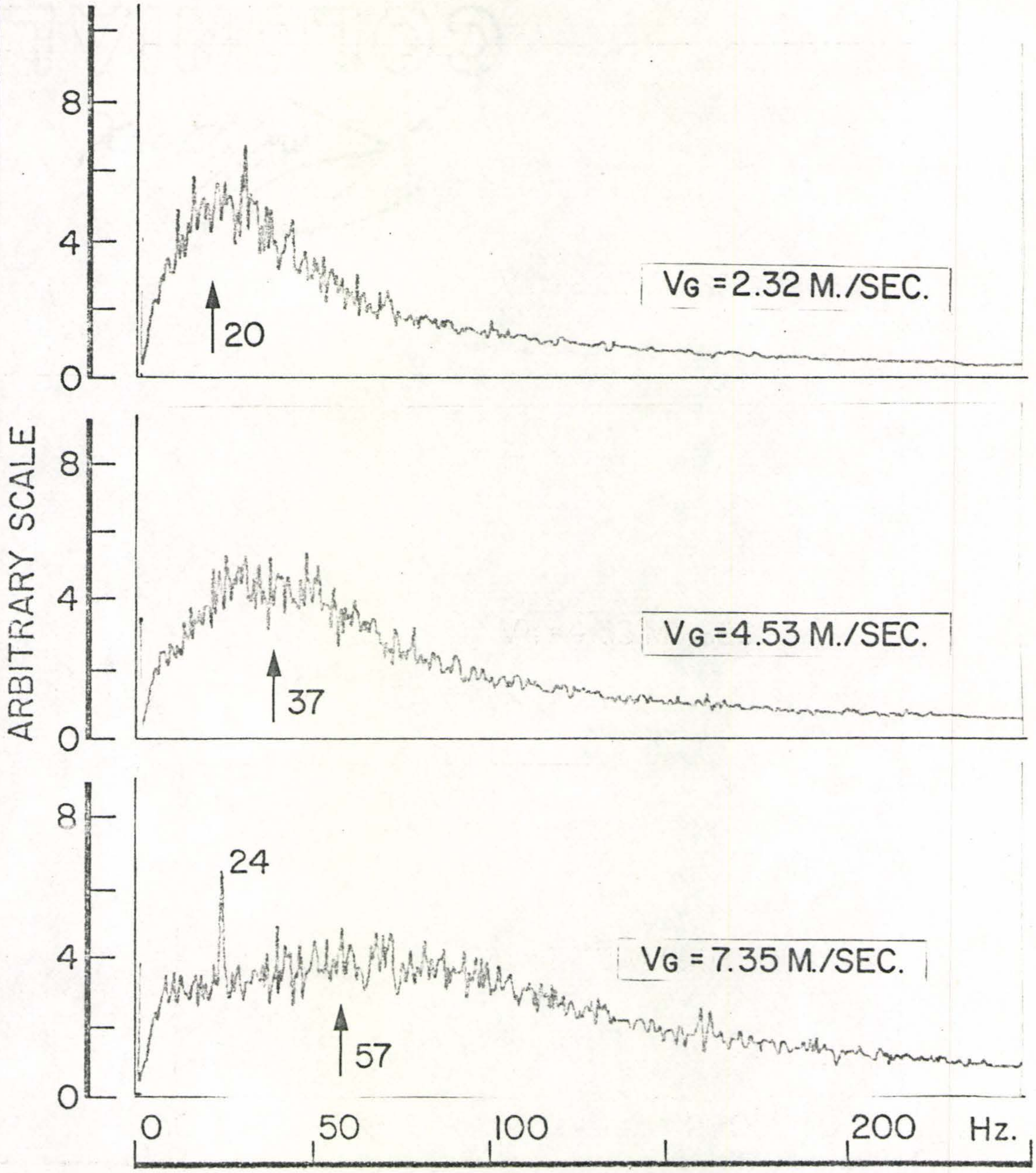


VELOCITY POWER-SPECTRA FOR 15 UPSTREAM ROWS

FIGURE 5.21

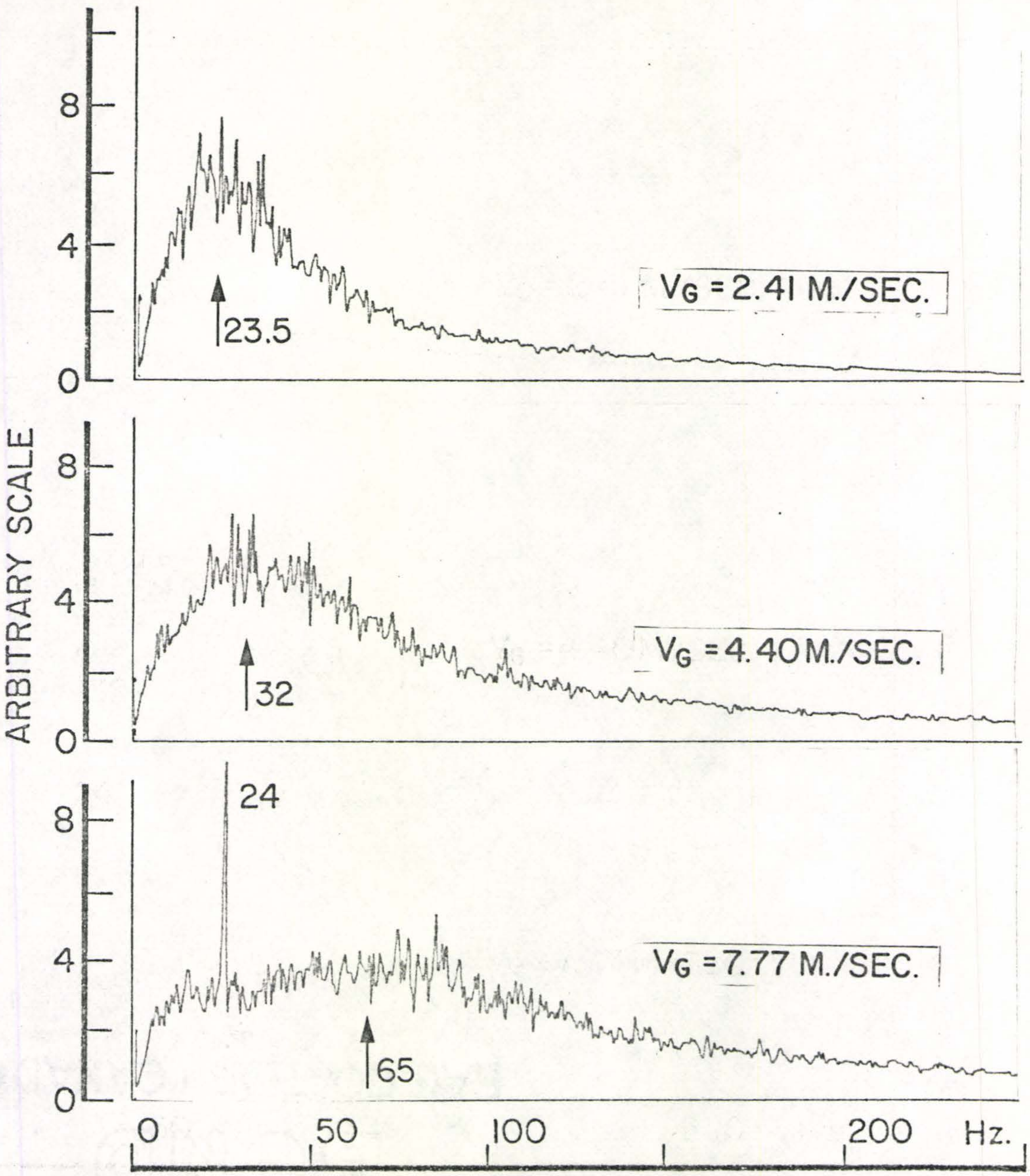


VELOCITY POWER-SPECTRA FOR 17 UPSTREAM ROWS

FIGURE 5.22

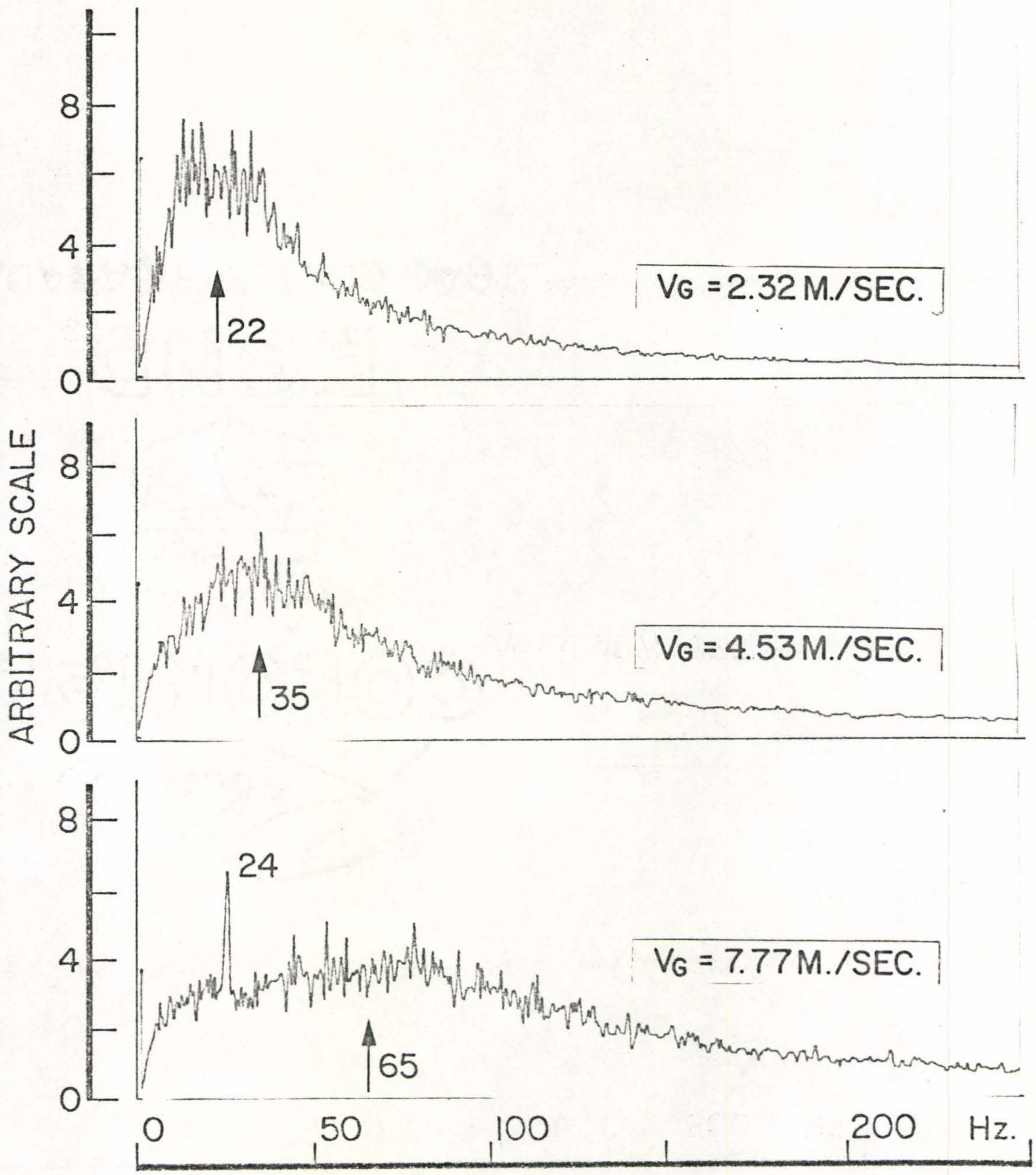


VELOCITY POWER-SPECTRA FOR 19 UPSTREAM ROWS

FIGURE 5.23

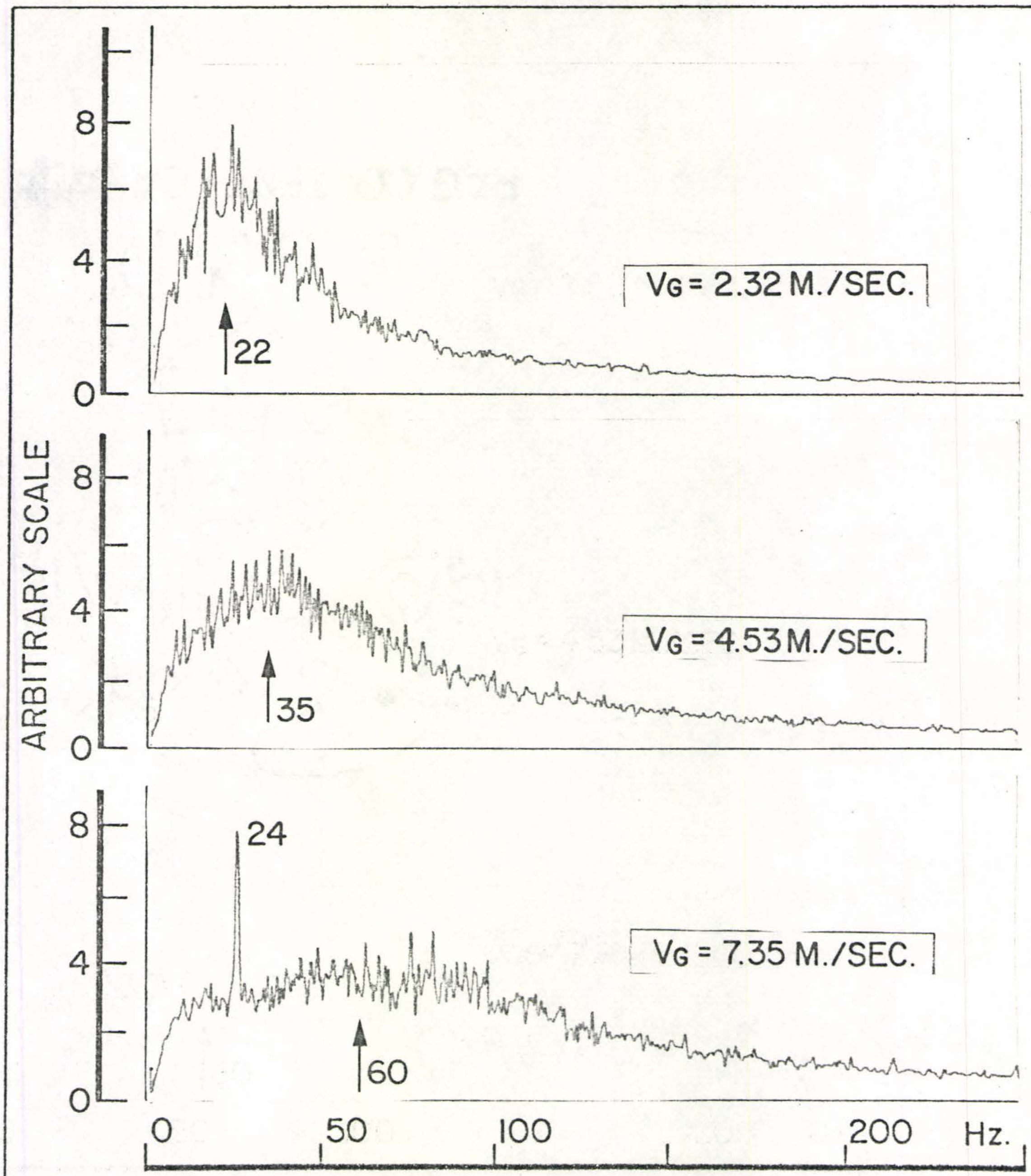


VELOCITY POWER-SPECTRA FOR 21 UPSTREAM ROWS
(FULL ARRAY)
FIGURE 5.24

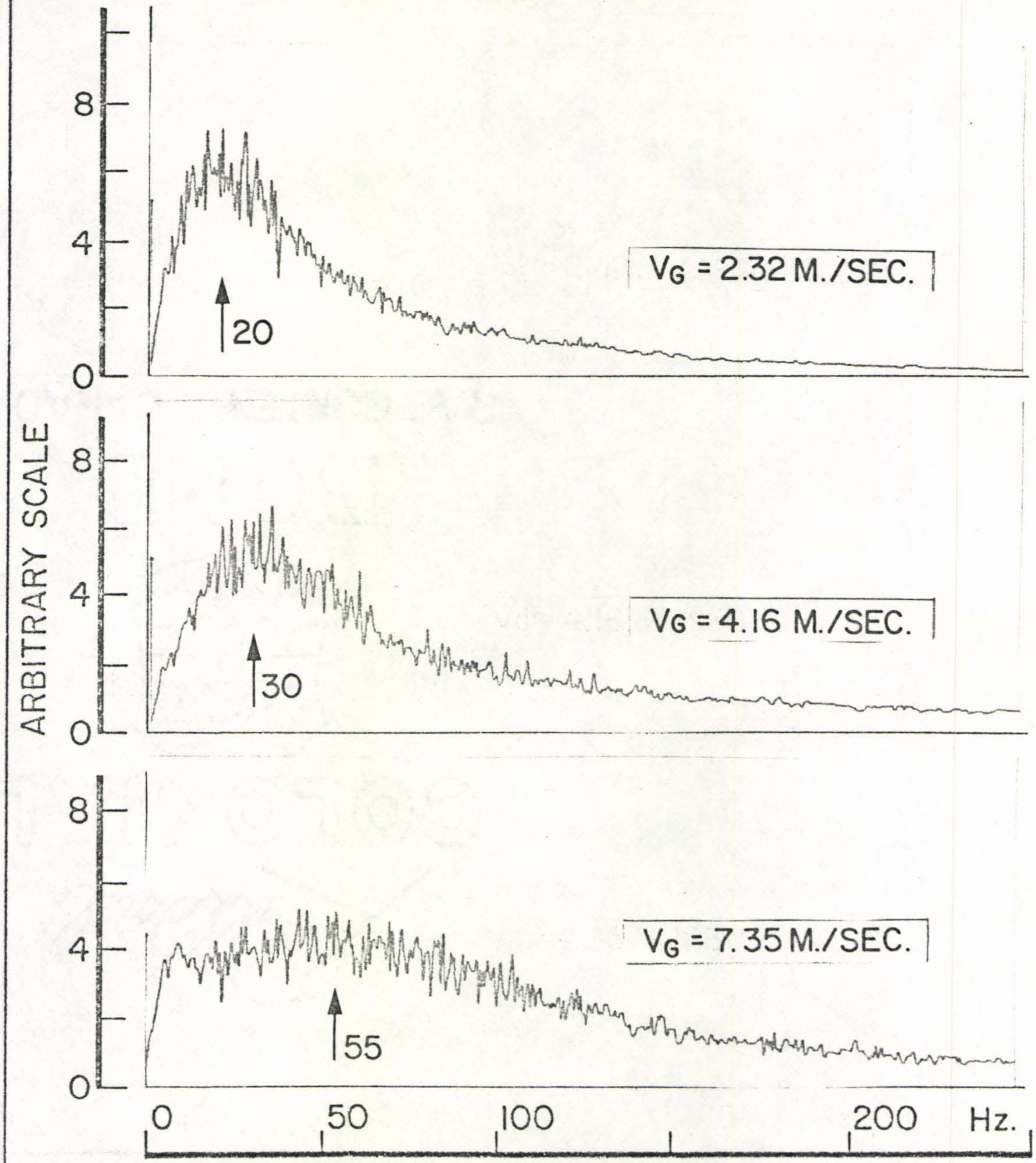


VELOCITY POWER-SPECTRA FOR 21 UPSTREAM ROWS
(MOVABLE TUBES TUNED TO $\delta$ = 0.04)
FIGURE 5.25

TABLE 5.2

| Number of Upstream Rows | Average Velocity in the Minimum-Gap $V_G$ = (m./sec.) | Peak Frequency in the Frequency Spectrum f = (Hz.) | Computed Strouhal Number $S_G = fd/V_G$ |
|---|---|---|---|
| 13 | 2.32 | 19 | 0.21 |
| | 4.64 | 40 | 0.22 |
| | 7.91 | (24) 65 | 0.21 |
| 14 | 2.32 | 18 | 0.20 |
| | 4.53 | 36 | 0.20 |
| | 7.63 | (24) 70 | 0.23 |
| 15 | 2.32 | 20 | 0.22 |
| | 4.53 | 37 | 0.21 |
| | 7.35 | (24) 57 | 0.20 |
| 16 | 2.32 | 21 | 0.23 |
| | 4.53 | 35 | 0.20 |
| | 7.35 | (24) 63 | 0.22 |
| 17 | 2.41 | 23.5 | 0.25 |
| | 4.40 | 32 | 0.19 |
| | 7.77 | (24) 65 | 0.21 |
| 18 | 2.32 | 22 | 0.24 |
| | 4.40 | 32.5 | 0.19 |
| | 7.77 | (24) 70 | 0.22 |
| 19 | 2.32 | 22 | 0.24 |
| | 4.53 | 35 | 0.20 |
| | 7.77 | (24) 65 | 0.21 |
| 20 | 2.32 | 20 | 0.22 |
| | 4.53 | 35 | 0.20 |
| | 7.35 | (24) 60 | 0.21 |
| 21 | 2.32 | 22 | 0.24 |
| | 4.53 | 35 | 0.20 |
| | 7.35 | (24) 60 | 0.21 |
| 21 With all the movable tubes tuned to $\delta = 0.04$ | 2.32 | 20 | 0.22 |
| | 4.16 | 30 | 0.19 |
| | 7.35 | 55 | 0.19 |

cause of a constant Strouhal number equal to 0.21 could be that the peak in the turbulence spectrum is originated from the separating shear layers from the surface of the tube and whose frequency of separation is equal to the vortex-shedding frequency from a single circular cylinder based on the minimum-gap velocity through the array. However, this argument has still to be verified and it remains a surprise that the peaks in the spectra occur at the Strouhal number for a single circular cylinder. The Reynolds number range for these experiments was $1.8 \times 10^3$ to $2 \times 10^4$ based on mean velocity through the minimum gap.

The frequency at the peak of the frequency spectra obtained from the present experiments is predicted fairly well (about 10% lower, see table 5.3) by Owen's [100] expression developed from theoretical formulations. Owen's model is based on a completely turbulent flow inside the tube-bundle and he balanced the rate of dissipation of turbulent energy and the rate at which the work is done on the gas by the mean pressure gradient. The following relationship resulted:

$$\frac{f\ell}{V_T} \cdot \frac{T}{d} = C\,(1 - \frac{d}{T})^2$$

where C is a constant to be derived experimentally. As the frequency at the peak in the frequency-spectra obtained from the present experiments can be predicted equally well by a simple Strouhal number relationship, it should be preferred over Owen's relatively complex relationship.

Putnam's [128] empirical relationship predicts the

TABLE 5.3

| S. No. | Gap Velocity $V_G$ = (m./sec.) | | Peak frequency from present experiments f = (Hz.) | Comparison with the peak frequency as predicted by the relationship of: | | | |
|---|---|---|---|---|---|---|---|
| | | | | Hill & Armstrong $f = V_u/\ell$ | Owen $\frac{f\ell}{V_T}\cdot\frac{T}{d} = 3.05(1-\frac{d}{T})^2 + 0.28$ | Putnam $\frac{f(T-d)}{V_T} = 0.12(\frac{2T-\ell}{d})$ | Walker & Reising $f = \frac{V_G}{4\ell}$ |
| | | | | $f_H$ = (Hz.) | $f_o$ = (Hz.) | $f_p$ = (Hz.) | $f_w$ = (Hz.) |
| 1 | 0.53 | REGULAR VORTEX-SHEDDING REGION | 18 | 8 | 4 | 4 | 8 |
| 2 | 0.69 | | 24 | 10 | 5 | 5 | 10 |
| 3 | 1.10 | TURBULENT BUFFETING REGION | 11 | 17 | 8 | 7 | 16 |
| 4 | 2.32 | | 20 | 36 | 17 | 15 | 33 |
| 5 | 4.53 | | 35 | 71 | 33 | 30 | 65 |
| 6 | 7.35 | | 60 | 115 | 54 | 48 | 105 |

present data to within about 20% (see table 5.3). However, his relationship is also more complicated than a simple Strouhal number relationship. In his map of Strouhal number as a function of spacing for staggered tube arrays most of the data is derived from Hill and Armstrong's [95] experiments, which are discussed below.

Hill and Armstrong's [95] relationship (see table 5.3) although simple in form, predicts about double the frequencies actually obtained in the present experiments. This relationship is based on the argument of successive compression and expansion of the gas as it flows through the tube-bank. Their data is reproduced in table 5.4 and has been recomputed to derive Strouhal number values ($S_G$) based on minimum-gap velocity. They used a three row staggered tube arrangement in which the distance between the first two rows was fixed and the position of the third row was varied so as to obtain a range of longitudinal pitches. It is seen that their data indicates a large variation in Strouhal number values. The last three points show a wider discrepancy from the first six points. The possible cause for this could be that as the third row of tubes is removed from the first two rows in this three-row staggered arrangement, the conditions of a typical tube-bundle no longer exist. In addition, Fitzpatrick and Donaldson [144] have recently shown that the results obtained from only a few rows of tubes may not be applicable to a deep tube-bundle. Stallbrass [88] has observed that in his experiments when four rows of cylinders were used, a highly turbulent flow existed behind

TABLE 5.4

Hill & Armstrong's Data

The test array was a three-row staggered array in which the distance between the first two rows was fixed ($\ell$ = 1.125 in., $X_L$ = 1.33) and the distance between the second and third row (= $L_1$) was varied.

Transverse pitch ratio = $X_T$ = T/d = 2/0.846 = 2.36

| S. No. | $L_1$ inches | $X_{L_1}$ = $L_1/d$ | Strouhal Number as given by Hill & Armstrong $S_T$ = | Recomputed Strouhal Number using minimum-gap velocity $S_G$ = |
|---|---|---|---|---|
| 1 | 0.81 | 0.96 | 0.61 | 0.46 |
| 2 | 0.93 | 1.00 | 0.50 | 0.44 |
| 3 | 1.09 | 1.29 | 0.45 | 0.48 |
| 4 | 1.20 | 1.42 | 0.37 | 0.42 |
| 5 | 1.28 | 1.51 | 0.39 | 0.44 |
| 6 | 1.30 | 1.54 | 0.34 | 0.40 |
| 7 | 1.58 | 1.87 | 0.28 | 0.32 |
| 8 | 1.62 | 1.92 | 0.28 | 0.32 |
| 9 | 1.95 | 2.31 | 0.26 | 0.30 |

the 2nd and subsequent rows only. The present experiments have indicated that at least four rows of tubes are required to establish conditions typical of those deep inside a tube-bank.

Walker and Reising's [90] correlation also predicts double the frequencies obtained in the present experiments (table 5.3). The authors have claimed a precision of only $\pm$ 30% for their relationship. Their correlation had been derived from the available field data.

Heinecke [132] has obtained a single frequency spectrum for a staggered tube-bundle of $X_T = 1.86$ and $X_{2L} = 1.5$ at a Reynolds number of $4.1 \times 10^4$. If velocity through the minimum-gap is used as the reference, the peak in the spectrum can be predicted by a Strouhal number equal to 0.23. He computes a value of 0.5 which is probably based on the velocity between two adjacent tubes in a row.

Stallbrass [88] conducted tests on a finned tube staggered array for $X_T = 2.2$ and $X_{2L} = 5.6$. He recorded acoustic resonance at $R = 2.64 \times 10^4$ (based on minimum-gap velocity). The present author computed the Strouhal number from this data and found $S_G = 0.21$. Stallbrass showed that for his experiments, Hill and Armstrong's relationship gave good predictions whereas Owen and Putnam's formulae predict too low a frequency. This is contrary to observations with the present data using minimum-gap velocity for reference and is an indication of the lack of confidence one has in the currently available predictive methods.

Based on the relationship $f\ell = V_u$, the frequencies recorded by Stallbrass and Hill and Armstrong are predicted correctly. However, this relationship predicts about twice the frequency values recorded in the present experiments. The possible cause for this wide discrepancy could be (a) the longitudinal pitch $X_{2L}$. For stallbrass's array $X_{2L} = 5.6$ and for Hill and Armstrong's experiment, minimum $X_{2L} = 2.3$. The present experiments were conducted at $X_{2L} = 1.375$. Therefore, it is likely that the relationship $fL = V_u$ ceases to be valid for small values of $X_L$. (b) the hypothesis on which the above relationship is based is not very sound. This appears to be a more likely cause. Hill and Armstrong have suggested that acoustic coupling is with the frequency of alternating compression and rarefaction of the gas as it flows through the tube-bank. They rejected the idea of coupling due to vortex-shedding by running a test on a single row of tubes and by observing no acoustic resonance. However, Connars [78] and Keefe [37] have recorded noise due to acoustic coupling at the vortex-shedding frequency even when there was only one circular cylinder in the wind-tunnel. This suggests a probable anomaly in the experiments conducted by Hill and Armstrong for one row of tubes and further indicates that the nature of flow fluctuations that cause acoustic coupling in a tube-bundle is not completely understood yet.

The above analysis clearly indicates that the relationship of a constant Strouhal number equal to 0.21 (approximately) based on minimum-gap flow velocity can be used to correctly predict nearly all of the available experimental data on staggered tube arrays.

Grotz and Arnold [91] have measured vortex-shedding frequencies (based on acoustic coupling) through 20 different in-line tube-bundles. The data has been reproduced in table 5.5. This data is expected to be of limited precision only as the authors have claimed a maximum error of as much as 30%. They have not computed the Strouhal numbers for their arrays. If the Strouhal numbers are computed from their data it is seen that (table 5.5) most of the values seem to be falling around 0.2 (keeping in view the claimed accuracy of the data). Some of the data points are close to double this value, indicating the possibility of a 2nd acoustic mode being excited. A close scrutiny of the remaining points which do not fall either around 0.2 or around 0.4 suggests the possibility of some gross error in the measurement of velocity or frequency values. Although not enough data on in-line tube arrays are available, it appears that the dominant frequency in such arrays can also be predicted by a constant Strouhal number equal to about 0.2.

In summary, the present data and most of the data available in the open literature for both staggered and in-line tube-banks may be collapsed to a Strouhal number of about 0.21 if the computation is based on minimum-gap velocity and tube diameter. It is peculiar that so much of the previous Strouhal numbers reported were computed using mean flow velocities other than minimum-gap velocity. The latter is the

TABLE 5.5

GROTZ & ARNOLD'S DATA
IN-LINE ARRAYS

Abbreviations

C.W.(x): Compare with S.No.x
C.B.: Could be

| S. No. | d in. | ℓ in. | T in. | $V_T$ ft./sec. | Remarks on $V_T$ | Computed Frequency $f_H^*$ = (Hz) | Observed Frequency $f_G$ = (Hz) | Remarks on $f_G$ | Computed Strouhal Number $S_G^{**}$ = |
|---|---|---|---|---|---|---|---|---|---|
| 1 | .065 | .196 | .238 | 30.1 | | 1340 | 1040 | | 0.19 |
| 2 | .25 | .313 | .375 | 90.0 | | 1150 | 1900 | C.B. 2nd Mode | 0.45 |
| 3 | .315 | .468 | .468 | 97.9 | | 820 | 1330 | C.B. 2nd Mode | 0.42 |
| 4 | .375 | .936 | .468 | .163 | C.W.(6) C.B. Lower | 415 | 688 | | 0.13 |
| 5 | .315 | .468 | .563 | 87.1 | | 984 | 1330 | | 0.48 |
| 6 | .375 | .936 | .563 | 131 | | 560 | 704 | | 0.17 |
| 7 | .375 | .75 | .563 | 103.5 | | 554 | 670 | | 0.20 |
| 8 | .375 | .75 | .75 | 78.4 | | 627 | 685 | | 0.27 |
| 9 | .375 | .936 | .563 | 123 | | 527 | 605 | | 0.16 |
| 10 | .312 | .468 | .563 | 57.5 | C.W.(5) C.B. Higher | 656 | 687 | | 0.31 |
| 11 | .312 | .936 | .563 | 183 | C.W.(6) C.B. Lower | 1046 | 650 | $f_G$ usually $>f_H$ | 0.09 |
| 12 | .312 | .468 | .468 | 53.8 | C.W.(5) C.B. Higher | 460 | 694 | | 0.34 |
| 13 | .312 | .936 | .468 | 123 | C.B. Lower | 526 | 680 | | 0.14 |
| 14 | .312 | .936 | .936 | 98 | | 833 | 690 | | 0.18 |
| 15 | .375 | .936 | .468 | 185 | C.W.(6) C.B. Lower | 472 | 688 | | 0.12 |
| 16 | .315 | .936 | .936 | 90 | | 765 | 687 | | 0.24 |
| 17 | .312 | .75 | .563 | 94 | | 670 | 678 | | 0.19 |
| 18 | .312 | .75 | .75 | 84 | | 786 | 688 | | 0.21 |
| 19 | .375 | .563 | .936 | 81 | | 1033 | 677 | | 0.26 |
| 20 | .315 | .945 | .936 | 117 | C.W. (16) C.B. Lower | 985 | 679 | | 0.16 |

* Using Hill & Armstrong's relationship $f_H = V_u/\ell$

** Recomputer Strouhal number by the present author $S_G = \frac{f_G d}{V_T}$

only one which appears to be physically meaningful in terms of the flow separation occurring at each tube. It is remarkable that this agrees so closely with the value for a single cylinder. It should be recalled that this holds true only for sufficiently high Reynolds numbers deep inside a tube-bank. While there is significant evidence to support the concept of a universal Strouhal number for tube-banks, more data is required, particularly for in-line arrays, to fully support this relationship.

### 5.3 Tube-Response at Higher Reynolds Numbers

In the full array as the flow velocity was increased, the instrumented tube (tube no. 5, figure 5.1) responded to turbulence in the flow-field. Two capacitance probes as described in Chapter 4 were installed perpendicular to each other at the top of the instrumented tube. The outputs from these probes were fed into an oscilloscope to observe the tube motion. The movable tubes were tuned to 24 $\pm$ 0.04 Hz and the logarithmic decrement of damping for the instrumented tubes was 0.007.

#### 5.3.1 Effect of Flow-Field on Tube Response

A typical tube response as seen on the oscilloscope screen was photographed at a number of flow velocities and has been reproduced in figure 5.26. Up to about 3.2 m./sec. the tube response was very small and random in character. The random response of the tube is shown on a time scale in

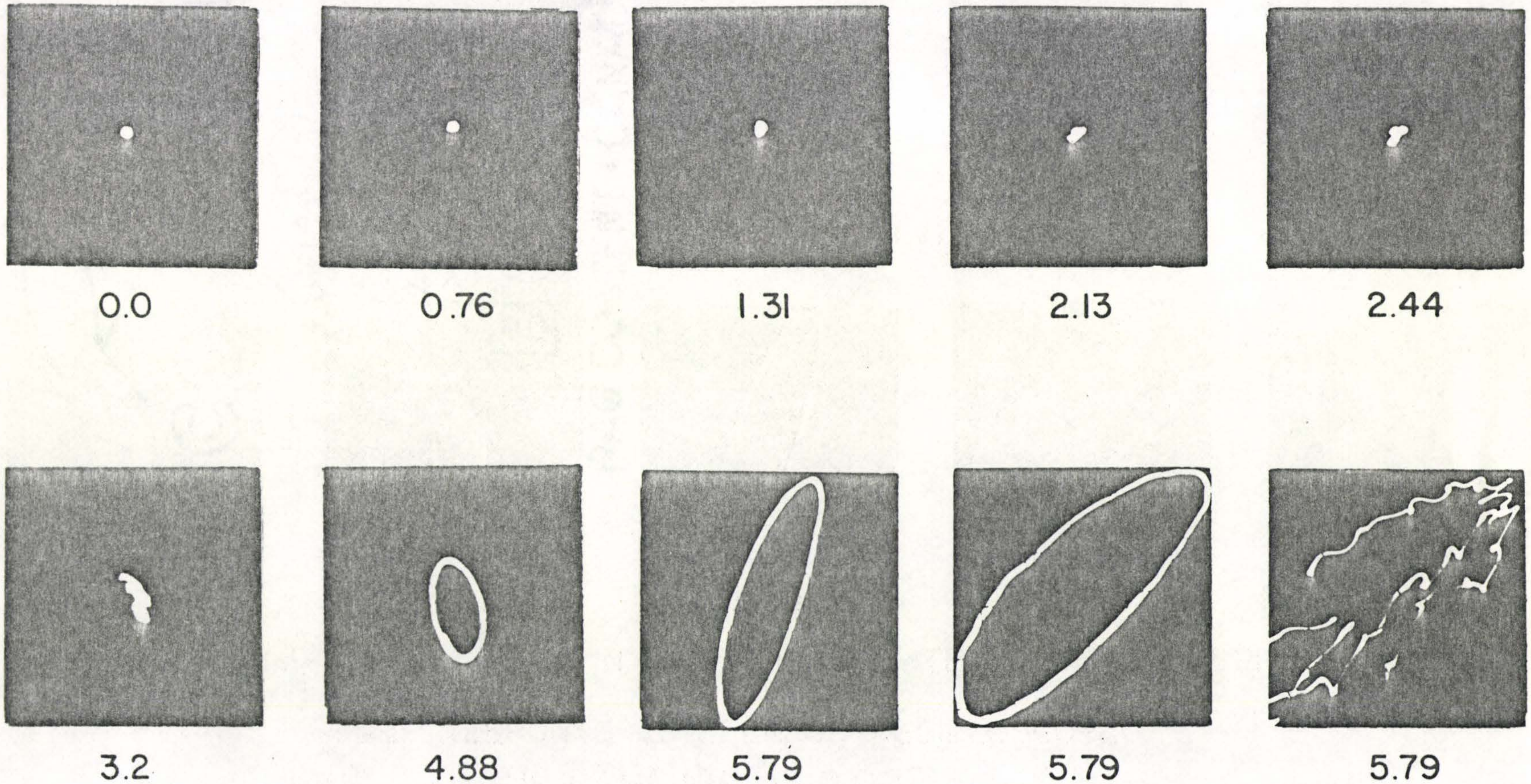


MINIMUM-GAP VELOCITY IN M/SEC. IS INDICATED UNDER EACH PICTURE

TUBE RESPONSE AS SEEN ON OSCILLOSCOPE

(AIR DAMPING $\delta = 0.007$)

FIGURE 5.26

figure 5.27. The output was also recorded on a U.V. recorder from which the maximum amplitude of the tube occurring in a time period of 30 secs. was computed. The maximum amplitude rather than R.M.S. amplitude was computed because, from a tube-damage standpoint, peaks are more important than R.M.S. value of the amplitudes.

The maximum amplitudes have been plotted against minimum-gap velocities in figure 5.28. Portion AB of the response curve is due to forced random response of the tube. In this region the peak to peak maximum amplitude is seen to be directly proportional to the minimum-gap velocity. However, Zdrakovich [112] has found that the maximum amplitude response due to turbulence in his experiments was proportional to the square of the flow velocity. The present results suggest less correlation of forces along the length of the tube in the present array than that tested by Zdrakovich, which is not surprising considering that Zdrakovich conducted his tests on only one-, two- and three-row in-line arrangements.

As the flow velocity was further increased the tube responded at larger amplitudes. The random response of the tube seen so far shifted to regular oscillations of the tube at its natural frequency. Elliptical orbital patterns were observed on the oscilloscope as shown in figure 5.26. The motion of the tube was predominantly in the transverse direction to the flow, shifting to within $\pm$ 45$^{o}$ of this direction and occasionally drifting to the streamwise direction. The amplitude of tube vibration was not constant. The

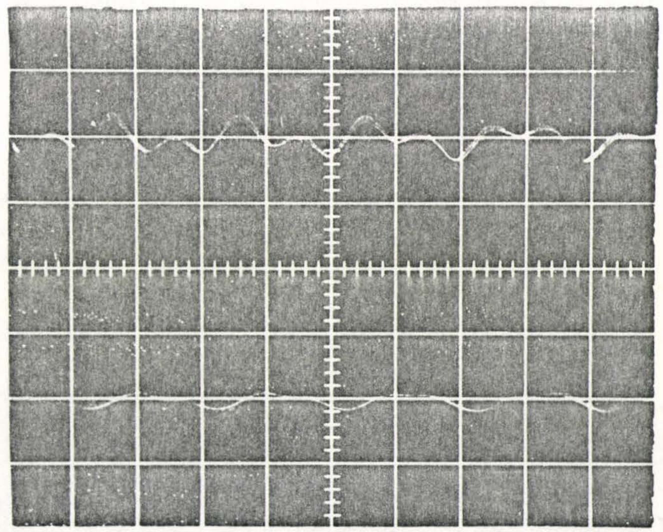

CHANNEL - I

CHANNEL - 2

LOCATION OF CHANNELS — I,2
IS SHOWN IN FIGURE 4

HORIZONTAL SCALE I DIV. = 20 M.SEC.

A TYPICAL RECORD OF TURBULENCE RESPONSE
OF A MOVABLE TUBE (TUNED NATURAL FREQUENCY = 24 Hz)

FIGURE 5.27

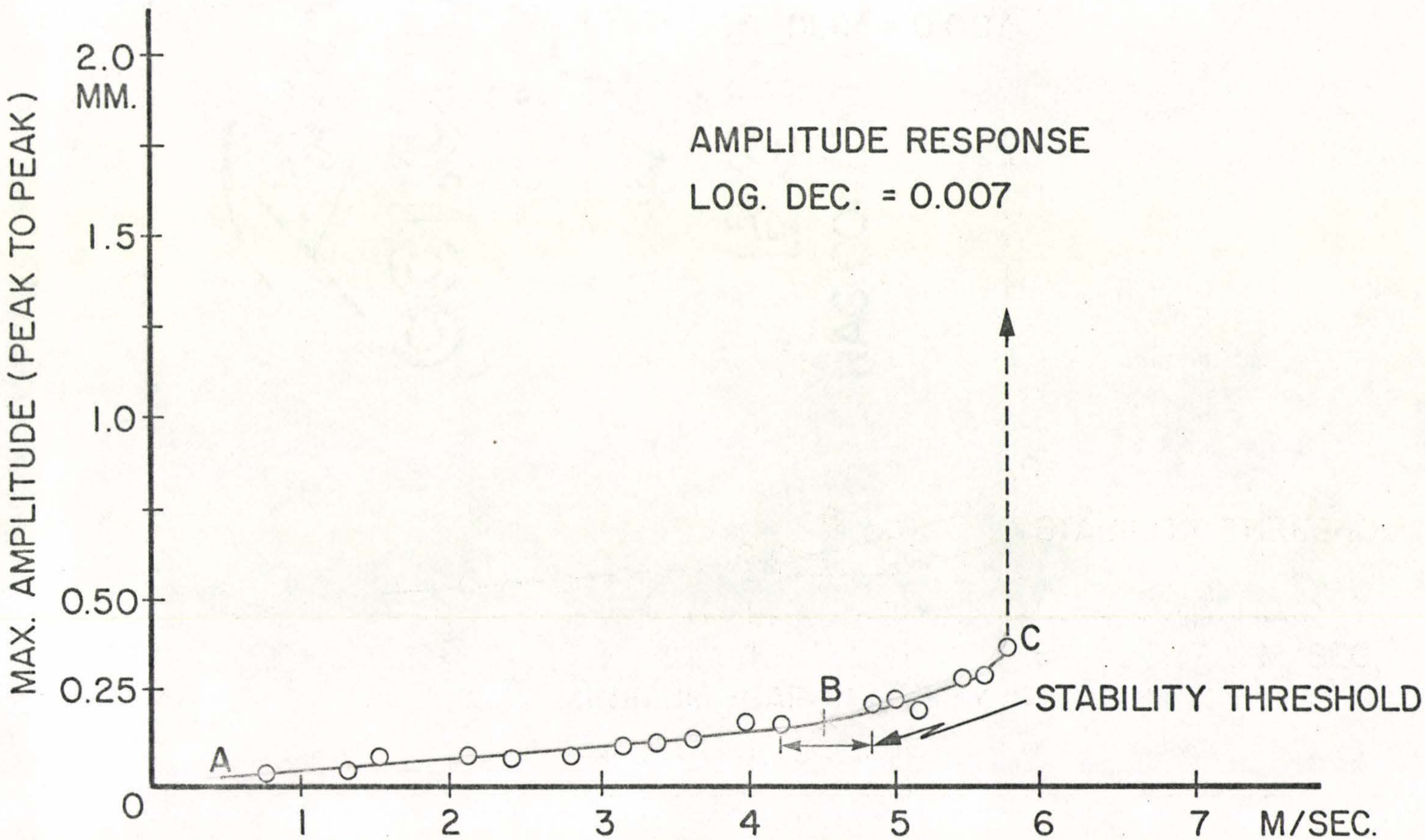
2.0
MM.
1.5
1.0
0.50
0.25
MAX. AMPLITUDE (PEAK TO PEAK)
AMPLITUDE RESPONSE
LOG. DEC. = 0.007
A
B
C
STABILITY THRESHOLD
0
1
2
3
4
5
6
7
M/SEC.
MINIMUM-GAP VELOCITY

FIGURE 5.28

capacitive probe signal varied between levels of maximum amplitude and null points with time as shown in figure 5.29. This amplitude modulation is undoubtedly due to turbulence and coupling effects from adjacent tubes. With still further increase in flow velocity the maximum tube amplitude kept on building up rapidly till the piano-wire started to hit the capacitive probes. Unlike Chen's [89] vortex-shedding resonance response of tubes inside a tube-bundle, the tubes in the present experiments continued to vibrate at their natural frequency as the flow velocity was increased past some critical threshold value. The large amplitude vibrations being observed are thought to be due to fluidelastic instability. Fluidelastic response is characterized by a critical flow velocity, below which the oscillations are small and random in nature and above which the amplitudes increase significantly and the tube frequency and mode shape become regular. The tube response is similar to that observed by Connars [78] except for the mode shapes which appear to be primarily in the transverse direction rather than alternating tubes vibrating in streamwise and transverse orbital patterns.

As the tube amplitude is irregular, the significant value is considered to be the maximum amplitude in a 30 second recording, as explained above. This maximum amplitude was seen to occur quite frequently during this time period. The output of two capacitive probes was recorded on a U.V. recorder and is shown in figure 5.29. The square of the maximum amplitude was given by the sum of the squares of amplitudes

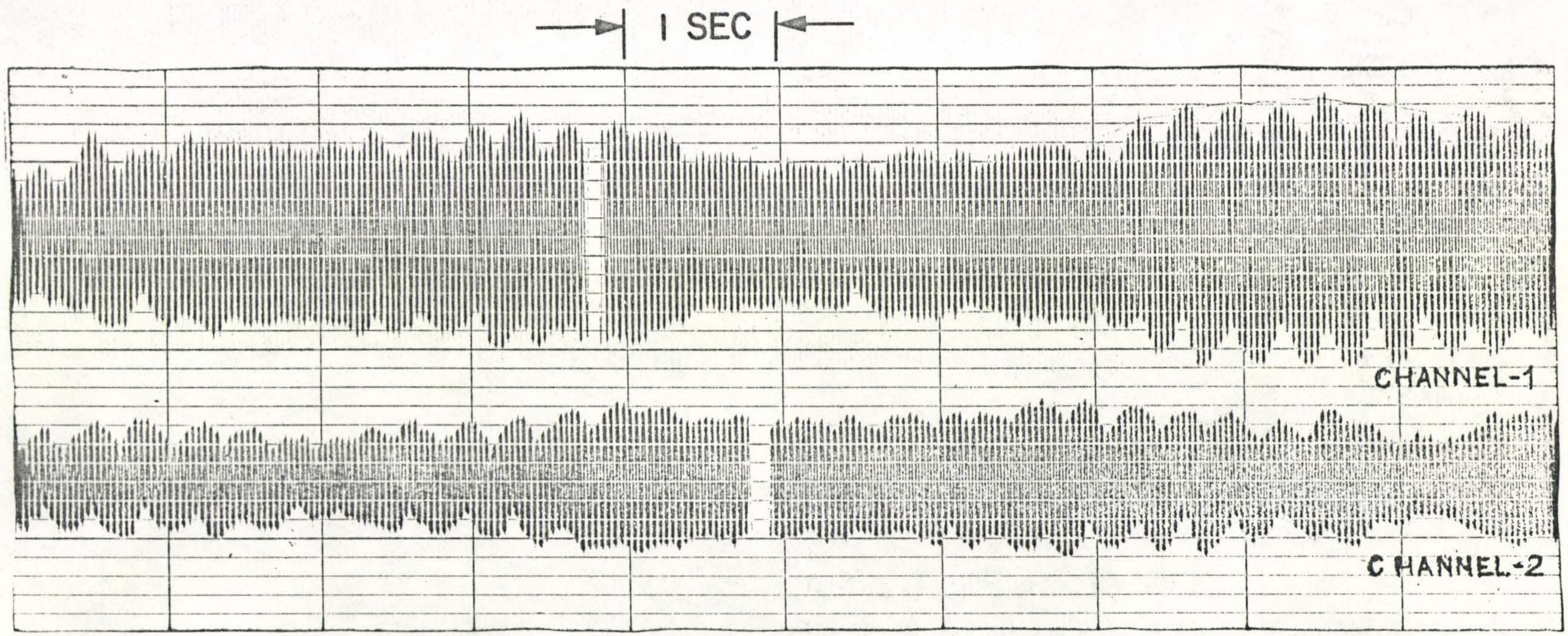


AMPLITUDE RESPONSE
IN THE FLUID-ELASTIC REGION

LOGARITHMIC DECREMENT = 0.010

FIGURE 5.29

from the recording of two channels where the maximum amplitude was seen to have occurred. The maximum amplitude (peak to peak) was then plotted against the gap velocity as shown by the curve BC in figure 5.28. A distinct change of slope is seen around point B. The gap velocity at which the slope of the amplitude response diagram changes is defined as the fluidelastic 'stability threshold' for the tube. As it is difficult to determine precisely where the change of slope occurs, a certain band of gap velocities as shown in figure 5.28 has been designated as the region of the stability threshold and is an indication of uncertainty involved in determining precisely the critical flow velocity. Many other investigators [81] have experienced the same problem in precisely locating the stability threshold. In the present experiments, it appears that using the criterion of change of tube response from random to regular motion, is a better indicator of fluidelastic instability than a change in the slope of the amplitude-response curve of the tube, especially for higher damping.

At the gap velocity corresponding to point 'C' in figure 5.28 the amplitude of the tube kept on increasing without any further increase in the flow velocity. This amplitude build-up was limited by the contact with the capacitive probes as shown in the last picture of figure 5.26. Such behaviour was not observed by Zdrakovich [110] who studied the tube responses in up to three rows of in-line movable tubes. However, a very high rate of amplitude build-up was recorded by Connars [78]. The higher level of response in the present experiments may be attributed to fluid coupling with the surrounding tubes which are vibrating at the same frequency. In addition, damping is probably an important factor in amplitude build-up as is seen later in this chapter.

The response of another tube in the bundle (tube no. 2, see figure 5.1) was similarly recorded and is plotted in figure 5.30 as the maximum peak to peak amplitude vs. gas velocity. The logarithmic decrement of damping of tube no. 2 is 0.015 which is about double that recorded for tube no. 5. The basic character of the amplitude-response curve remains the same, i.e., a turbulence response followed by a large amplitude self-excited response of the tube. In the fluid-elastic region the tube vibrated at its natural frequency. However, the shape of the response curve is different from that obtained for tube no. 5 and the stability threshold occurs at higher gap velocities. This indicates that the precise shape of the amplitude-response curve depends on the damping of the tube although all the movable tubes finally exhibit large amplitude vibrations.

Some hysteresis in self-excited vibrations was noticed. The vibrations always started at a higher flow velocity when the velocity was increasing and ceased at a lower flow velocity when the flow velocity was being reduced. This is typical of fluidelastic phenomena where flow periodicity is caused by the motion of the structure.

Figure 8 shaped lissajous figures were occasionally

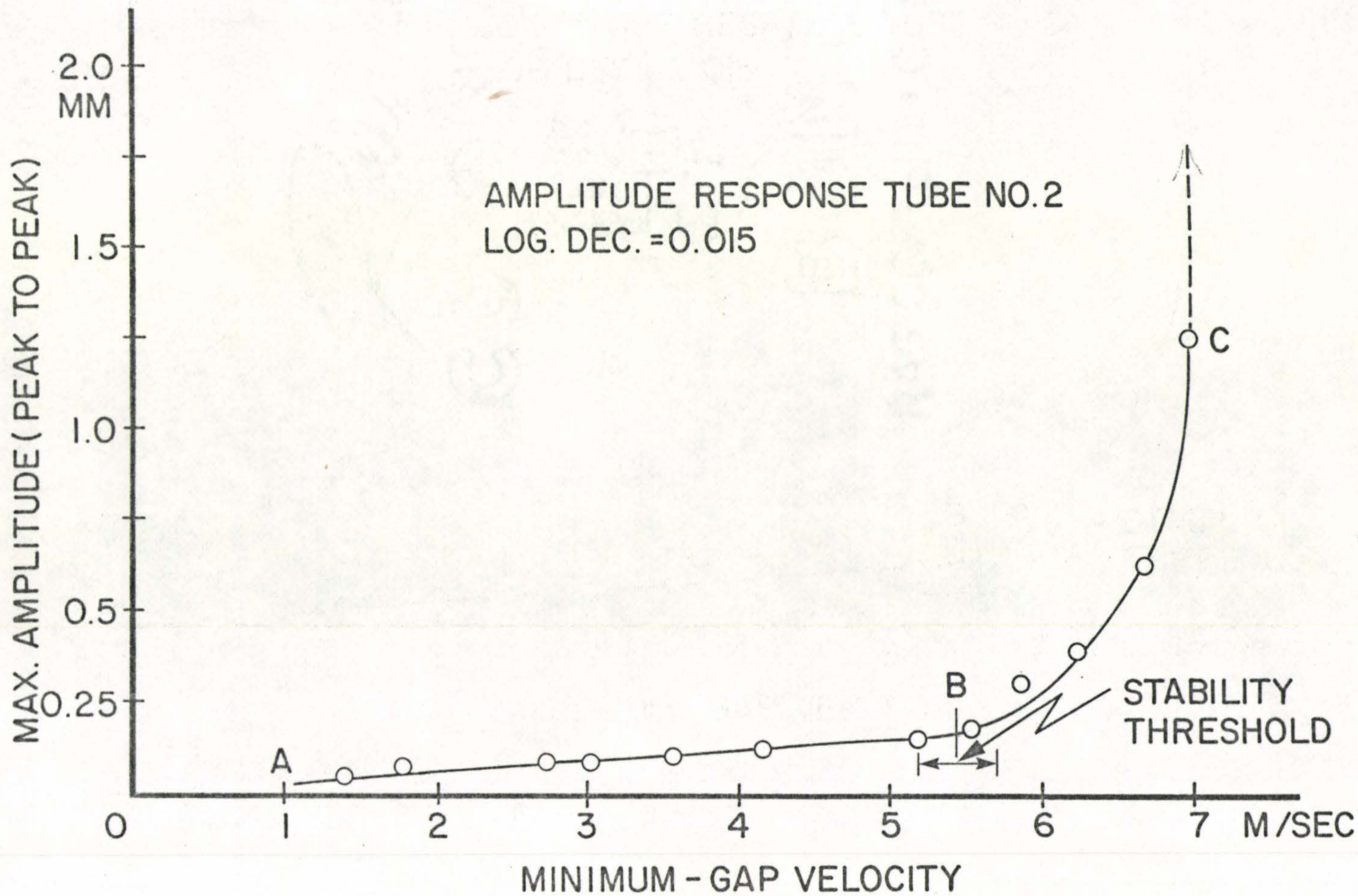
AMPLITUDE RESPONSE TUBE NO.2
LOG. DEC. =0.015
MAX. AMPLITUDE ( PEAK TO PEAK)
2.0
MM
1.5
1.0
0.5
0.25
0
1
2
3
4
5
6
7
M/SEC
A
B
C
STABILITY
THRESHOLD
MINIMUM - GAP VELOCITY

FIGURE 5.30

observed on the oscilloscope screen, thus indicating a frequency in the drag direction equal to twice the lift frequency. An amplitude power-spectrum was computed from the output of the capacitive probe and is shown in figure 5.31. A sharp peak at the natural frequency of the monitored tube (32 Hz) and another sharp but smaller peak at double the natural frequency of the tube is seen. This result points to the possibility that as the tube begins to vibrate at large amplitudes it starts shedding vortices at its own natural frequency. However, this argument has still to be verified. The sharp peaks of the amplitude power-spectrum also indicates the excellent linear characteristics of the designed movable tube as well as the absence of any rocking mode.

### 5.3.2 Flow-Field Velocity Power-Spectrum

A velocity power-spectrum similar to the ones described in section 5.2 was computed at location 'H' in the tube array (see figure 5.1), when the movable tubes were vibrating at large amplitudes. The power spectrum so obtained is shown in figure 5.32. Initiation of tube vibration did not change the basic shape of the frequency spectrum except that a large peak at the natural frequency of the movable tubes (24 Hz) has appeared. The peak at 24 Hz in the bottom traces of figures 5.20-5.24 referred to in section 5.2.4 are all due to fluid-elastic tube vibration. No such peak occurred at the same flow velocity when the movable tubes were not vibrating (being either heavily damped or prevented from moving) as shown in figure

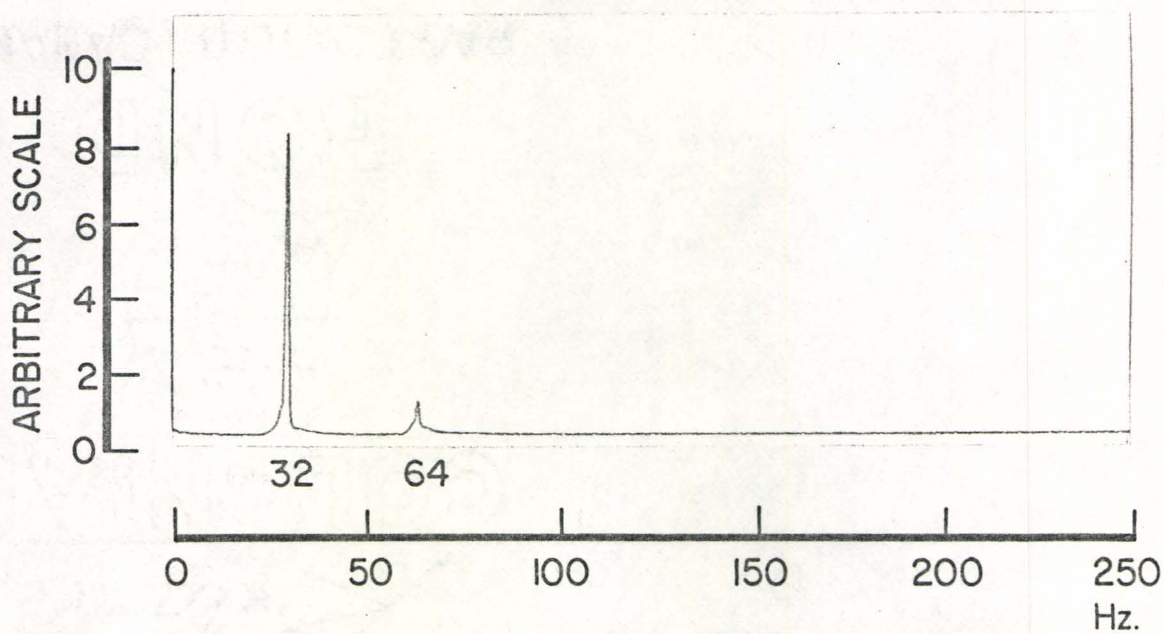


AMPLITUDE-POWER SPECTRUM OF TUBE RESPONSE
(TUNED NATURAL FREQUENCY OF TUBE = 32 Hz.)

FIGURE 5.31

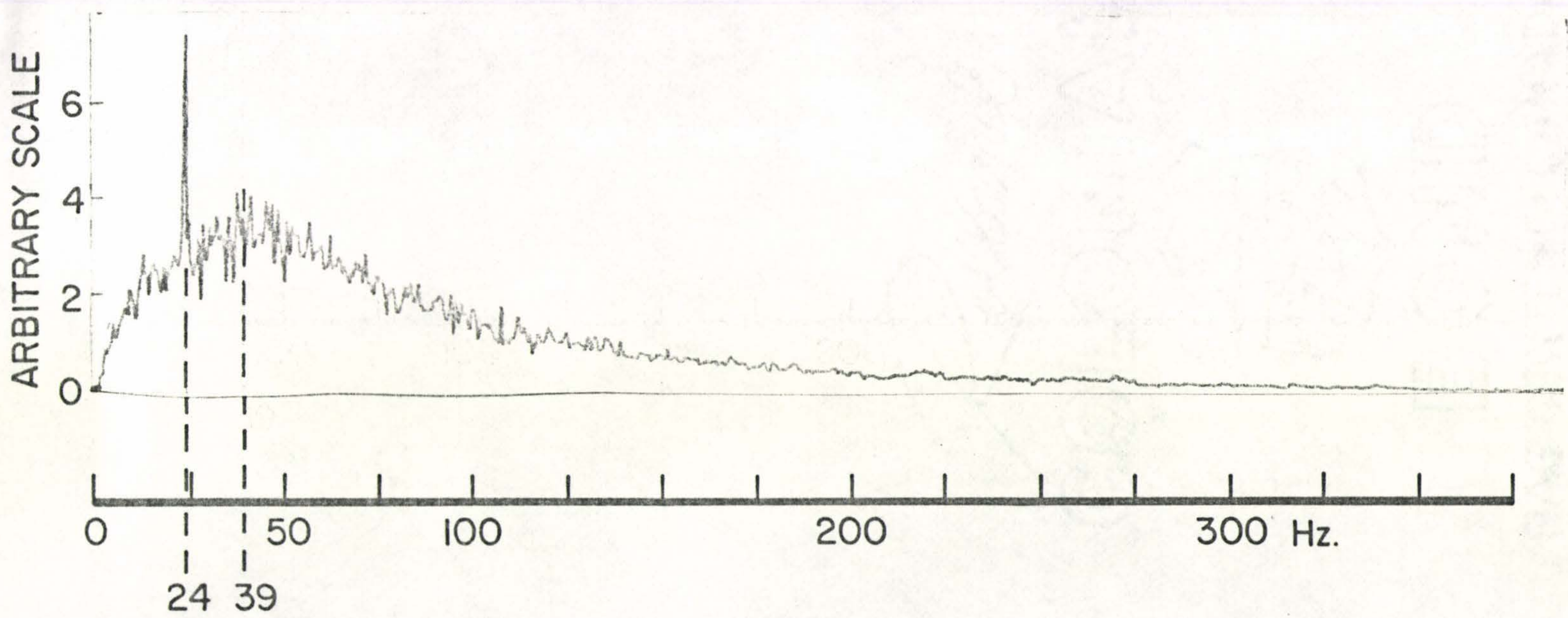


A TYPICAL RECORD OF FLOW-FIELD VELOCITY POWER SPECTRUM
(MOVABLE TUBES VIBRATING WITH LARGE AMPLITUDES)
(TUNED NATURAL FREQUENCY OF TUBES = 24 Hz.)

FIGURE 5.32

5.25. The large peak at 24 Hz is therefore caused by the tube vibration and is probably due to the capacity of the vorticity fields to be excited and amplified over rather broad frequency bands, in the sense described by Morkovin [29].

### 5.3.3 Relative Mode Shapes of the Movable-Tubes

A movie film was taken of the vibrating movable tubes at 200 frames/sec. The film was shot when the tubes were vibrating at large amplitudes in the fluidelastic region. The film was projected at slow speed in order to observe in detail the motion of the tubes and their relative mode shapes. From this film it was observed that the predominant direction of motion appears to be transverse to the flow. Groups of tubes vibrate in unison such that their amplitudes increase and decrease simultaneously. It appears that coupling between adjacent tubes causes an increase in vibration amplitude up to some threshold value whereupon the coupling is destroyed and the amplitude rapidly decreases. The outside tubes had lower amplitudes compared to those in the core of the bundle. This is likely due to the adjacent tubes being fixed and therefore, being unable to couple dynamically with the movable tubes. No unique relative mode shapes of the tubes could be discerned. Any two adjacent tubes seemed to be vibrating alternatively in-phase and out-of-phase and randomly reverting from one phase to another.

### 5.3.4 Effect of Surrounding Tube Motion

The effect of surrounding tube motion on the tube response was studied next. The amplitude-response of the monitored tube was recorded when the surrounding tubes were free to vibrate. The motion of the surrounding movable tubes was then physically blocked from outside the test section (using acrylic strips). The amplitude-response of the monitored tube was recorded again. For comparison the two responses so obtained have been plotted together in figure 5.33. It is significant that the monitored tube vibrated at large amplitudes due to fluidelastic instability even when all its surrounding tubes did not move. However, the comparison shows that adjacent tube motion has a strong influence on the amplitude-response of the monitored tube. In the fluidelastic region much smaller tube amplitudes have been recorded when the surrounding tubes were blocked (the tube oscillations were still predominantly transverse to the direction of flow). No significant difference in turbulence response is evident. The stability thresholds in the two cases appear to be very close to each other, thus suggesting that from a stability threshold standpoint, only one movable tube in the bundle is required. On the oscilloscope screen it was observed that in the fluidelastic region the monitored tube oscillated more frequently about its predominantly transverse mode when the surrounding tubes were vibrating than when their motion had been blocked. Heinecke [132] observed that with small longitudinal spacing the boundary layer separates

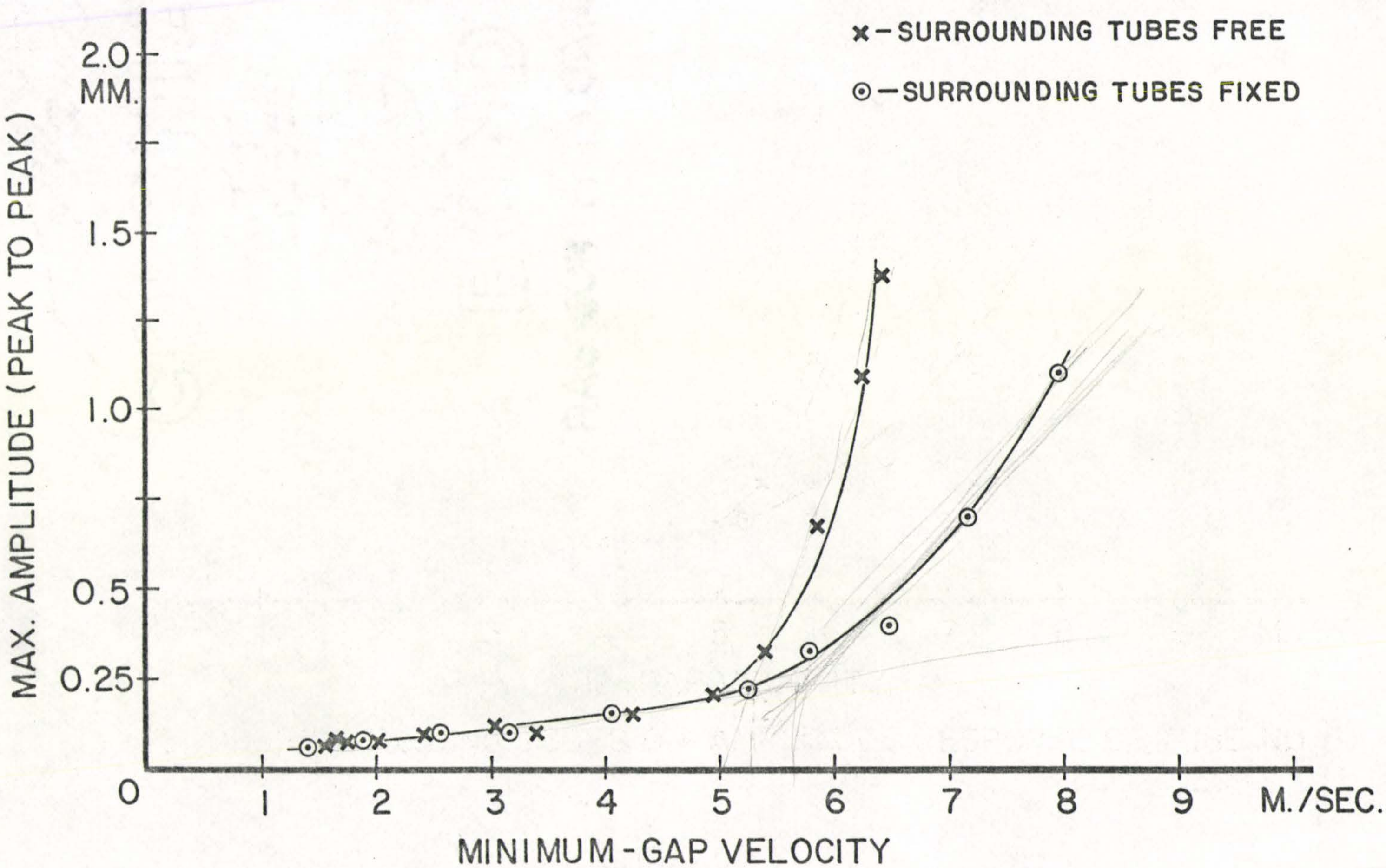


EFFECT OF SURROUNDING TUBES ON AMPLITUDE RESPONSE OF TUBE NO. 5
(LOG. DEC. = 0.01)

FIGURE 5.33

further downstream than in arrays with greater longitudinal pitches. Thus a variation in longitudinal spacing results in variations of the separation point on the tube. The vibration of the surrounding tubes leads to more rapid variation in longitudinal pitch, which probably explains why the monitored tube oscillated more frequently about its predominantly transverse mode when the surrounding tubes were also vibrating.

### 5.3.5 Discussion

It is observed from the present experiments that as the flow velocity increases, the amplitude-response due to turbulence increases until sufficient energy is available for the tubes to become self-excited. The flow-field random turbulence has a peak which is probably due to the frequency of vortex-shedding varying over the narrow range about $S_G \simeq 0.21$. The frequency in the turbulence coinciding with the natural frequency of the tube is amplified by the tube's motion. This amplification is probably due to both fluid coupling with the surrounding tubes and a better correlation of forces along the length of the tube usually associated with large amplitude oscillations.

The peak in the turbulence spectrum which occurs at $S_G = 0.21$ (as shown in section 5.2.4) , is useful for predicting only the acoustic resonance in the tube-bank. Contrary to Owen's [100] hypothesis, a match between the frequency at the peak in the turbulence spectrum and the natural frequency of the tube is not necessary in order to initiate the mechanical vibrations of the tube. The tubes in the present experiments started to vibrate at large amplitudes only after the peak in the velocity power-spectrum was significantly higher than the natural frequency of the tube. No periodic tube response was observed when the velocity power-spectrum peak coincided with the tube natural frequency. The effect of scale of turbulence on the tube response has not been studied here.

The present experiments have also shown that the tubes deep inside a tube-bundle are susceptible to large-amplitude flow-induced vibrations, contrary to the assumption of Roberts [77] who stated that the failures in the tube-bundles were observed to be confined to the rear rows of tubes only. His model for a single row of tubes was based on a jet-switch mechanism. The movable tubes in the present array vibrated at large amplitudes predominantly in the transverse direction, which is again contrary to Roberts' observation. He found that the vibratory motion in the practical situation is primarily in the free-stream direction and subsequently based his mathematical model on the assumption that tube vibration is under the influence of time-varying drag force, which gives rise to and maintains the vibration.

In summary, the present experiments have clearly shown that the response of a tube deep inside a tube-bundle can be divided into two distinct regions (1) Turbulence response and (2) Fluidelastic response. The amplitude-response of the tube is qualitatively similar to the tube responses observed by Connars [78], Zdrakovich [110] and Gorman [113].

## 5.4 Fluidelastic Stability Boundary for the Array

As described in Chapter 1, the fluidelastic stability boundary for the array may be plotted in the form of velocity parameter against damping parameter. The location of this boundary is expected to be a function of tube pitch and geometry of the array. Connors [78] coined the concept of a fluidelastic boundary for the tube array. However, his experiments were conducted on a single row of tubes only.

In order to realise a range of damping values in the present experiments, discrete damping devices of the type described in Chapter 4 were used to vary the damping of the tubes. The device consisted essentially of a small cup and paddle assembly installed one each at the top and bottom of the movable tubes. The damping could be varied by pouring different grades of motor oils in varying quantities into the damping cups. The damping control was found to be excellent.

The movable tubes were fixed at 24 $\pm$ 0.04 Hz, while their damping values were tuned at $\delta$ = 0.04, 0.07, 0.10 and 0.15 respectively.

The procedure for tuning a tube to a certain desired value of damping was as follows:

(1) From the performance results of the single tube assembly described in Chapter 4, the type of oil required (SAE 10, 20 or 30) to obtain the desired value of damping was selected. The approximate level of this oil in the cups was also noted.

(2) The selected oil in the desired quantity was then poured into the top and bottom cups of the movable tube.

(3) The tube was instrumented to record its motion on a U.V. recorder.

(4) A amplitude-decay trace was obtained by plucking and releasing the tube from its static equilibrium position.

(5) The logarithmic decrement of damping was computed from this damping trace over 5-10 cycles.

(6) Oil was then added or taken out from the damping cups depending on whether the computed value of logarithmic decrement was lower or higher than the desired value of damping. A new amplitude-decay trace was then recorded and another value of damping was similarly computed. This procedure was repeated until the desired value of damping had been obtained.

(7) Steps (1)-(6) were repeated for each of the 19 movable tubes until they had all been tuned to the desired value of damping.

(8) Steps (1)-(7) were repeated for each desired value of damping.

The logarithmic decrement of damping for each of the 19 movable tubes as they were tuned to a nominal value of 0.04, 0.07, 0.10 and 0.15 respectively is given in table 5.6. Care was taken to keep the spread in the damping very small and the data indicates that excellent control could be obtained.

### 5.4.1 Tube Response at Higher Values of Damping

The amplitude-response of the monitored tube was recorded for various values of damping by following the procedure described in section 5.3.1.

The amplitude response of the monitored tube when the movable tubes were tuned to a damping of $\delta = 0.04$ is shown in figure 5.34. The response in region AB is due to turbulence in the flow, random oscillations being seen on the oscilloscope screen. In the region BC the tube responded at its natural frequency only, the motion having changed from random to periodic. The transition region from turbulence response to fluidelastic response is fairly small and defines the stability threshold for the array. The damping of the movable tubes was now increased to $\delta = 0.07$ and an amplitude-response of the monitored tube was similarly plotted as shown in figure 5.35. The basic character of the tube response remains the same, viz., turbulence response region followed by the fluidelastic region. The transition region is wider than when the tubes were tuned at $\delta = 0.04$.

The logarithmic decrement of damping of the tubes was

TABLE 5.6

TUNED OIL-DAMPING OF MOVABLE TUBES

| Tube No. | Set-1 | Set-2 | Set-3 | Set-4 |
|---|---|---|---|---|
| 1 | 0.040 | 0.071 | 0.105 | 0.156 |
| 2 | 0.042 | 0.071 | 0.103 | 0.154 |
| 3 | 0.042 | 0.069 | 0.103 | 0.150 |
| 4 | 0.041 | 0.072 | 0.105 | 0.150 |
| 5 | 0.040 | 0.071 | 0.098 | 0.151 |
| 6 | 0.040 | 0.070 | 0.103 | 0.153 |
| 7 | 0.040 | 0.072 | 0.098 | 0.156 |
| 8 | 0.040 | 0.072 | 0.100 | 0.155 |
| 9 | 0.041 | 0.070 | 0.102 | 0.156 |
| 10 | 0.039 | 0.069 | 0.097 | 0.152 |
| 11 | 0.042 | 0.071 | 0.101 | 0.155 |
| 12 | 0.041 | 0.071 | 0.101 | 0.150 |
| 13 | 0.040 | 0.069 | 0.098 | 0.154 |
| 14 | 0.040 | 0.070 | 0.097 | 0.150 |
| 15 | 0.039 | 0.071 | 0.102 | 0.156 |
| 16 | 0.040 | 0.071 | 0.101 | 0.151 |
| 17 | 0.041 | 0.072 | 0.105 | 0.151 |
| 18 | 0.041 | 0.070 | 0.105 | 0.150 |
| 19 | 0.041 | 0.072 | 0.100 | 0.150 |
| Mean | $0.041^{+0.001}_{-0.002}$ | $0.071^{+0.001}_{-0.002}$ | $0.101 \pm 0.004$ | $0.153 \pm 0.003$ |

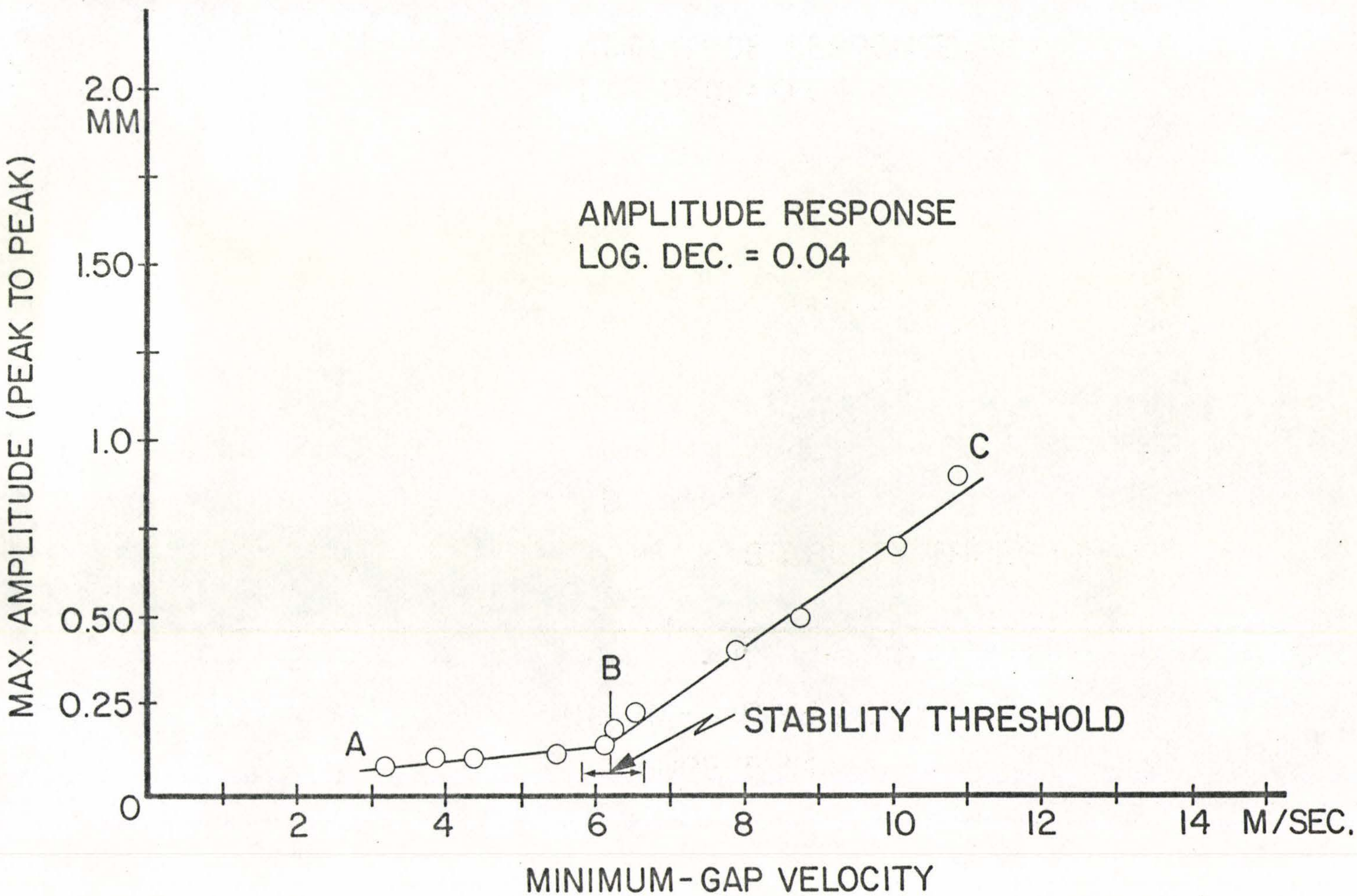

2.0
MM
1.50
1.0
0.50
0.25
0
MAX. AMPLITUDE (PEAK TO PEAK)
AMPLITUDE RESPONSE
LOG. DEC. = 0.04
A
B
C
STABILITY THRESHOLD
2
4
6
8
10
12
14
M/SEC.
MINIMUM-GAP VELOCITY


FIGURE 5.34

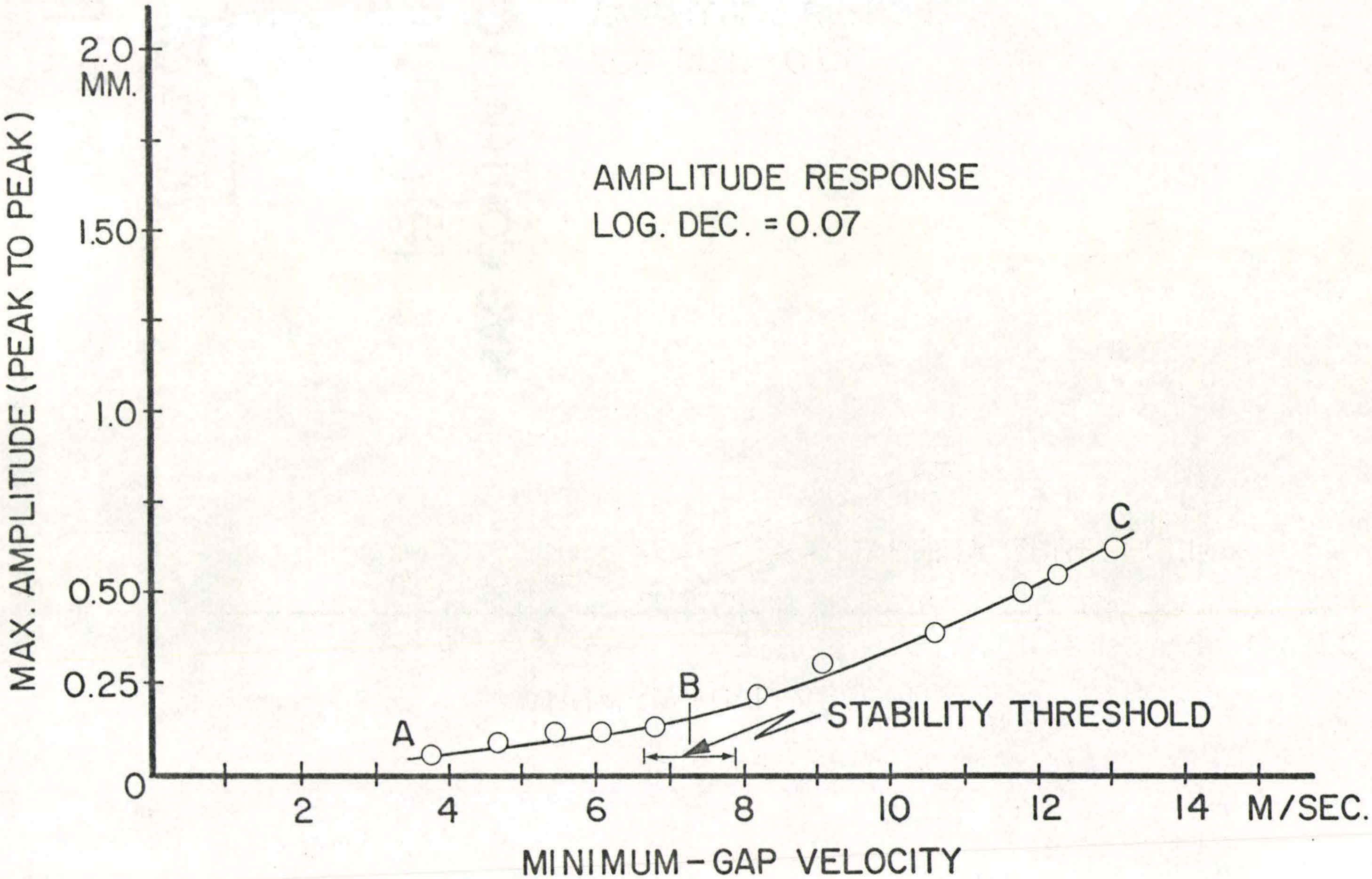
2.0
MM.
1.50
1.0
0.50
0.25
0
MAX. AMPLITUDE (PEAK TO PEAK)
AMPLITUDE RESPONSE
LOG. DEC. = 0.07
A
B
C
STABILITY THRESHOLD
2
4
6
8
10
12
14
M/SEC.
MINIMUM-GAP VELOCITY

FIGURE 5.35

next increased to 0.10. The amplitude-response of the instrumented tube was computed and has been plotted in figure 5.36. The two regions due to turbulence response and fluid-elastic response are again separated by a change in the slope of the curve defining the 'stability threshold'. The response of the tube in the fluidelastic region was at the natural frequency of the tube and a typical response recorded on a U.V. recorder is shown in figure 5.37. As before, it is noticed that the amplitude of the tube vibration does not stay constant. However, the response is different from that recorded for very low values of damping ($\delta = 0.01$, see figure 5.29) in that the modulation frequency appears to increase with increased damping.

The movable tubes were finally tuned to a damping of $\delta = 0.15$ and the amplitude-response is shown in figure 5.38. Here the transition from turbulence to fluidelastic response is very gradual resulting in greater uncertainty in properly locating the 'stability threshold'. Even on the oscilloscope screen when the wind-tunnel was operating at gap velocities corresponding to 'stability threshold' region in figure 5.38, the tube response shifted indiscriminately from exhibiting random response to a periodic response at the natural frequency of the tube. The response at higher flow velocities was similar to that obtained for $\delta = 0.10$ except that the amplitude modulation occurred at a higher frequency. The highest flow velocity reached was 13 m./sec. which corresponded to a Reynolds number of $2.21 \times 10^4$. The

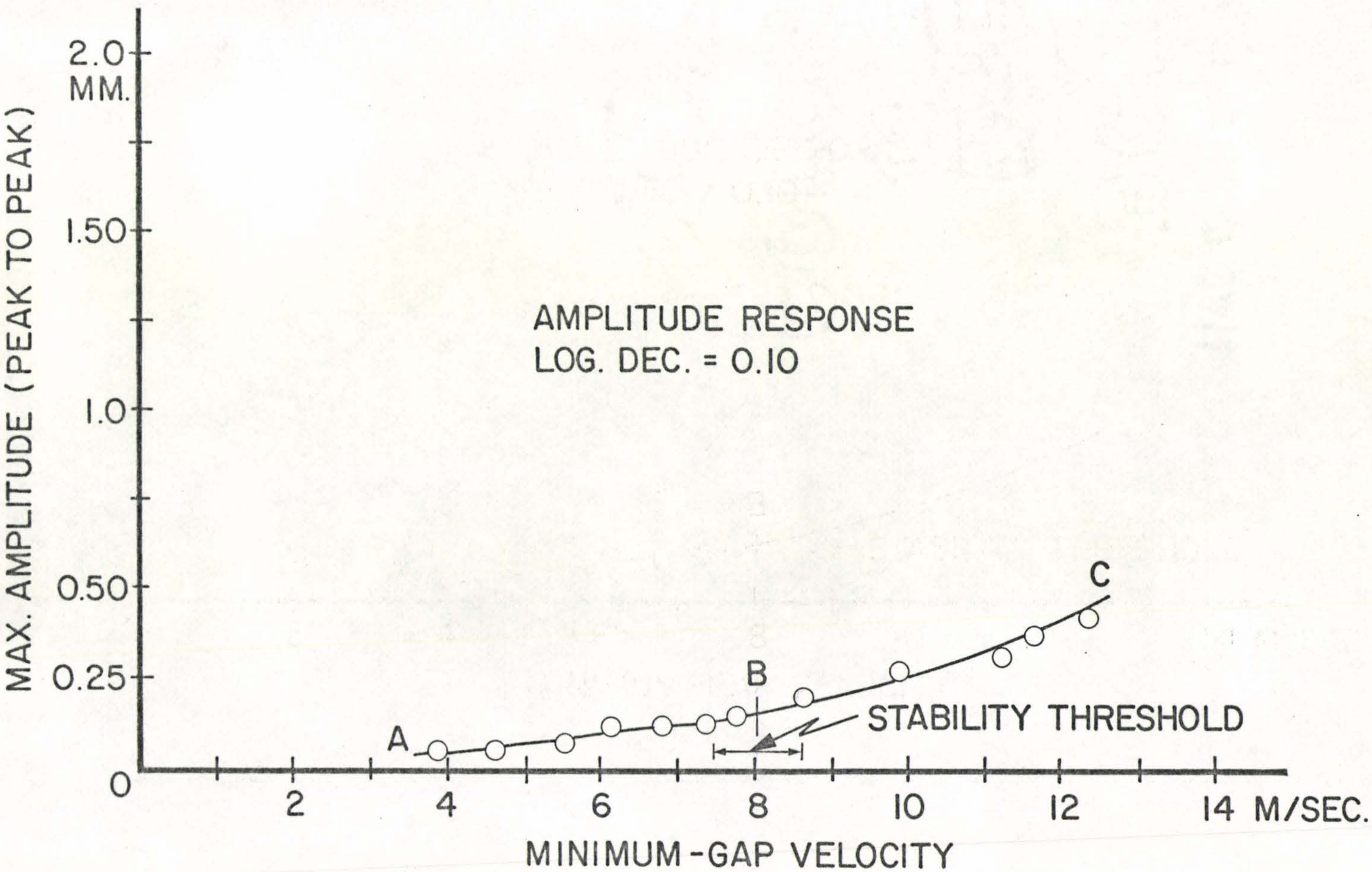
2.0
MM.
1.50
1.0
0.50
0.25
0
MAX. AMPLITUDE (PEAK TO PEAK)
AMPLITUDE RESPONSE
LOG. DEC. = 0.10
A
B
C
STABILITY THRESHOLD
2
4
6
8
10
12
14 M/SEC.
MINIMUM-GAP VELOCITY

FIGURE 5.36

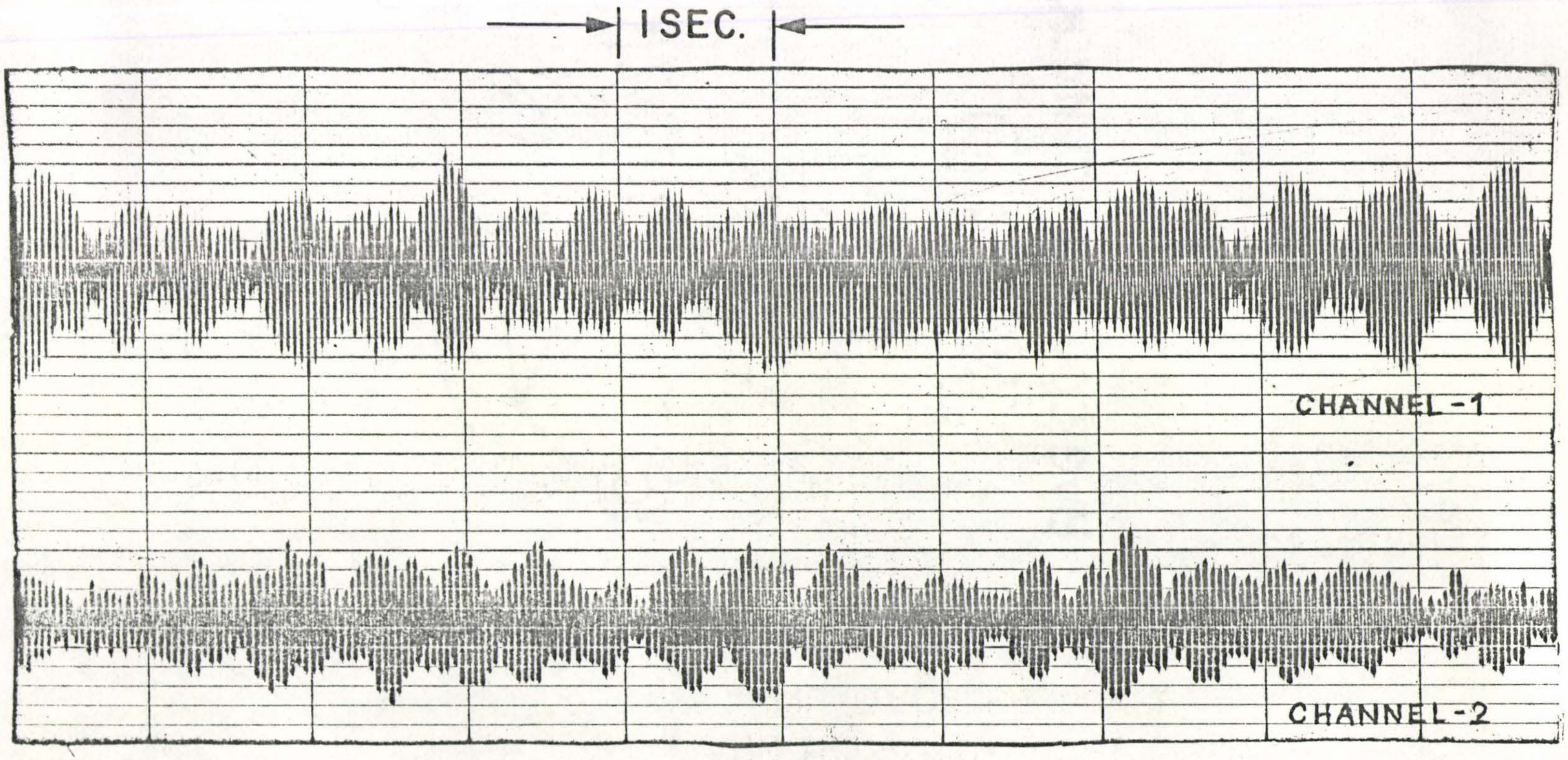


AMPLITUDE RESPONSE
IN THE FLUID-ELASTIC REGION

LOGARITHMIC DECREMENT = 0.10

FIGURE 5.37

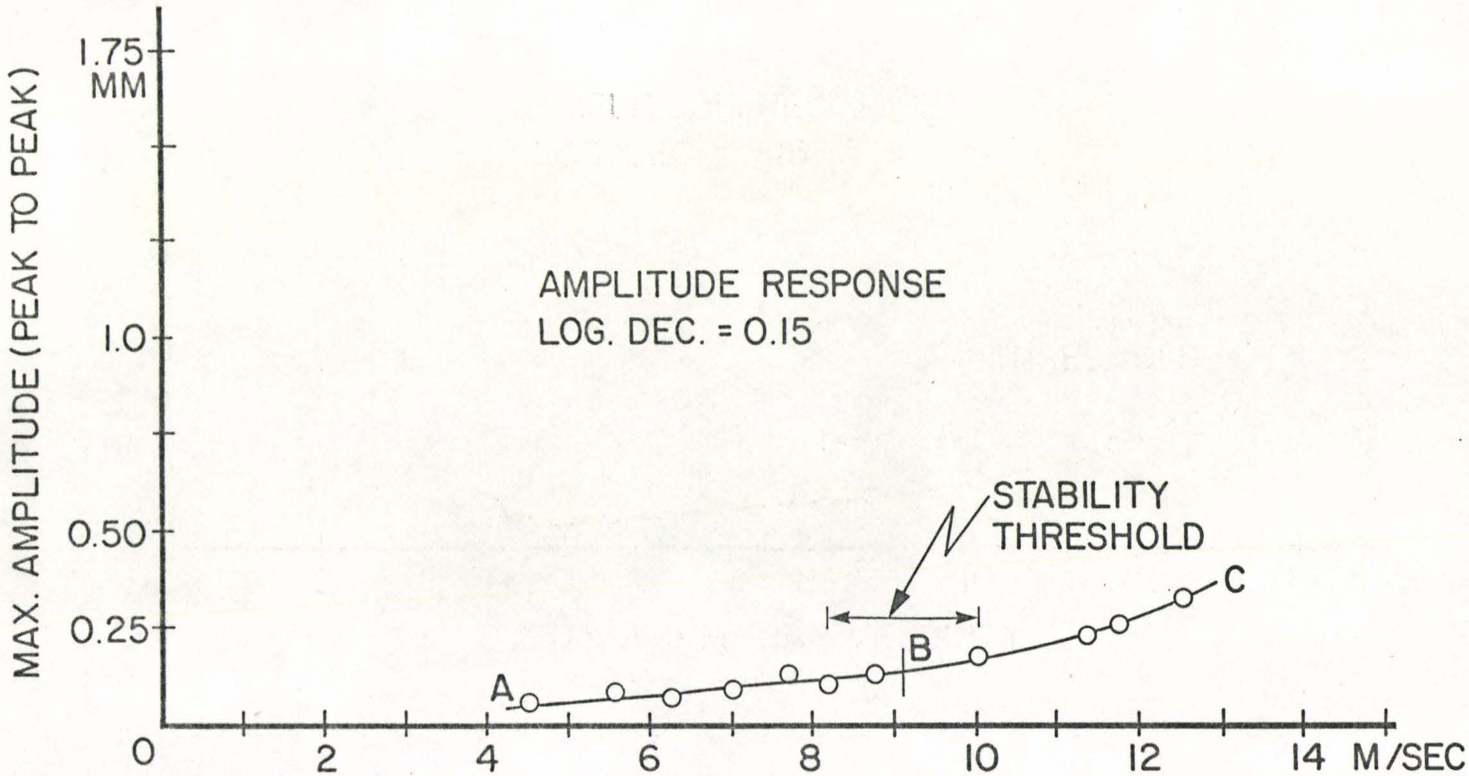


MINIMUM-GAP VELOCITY

FIGURE 5.38

oscillations of the tube in the fluidelastic region were predominantely in the transverse direction and drifted frequently within $\pm$ 45$^o$ to this direction.

The amplitude responses recorded for various values of damping have been plotted together in figure 5.39. Curves A and D are for damping values obtained without any oil in the damping cups and curve B has been described later in this section. The upper and lower limits of the range for stability threshold for each value of damping have been joined together by straight lines to give a 'transition region' shown in figure 5.39. The transition appears to be occurring at flow velocities for which the peak to peak tube amplitude reaches between 0.14-0.25 mm., depending on the damping in the tube. Apparently, the peak amplitude at which instability occurs decreases slightly as damping increases. It is noticed as well that the critical flow velocity for fluidelastic instability increases with an increase in damping and becomes progressively more difficult to determine precisely.

### 5.4.2 The Stability Boundary

The critical flow velocities ($V_G$) were non-dimensionalized to reduced velocity and plotted against the damping parameter as shown in figure 5.40. The data point 'C' was obtained by recomputing the amplitude-response of the monitored tube, after the experimental rig had been operating for about six months and the damping of the tube was noticed to have increased from $\delta$ = 0.007 to $\delta$ = 0.01. The Reynolds numbers

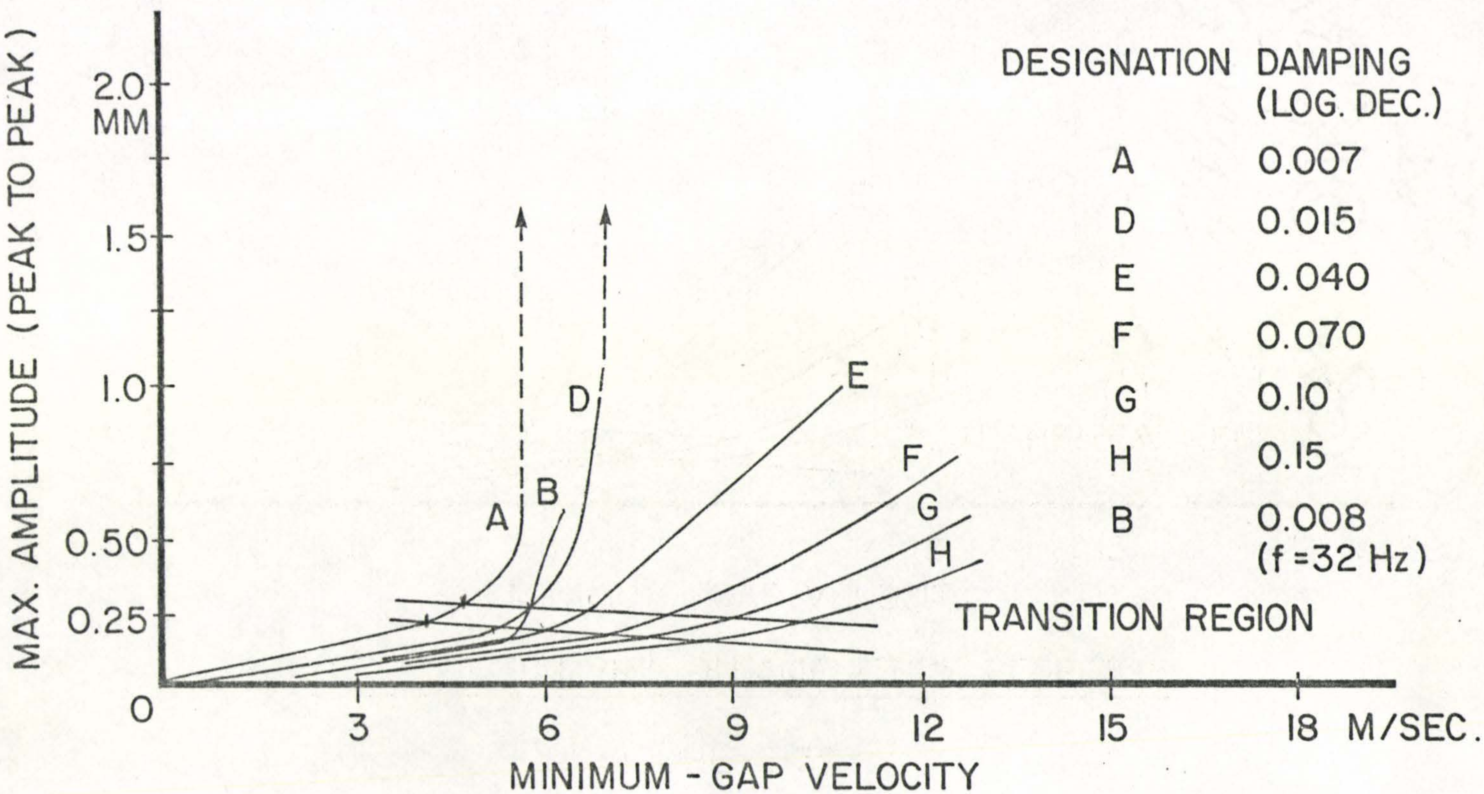


EFFECT OF DAMPING ON AMPLITUDE RESPONSE

FIGURE 5.39

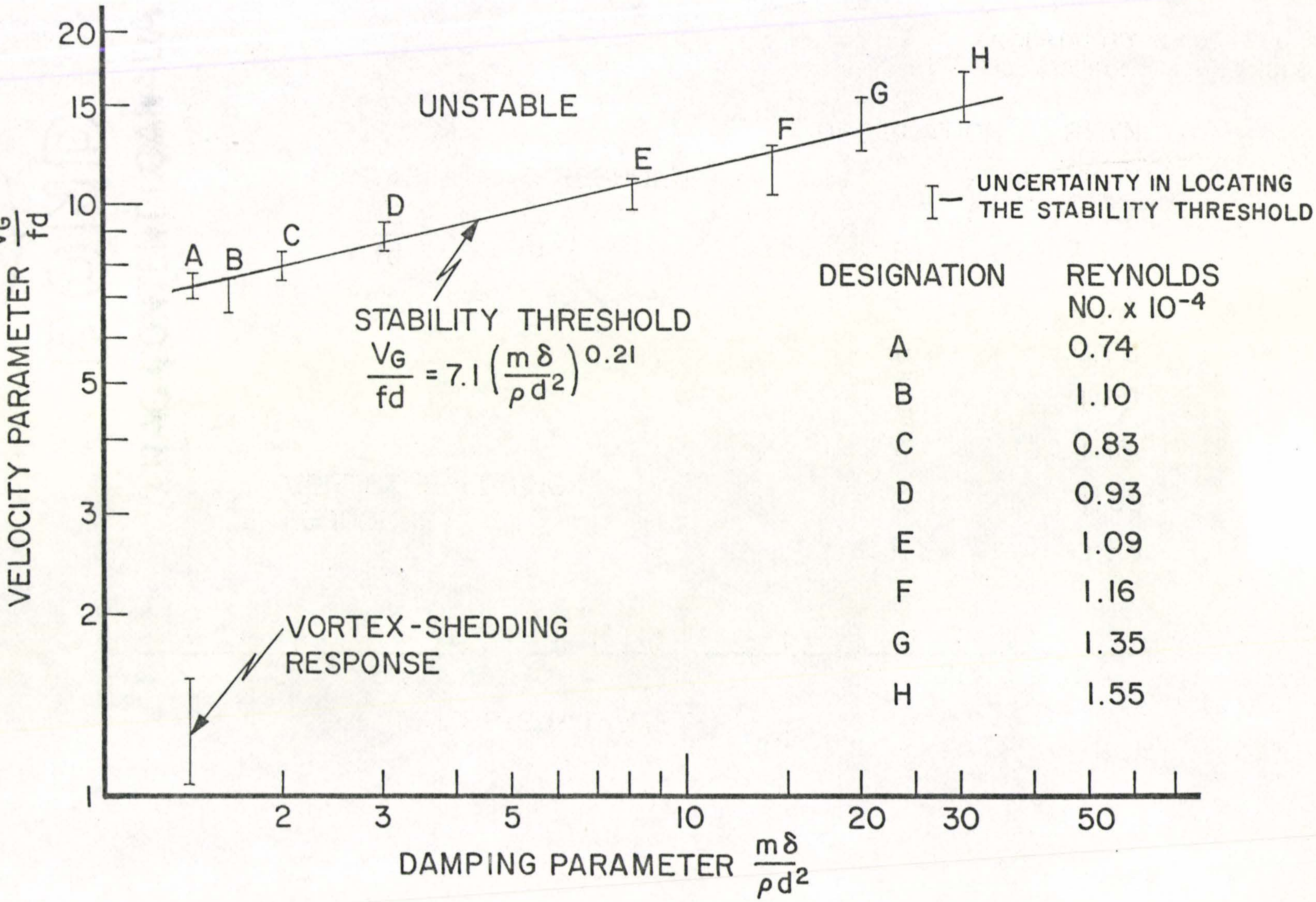
UNSTABLE
A
B
C
D
E
F
G
H
UNCERTAINTY IN LOCATING THE STABILITY THRESHOLD
STABILITY THRESHOLD
$\frac{V_G}{fd} = 7.1\left(\frac{m\delta}{\rho d^2}\right)^{0.21}$
DESIGNATION
REYNOLDS NO. x $10^{-4}$
A 0.74
B 1.10
C 0.83
D 0.93
E 1.09
F 1.16
G 1.35
H 1.55
VORTEX-SHEDDING RESPONSE
VELOCITY PARAMETER $\frac{V_G}{fd}$
DAMPING PARAMETER $\frac{m\delta}{\rho d^2}$
1
2
3
5
10
15
20
2
3
5
10
20
30
50

FIGURE 5.40

corresponding to various critical flow velocities have also been tabulated in figure 5.40.

A least square straight line fit through the points A and C-H was computed and is drawn as shown. Point 'A' was obtained at $R_G = 0.74 \times 10^4$ whereas point 'H' was recorded at $R_G = 1.55 \times 10^4$. Although both of these points lie within the subcritical range for a single cylinder, it was suspected that there might be some Reynolds number effect for the tube-bundle in this range. A simple test as described below was conducted to resolve this question.

The tuned natural frequency of the movable tubes was increased from 24 Hz to 32 Hz and the oil was completely removed from the damping cups. The increase in frequency resulted in a decrease of computed logarithmic decrement of the monitored tube from 0.01 to 0.008. A test was then run to determine the response and the results for the monitored tube are plotted in figure 5.41. Distinct regions due to turbulence response and fluidelastic response are apparent. The tube response has been replotted as curve 'B' in figure 5.39 refered to earlier in this section. The critical velocity has been plotted as point 'B' in the stability diagram of figure 5.40. The effect of increasing the natural frequency from 24 to 32 Hz was to increase the critical velocity from a Reynolds number of $0.83 \times 10^4$ to $1.10 \times 10^4$ (about 33%). However, within the limits of experimental uncertainty the corresponding reduced velocities fall on the same straight line. This suggests that no significant Reynolds number effects

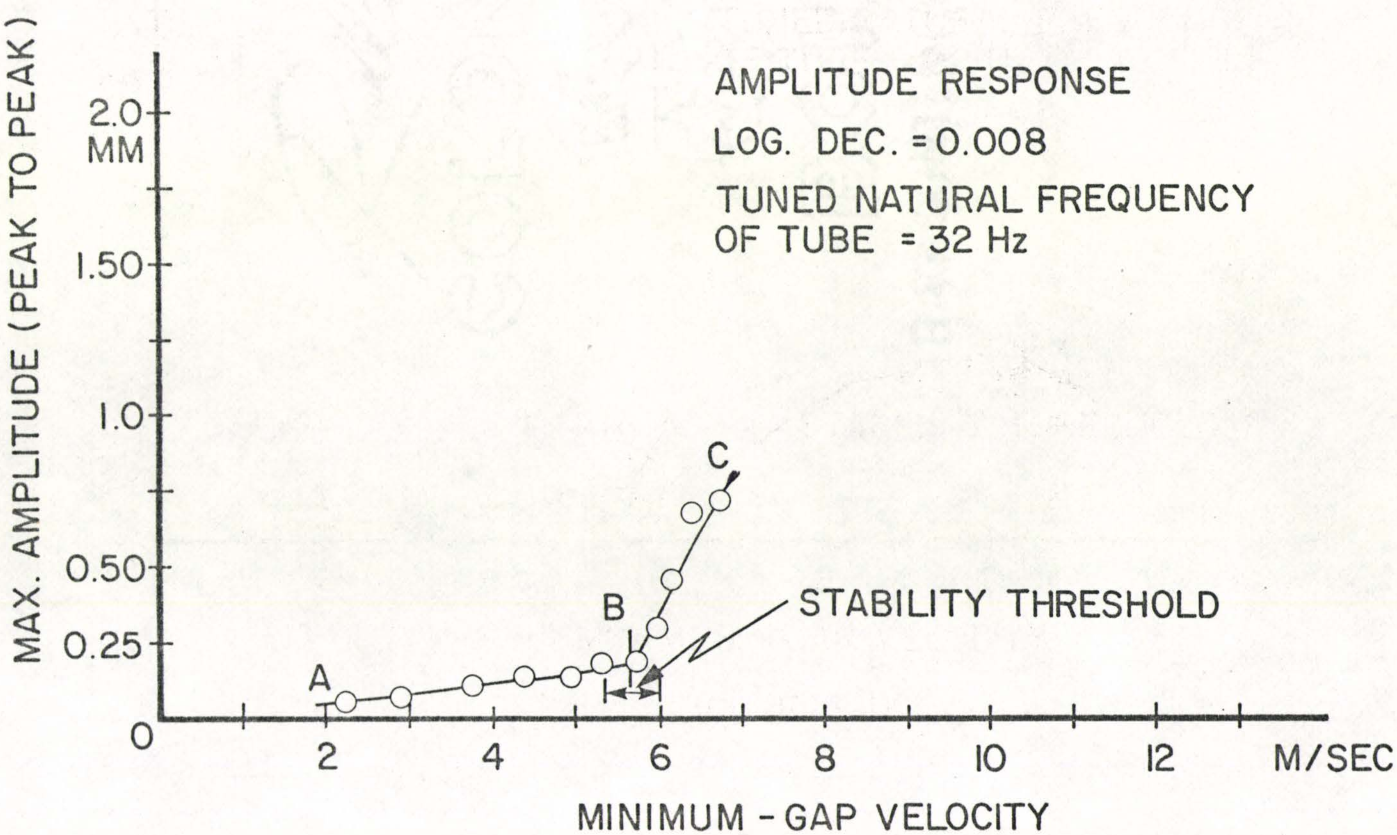
AMPLITUDE RESPONSE
LOG. DEC. = 0.008
TUNED NATURAL FREQUENCY
OF TUBE = 32 Hz
MAX. AMPLITUDE (PEAK TO PEAK)
2.0
MM
1.50
1.0
0.50
0.25
0
2
4
6
8
10
12
M/SEC
A
B
C
STABILITY THRESHOLD
MINIMUM - GAP VELOCITY

FIGURE 5.41

can be discerned within the range of values tested. Batham [111] conducted tests on an in-line array of stationary tubes for p/d = 1.25 and observed no Reynolds number effects on mean and fluctuating pressure coefficients in the range $2.8 \times 10^4$ to $10^5$.

The least-square fit to a straight line drawn in figure 5.40 is designated the 'stability boundary' for the array tested in the present experiments. The boundary can be defined by

$$\frac{V_G}{fd} = 7.1 \left(\frac{m\delta}{\rho d^2}\right)^{0.21} \qquad (1)$$

(Experimental points fall within $^{+4\%}_{-8\%}$ of this line.)

In the region below the 'stability boundary' the tube responds randomly at small amplitudes to turbulence in the flow. Above this boundary large amplitude vibrations of the tube occur at its natural frequency due to a fluidelastic mechanism and the whole array becomes unstable. The two parameter ranges for which this 'stability boundary' has been obtained are:

Damping parameter $\frac{m\delta}{\rho d^2}$ = 1.4 to 30

Velocity parameter $\frac{V_G}{fd}$ = 1.1 to 15.5

In the relationship (1), for a particular heat-exchanger m, $\rho$, d and f would normally be constants, therefore, there should be a direct relation between $V_G$ and $\delta$. For the present array it is obviously $V_G \propto \delta^{0.21}$ [$V = 44.4\ \delta^{0.21}$ for f = 24 Hz].

Dumpleton [76] in his experiments obtained $V_G \alpha \delta^{0.33}$. However, the geometry of his array is not known and also the number and range of data points used to derive this relationship is not known.

### 5.4.3 Discussion

The available information on critical flow velocities for tube arrays has been compiled by Shin and Wambsgnass [81] in the form of a stability diagram and is reproduced in figure 5.42. Connars' [78] stability threshold for a single row of tubes is given by a 0.5 power law, i.e.,

$$\frac{V_G}{fd} = 9.9 \left(\frac{m\delta}{\rho d^2}\right)^{0.5}$$

There are only four points in the data of figure 5.42 which can be possibly used for comparison with the present data. Three points are from Pettigrew marked 'P2' and one point is from Gorman marked 'G' for a parallel-triangular configuration (p/d value employed by Pettigrew and Gorman are slightly different from the present array). These four points along with the present data have been replotted in another stability diagram shown in figure 5.43 in order to avoid confusion. Three additional points from Hartlen [135] which were not included in Shin and Wambsgnass's stability diagram and two more data points from Gorman [113] obtained from his recent paper have also been included in figure 5.43. The dashed line for K = 3.3 is the threshold line suggested by Gorman.

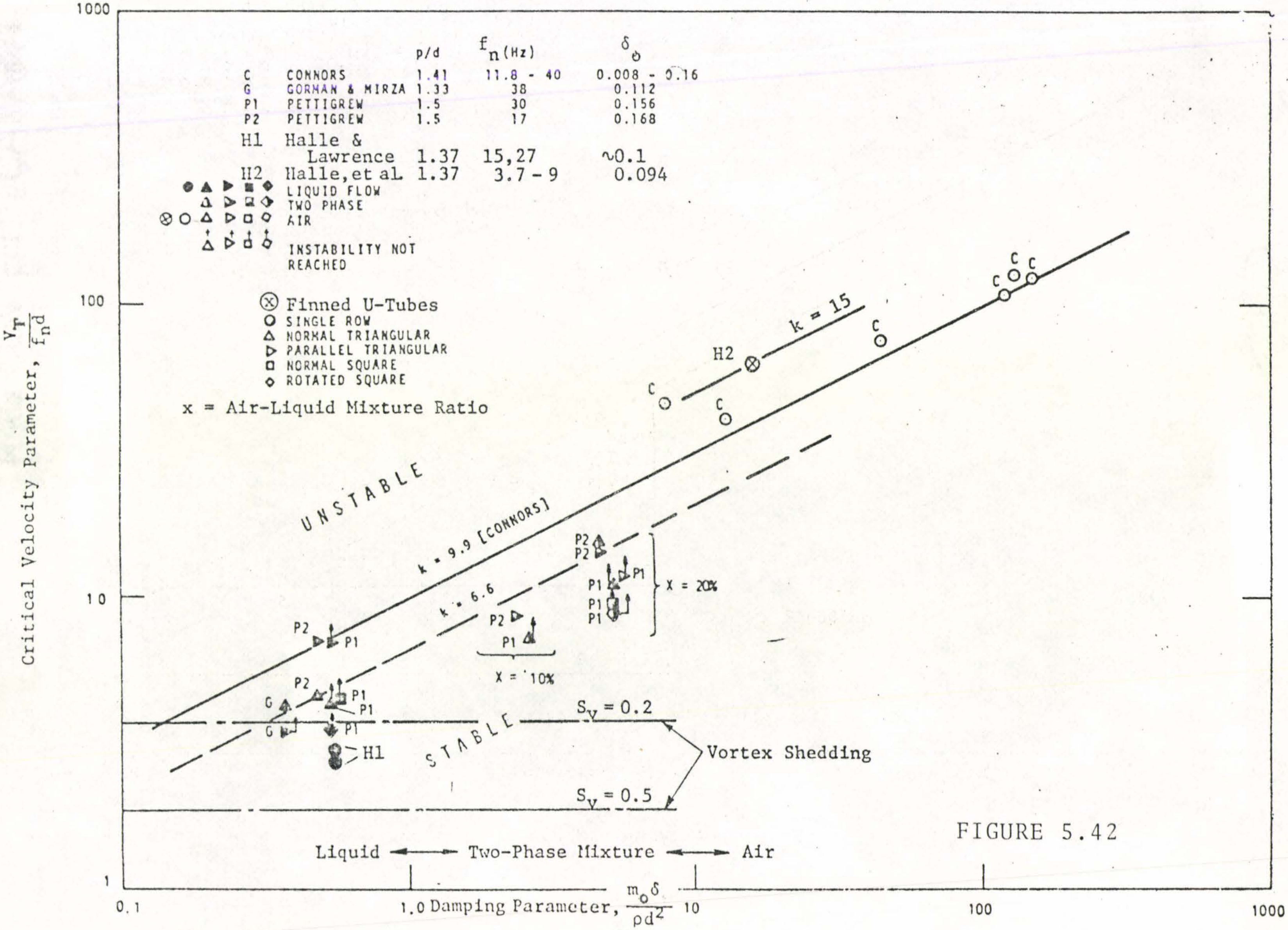


FIGURE 5.42

Stability Diagram for Tube Arrays.

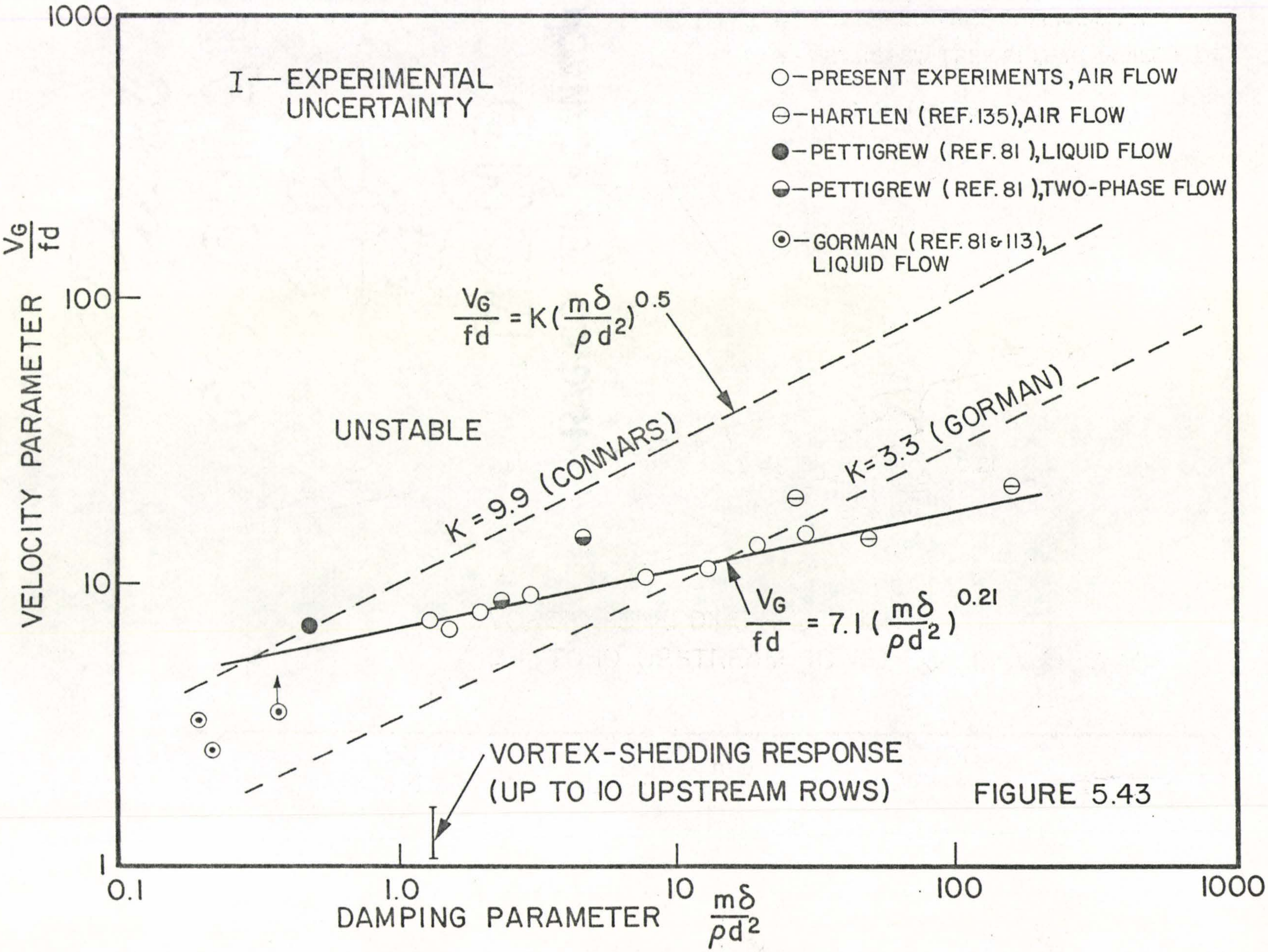
I — EXPERIMENTAL UNCERTAINTY
○ — PRESENT EXPERIMENTS, AIR FLOW
⊖ — HARTLEN (REF. 135), AIR FLOW
● — PETTIGREW (REF. 81), LIQUID FLOW
◒ — PETTIGREW (REF. 81), TWO-PHASE FLOW
⊙ — GORMAN (REF. 81 & 113), LIQUID FLOW
UNSTABLE
$\frac{V_G}{fd} = K\left(\frac{m\delta}{\rho d^2}\right)^{0.5}$
K = 9.9 (CONNARS)
K = 3.3 (GORMAN)
$\frac{V_G}{fd} = 7.1\left(\frac{m\delta}{\rho d^2}\right)^{0.21}$
VORTEX-SHEDDING RESPONSE
(UP TO 10 UPSTREAM ROWS)
VELOCITY PARAMETER $\frac{V_G}{fd}$
DAMPING PARAMETER $\frac{m\delta}{\rho d^2}$
1000
100
10
1
0.1
1.0
10
100
1000

FIGURE 5.43

Gorman's tests were conducted in a water-tunnel at damping parameter ($\frac{m\delta}{\rho d^2}$) values from 0.20-0.39 only. The following observations are warranted from figure 5.43.

(1) Gorman's points where stability threshold had been reached lie about 36-51% below the line obtained by extrapolating the present stability boundary.

(2) Pettigrew's point at $\frac{m\delta}{\rho d^2}$ = 0.49 for liquid flow is 13% above the extrapolated stability boundary. The uncertainty in Pettigrew's point is not known.

(3) Pettigrew's point at $\frac{m\delta}{\rho d^2}$ = 2.3 for two-phase flow (x = 10%) is only 4% above the present stability line.

(4) The third point of Pettigrew at $\frac{m\delta}{\rho d^2}$ = 4.7 which is again for two-phase flow (x = 20%) is 46% above the stability line.

(5) The two data points of Hartlen at $\frac{m\delta}{\rho d^2}$ = 50 and 166 are predicted within 10% of the present stability boundary extrapolated. However, Hartlen obtained this data in simple laboratory experiments to obtain design information and has stated that it may not be very precise.

(6) The third data point of Hartlen at $\frac{m\delta}{\rho d^2}$ = 28.6, for which better accuracy has been claimed, lies 33% above the present stability line. This difference could be due to the fact that Hartlen observed the onset of instability in the array only visually and hence the boundary will be unconservative.

While there is some scatter in the above data its agreement with the present results is very encouraging. The scatter may be attributed to the slightly different geometries tested as well as the different data collection procedures. The important point is that the present results are corroborated by experiments with tube-banks of different geometric scales and different shell side fluids. The implications of these results are extremely significant. The slope of the stability threshold is much less than that indicated by Connars (for a single row to tubes) and commonly used for tube-banks as it previously represented the only available data obtained for a range of reduced damping.

The present data has also been replotted on a fluid-elastic stability diagram suggested by Chen [131] and is shown in figure 5.44. The ordinate of this diagram is $\xi = \frac{R\ V_R}{X_T}$ rather than the velocity parameter (R = Reynolds number, $V_R$ = Reduced Velocity, $X_T$ = Transverse pitch = T/d). Chen has predicted that the data should fall around a line given by:

$$\xi = C\ \left(\frac{m\delta}{\rho d^2}\right)^{0.6}$$

where the value of C suggested by Chen is $0.35 \times 10^6$. The present data gives a constant of $C = 0.009 - 0.013 \times 10^6$ only, which is a very poor agreement with Chen's value. However, the present data does fall on the line:

$$\xi = 10^4\ \left(\frac{m\delta}{\rho d^2}\right)^{0.45} \quad \text{within} \ {}^{+\ 20\%}_{-\ 15\%}$$

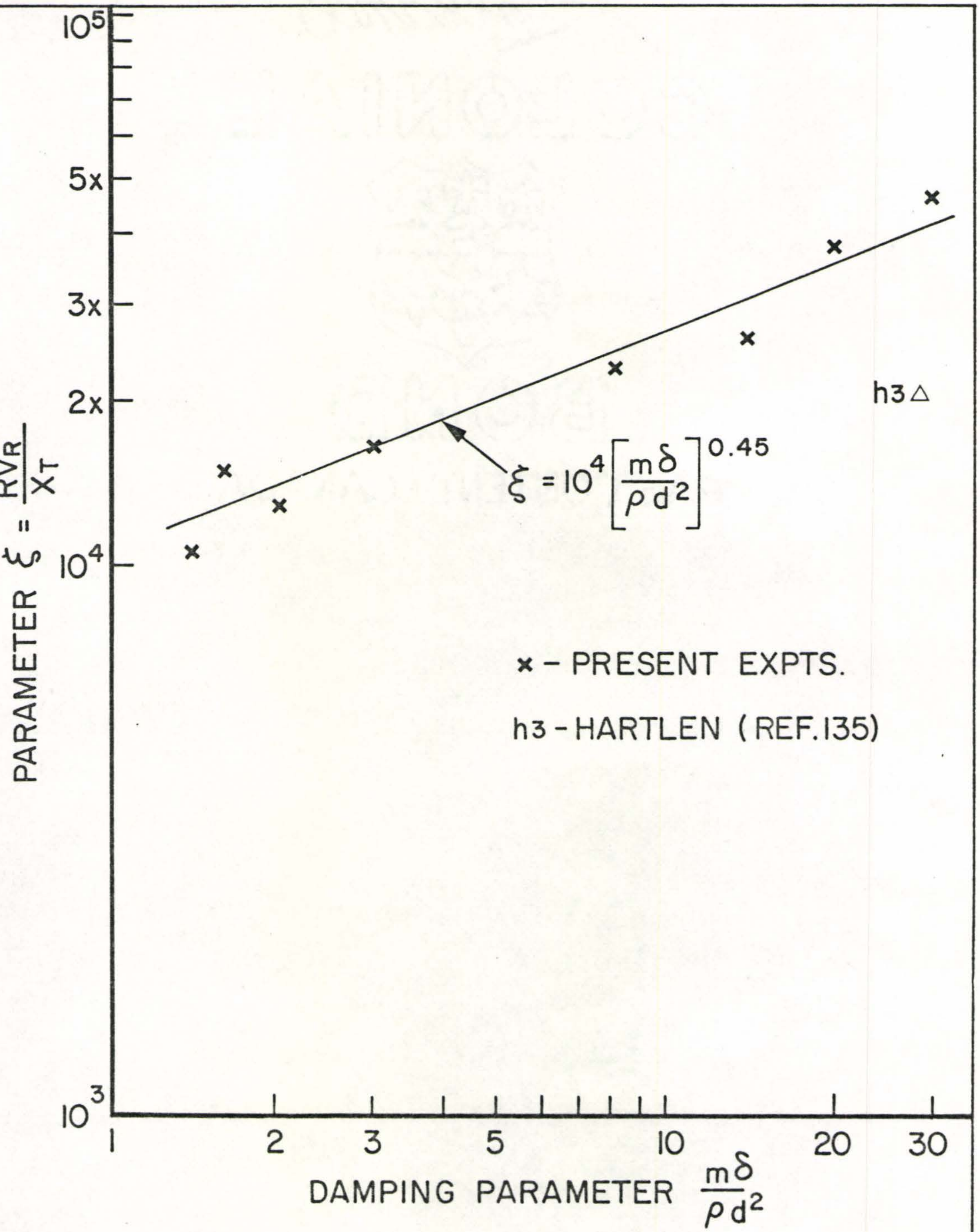


DATA POINTS ON STABILITY DIAGRAM OF CHEN (REF. 131)

FIGURE 5.44

which gives a constant $C' = \xi(\frac{m\delta}{\rho d^2})^{-0.45} = 10^4$.

Hartlen's data points have also been replotted in figure 5.44 and it is seen that their agreement with the present data becomes worse when plotted using the two dimensionless parameters suggested by Chen. It appears that in Chen's suggested stability diagram the effect of including Reynolds number is exaggerated out of proportion and it is difficult to realistically compare data from different experimenters (Pettigrew's data when plotted on this diagram goes completely off the scale).

No data exists in the literature from a systematic investigation of a stability boundary for any closely packed tube-bundle. The present investigation is the first attempt to vary the damping of tubes deep inside a tube-bundle over a wide range of values in order to obtain the fluidelastic stability boundary for the array. As this stability boundary is expected to be a function of geometry of the array, further experiments along the same lines are required to generate a family of threshold boundaries for various geometries of tube-bundles.

## 5.5 Coefficient of Lift in the Fluidelastic Region

The movable tubes were designed to give a linear response for up to $\pm$ 1 mm. of tube deflection. This feature can be used to compute the coefficient of lift as described in Appendix F. This method of determining the lift forces gives a 'gross effect' only and gets around the tedious problem of estimating the temporal and spatial distribution of forces along the length and around the circumference of the tube.

The lift-coefficients so obtained are shown in figure 5.45. It is seen that the coefficient of lift varies between 0.01-0.045. This value is much lower than the coefficient of lift obtained for the vortex-shedding response of the tube (section 5.1). It shows the misleading effect of normalizing lift forces with velocity head. For the same forces, the lift coefficient for fluidelastic oscillations will be much less than for vortex-shedding because of the much higher flow velocities.

The lift-coefficient is seen to be a function of amplitude of vibration and Reynolds number. The range of Reynolds numbers covered is from $0.7 \times 10^4$ to $2.2 \times 10^4$ (based on minimum-gap velocity) for which the corresponding $C_L$ has increased by a factor of about four. As expected, the lift coefficient increases with an increase in vibration amplitude. The arrows at the end of the two vertical dashed lines indicate the self-excited build up of amplitude of tube vibration without any further increase in the flow velocity.

No data is available in the literature on $C_L$ values obtained in the fluidelastic region for any tube array. For a single row of movable tubes in the range $R_T = 0.8\text{-}1.4 \times 10^5$ and for $y/d = 0.265$, Connars [78] obtained $C_L = 0.09\text{-}0.10$. This Reynolds number range is higher than that obtained in the present experiments and $C_L$ has been obtained at much higher y/d. Also as only one row of tubes was used the

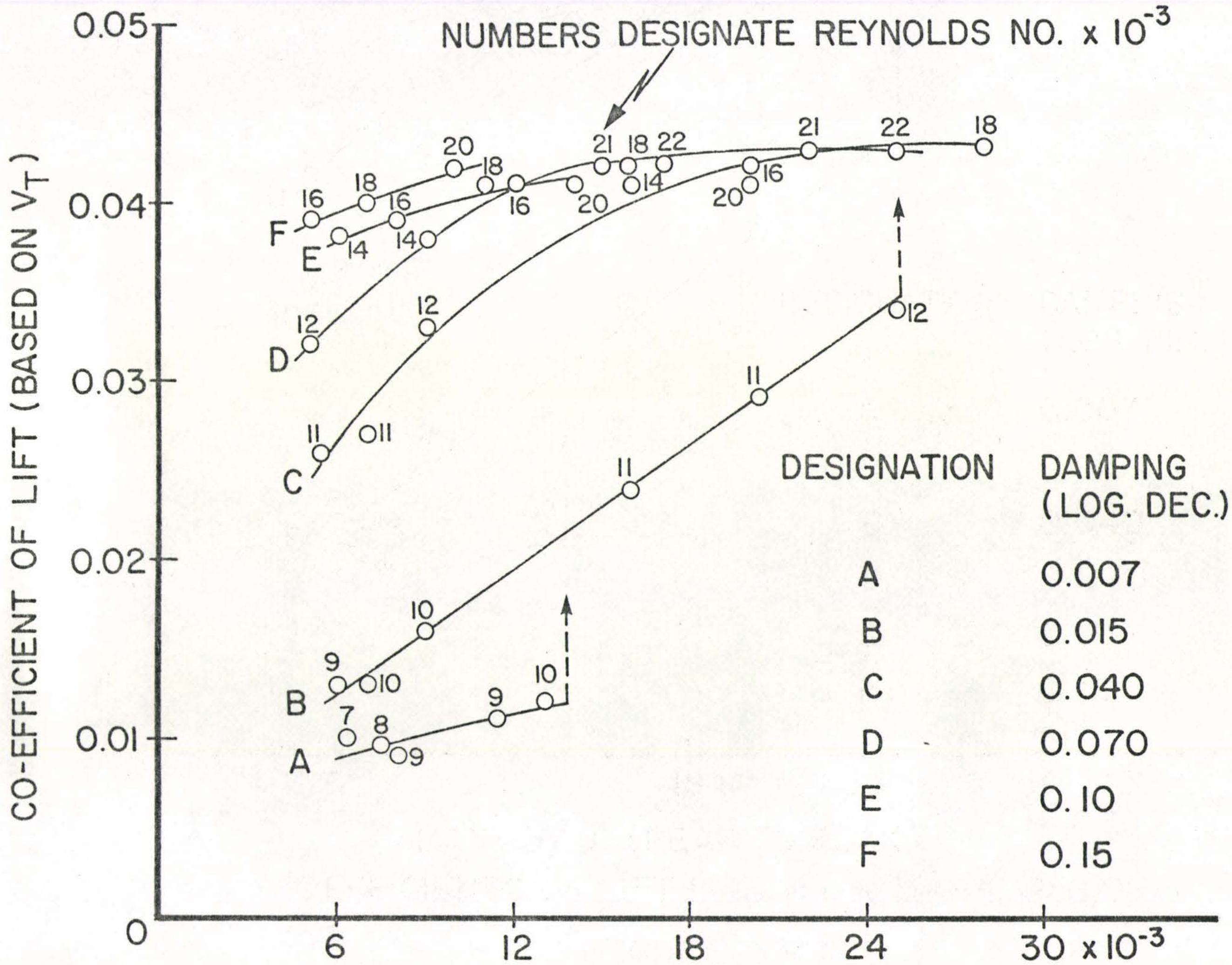


MAX. $y/d$ (PEAK TO PEAK)

CO-EFFICIENTS OF LIFT IN FLUID-ELASTIC REGION

FIGURE 5.45

correlation of forces along the length of the tube is expected to be better than that in a closely-pitched array.

At higher Reynolds numbers of about $2 \times 10^4$ it is seen that $C_L$ tends to reach a constant value, thus indicating that $C_D$ has become constant, which appears to be true as seen from figure 2.11 of Chen and Weber's paper [142]. In this figure they have shown that for staggered arrays $C_D$ decreases only up to $R_T = 6 \times 10^4$ and thereafter it stays constant till about $R_T = 10^5$. This point is also substantiated by referring to figure 5 of Chen's paper [97] where it is shown that for a circular cylinder, in the high subcritical range of $R = 5 \times 10^3$-$6x10^4$ the separation angle of the boundary layer stays constant at about $85^o$ from the front stagnation point.

For higher values of damping, the data appears to be converging to an upper bound for lift coefficient of about 0.043. The implication is that a further increase in the flow velocity produces no additional significant coupling effects or increased correlation of forces along the tubes.

The pressure-drop across the present tube-bundle was obtained by using two pitot-probes installed one upstream and the second downstream of the tube-bundle and the data obtained has been plotted against Reynolds number in figure 5.46. It is seen that the rate of decrease in pressure-drop is more rapid at lower Reynolds numbers. Wallis [99] and Chen [142] observed a decrease in pressure-drop in their arrays till about $R = 4 - 6 \times 10^4$ and thereafter the pressure-drop

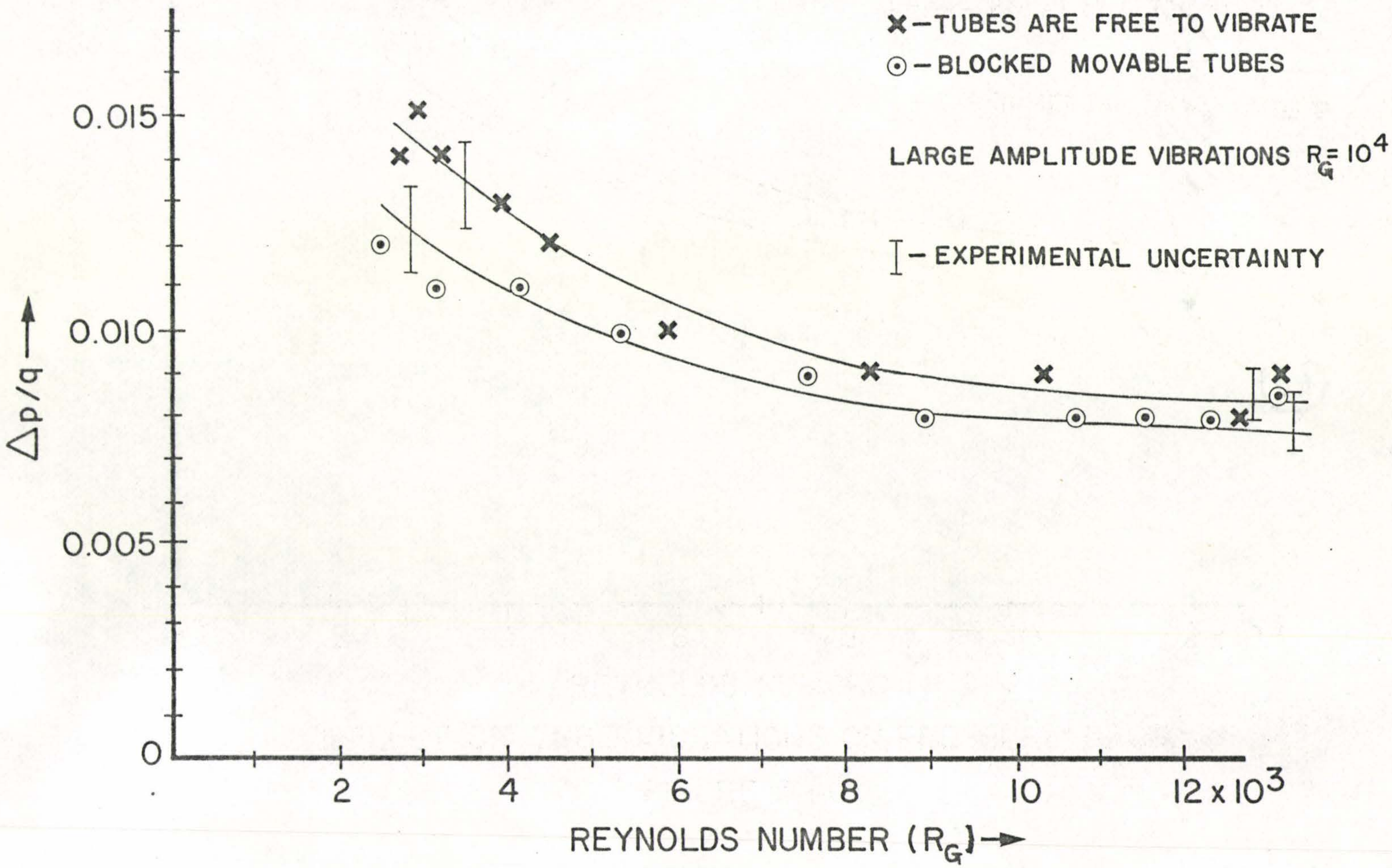


EFFECT OF TUBE VIBRATIONS ON PRESSURE DROP

FIGURE 5.46

attained a constant value. As the pressure-drop in the array is highly dependent on the geometry of the array, on the surface finish of the tubes and on the upstream flow conditions, only a qualitative comparison with the work of these authors can be afforded.

The effect of vibration of the movable tubes on pressure-drop was studied and it was found that the tube vibrations resulted in an increase in pressure-drop across the array as shown in figure 5.46. The small difference is undoubtedly due to an additional expenditure of flow energy required for maintaining the vibrations of tubes in the array. It should be remembered here that only 19 tubes were vibrating in the array having a total of 135 tubes (about 14% movable tubes).

## 5.6 Effect of Number of Upstream Rows on the Fluidelastic Stability Threshold

The effect of tube-bundle size on the critical velocity of the monitored tube was determined. The movable tubes were tuned at 24 $\pm$ 0.04 Hz and the damping of the monitored tube was $\delta$ = 0.007. The amplitude-response of the tube was recorded for the full array (14 rows upstream of tube no. 5) by following the procedure described in section 5.3.1. The stability threshold (critical velocity) was determined and plotted in figure 5.47. This procedure was repeated, removing one row of stationary tubes from the front of the remaining tube-bundle at a time, till the movable tube no. 8 (see

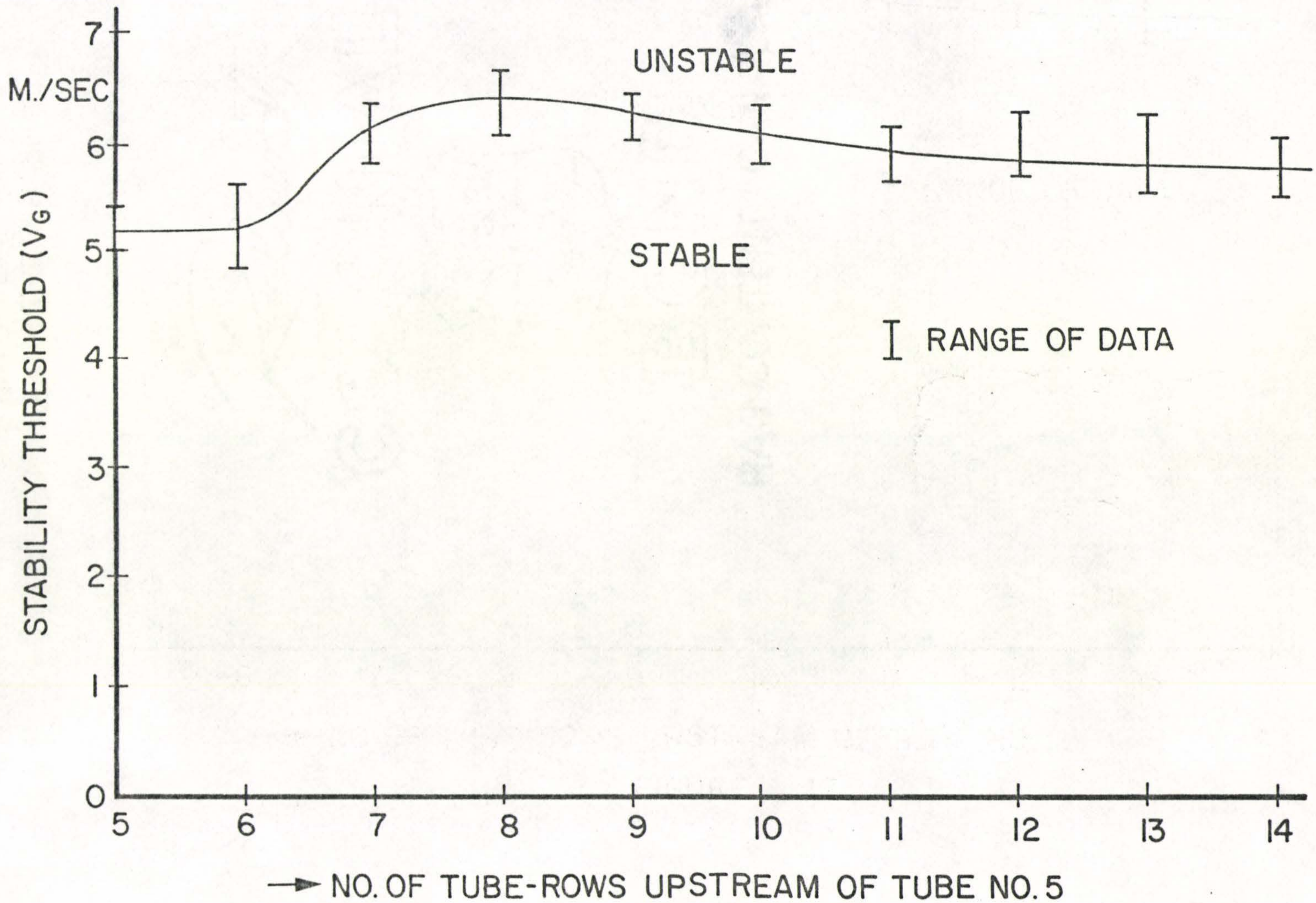

UNSTABLE
STABLE
RANGE OF DATA
M./SEC
STABILITY THRESHOLD ($V_G$)
0
1
2
3
4
5
6
7
5
6
7
8
9
10
11
12
13
14
NO. OF TUBE-ROWS UPSTREAM OF TUBE NO. 5


FIGURE 5.47

figure 5.1) was directly facing the upstream flow. The complete experiment was repeated three times and the results plotted in figure 5.46. A smooth curve was drawn through the bands representing experimental uncertainty.

A surprising result was obtained, in that the critical flow velocity was seen to vary with the size of the tube-bundle. The stability threshold is highest when the number of tube-rows upstream of the monitored tube were equal to eight. The threshold was lowest for minimum number of upstream rows (equal to five) and tended to level off as the number of rows upstream of the monitored tube were made about 10.

On the oscilloscope screen it was observed that the rate of amplitude build up of the tube appeared to be most rapid when there were no rows of stationary tubes upstream of the movable-tube bundle as compared to when the size of the upstream tube-bundle was bigger. A possible cause for this could be that when the movable-tubes bundle was directly facing the upstream flow, there is a better spanwise correlation of forces on the tubes and the turbulence intensity is certainly lower. This observation indicates that the sharpness of the stability threshold is also a function of number of upstream rows (in addition to that of damping as described in previous sections). It is not unexpected then to find that Connars [78] working only on a single-row of tubes, obtained relatively sharp thresholds.

Figure 5.47 shows that there is an increase in critical flow velocity by about 23% when the number of upstream rows is increased from 5 to 8 and there is a drop in the critical velocity of about 12% as the number of upstream rows is further increased from 8 to 14. The increase in critical velocity as the number of upstream rows increases from 5 to 8 could be explained by the increase in the upstream turbulence intensity. This could delay the commencement of large amplitude vibrations to higher flow velocities and decrease the rate of amplitude build-up. The same observation has also been recorded by Zdrakovich [110]. The 12% drop in critical velocity with a further increase in the number of upstream rows could be explained by the flow's becoming rather regularised having achieved a maximum turbulence level. Once the flow is established well inside the tube-bundle (before reaching the movable-tubes) no dramatic changes occur and the stability boundary does not appear to change further.

These results have several important implications for future design and experimentation. It appears that the first tubes to become unstable in a particular tube-bundle will be in the first few rows. That is, the tubes deep inside a tube-bundle are not the critical ones. In addition, experiments on a tube-bundle with only four or five rows of tubes should be adequate for establishing the critical fluidelastic stability boundary for that array. It should also be noted that some discrepancy between data obtained by different researchers using different sized arrays is to be expected.

# CHAPTER 6

## SUMMARY AND CONCLUDING REMARKS

The author's aim was to study cross-flow-induced vibrations of a model tube-array in the parameter range where both vortex-shedding and fluidelastic types of instabilities were expected to occur. It was intended to determine whether vortex-shedding occurs deep inside a tube-bundle and what would be the effect of tube-bundle size on the vibration and flow-field characteristics of the tube-array. It was also desired to investigate the nature of the fluidelastic instability deep inside a tube-array.

The experiments were conducted in a low-speed wind-tunnel having 305 x 305 mm. (12" x 12") working section. The tube-bundle was a parallel-triangular array of tubes having pitch/diameter = 1.375. The array was 27 rows deep with 5 tubes in each row. Nineteen identical tubes in the middle of the tube-array were movable and were specially designed so that their natural frequency and damping could be controlled precisely over a range of values. The remaining tubes were fixed tubes and were designed such that they could be conveniently removed from outside the wind-tunnel, in order to facilitate studying the effect of tube-bundle size on vibration and flow characteristics. The experiments were conducted over a Reynolds number range from 700 to $2.2 \times 10^4$ (based on tube diameter and minimum-gap velocity).

Discrete periodicity in the flow has been recorded up to a Reynolds number of about $10^3$. (While no response of the tubes was seen for a large number of rows, there still existed discrete vortex-shedding at low Reynolds numbers). The Strouhal number based on minimum-gap stream velocity is 0.83. As the Reynolds number or the number of rows in the array is increased, this well-defined periodicity in the flow breaks down and the flow-field shows a narrow-band velocity power-spectrum. The coefficient of lift of a vibrating tube while in resonance with vortex-shedding frequency is 0.41. The response of a tube due to vortex-shedding would depend on Reynolds number and the number of upstream rows of tubes. However, the vortex-shedding response occurs at such low flow velocities (high Strouhal numbers) that the von Karman vortex effect is believed to be a negligible factor in promoting damaging tube vibration at least when the fluid on the shell-side of the tubes is a gas.

At higher Reynolds numbers ($> 10^3$), the frequency corresponding to the maximum level of energy in the velocity power-spectra obtained from the present tube-array can be predicted by a Strouhal number of 0.21 over the Reynolds number range tested. From the flow-field velocity power-spectra obtained for the array used in the present experiments and from the available data existing in the literature it is seen that there is a strong possibility of predicting the dominant frequency of flow in any tube-bundle from a universal Strouhal number equal to 0.21 (based on the minimum-gap flow velocity). The peak frequency computed from the universal Strouhal number would be useful for predicting and avoiding the acoustic resonance only, because the mechanical vibrations of the tubes in the array occur even when their natural frequencies are mismatched to this peak frequency.

Self-excited vibrations of the movable tubes were observed at their natural frequencies as the flow rate was increased beyond a certain critical flow velocity. The mode shape of vibration of the tube appeared to be predominantly in the transverse direction but the tube frequently oscillated within about $\pm 45^{\circ}$ to this direction. A fluidelastic stability boundary for the array has been derived and the periodic self-excited vibrations in the array can be predicted by the relationship:

$$\frac{V_G}{fd} = 7.1 \left(\frac{m\delta}{\rho d^2}\right)^{0.21}$$

(formulated for a damping parameter range from 1.4 to 30). It is believed that a tube deep inside a tube-array starts to vibrate when enough fluid-dynamic energy is available at the tube's natural frequency to overcome the damping of the tube. Once a vibration of sufficient amplitude is produced, the tube's motion amplifies and controls flow periodicity at the tube's natural frequency and the tube amplitude continues to increase until restricted by system non-linearity and damping. This type of vibration occurs at higher flow velocities than vortex-shedding and may lead to tube failure.

For the first time a fluidelastic stability boundary as a function of damping parameter for the array has been determined experimentally. It is found that the slope of this boundary is significantly different from that derived by previous authors from theoretical considerations based on very simple geometrical configurations and which forms the foundation for current design practice.

The results from the study of a number of tube-rows in a tube-bundle on its vibration characteristics (in the fluidelastic region) have several important implications for future design and experimentation. It appears that the first tubes to become unstable in a particular tube-bundle will be in the first few rows. That is, the tubes deep inside a tube-bundle are not the critical ones. In addition, experiments on a tube-bundle with only four or five rows of tubes should be adequate for establishing the critical fluid-elastic stability boundary for that array.

Although the present research work has answered some very important questions and has improved our understanding of the dynamic behaviour of tubes deep inside a tube-bundle, it has undoubtedly raised a number of new questions. Some of the specific areas requiring future research in the area are enumerated below:

(a) The dimensionless damping parameter currently used for design is in fact a combination of two dimensionless parameters, viz., mass ratio and logarithmic decrement of damping. Therefore, it is anticipated that the two parameters could behave independently of each other. If this is so the fluidelastic boundary which is obtained by varying the damping parameter would be different from that obtained by varying the mass ratio.

(b) The fluidelastic stability boundary has been obtained for a single tube-bundle only. The stability boundary is expected to vary with the geometry of the array and it is desired to obtain these stability boundaries for a range of different tube patterns, especially for in-line arrays where the fluidelastic vibration threshold is expected to be much sharper.

(c) In the present investigation the Reynolds numbers for which vortex-shedding response was observed were above those for which discrete vortex-shedding occurred. It would be worthwhile to examine the response of the tubes with lower natural frequencies so that the region of discrete vortex-shedding overlapped the tube frequency.

(d) The present research has also indicated that vortex-shedding response is a function of Reynolds number and the number of upstream tubes in the array. There is a need to obtain and correlate this information for different patterns of the tube arrays.

(e) In regard to turbulent buffeting within the tube banks, additional experimental results are required to further evaluate the hypothesis of a universal Strouhal number for predicting the dominant frequency of the flow-field in any tube-bundle.

(f) The quasi-steady model developed by Connars [78] assumes a mode shape different from that observed in the present experiments. It also requires the coupled motion of the adjacent tubes, which led Blevins [79] to the conclusion that detuning of adjacent tubes will eliminate the vibration problem. However, the present study indicates that coupling of adjacent tubes is not necessary. It would be very useful to investigate experimentally the effect of detuning adjacent tubes on the stability threshold and velocity power-spectra.

# REFERENCES


1. Symposium on "Fluid-solid interaction", presented at ASME Winter annual meeting, Pittsburgh, Nov.-1967. Ed. J. E. Greenspon.

2. Oldaker, I. E., Et al., "An overview of the Canadian program to investigate vibration and fretting in nuclear fuel assemblies", CSME paper no. 73-CSME-89.

3. IUTAM/IAHR, 1974 Proc. of Symp. on flow-induced structural vibs., Karksruhe, Germany. Springer-Verlag, Berlin. Ed. E. Naudascher.

4. Weaver, D. S., "On flow-induced vibrations in hydraulic structures and their alleviation", Canadian J. of Civil Engg., Vol. 3, No. 1. 1976.

5. Nelms, H. A., Segaser, C. L., "Survey of nuclear reactor system primary circuit heat-exchangers", April 1969, ORNL-4399, Oak-ridge.

6. Int. Symp. on vib. problems in industry, Keswick, England, 1973. (U.K. Atomic energy authority at Windscale, N.P.L.).

7. Proceedings of the wind effects on buildings and structures conference, NPL, Teddington, England, June 1963.

8. Toebes, G. H., "Flow-induced structural vibrations", J. Engineering Mechanics Division, ASCE, EMG, 1965, pp. 39-65.

9. Flax, A. M., "Aero and Hydroelasticity", Proc. of the first symp. on Naval Struc. Mechanism, Pergamon Press, New York, 1960, p. 285.

10. Abramson, H. N., "Hydroelasticity - some problems and some solutions", ASME Symp. onf fluid-solid interaction, 1967, p. 187.

11. Benjamin, T. Brooke, "The threefold classification of unstable disturbances in flexible surfaces bounding inviscid flow", J. Fluid Mechanics, Vol. 16, 1963, p. 436.

12. Naudascher, E., "From flow instability to flow-induced excitation", ASCE, J. of Hydraulics Div., HY4, 1967.

13. Cooper, K. R., Wardlaw, R. L.: "Aeroelastic instabilities in wakes", Proc. 3rd Int. Conf. Wind Effects on Bldgs. and Structures, Tokyo, IV, (1971).

14. Simpson, A., "Stability of subconductors of smooth circular cross-section. Proc. Inst. Elect. Engrs. 117, 4, (April 1970).

15. Davis, D. A., et al., "Investigation of conductor oscillation on the 275 kV crossing over the Rivers Severn and Wye. Proc. Inst. of Elec. Engrs. 110, 1, (1963).

16. Bisplinghoff, R. L., Ashley, Holt, Halfman, R. L., "Aeroelasticity", Addison-Wesley, Cambridge, Mass., 1955.

17. Bolotin, V. V., "Nonconservative problems of the theory of elastic stability", Pergamon Press, New York, 1963.

18. Baker, W. E., Westine, P. S. and Dodge, F. T., "Similarity Methods in Engineering Dynamics", Hayden Book Co., New Jersey.

19. Den Hartog, J. P., "Recent technical manifestations of von Karman's vortex wake", Engineering, Vol. 40, 1954, pp. 155-157.

20. Marris, A. W., "A review on vortex streets, periodic wakes, and induced vibration phenomena", J. of Basic Engg., June 1964.

21. Roshko, S., "Experiments on the flow past a circular cylinder at very high Reynolds number", J. of Fluid Mechanics, Vol. 10, 1961, pp. 345-356.

22. Wille, R., "Karman vortex streets", Adv. Appl. Mech. (1960), Vol. 6, p. 273.

23. Abernathy, F. H. and Kronauer, R. E., "The formation of vortex streets", J. Fluid Mech., 13, 1, (1962).

24. Fage, A., and Johansen, F. C., "Structure of vortex streets", Phil. Mag. S.7, vol. 5, No. 28, Feb. 1928, pp. 417-441.

25. Papailiou, D. D., and Lykoudis, P. S., "Turbulent vortex streets and the entrainment mechanism of the turbulent wake", J. of Fluid Mechanics (1974), vol. 62, part 1, pp. 11-31.

26. Prandtl, L., "The generation of vortices in fluids of small viscosity", The J. of the Royal Aeronautical Society, (1928), pp. 720-741.

27. Fromm, J. E. and Harlow, F. H., "Numerical solution of the problem of vortex street development", The Physics of Fluids, Vol. 6, No. 7, July 1963, pp. 975-982.

28. Birkhoff, G., "Formation of vortex streets", J. of Applied Physics, Vol. 24, No. 1, pp. 98-103.

29. Morkovin, M. V., "The interaction of vorticity and pressure fields", Symp. on flow-induced vib. in heat-exchangers, ASME, New York, 1970.

30. Lenharth, W., and Corell, R. W., "Thoughts on the relationship between Reynolds and Strouhal numbers", J. of Sound and Vibration (1974) 36 (1), pp. 147-149.

31. Scruton, C., "On the wind-excited oscillations of stacks, Towers, and Masts", N.P.L. Symp. on wind effects on bldgs. and struc., 1963.

32. Weaver, W., "Wind-induced vibrations in Antenna members", J. Engg. Mech. Div., Proc. ASCE, Vol. 87, 1961.

33. Ferguson, N., and Parkinson, G. V., "Surface and wake flow phenomena of the vortex-excited oscillation of a circular cylinder", ASME paper 67-Vibr.-31.

34. Gerrard, J. H., "An experimental investigation of the oscillating lift and drag of a circular cylinder shedding turbulent vortices", J. of Fluid Mechanics, Vol. 11, part 2, 1961, pp. 244-256.

35. Bishop, R. E. D., and Hassan, A. Y., "The lift and drag forces on a circular cylinder in a flowing fluid", Proc. Roy. Soc. A, vol. 277, pp. 32-50.

36. Fung, Y. C., "Fluctuating lift and drag acting on a cylinder in a flow at supercritical Reynolds number", J. of Aerospace Science (1960), Vol. 27, pp. 801-14.

37. Keefe, R. T., "An investigation of the fluctuating forces acting on a stationary circular cylinder", Univ. of Toronto, UTIA Report no. 76, 1961.

38. Rouse, H., "Fluid Mechanics for Hydraudlic Engineers", Dover publications, Inc. New York.

39. Chen, Y. N., "Flow-induced vibrations in tube-bundle heat-exchangers", Symp. on flow-induced vib. in heat-exchangers, ASME, New York, 1970.

40. Griffin, O. M., "Flow near self-excited and forced vibrating circular cylinders", ASME paper no. 71-vibr-25.

41. Griffin, O. M., "Flow near self-excited and forced vibrating circular cylinders", ASME paper no. 71-Vibr-25.

42. Griffin, O. M., "Instability in the vortex street wakes of vibrating bluff bodies", J. of Fluids Engineering, Dec. 1973, pp. 579-81.

43. Bishop, R. E. D., and Hassan, A. Y., "The lift and drag forces on a circular cylinder oscillating in a flowing fluid", Proc. Roy. Soc. A, Vol. 277, pp. 51-75.

44. Collins, W. M., and Dennis, S. C. R., "Flow past an impulsively started circular cylinder", J. Fluid Mech. (1973), vol. 60, part 1, pp. 105-127.

45. Heinzer, A., and Dalton, C., "Wake observations for oscillating cylinders", J. of Basic Engineering, Dec. 1969, pp. 850-852.

46. Ferguson, N. and Parkinson, G. V., "Surface and wake flow phenomena of the vortex-excited oscillation of a circular cylinder", ASME paper no. 67-Vibr.-31.

47. Hartlen, R. T., and Curie, I. G., "Lift-oscillator model of vortex-induced vibration", ASCE, J. of Engg. Mech. Div., EM-5, Oct. 1970, pp. 577-591.

48. Landl, R., "Theoretical model for vortex excited oscillations", paper No. 114 of Ref. No. 6.

49. Currie, I. G., et al., "The response of circular cylinders to vortex shedding", Pages 128-142 of Ref. No. 3.

50. Chen, Y. N., "The relationship between the von Karman vortex street and the steady drag of a single circular cylinder", Symp. on flow induced vib. in heat-exchangers, ASME, New York, 1970.

51. Iwan, W. D., and Blevins, R. D., "A model for vortex-induced oscillation of structures", J. of Applied Mechanics, Sept. 1974, pp. 581-586.

52. Parkinson, G. V., "Mathematical models of flow-induced vibrations of bluff bodies", General lecture; pages 81-127 of Ref. No. 3.

53. Shaw, T. L., "Effect of side walls on flow past bluff bodies", ASCE, J. of Hydraulics Div., Jan. 1971, pp. 65-79.

54. Ramamurthy, A. S., and Lee, P. M., "Wall effects on flow past bluff bodies", J. of Sound and Vibration (1973) 31(4), pp. 443-451.

55. Apelt, C. J., et al., "The effects of wake splitter plates on the flow past a circular cylinder in the range $10^4 < R < 5 \times 10^4$", J. of Fluid Mechanics (1973), Vol. 61, part 1, pp. 187-198.

56. Petrie, A. M., "Effect of free-stream turbulence on vortex-shedding in the wakes of cylinders in cross-flow", Journal of Sound and Vibration (1974) 34(2), pp. 287-290.

57. Kestin, J., "The effect of freestream turbulence of heat-transfer rates", Advances in Heat Transfer, Vol. 3, 1964, pp.1-32.

58 Maull, D. J., and Young, R. A., "Vortex shedding from bluff bodies in a shear flow", J. of Fluid Mechanics (1973), Vol.60, part 2, pp. 401-409.

59. Vickery, B. J., "Fluctuating lift and drag on a long cylinder of square cross section", J. of Fluid Mechanics, Vol. 25, part 3, 1966, p. 481.

60. Protos, A., et al., "Hydroelastic forces on bluff cylinders", J. of Basic Engineering, Trans. ASME, Series D, No. 3, Sept. 1966, pp. 378-386.

61. Modi, V. S., and Wiland, E., "Unsteady aerodynamics of stationary elliptic cylinders in sub-critical flow", AIAA Journal, Vol. 8, No. 10, 1970, pp. 1814-1821.

62. Gaster, M., "Vortex shedding from slender cones at low Reynolds Numbers", J. of Fluid Mechanics, Vol. 21, No. 38, 1969, pp. 565-576.

63. Paidoussis, M. P., "An experimental study of vibration of flexible cylinders induced by nominally axial flow", Nuclear Science and Engg., 35 (1969), pp. 127-138.

64. Reavis, J. R., "Vibration correlation for maximum fuel-element displacement in parallel turbulent flow", Nuclear Science and Engineering, 38 (1969), pp. 63-69.

65. Burgreen, D., "Vibration of rods induced by water in parallel flow", Trans. ASME, July 1958, pp. 991-1003.

66. Basile, D., "Experimental study on the vibrations of various fuel rod models in parallel flow", Nuclear Engg. and Design 7 (1968), pp. 517-534.

67. Fung, Y. C., "Fluctuating lift and drag on a cylinder at supercritical Reynolds Number", J. Aerospace Sci., Vol. 27, 1960.

68. Spival, H. M., "Vortex frequency and flow pattern in the wake of two parallel cylinders at varied spacing normal to an air stream", J. of the Aeronautical

Sciences, June 1946, pp. 289-301.

69. Thomas, D. G., and Kraus, K. A., "Interaction of vortex streets", Journal of Applied Physics, Vol. 35, No. 12, Dec. 1964, pp. 3458-59.

70. Zdravkovich, M. M., "Flow-induced vibrations in irregularly staggered tube bundles, and their suppression", Paper No. 413 of Ref. No. 6.

71. Chen, S. S., "Dynamic responses of two parallel circular cylinders in a liquid", J. of Pressure Vessel Technology, Trans. ASME, May 1975.

72. Biermann, D., and Herrnstein, W. H., "The interference between struts in various combinations", from Ref. No. 73.

73. Wilson, J. F., and Caldwell, H. M., "Force and stability measurements on models of submerged pipelines", J. of Engineering for Industry, Nov. 1971, pp. 1290-1298.

74. Livesey, J. L., and Dye, R. C. F., "Vortex-excited vibration of a heat exchanger tube row", J. of Mech. Engg. Science, Vol. 4, No. 4, 1962, pp. 349-52.

75. Dye, R. C. F., "Vortex-excited vibration of a heat-exchanger tube row in cross-flow, Paper No. 417 of Ref. No. 6.

76. Dumpleton, O. W., "Tube vibrations: Interim report on experiments with gas-excited vibrations of boiler tubes", E. D. Report 4, EC/1, Babcock and Wilcox Ltd., (1959), from Ref. No. 74.

77. Roberts, B. W., "Low frequency, aeroelastic vibrations in a cascade of circular cylinders", Monograph No. 4, Inst. of Mech. Engrs., England, Sept. 1966.

78. Connars, H. J., "Fluidelastic vibration of tube arrays excited by cross-flow", Symp. on flow-induced vibs. in heat-exchangers, ASME, Dec. 1970.

79. Blevins, R. D., "Fluid elastic whirling of a tube row", J. of Pressure Vessel Technology, Trans. ASME, Nov. 1974, pp. 263-267.

80. Chen, S. S., "Vibrations of a row of circular cylinders in a liquid", J. of Engg. for Industry, Trans. ASME, 97, 1212-1218 (1975).

81. Shin, Y. S., and Wambsganss, M. W., "Flow-induced vibration in LMFBR steam generators", ANL-75-16, A.N.L. Argonne.

82. Savkar, S. D., "A survey of flow-induced vibrations of cylindrical arrays in cross-flow", ASME paper 76-WA/FE-21.

83. Chenoweth, J. M., Kistler, R. S., "Tube vibrations in shell-and tube heat exchangers", Report from HTRI California, Sept. 1976.

84. Hartlen, R. T., "Recent field experience with flow-induced vibration of heat-exchanger tubes", Paper No. 611 of Ref. No. 6.

85. Borges, A. R. J., "Vortex-shedding frequencies of the flow through two-row branks of tubes", J. of Mech. Engg. Sci., Vol. 11, No. 5, 1969, pp. 498-502.

86. Baird, R. C., "Pulsation-induced vibration in utility steam-generating units", COMBUSTION, Vol. 25, April 1954, pp. 38-44.

87. Halliday, John, "Boiler vibration caused by combustion gas-flow", ASME paper No. 56-A-216.

88. Stallabrass, J. R., "Aerodynamic noise in heat-exchangers", N.R.C. Ottawa, DME/NAE Quarterly, April 1966.

89. Chen, Y. N., "Flow-induced vibration and noise in tube-bank heat-exchangers due to von Karman streets", J. of Engg. for Industry, Vol. 90, No. 1.

90. Walker, W. M. and Reising, G. F., "Flow-induced vibrations in cross-flow heat-exchangers", Chemical and Process Engg., Nov. 1968, pp. 95-103.

91. Grotz, B. J. and Arnold, F. R., "Flow-induced vibrations in heat-exchangers", Stanford Univ. report AD-104-568, Aug. 1956.

92. Kays, W. M., and Loeschner, T. R., "Heat-transfer and flow friction characteristics of an elliptical pin-fin heat exchanger", Stanford Univ. report AD-228-668, Sept. 1959.

93. Putnam, A. A., "Flow-induced noise and vibration in heat-exchangers", ASME paper No. 64-WA/HT-21, 1964.

94. Dye, R. C. F., and Abrahams, C. G. M., "An investigation of the aerodynamic stability of a cross-flow type finned tube heat-exchanger", ASME paper No. 68-WA/HT-19.

95. Hill, R. S., and Armstrong, C., "Aerodynamic sound in tube-banks", Proc. Physical Society, Vol. 79, Part 1, No. 507, 1962, pp. 225-227.

96. Chen, Y. N., "Frequency of the von Karman vortex-street in tube banks", J. of the Royal Aeronautical Society, London, Vol. 71, 1967.

97. Chen, Y. N., "Fluctuating lift forces of the von Karman vortex-streets on single circular cylinders and in tube-bundles", ASME paper 71-Vibr-13.

98. Fitz-Hugh, J. S., "Flow-induced vibration in heat-exchangers", Paper No. 427, Ref. No. 6.

99. Wallis, R. P., "Photographic study of fluid flow between banks of tubes", ENGINEERING, Oct. 13, 1939, pp. 423-426.

100. Owen, P. R., "Buffeting excitation of boiler tube vibration", J. of Mech. Engg. Sci., Vol. 7, No. 4, 1965, pp. 431-439.

101. Gainsboro, N. R., "Tube vibration in a large bearing water cooler", Chemical Engineering Progress, Vol. 64, No. 3, 1968, pp. 85-88.

102. Coit, R. L., Peake, C. C. and Lohmeier, A., "Design and manufacture of large surface condensers", Proc. American Power Conf., 1966, pp. 469-483.

103. Wambsganss, M. W., "Vibration of reactor core components", Reactor and Fuel-Processing Technology, Vol. 10, No. 3, 1967, pp. 208-219.

104. Sebald, J. F. and Nobles, W. D., "Control of tube vibration in steam surface condensers", Proc. American Power Conf., 1962, pp. 630-642.

105. Kissel, J. H., "Flow-induced vibrations in heat-exchangers", Machine Design, May 3, 1973, pp. 104-107.

106. Cohan, L. J., and Deane, W. J., "Elimination of destructive vibrations in large, gas-and oil-fired utility units", Combustion, Oct. 1964, pp. 26-32.

107. Erskine, J. B. and Waddington, W., "A review of some tube vibration failures in shell and tube heat-exchangers", Paper No. 421, Ref. No. 6.

108. Zdravkovich, M. M. and Nuttall, J. A., "On the elimination of aerodynamic noise in a staggered tube bank", J. of Sound and Vibration (1974) 34(2), pp. 173-177.

109. Zdravkovich, M. M., "Flow-induced vibrations in irregularly staggered tube bundles, and their suppression", Paper No. 413, Ref. No. 6.

110. Southworth, P. J., Zdravkovich, M. M., "Cross-flow induced vibrations of finite tube banks in in-line arrangements", J. of Mech. Engg. Sci., Vol. 17, No. 4, 1975, pp. 190-198.

111. Batham, J. P., "Pressure distributions on in-line tube arrays in cross-flow", Paper No. 411, Ref. No. 6.

112. Southworth, P. J., and Zdravkovich, M. M., "Effect of grid-turbulence on the fluid-elastic vibs. of in-line tube banks in cross flow", J. of Sound and Vibration (1975) 39(4), pp. 461-469.

113. Gorman, D. J., "Experimental development of design criteria to limit liquid cross-flow-induced vibration in nuclear reactor heat exchange equipment", Nuclear Sci. and Engg., 61 (1976), pp. 324-336.

114. Langhaar, H. L., "Dimensional Analysis and theory of models", John Wiley and Sons, 1967.

115. Beavers, G. S., and Plunkett, R., "Modelling of flow-induced vibrations in heat-exchangers", ASME Paper No. 74-FE-31.

116. Pankhurst, R. C. and Holder, D. W., "Wind-tunnel technique", Sir Isaac Pitman and Sons Ltd., London, 1968.

117. Pope, A. and Harper, J. J., "Low-speed wind-tunnel testing", John Wiley and Sons, Inc., New York.

118. Gorlin, S. M., and Slezinger, I. I., "Wind-tunnels and their instrumentation", Translated from Russian Israel program for Scientific Translations, Jerusalem, 1966.

119. Smith, R. H. and Wang, Chi-Teh, "Contracting cones giving uniform throat speeds", J. of the Aeronautical Sciences, Oct. 1944.

120. Whitehead, L. G., Wu, L. Y. and Waters, M. H. L., Contracting ducts of finite length", The Aeronautical Quarterly, Feb. 1951.

121. Bloomer, N. T., "Notes on the mathematical design of nozzles and wind-tunnel contractions", The Aeronautical Quarterly, Aug. 1957.

122. Harrop, R., "A method for designing wind-tunnel contractions", J. of the Royal Aeronautical Society, March 1951.

123. Tsien, Hsue-Shen, "On the design of the contraction cone for a wind-tunnel", J. of the Aeronautical Sciences, Feb. 1943.

124. Szczeniowski, B., "Contraction cone for a wind-tunnel", J. of the Aeronautical Sciences, Oct. 1943.

125. Wade, J. H. T. and Fowler, H. S., "An introductory note on diffuser design and performance", ME-73-TF-1, McMaster Univ., Hamilton.

126. Laird, A. D. K., Warren, R. P., "Groups of vertical cylinders oscillating in water", J. of Engg. Mech. Div., Proc. ASCE., Feb. 1963.

127. Mabey, D. G., "Aerodynamically induced vibration in coolers", J. of the Royal Aeronautical Society, Dec. 1965, pp. 876-77.

128. Putnam, A. A., "Flow-induced noise in heat-exchangers", J. of Engg. for Power, Oct. 1959, pp. 417-422.

129. Thorngren, J. T., "Predict exchanger tube damage", Hydrocarbon Processing, April 1970, pp. 129-131.

130. Thompson, H. A., "Fatigue failures induced in heat-exchanger tubes by vortex-shedding", ASME paper No. 69-Pet-6.

131. Chen, Y. N., "The orbital movement and damping of the fluid elastic vibration of tube banks due to vortex formation", ASME paper No. 73-DET-146.

132. Heinecke, E., "Stationary and instationary flow phenomena in and behind staggered and in-line tube banks", Paper No. 412, Ref. No. 6.

133. Baylac, G., Bai, D. and Gregoire, J. P., "Study of flow and acoustic phenomena in a tube-bank", Paper No. 219, Ref. No. 6.

134. Brown, R. D., "Turbulent Buffeting of high pressure feed heater tubes", Paper No. 423, Ref. No. 6.

135. Hartlen, R. T., "Wind-tunnel determination of fluid elastic vibration thresholds for typical heat-exchanger tube patterns, Ontario Hydro, Research Division Report No. 74-309-K.

136. Blevins, R. D., "Fluid elastic whirling of tube rows and tube arrays", ASME Paper No. 76-WA/FE-26.

137. Chen, S. S., "Dynamics of heat-exchanger tube banks", ASME Paper No. 76-WA/FE-28.

138. Chen, S. S., "A mathematical model for cross-flow-induced vibrations of tube rows", Technical Report ANL-CT-77-4, A.N.L. Argonne, Illinois, Sept. 1976.

139. Fraas, A. P., and Ozisik, M. N., "Heat-exchanger design", John Wiley and Sons, Inc., New York.

140. Kays, W. M., and London, A. L., "Compact heat-exchangers", McGraw-Hill Book Co., New York, 1964.

141. Schneider, W. and Wade, J. H. T., "Investigation of flow in the Mechanical Engg. Dept. Laboratory Air Jet", Mech. Engg. Dept., McMaster Univ., 1963.

142. Chen, Y. N., and Weber, M., "Flow-induced vibrations in tube bundle heat-exchangers with cross and parallel flow", Symp. on Flow-Induced Vibration in Heat-Exchangers, ASME, 1970, pp. 57-77.

143. Lazan, B. J., "Damping of Materials and Members in Structural Mechanics, Pergamon Press, New York, 1968.

144. Fitzpatrick, J. A., and Donaldson, I. S., "A Preliminary study of flow and acoustic phenomena in tube-banks", A.S.M.E. paper No. 77-FE-7.

# APPENDIX A

## (1) Power Requirements for the Wind-Tunnel

Apart from those associated with the inefficiency of the driving unit, the losses which occur in a typical wind-tunnel are due to vorticity and eddying motion (arising from skin friction, flow separation, turbulence, etc.), due to blockage of model in the working section and in an open circuit tunnel, due to the rejection of kinetic energy at the diffuser exit. The magnitude of the losses is estimated by summing the losses due to each component of the tunnel. However, in the present wind-tunnel the power requirements will be governed mainly by the pressure drop across the tube-bundle in the working section. The power requirements of the wind-tunnel shown in figure 4.1 are computed as follows:

(a) Losses due to skin-friction at the walls:

The local coefficient of friction is defined by the expression (Ref. Pankhurst [116]).

$$C_f = \frac{\text{Frictional force}}{1/2\ \rho\ V^2\ A'}$$

where $A'$ = surface area of the solid boundary which is subject to the frictional force.

For turbulent flow in a channel with smooth walls the frictional coefficient is given approximately by:

$$C_f = 0.0018 + 0.1526\ R^{-0.35}$$

where $R$ = Reynolds number based on the diameter of the channel.

And considering the flow in a channel of x-sectional perimeter L, the loss of total head due to skin-friction is given by:

$$\Delta H = \quad C_f\ \frac{1}{2}\ \rho\ V^2\ \frac{L}{A}\ ds$$

where ds is an element of length in the direction of the flow and A the cross-sectional area, the integral being taken over the length of the channel.

Using mean dimensions and flow-velocities, the pressure drops due to skin-friction across various components of the wind-tunnel were computed and are tabulated below:

1. at contraction = 1.5 N./m$^2$. (0.0322 lbf./ft$^2$.)
2. at working-section = 11.2 N./m$^2$. (0.233 lbf./ft$^2$.)
3. at diffuser = 28.1 N./m$^2$. (0.587 lbf./ft$^2$.)

Total $\Delta H$ due to skin-friction = 40.8 N./m$^2$. (0.852 lbf./ft$^2$.)

(b) Diffuser losses:

Corresponding to a maximum design velocity of 18.3 m./sec. (60 ft./sec.) at the working section, velocity at the exit of the diffuser is 4.6 m./sec. (15 ft./sec.).

Theoretical gain of kinetic energy in the diffuser

$$= \frac{1}{2}\ \rho\ V_1^2 - \frac{1}{2}\ \rho\ V_2^2$$

$= \quad 192\ N./m^2.\ (4\ lbf./ft^2.)$

where $V_1$ = velocity at the entrance to the diffuser

and $V_2$ = velocity at the exit of the diffuser

As the diffuser design is based on 90% efficiency, therefore, losses due to local separation of flow are:

$= 0.1 \times 192 = 19.2\ N./m^2.\ (0.4\ lbf./ft^2.)$.

There is loss due to unrecovered kinetic energy flowing out at the exit of the diffuser:

$$= \frac{1}{2} \rho V_2^2$$

$$= 13\ N./m^2.\ (0.267\ lbf./ft^2.)$$

(c) Pressure-drop across the array

No design data for the pressure-drop across the array being tested exists (P/d = 1.375, d = 0.0254 m. [1 in.] parallel-triangle array, 27 rows deep, 5 tubes/row). An exact estimate for the pressure-drop is, therefore precluded. However, a very rough estimate can be obtained by using the performance data provided by Fraas and Ozisik [139] for a staggered tube-bundle of P/d = 1.50 containing 10 rows with 9 tubes/row. He gives $\Delta p/q = 0.6$ where q = dynamic head and $\Delta p$ = pressure-drop across the array.

Using a maximum flow velocity of 18.3 m.sec. (60 ft./sec.)

$q = 205\ N./m^2.\ (4.27\ lbf./ft^2.)$

therefore,

$$\Delta p = 0.6 \times 205 = 123\ N./m^2.\ (2.56\ lbf./ft^2.).$$

For the present array let us take $\Delta p = 192$ N./m$^2$. (4 lbf./ft$^2$.).

(d) Total pressure drop:

The total pressure drop across the wind-tunnel is then the sum of all the pressure drops computed above viz:

$$\Delta H = 40.8 + 19.2 + 13 + 192 = 265 \text{ N./m}^2. \ (5.52 \text{ lbf./ft}^2.)$$

$$= 0.027 \text{ m. water (static pressure) } (= 1.07 \text{ in.}).$$

Therefore, the fan at the end of the wind-tunnel must be able to develop at least 0.025 m. (1 in.) static pressure. The actual power required will depend on the type of fan used.

(ii) Specifications of the fan

A vaneaxial fan manufactured by Buffalo Forge Company, N.Y. and distributed by Canadian Blower and Forge Co. Ltd., Kitchener (Ontario), was used. The maximum ratings of the fan are as follows:

| | | |
|---|---|---|
| Static pressure | = | 0.076 m. (3 in.) water |
| Horse power | = | 7.32 |
| R.P.M. | = | 2320 |
| Free flow rate | = | 4.6 m$^3$./sec. (9640 C.F.M.) |

The "swirling" of air leaving the fan blades produces no useful effect, it is actually responsible for a reduction in the fan efficiency. To correct the swirling motion of the air leaving the blades and thus improve efficiency, the fan is installed with a set of stationary vanes at the discharge side of the wheel. These vanes straighten out the air leaving the wheel so that it travels from the vanes in a true axial direction. A vaneaxial fan is a coined word adopted by the National Association of Fan Manufacturers of America to designate an axial flow fan in a cylindrical drum type housing equipped with stationary directional vanes.

(iii) Specifications of the motor

For running the fan a 250 volt, DC shunt/compound wound motor was installed on top of the fan. The motor had the following speed-control characteristics.

(a) 10 H.P., constant horsepower, over a speed range of 3000/5000 R.P.M. obtained by shunt control.

(b) 10/1.67 H.P., constant torque, over a speed range of 3000/500 R.P.M. obtained by armature control

(iv) Speed-control unit for the motor

The Ward Leonard system for speed control and the associated equipment was designed and manufactured by Bepco Canada Ltd., Toronto.

The motor-generator set consisted of a 25 H.P., A.C. driving motor and two 7 1/2 KW. D.C. generators. The A.C. motor is connected to the line in the usual manner and the generator of the motor generator set is connected to the dynamometer in the normal Ward Leonard connection for driving the dynamometer as a motor.

The speed control is obtained by armature and shunt control for two ranges of speeds. For higher speed range; 3000/5000 R.P.M. the speed was varied by shunt control at a constant horsepower of 10 H.P. Armature control was used to cover a speed range of 3000/500 R.P.M. Corresponding variation in horsepower was 10/1.67 H.P. at constant torque. To obtain very low speeds of motor an additional rheostat was installed in the armature circuit.

Using this arrangement an excellent control over the speed range was obtained. At the higher end of the speed range the motor speed stayed constant to within $\pm$ 5 R.P.M. while at lower speeds the fluctuations were only $\pm$ 2 R.P.M.

A schematic of the control circuit is shown in figure A.1. Although two dynamometers are shown in the circuit only one of them was used as a motor on top of the vaneaxial fan.

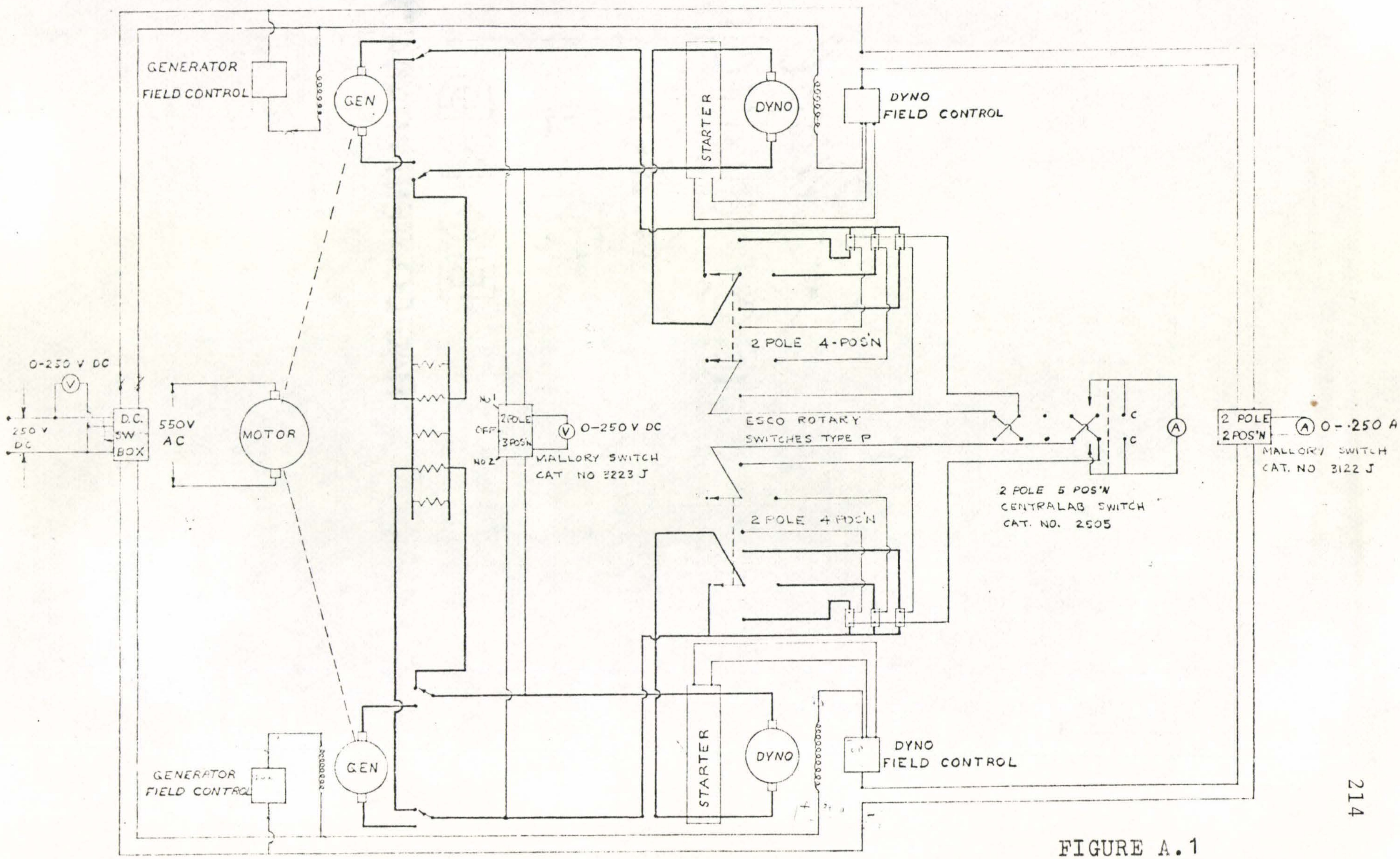
GENERATOR
FIELD CONTROL
GEN
STARTER
DYNO
DYNO
FIELD CONTROL
2 POLE 4-POS'N
0-250 V DC
250 V
DC
D.C.
SW
BOX
550V
AC
MOTOR
No 1
OFF
No 2
2 POLE
3 POS'N
0-250 V DC
MALLORY SWITCH
CAT NO 3223 J
ESCO ROTARY
SWITCHES TYPE P
2 POLE 5 POS'N
CENTRALAB SWITCH
CAT. NO. 2505
2 POLE
2 POS'N
0-250 A
MALLORY SWITCH
CAT. NO 3122 J
2 POLE 4 POS'N
STARTER
DYNO
DYNO
FIELD CONTROL
GEN
GENERATOR
FIELD CONTROL

FIGURE A.1

## APPENDIX B

## BEATING RESPONSE OF THE TUBE

The output of the proximity transducer while being used to record the free oscillations of the first tube-model (where compression-coil springs were used to control the stiffness of the tube) occasionally showed beating form of tube oscillations. The beats were, at first, thought to be due to the coupling of natural frequency of the tube with that of the frame but a computer analysis of the problem showed that the beat response is due to the slightly different spring rates of the tube along two mutually perpendicular directions.

Two uncoupled equations of motion for free vibrations (neglecting damping) along two mutually perpendicular directions (having slightly different spring rates) were written and time-history of tube motions was computed assuming a prescribed initial plucking position. The computer output when spring rates along two mutually perpendicular directions were different, showed that the tube oscillations are orbital and a vibration pick-up installed in x-direction will record a beating type of phenomenon. Another programme was written to obtain x-component of the instantaneous positions of tube oscillations and the output has been shown in figure B.1 against the time axis. $f_1$ and $f_2$ are the natural frequencies

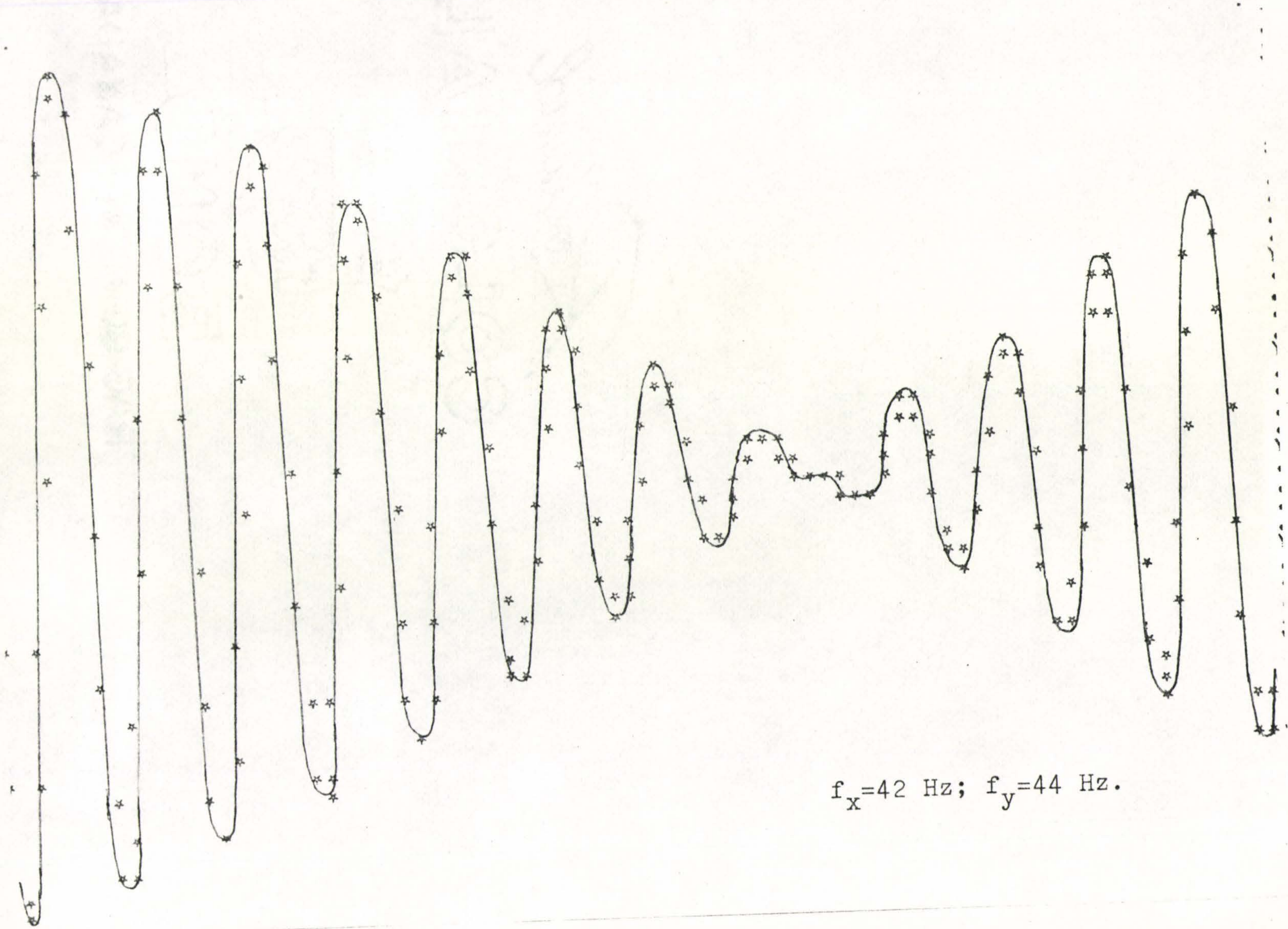


FIGURE B.1

in directions x and y respectively. The listing of the computer programmes is given in figure B.2.

```
      PROGRAM TST (INPUT,OUTPUT,TAPE5=INPUT,TAPE6=OUTPUT)
C     TIME-AMPLITUDE PLOT OF TUBE VIBRATING AT ITS NATURAL
C     ANGULAR FREQUENCY WHEN ITS NATURAL ANGULAR FREQUENCY IN TWO
C     PERPENDICULAR PLANES DIFFER BY DOMEGA. DAMPING NEGLECTED
C     AND PLANAR VIBRATIONS ASSUMED.
      OMEGA=372.
      DOMEGA=35.
      SIGMA=31.
      OMEGAD=OMEGA+DOMEGA
      DO 10 I=1,50
      T1=I-1
      T=T1/200.
      P=0.500*COS(OMEGA*T)
      Q=0.500*COS(OMEGAD*T)
      Y=P+Q
      Y1=COS(SIGMA*T)
      Y=Y1*Y
      WRITE(6,20) T,Y
   20 FORMAT(2F10.5)
      CALL PLOTPT(T,Y,4)
   10 CONTINUE
      CALL OUTPLT
      STOP
      END
```

```
      PROGRAM TST (INPUT,OUTPUT,TAPE5=INPUT,TAPE6=OUTPUT)
      OMEGAX=350.
      OMEGAY=353.5
      DO 10 I=1,157,52
      A1=I-1
      ALPHA=A1/100.
      AX=COS(ALPHA)
      AY=SIN(ALPHA)
      DO 20 J=1,50
      T1=J-1
      T=T1/200.
      X=AX*SIN(OMEGAX*T)
      Y=AY*SIN(OMEGAY*T)
      WRITE(6,30) X,Y
   30 FORMAT(2F10.5)
      CALL PLOTPT(X,Y,4)
   20 CONTINUE
      CALL OUTPLT
   10 CONTINUE
      STOP
      END
```



FIGURE B.2

## APPENDIX C

## IMPROVED PROTOTYPE TUBE-MODEL

The feasibility of using a light aluminum tube sprung on a piano-wire was examined anaytically and it was found that there is a good possibility of obtaining a dimensionless parameter ($m\delta/\rho d^2$) down to approximately three. Also by eliminating compression-coil springs the large scatter in damping values and directional variation in tube stiffness of the previous prototype tube-model is expected to be reduced. Tension in the piano-wire could be used to regulate the natural frequency of the tube. Wire material damping and windage will provide the necessary low damping values required whereas high damping values will be obtained from various fluids using an arrangement similar to the previous tube-model.

The analytical model has been developed in the following pages (for use in this appendix only, T = initial tension in the wire, $\ell$ = length of wire as shown in figure C.1).

<u>Analytical Development</u>

Strain in piano-wire due to displacement 'x' is

$$= \frac{(\ell^2+x^2)^{1/2}-\ell}{\ell}$$

$$= (1 + \frac{x^2}{\ell^2})^{1/2} - 1$$

$$\simeq x^2/2\ell^2$$

Corresponding tensile force in the wire is:

$$T + A\left(E\frac{x^2}{2\ell^2}\right)$$

and the restoring force acting on mass 'm' will be

$$2\left[\left(T+AE\frac{x^2}{2\ell^2}\right)\frac{x}{(\ell^2+x^2)^{1/2}}\right]$$

$$\simeq 2\left[\left(T+AE\frac{x^2}{2\ell^2}\right)\frac{x}{\ell}\right] \simeq 2\left[T+AE\frac{x^2}{2\ell^2}\right)\frac{x}{\ell}]$$

$$= \frac{2Tx}{\ell} + AE\frac{x^3}{\ell^3}$$

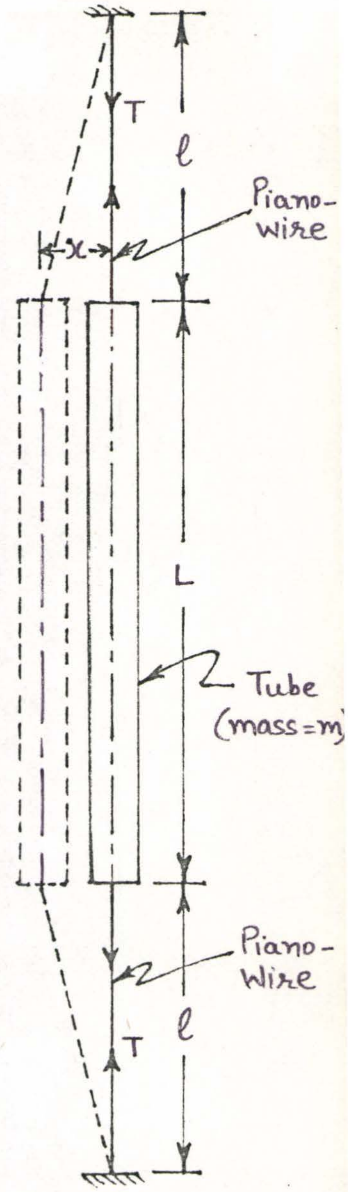


FIGURE C.1

The equation of motion of mass 'm' thus becomes:

$$m\ddot{x} + 2T\frac{x}{\ell} + AE\frac{x^3}{\ell^3} = 0$$

This is a non-linear differential equation. It can be considered linear for small deflections 'x' and high initial tensile force 'T'. The linearised equation is (neglecting AE $\frac{x^3}{\ell^3}$ compared to 2T $\frac{x}{\ell}$

$$m\ddot{x} + 2T\frac{x}{\ell} = 0$$

and for simple harmonic motion of mass 'm', the solution of this second order differential equation will lead to:

$$f = \frac{1}{2\pi} \sqrt{\frac{2T}{m\ell}}$$

where f = Natural frequency of mass 'm' (and an implicit assumption in this formulation is that the mass of the wire is negligible as compared to the total central mass 'm').

Thus for a fixed length of the wire and mass of the tube, the natural frequency of the system is directly proportional to the square root of the tension in the wire.

Feasibility evaluation

It was decided to use a commerically available 0.001 m. (0.041 in.) diameter piano-wire weighing 0.0066 Kg./m (0.0044 lb./ft.). The tensile strength of this wire is 2.28 x $10^6$ kN/$m^2$ (330, 750 p.s.i.).

If the same tube as of the previous model is used, weighing 0.040 Kg. (0.089 lb.) and use 0.15 m. (6 in.) length of piano-wire at each end of it, then the weight of the wire/total weight of tube =

= 0.0066/(0.040 + 0.0066) = 0.0471.

This is a small value and thus satisfies the implicit assumption of the above analytical development.

Now

$$f = \frac{1}{2\pi} \sqrt{\frac{2T}{m\ell}}$$

or

$$T = \frac{m\ell}{2} (2\pi f)^2$$

$$= \frac{1}{2} \cdot m. \ \ell \, (2\pi)^2 \ f^2$$

$$= \frac{1}{2} \cdot \frac{0.040}{9.81} \times 0.15 \times (2 \times 3.14)^2 \ f^2$$

or $\quad T = 0.014\ f^2$ Kgs. $\quad$ (1)

the corresponding stress in the wire would be:

$$\sigma = \frac{T}{A}$$

$$= \frac{0.014\ f^2}{\frac{\pi}{4}\ (0.001)^2}$$

or $\quad \sigma = 157.3\ f^2\ kN/m^2$ $\quad$ (2)

the strain in the wire, taking $E = 207 \times 10^6\ kN/m^2$ ($30 \times 10^6$ p.s.i.) for steel, is:

$$\varepsilon = \frac{\sigma}{E}$$

$$= \frac{157.3\ f^2}{207 \times 10^6}$$

$$= 0.76 \times 10^{-6}\ f^2$$

And for 0.15 m. (6 in.) length of wire, the wire at each end of the tube should be stretched by:

$$\delta = \varepsilon . \ell .$$

$$= 0.76 \times 10^{-6}\ f^2 \times 0.15 \text{ m.}$$

$$= 0.11 \times 10^{-6}\ f^2 \text{ m.} \qquad (3)$$

The ranges of the two dimensionless parameters in the stability diagram which are desired in the current research are:

1) Velocity parameter $\frac{V_G}{fd} = 3$ to 100
2) Damping parameter $\frac{m\delta}{\rho d^2} = 3$ to 50.

For the given tube of 0.0254 m. (1 in.) outside diameter and weighing 0.040 Kg. (0.089 lb.) and air as the external flow medium, these parameters reduce to:

1) $\dfrac{V_G}{fd} = \dfrac{V_G}{f\text{x}0.0254} = 39\ \dfrac{V_G}{f}$

2) $\dfrac{m\delta}{\rho d^2} = 167\ \delta$

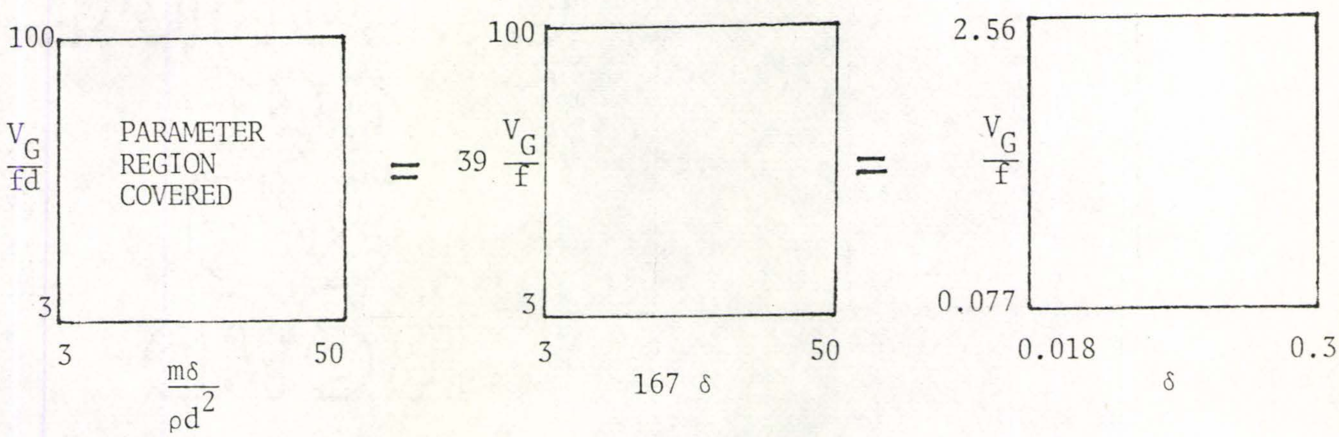


Hence, there are only three parameters left to be controlled.

1) $V_G$ = minimum-gap velocity

In the wind-tunnel constructed for these experiments we can cover a range of gap velocities up to 50 m./sec.

2) f = Natural frequency of vibration of the tube.

This is controlled by tension in the wire and limited by the tensile strength of the wire and the availability of an adequate support.

3) $\delta$ = logarithmic decrement of damping.

This depends primarily upon the wire material, support conditions, aerodynamic damping and external fluid damping (if used).

It is obvious that to scan the above region, V and f will be inter-related whereas $\delta$ can be varied independently. These two sets of parameters are evaluated as follows:

(a) Logarithmic decrement of damping:

From Lazan's book [143] on "Damping of Materials and Members in Structural Mechanics", an approximate value of $\eta_s$ (called loss factor) for stainless steel in bending is $10^{-3}$.

Logarithmic decrement $\delta$ is defined as $\pi \eta_s = 0.00314$.

As there will be additional damping due to support conditions and contribution due to aerodynamic damping, the total damping obtained from the actual tube will be more than 0.00314. However, the minimum $\delta$ required is 0.018 and therefore, it is hoped that we will be able to obtain a value of total damping close to $\delta = 0.018$.

Higher damping values can be obtained by installing a cup and paddle arrangement similar to that used in the previous tube-model at each end of the tube and then using different fluids in it. It was found that with this kind of arrangement we can realise $\delta$ values as high as 0.44.

(b) Gap velocity and natural frequency of vibration of tube:

As we will like to keep the tension in the wire as low as possible, the limiting design case would be:

$$\frac{V_G}{f} = 0.077$$

If we take the minimum gap-velocity in the wind-tunnel as 3 m./sec., we must have $f = 3/0.077 \simeq 40$ Hz. From (1), (2) and (3) for $f = 40$ Hz. we have

$$T = 21.9 \text{ Kg}$$
$$\sigma = 2.5 \times 10^5 \text{ kN/m}^2$$
$$\delta = 0.0002 \text{ m.}$$

As these figures are safe, it indicates that we can obtain a natural frequency of 40 Hz. from the given piano-wire by stretching it about 0.0002 m.

Next, as the maximum gap-velocity available is 50 m./sec., keeping the same tension in the wire we can traverse $\frac{V_G}{f}$ up to $\frac{50}{40} = 1.25$ or $\frac{V_G}{fd}$ up to 48. As the vortex-shedding threshold is expected to be somewhere between $\frac{V_G}{fd} = 1.25$ to 5, this designed range of $\frac{V_G}{fd}$ up to 48 is satisfactory.

On the other end of the velocity parameter scale we need $\frac{V_G}{f} = 2.56$ and if we use a limiting upper gap-velocity of 50 m./sec we require $f = 50/256 = 19.2$ Hz. and this can be obtained by stretching the wire by $\delta = 0.00004$ m. for convenience if we keep $f = 19.2$ Hz. fixed and just vary $V_G$, we can cover a range of $\frac{V_G}{fd}$ from 6.26 to 100. As the stability threshold for fluidelastic mode of vibration is expected to move up with increasing values of the damping parameter, this lowest value of velocity parameter = 6.26 should be satisfactory.

Thus it is seen that for a certain value of damping if we set a constant f = 40 Hz. then by varying the gap velocity between its limiting design values we can cover a velocity parameter range from 3 to 48. Also by setting f at 20 Hz. the corresponding velocity parameter range covered will be 6 to 100. Similarly by setting f at various other values (depending on the damping value) a wide range of desired velocity parameters can be realised.

## Summary and Conclusions

An analytical study of a light aluminum tube sprung on a piano-wire has proven that such a prototype tube-model is feasible and the desired ranges of the various parameters can be obtained.

It is expected that this tube-model will give closer parameter control, improved directional accuracy and will be cheaper to manufacture than the coil-spring model.

## APPENDIX D

## SPECIFICATIONS OF THE INSTRUMENTS EMPLOYED

1. <u>Vibration Pick-up of Single Tube Assembly</u>

   (i) Proximity - Vibration transducer

   DISA Type 51D11 (Can measure up to $\pm$ 5 mm. deflections). This transducer has a built-in tank circuit so that it may be connected to the oscillator directly.

   (ii) Oscillator

   DISA Type 51E02

   (iii) Reactance converter

   DISA Type 51E01

   Supplier: DISA Elektronik A/S, DK2730 Herlev, Denmark.

2. <u>Vibration Pick-up of a Movable Tube in the Array</u>

   (i) Capacitive probe

   Wayne Kerr Type MC1 (0.010" full scale range)

   (ii) Vibration meter

   Wayne Kerr Type B731B

   (iii) Wayne Kerr low-pass filter; Model F731A,

   Supplier: The Wayne Kerr Company, Ltd., England.

3. Flow Measurements

(i) Pitot-static probe

Part No. PBC-18-G-16-KL

Supplier: United Electric Controls (Canada) Ltd., Mississauga.

(ii) Betz manometer

Supplied by: Thermovolt Instruments Ltd., Toronto, S. No. 11248.

(iii) $90^{o}$ miniature hot-wire probe

DISA Type 55P14

(iv) Hot-wire probe support

DISA Type 55H21

(v) Constant temperature anemometer

DISA Type 55A01

Supplier: DISA Elecktronik A/S, DK 2730 Harlev, Denmark.

4. Oscilloscopes

(i) Model 120B; Hewlett & Packard,

It is a general-purpose oscilloscope whose bandwidth extends from D.C. to 450 kc.

(ii) Tektronix; Type 564, Storage Oscilloscope.

With Type 3A72 Dual-trace amplifier and Type 2B67 Time base.

5. Recorder

(i) Visicorder Oscillograph,

Model 2106, Honeywell test instruments Inc., Denver, Colorado.

It is a direct writing 12-channel oscillograph that records at frequencies from D.C. to 13,000 Hz. The oscillograph uses a high-pressure mercury vapor lamp that emits high intensity ultra-violet light, which is reflected from miniature mirror galvanometers through a precision optical system into the recording paper.

(ii) Universal counter,

Model 5325B, Hewlett Packard,

Range: D.C. 0-20 M Hz.

A.C. 10 Hz. - 20 M Hz.

Accuracy: $\pm$ 1 count

6. Fourier Analysis

A combination of the following Hewlett Packard units;

(i) Control unit: Model 5475A

(ii) Computer: Moel 2100A

(iii) Display unit: Model 5460A

(iv) X-Y recorder: Model 7635B

(v) Tape reader: Model 2748B

7. Meters

(i) Electronic voltmeter

Type 2409, Bruel & Kjaer

(ii) Multimeter,

Model 3470, Hewlett Packard

(iii) Hand-held Tachometer,

Manfr. Hasler S.A. Berne, Switzerland.

# APPENDIX E

# INSTRUMENT CALIBRATION

## 1. Calibration of Displacement Transducer

Calibration of the proximity transducer (DISA Type 51D11) was done using an arrangement shown in figure E.1. The micrometer screw was turned in order to obtain a known variation of the gap between the aluminum plate and the electrode of the transducer. The corresponding output of the transducer system (in volts) was then recorded. The procedure was repeated for a range of gap widths and a complete calibration curve was drawn. Any nonlinearity in the calibration curve was corrected by adjusting the nonlinearity knob provided in the reactance converter (DISA type 51E01). Transducer circuitory was always balanced before starting the calibrations and also before any actual measurements were conducted. The calibration curves for the two transducers used are given in figures E.2 and E.3.

## 2. Calibration of Wayne-Kerr Transducer

The Wayne-Kerr transducer was calibrated by using joe-blocks (precision blocks) as shown in figure E.4. The gap between the block and face of the transducer was set by using a feeler-gage. The output of the transducer system (in volts) was recorded and the procedure was repeated

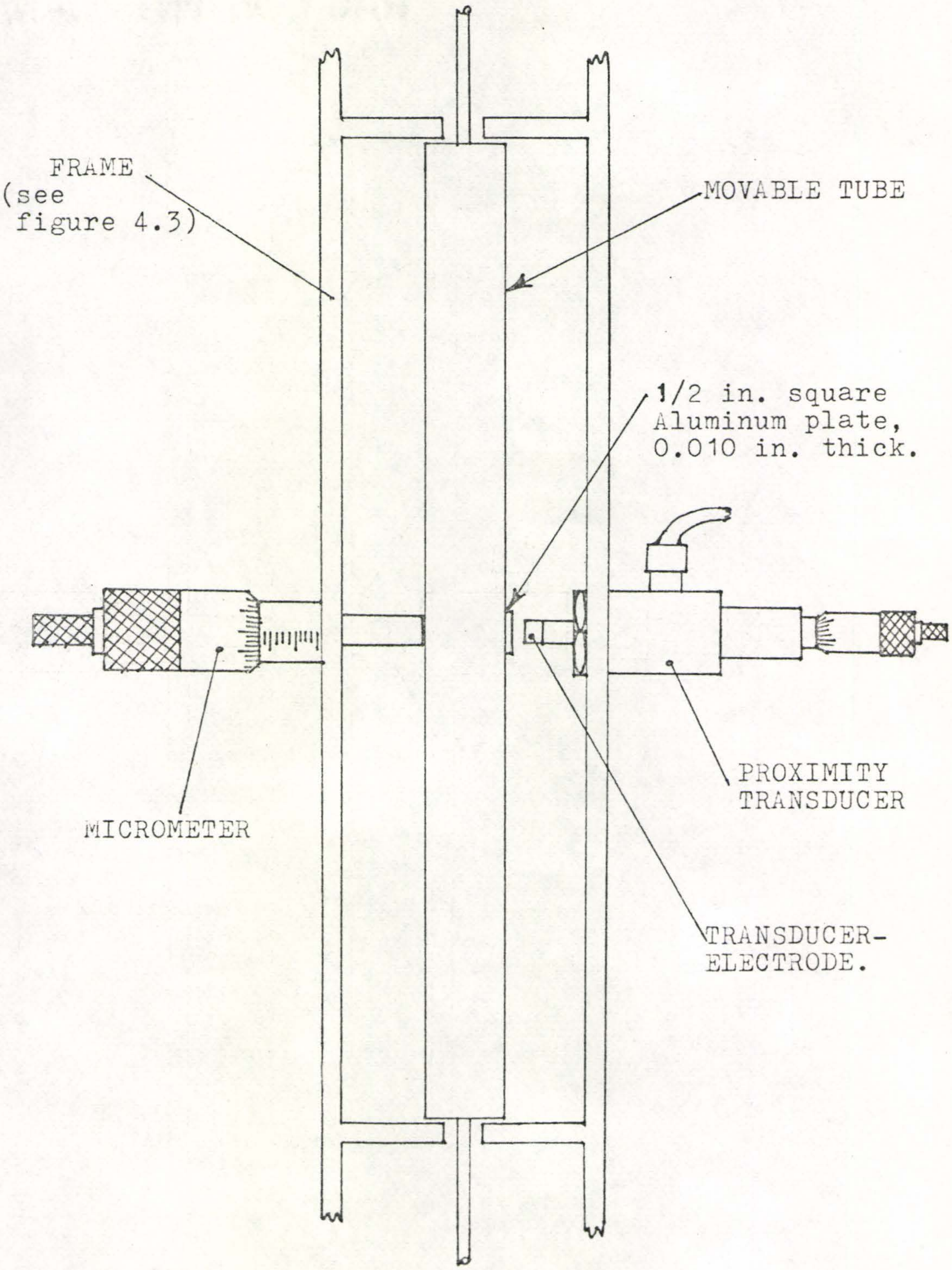


CALIBRATION OF DISPLACEMENT-TRANSDUCER

FIGURE E.1

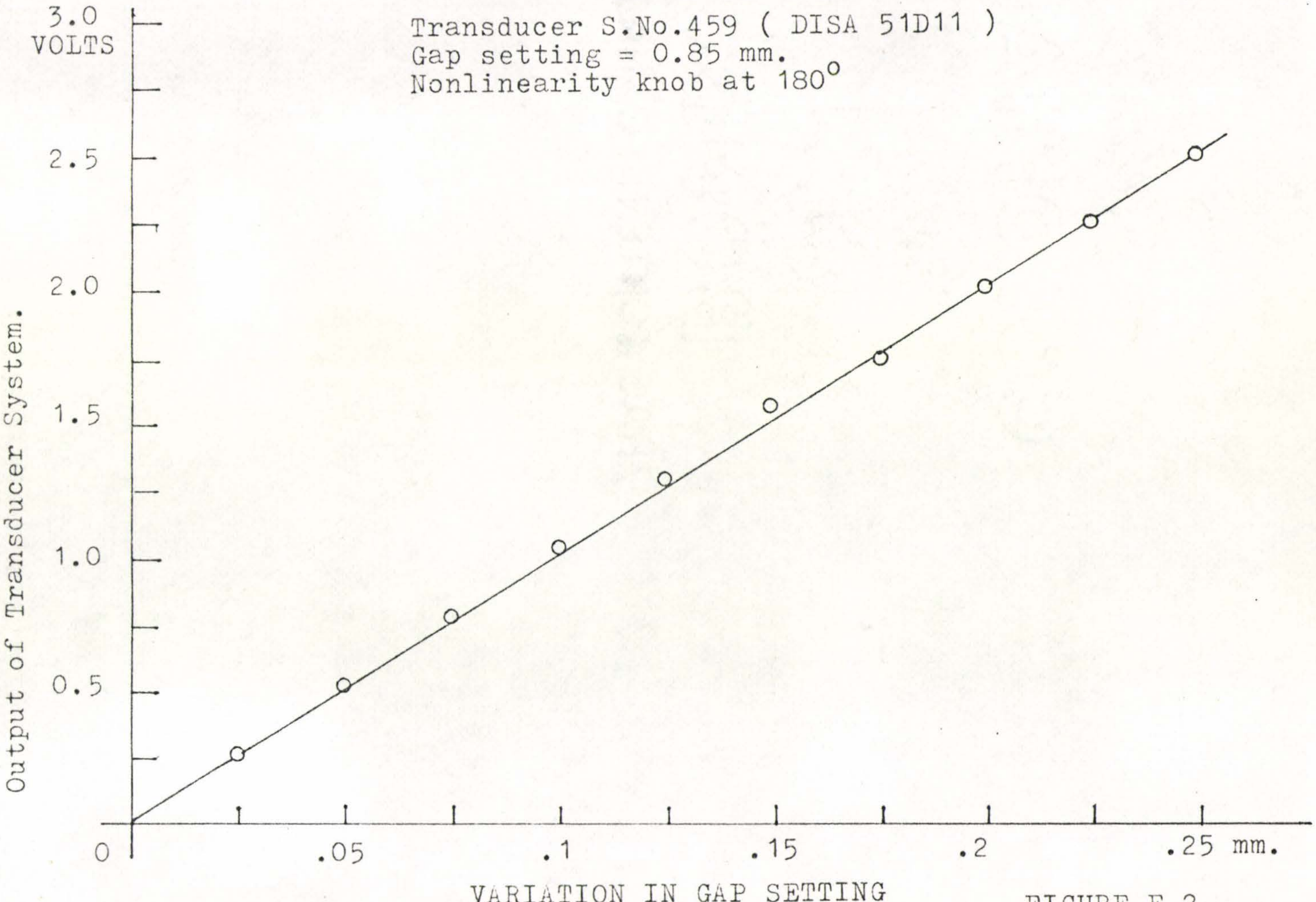
Transducer S.No.459 ( DISA 51D11 )
Gap setting = 0.85 mm.
Nonlinearity knob at 180°
3.0
VOLTS
2.5
2.0
1.5
1.0
0.5
Output of Transducer System.
0
.05
.1
.15
.2
.25 mm.
VARIATION IN GAP SETTING

FIGURE E.2

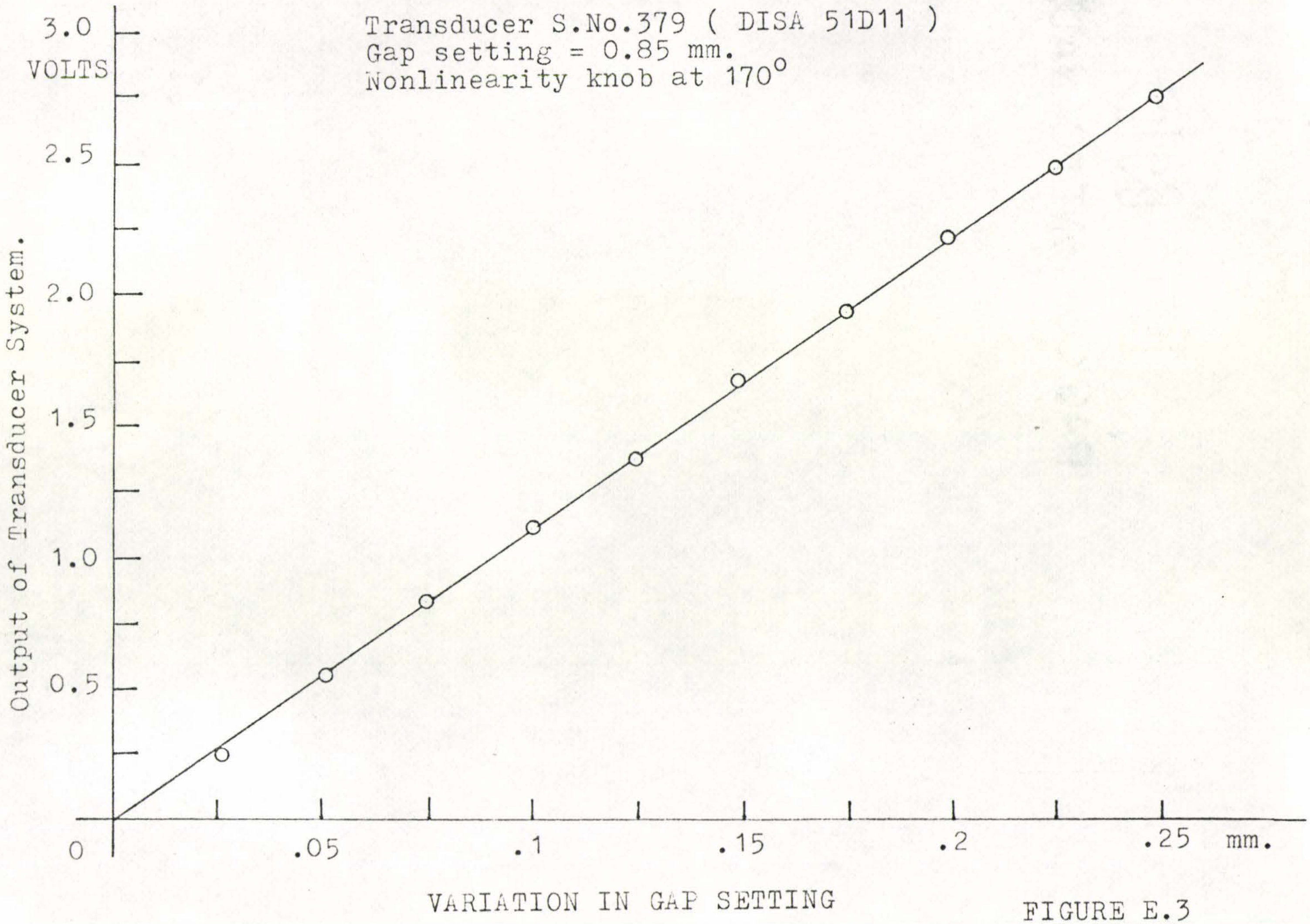
Transducer S.No.379 ( DISA 51D11 )
Gap setting = 0.85 mm.
Nonlinearity knob at 170°
3.0
VOLTS
2.5
2.0
1.5
1.0
0.5
0
Output of Transducer System.
.05
.1
.15
.2
.25
mm.
VARIATION IN GAP SETTING

FIGURE E.3

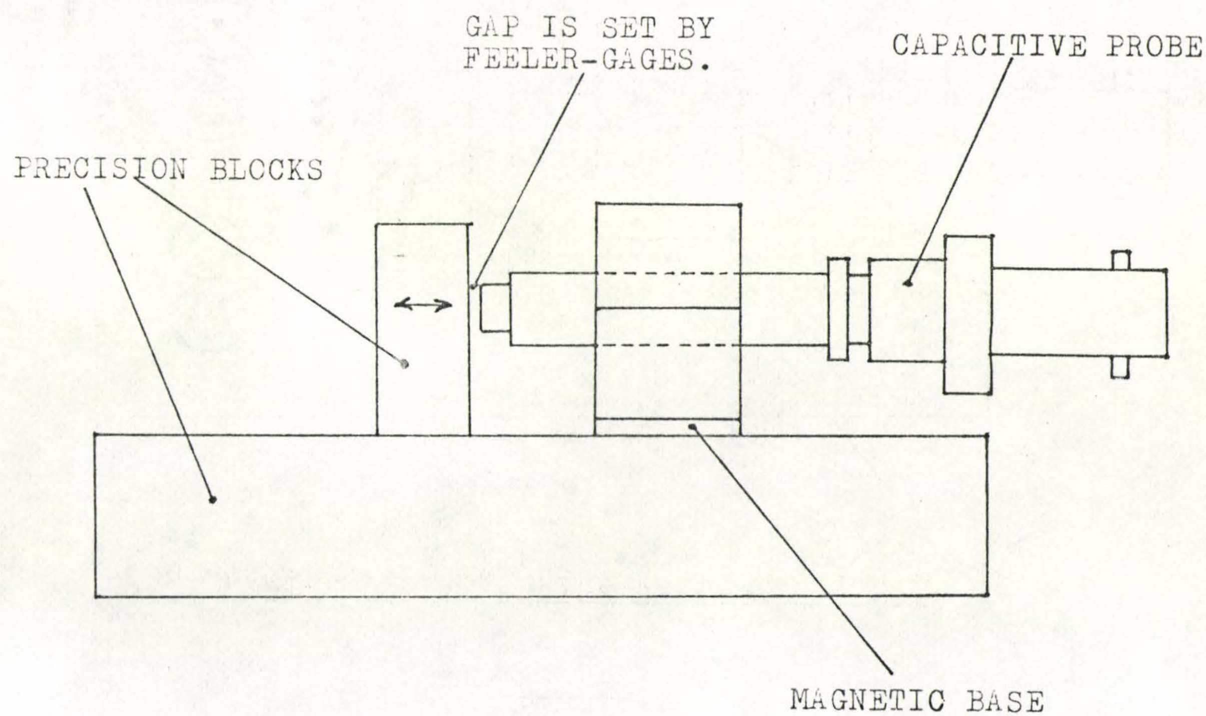


Calibration of Wayne-Kerr Transducer

FIGURE E-4

by setting different gaps by feeler-gages. The calibration curve for the transducer has been plotted in figure E.5. It is seen that the transducers are linear for up to approximately 0.4 mm. (0.016 in.) whereas the specification provided by the manufacturer is only 0.25 mm. (0.010 in.)

## 3. Calibration of the Movable-Tube

As the Wayne-Kerr displacement transducer was installed outside the wind-tunnel, close to the top end of the piano wire (see figure E.6), a calibration was conducted to establish a relationship between the deflection of the tube at the middle and that recorded by the Wayne-Kerr transducer. The arrangement is shown in figure E.6 and the data obtained has been plotted in figure E.7. It is evident that there is a linear relationship for tube deflections up to approximately $\pm$ 0.7 mm. ($\pm$ 0.028 in.)

## 4. Calibrations of the Hot-Wire Probes

The hot-wire probes were calibrated in a known flow field of good accuracy. A carefully constructed calibration nozzle giving a low turbulence potential core some 20 mm. (0.8 in.) in diameter was available in the department (figure E.8). This nozzle has been very carefully checked for flow uniformity and turbulence level (Ref. 141). The nozzle uses a contour, suitable for wind-tunnel contraction design, the curvature being arranged to give a flat velocity profile at the exit.

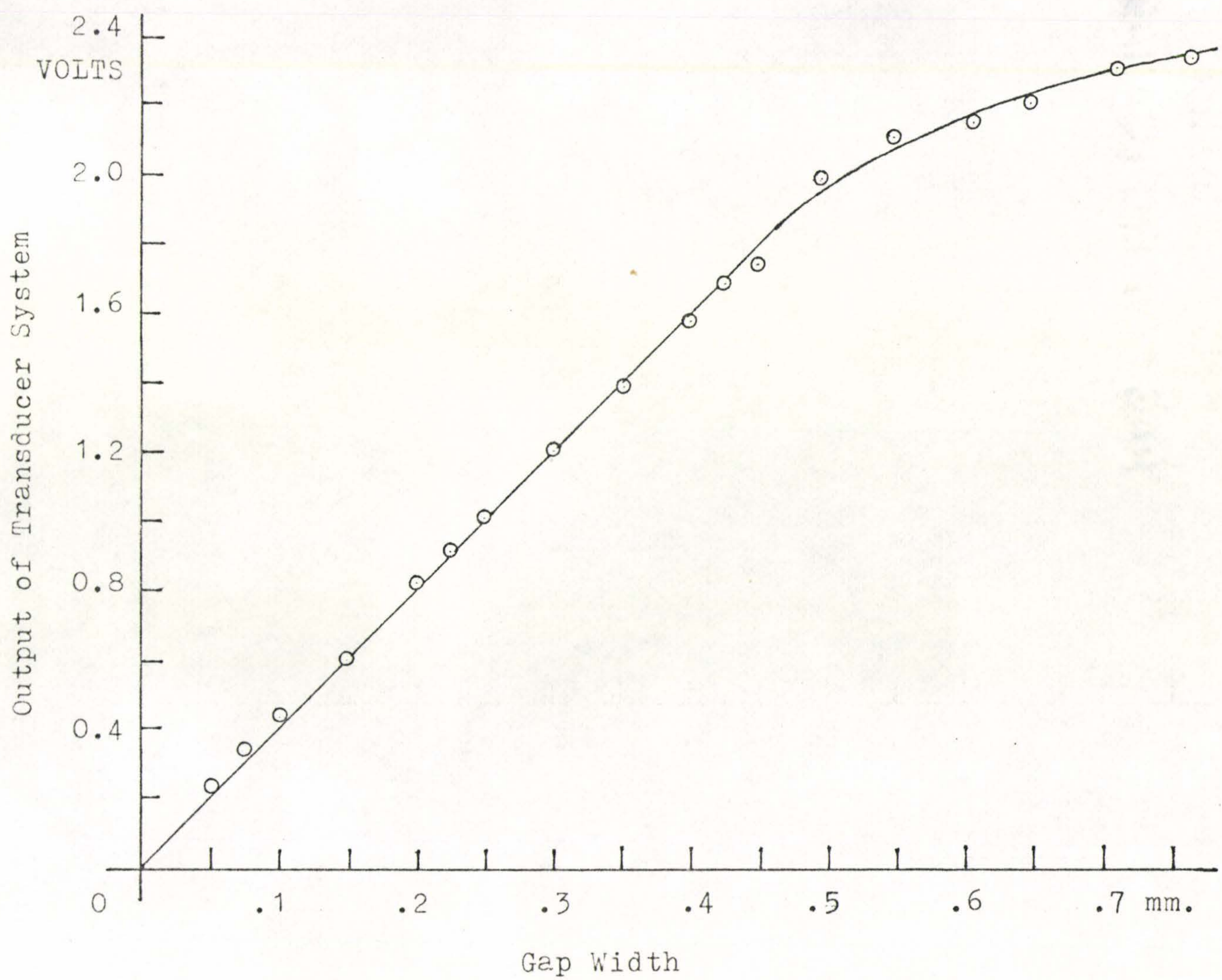
2.4
VOLTS
2.0
1.6
1.2
0.8
0.4
0
Output of Transducer System
.1
.2
.3
.4
.5
.6
.7 mm.
Gap Width

FIGURE E-5

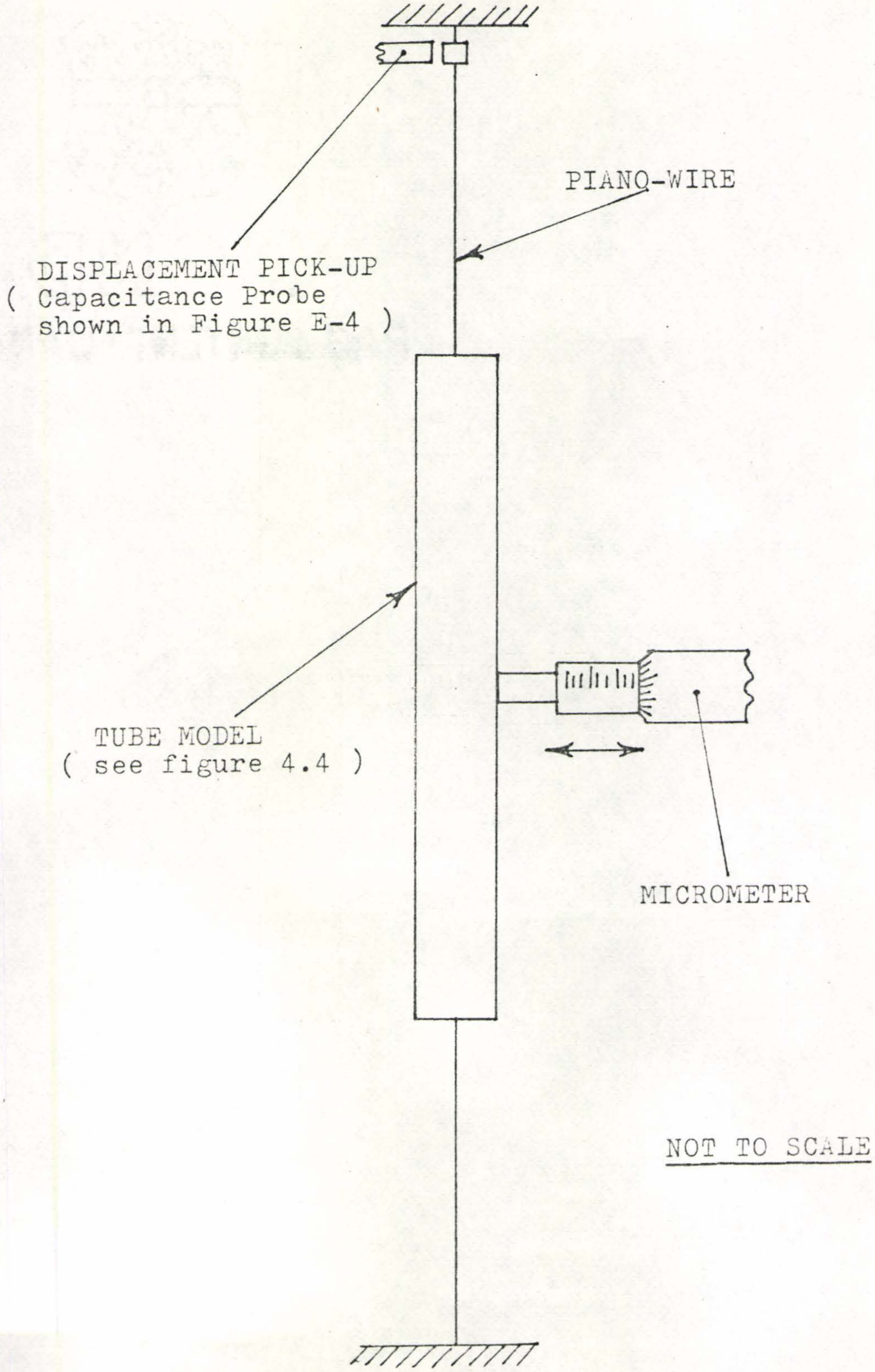
PIANO-WIRE
DISPLACEMENT PICK-UP
( Capacitance Probe
shown in Figure E-4 )
TUBE MODEL
( see figure 4.4 )
MICROMETER
NOT TO SCALE

FIGURE E.6

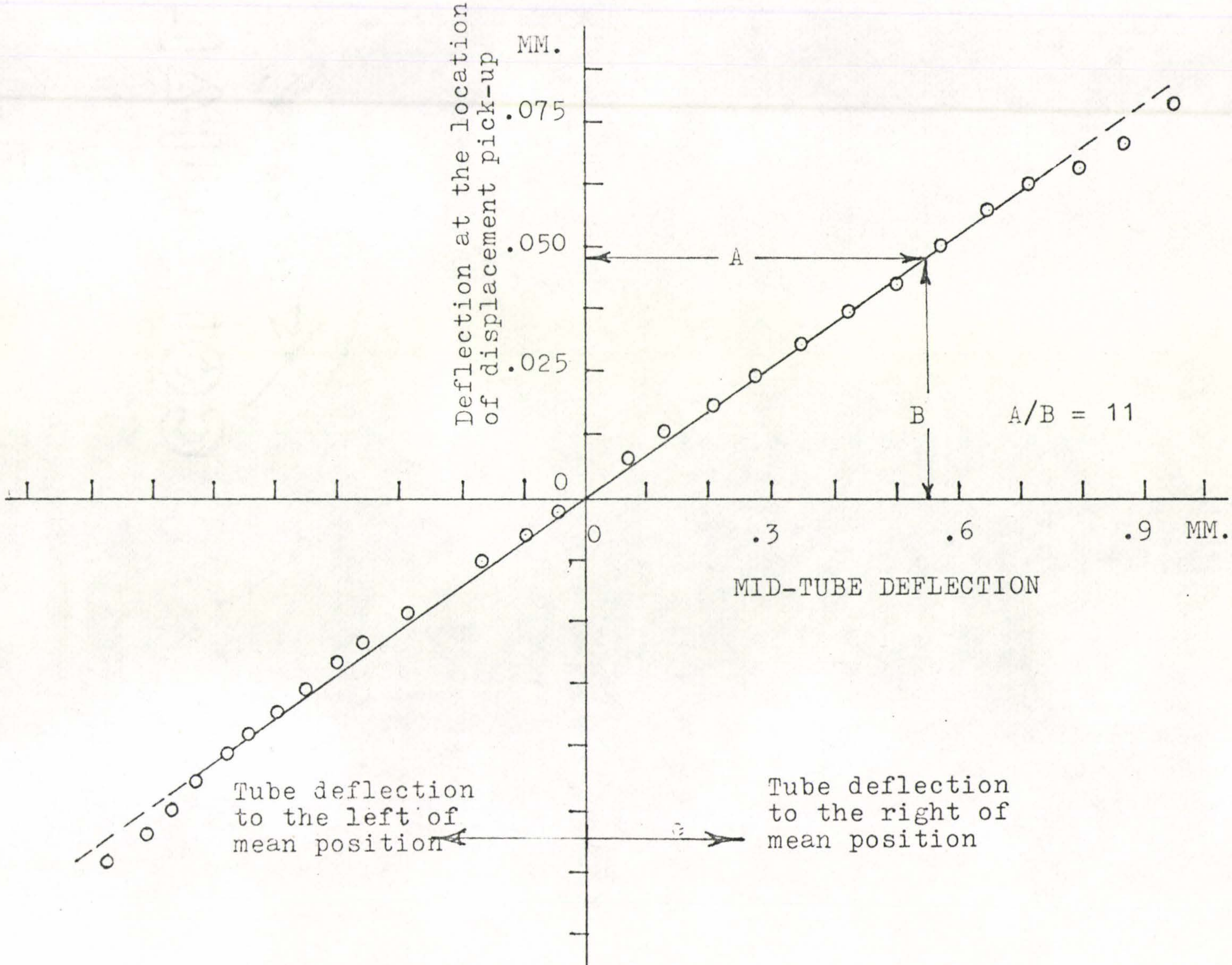
Deflection at the location of displacement pick-up
MM.
.075
.050
.025
0
A
B
A/B = 11
0
.3
.6
.9
MM.
MID-TUBE DEFLECTION
Tube deflection to the left of mean position
Tube deflection to the right of mean position

FIGURE E.7

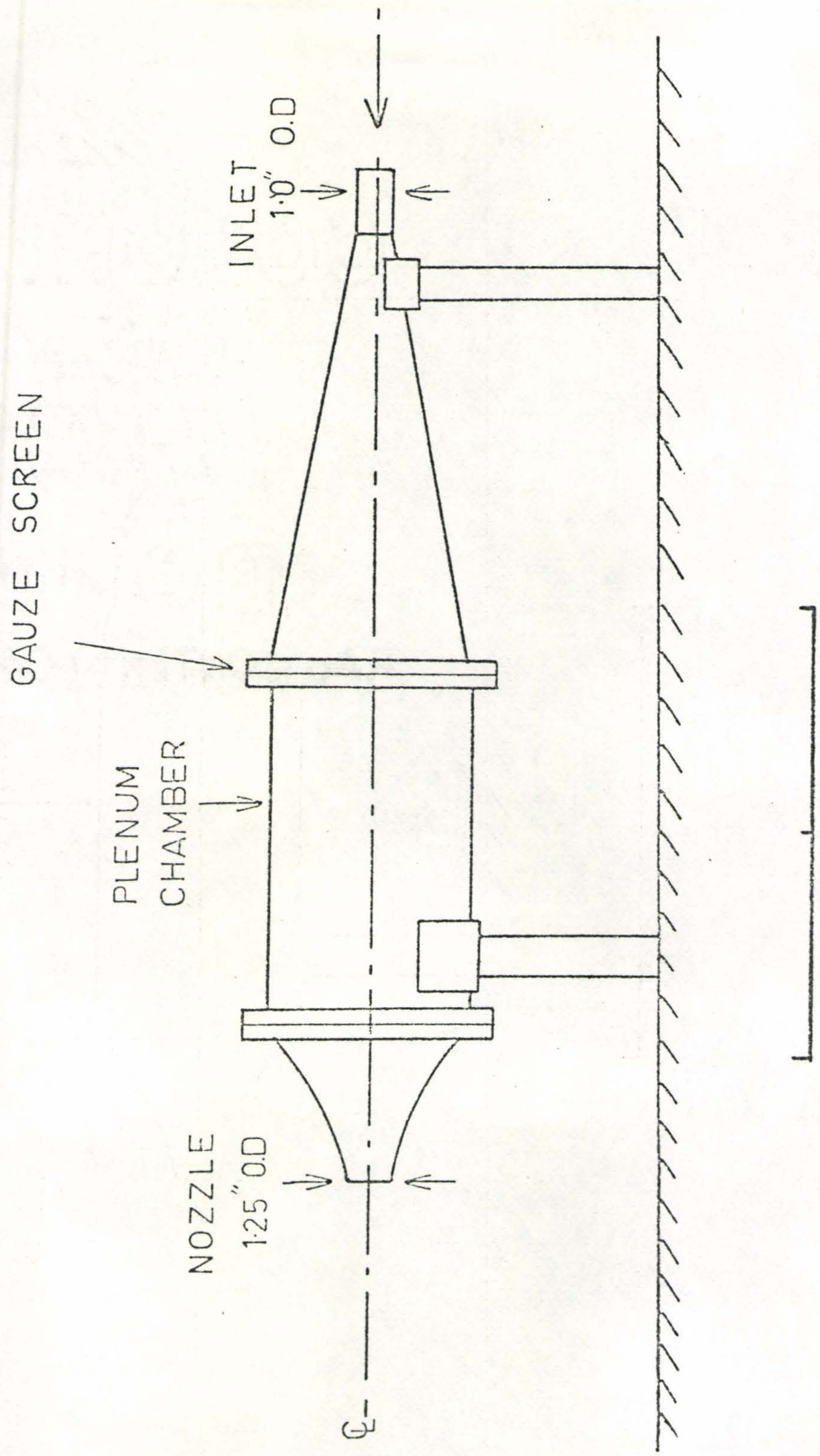


FIGURE E.8

The Calibration Nozzle

A pitot-probe and the hot-wire probe (to be calibrated) were mounted side by side at the exit of the nozzle. The blower was run at a constant speed and a steady air flow through the calibration nozzle was established. The outputs of hot-wire probe and the pitot-probe were recorded from a constant temperature anemometer and a Betz manometer respectively. The flow velocity (m./sec.) was plotted against the output of the hot-wire probe (volts). The procedure was repeated for a range of blower speeds and a complete calibration curve as shown in figure E.9 was drawn. For clarity the data points at very low flow velocities have been replotted in figure E.10. It is to be noted that this is a typical calibration curve. The calibration curves were obtained for each of the hot-wire probes used. The hot-wire probe was calibrated before each set of experiments and the calibration checked afterwards.

The maximum range of interest for the flow rates is up to $V_G$ = 13.7 m./sec. (45 ft./sec.) only. The above data for this range has been replotted in figures E.11 and E.12. It is evident that most of the data points seem to be following a 0.55 law rather than King's law based on a velocity exponent of 0.5.

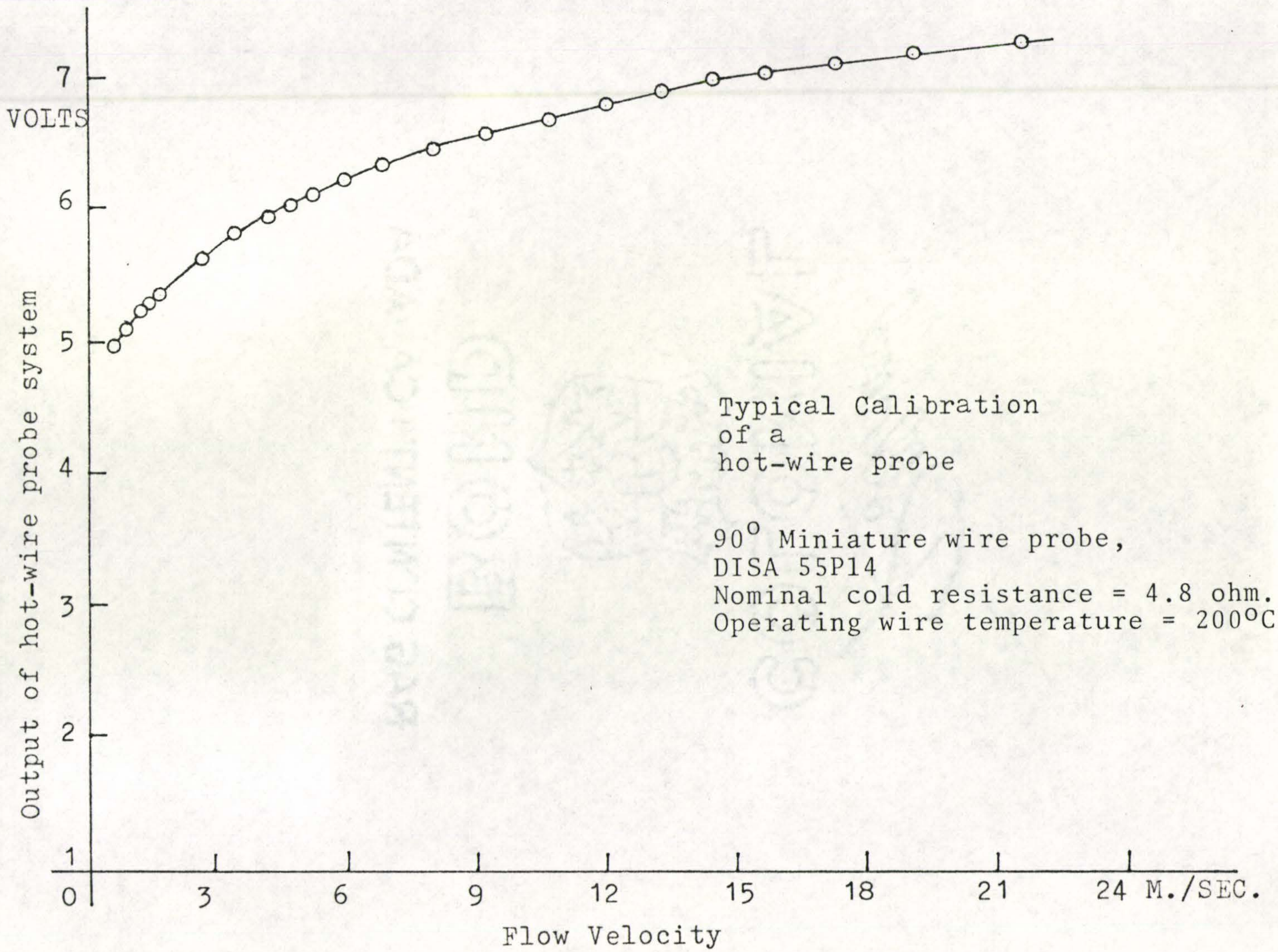
7
VOLTS
6
5
4
3
2
1
0
Output of hot-wire probe system
Typical Calibration
of a
hot-wire probe
90° Miniature wire probe,
DISA 55P14
Nominal cold resistance = 4.8 ohm.
Operating wire temperature = 200°C
3
6
9
12
15
18
21
24 M./SEC.
Flow Velocity

FIGURE E.9

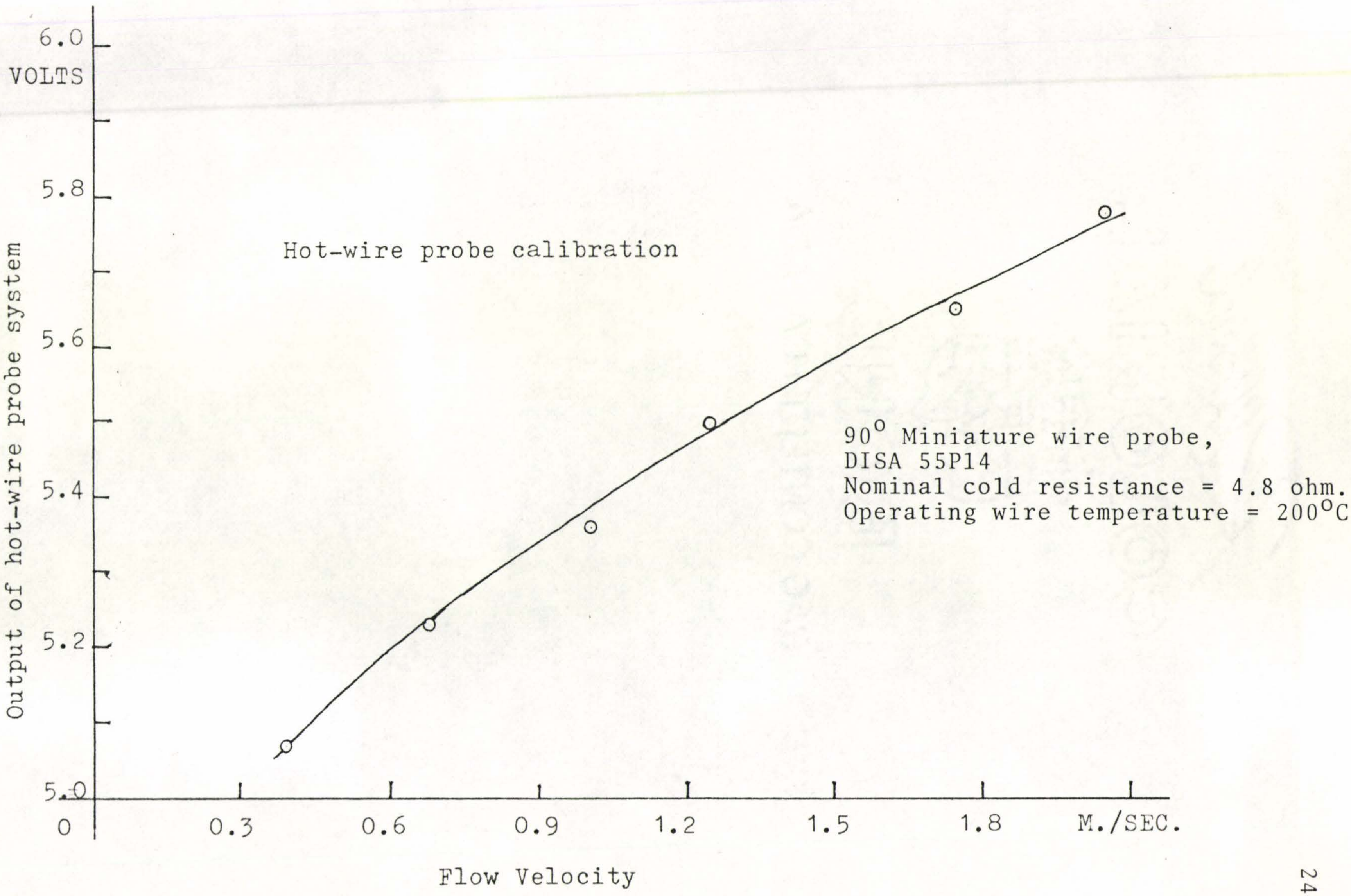
Hot-wire probe calibration
90° Miniature wire probe,
DISA 55P14
Nominal cold resistance = 4.8 ohm.
Operating wire temperature = 200°C
6.0
VOLTS
5.8
5.6
5.4
5.2
5.0
Output of hot-wire probe system
0
0.3
0.6
0.9
1.2
1.5
1.8
M./SEC.
Flow Velocity

FIGURE E.10

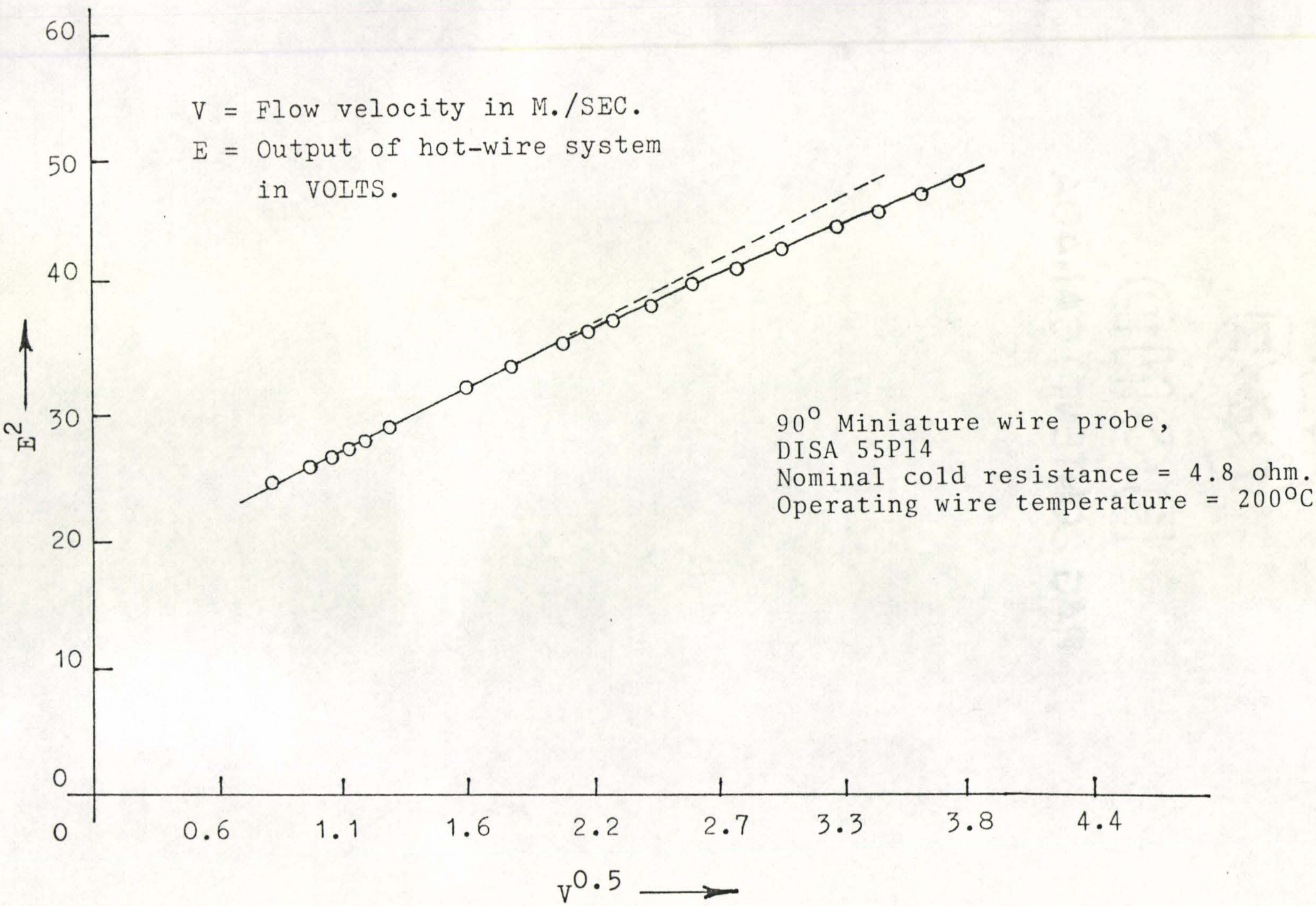
60
50
40
30
20
10
0
$E^2$
V = Flow velocity in M./SEC.
E = Output of hot-wire system in VOLTS.
90° Miniature wire probe,
DISA 55P14
Nominal cold resistance = 4.8 ohm.
Operating wire temperature = 200°C
0
0.6
1.1
1.6
2.2
2.7
3.3
3.8
4.4
$V^{0.5}$

FIGURE E.11

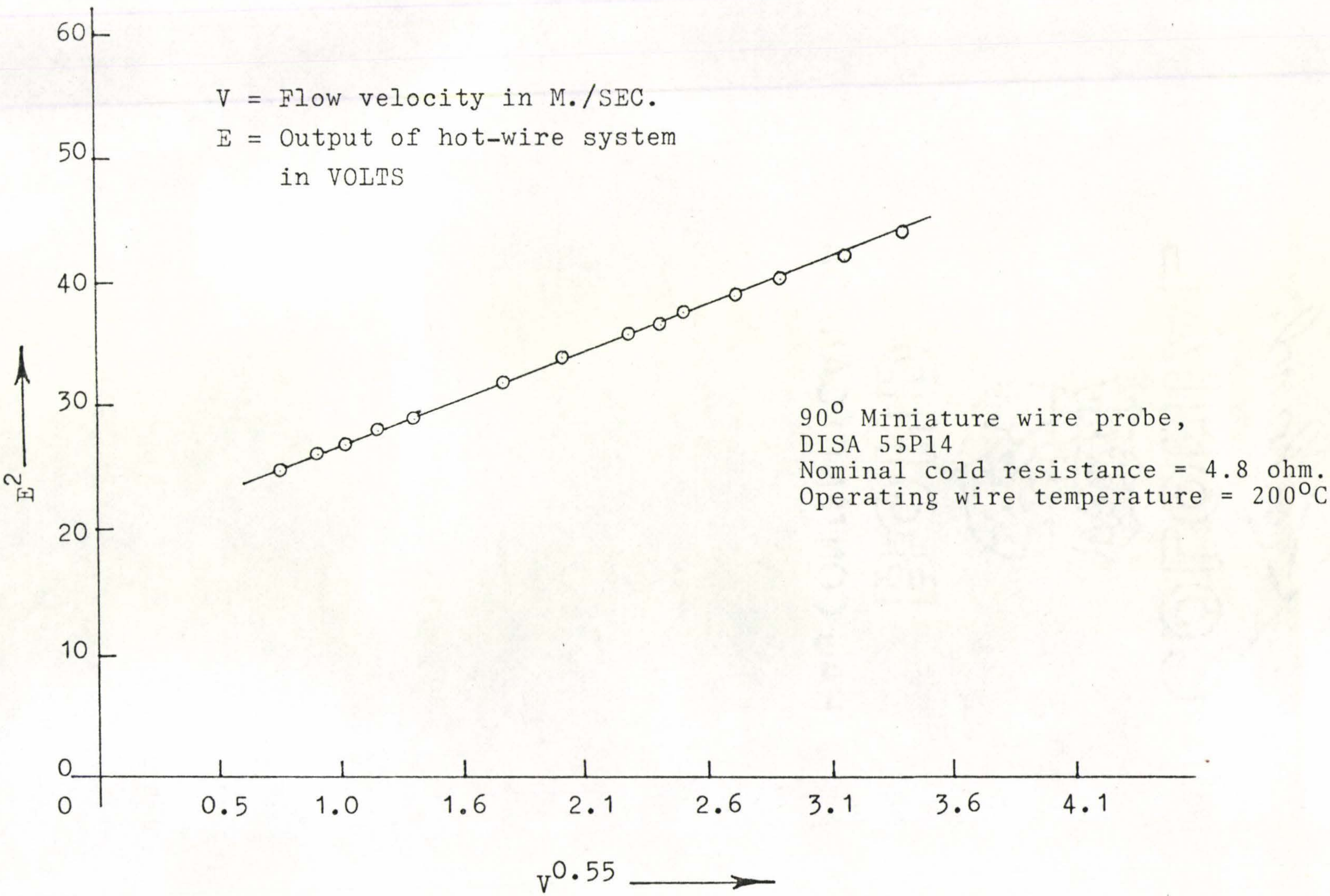

60
50
40
30
20
10
0
V = Flow velocity in M./SEC.
E = Output of hot-wire system in VOLTS
90° Miniature wire probe,
DISA 55P14
Nominal cold resistance = 4.8 ohm.
Operating wire temperature = 200°C
$E^2$
0
0.5
1.0
1.6
2.1
2.6
3.1
3.6
4.1
$V^{0.55}$


FIGURE E.12

# APPENDIX F

## COEFFICIENT OF LIFT OF THE TUBE

The movable tubes have been designed so as to give a linear load-deflection curve for up to $\pm$ 1 mm. of tube deflection. This novel feature of the tube was utilized to obtain an instantaneous value of lift-coefficient when the tube was vibrating at large amplitudes in the fluid-elastic region.

For a sinusoidal force input the equation of motion of the tube is:

$$m\ddot{x} + c\dot{x} + kx = F_o \sin \omega t \tag{1}$$

where $m$ = mass of the tube

$c$ = absolute damping of the tube

$k$ = effective stiffness of the tube

$F_o \sin \omega t$ = sinusoidal force input at frequency = $\omega$.

The steady-state solution of equation (1) is given by:

$$x = \frac{F_o/k}{\sqrt{(1-\frac{m\omega^2}{k})^2 + (\frac{c\omega}{k})^2}}$$

$$= \frac{F_o/k}{\sqrt{(1-\frac{\omega^2}{\omega_n^2})^2 + (\frac{c\omega}{k})^2}}$$

$$\omega_n = \sqrt{\frac{k}{m}} \quad = \text{Natural frequency of the tube.}$$

for $\quad \omega = \omega_n$ (at resonance)

$$X = \frac{F_o/k}{c\ \omega_n/k}$$

$$= F_o/c\ \omega_n \tag{2}$$

Logarithmic decrement of damping, for small values of damping, is given approximately by:

$$\delta = 2\pi\xi'$$

where $\quad \xi' =$ damping factor $= c/c_c$

$\quad c_c =$ critical damping factor $= 2\ m\ \omega_n$

Therefore,

$$\delta = 2\ \frac{c}{2\ m\ \omega_n}$$

or

$$c = \frac{\delta\ m\ \omega_n}{\pi}$$

Substituting in (2):

$$X = \frac{\pi\ F_o}{\delta\ m\ \omega_n^2}$$

or

$$F_o = \frac{X\ \delta\ m\ \omega_n^2}{\pi} \tag{3}$$

Next, by definition, the coefficient of lift is given by:

$$C_L = \frac{F_o}{\frac{1}{2}\ \rho\ V_G^2\ d}$$

Substituting for $F_o$ from (3):

$$C_L = 2 \frac{X \delta m \omega_n^2}{\pi \rho V_G^2 d} \tag{4}$$

When the movable tube is tuned to a known value of natural frequency ($\omega_n$) and damping ($\delta$) and is oscillating in steady state at a certain flow velocity ($V_G$), expression (4) can be used to compute the instantaneous value of the lift-coefficient ($C_L$) corresponding to any value of tube-amplitude (X).